Designing corneal stromal microenvironments based on supramolecular hydrogels

Document Version:
Publisher's PDF, also known as Version of Record (includes final page, issue and volume numbers)

Please check the document version of this publication:

• A submitted manuscript is the version of the article upon submission and before peer-review. There can be important differences between the submitted version and the official published version of record. People interested in the research are advised to contact the author for the final version of the publication, or visit the DOI to the publisher's website.
• The final author version and the galley proof are versions of the publication after peer review.
• The final published version features the final layout of the paper including the volume, issue and page numbers.

Link to publication

Download date: 08. Feb. 2024

DESIGNING CORNEAL STROMAL MICROENVIRONMENTS BASED ON SUPRAMOLECULAR HYDROGELS

Annika Vrehen

DESIGNING CORNEAL STROMAL MICROENVIRONMENTS BASED ON SUPRAMOLECULAR HYDROGELS

Annika Vrehen

Designing corneal stromal microenvironments based on supramolecular hydrogels

Anna Felicia Vrehen

Eindhoven University of Technology, The Netherlands

Cover design by Siri Hellenbrand & Annika Vrehen

Printed by Gildeprint

If not stated otherwise, the used quotes are citations of Jack Poels (Rowwen Hèze)

A catalogue record is available from the Eindhoven University of Technology Library.

" Woar ge ok loept en wat ge ok bint

Niemand di zeat ow wat good is of slecht

Niemand di wet wie verluust of wie wint

Ge komt op ut end beej ow zelf terecht "

Designing corneal stromal microenvironments based on supramolecular hydrogels

PROEFSCHRIFT

Ter verkrijging van de graad van doctor aan de Technische Universiteit Eindhoven,
op gezag van de rector magnificus prof. dr. S.K. Lenaerts,
voor een commissie aangewezen door het College voor Promoties,
in het openbaar te verdedigen op vrijdag 27 oktober 2023 om 13:30 uur.

Door

Anna Felicia Vrehen

Geboren te Nieuwstadt

Dit proefschrift is goedgekeurd door de promotoren en de samenstelling van de promotiecommissie is als volgt:

Voorzitter:	prof. dr. M. Merkx
Eerste promotor:	prof. dr. dr. P.Y.W. Dankers
Tweede promotor:	prof. dr. C.V.C. Bouten
Promotiecommissieleden:	prof. dr. J. de Boer
	prof. dr. Ing. L. De Laporte (RWTH Aachen)
	prof. dr. R. Nuijts (Maastricht UMC)
	dr. Ir. W. F. Daamen (Radboud UMC)
	dr. M. Baker (Maastricht UMC)

Voor Mia† en Fien

TABLE OF CONTENTS

Designing corneal stromal microenvironments based on supramolecular hydrogels

Covered by the tear film, the cornea is positioned at the outermost part of the eye. The main functions of the cornea within the human eye are protection of the inner parts of the eye, and refraction of light from the external world towards the retina. The thickest layer of the cornea is the corneal stroma. As such, the intrinsic characteristics of the stroma largely affect essential corneal properties, *i.e.* corneal transparency. In case of a damaged or diseased stroma, the ability of the cornea to ensure maximal focus of light on the retinal surface, is seriously hampered. Eventually, a corneal disease or injury to the cornea can result in visual impairment or even blindness. Very limited treatment options for patients with severe stromal disease or injury are currently available, resulting in an urgent need for the development of new successful biomaterials.

The characteristics of the native stromal microenvironment determine the design criteria of new successful biomaterials. Our aim is to design corneal stromal microenvironments based on hydrogels, using a supramolecular approach to vary the bioactivity and mechanical properties of the hydrogels, to support stromal keratocytes. Due to the viscoelastic nature and high water content, hydrogels closely mimic the natural environment of corneal stromal cells. To this end, hydrogels possess the desirable material characteristics to function as a stromal construct. Here, synthetic biomaterials based on supramolecular chemistry are designed with the ability to remodel, adapt and self-heal due to the dynamic and responsive nature of the materials. Due to their tunability, the needed biochemical cues to induce self-regeneration of the stromal tissue, can be incorporated within the synthetic hydrogel. Within this work, polymers based on supramolecular ureido-pyrimidinone (UPy) motifs were used as building blocks. These motifs

are able to form hydrogen bonds that induce self-assembly into supramolecular polymers, allowing to generate supramolecular hydrogels.

First, an injectable supramolecular hydrogel based on UPy-moieties with incorporated UPy-cRGD was designed. The biological and mechanical properties of this hydrogel were compared with a hybrid hydrogel, based on a combination of UPy-fibers and collagen type I fibers. Encapsulation of stromal keratocytes within the hydrogels resulted in 3D cell culture, providing the cells with the needed biochemical cues to support migration, proliferation, and differentiation. The combination of biocompatibility and injectability, results in a supramolecular hydrogel that holds a great potential as a synthetic stromal construct.

Besides UPy-cRGD, we synthetized, conjugated and characterized three additional bioactive peptide additives; a collagen type I binding peptide UPy-GCGGPAQMWVH, a collagen mimicking peptide UPy-GFOGER that showed a novel superstructure, and a short collagen mimicking peptide UPy-DGEA. All three peptide additives were individually incorporated within the synthetic supramolecular hydrogel. Characterization of UPy-GFOGER demonstrated the ability of the supramolecular conjugate to self-assemble into short nanofibers with brush-like outer features, suggesting trimerization into a triple helix. These conformational differences were associated with a difference in biological success, as the UPy-GFOGER supported the spreaded morphology and (re-)differentiation of the encapsulated keratocytes, while the UPy-DGEA only supported small round-shaped cells. The analysis of these bioactive additives indicated the importance of a complex structure to mimic the complex structure of natural collagen.

Furthermore, the supramolecular approach allowed for the formation of a large set of hydrogel-like networks upon introduction of a supramolecular polyaminoacid library. Both 2D and 3D cell culture were supported by the various hydrogel designs. Excitingly, our mixing approach allowed for the fabrication of transient networks comprising of a mix of amino acids. The fabrication of these mixtures resulted in a novel design tool to generate a library of functional biomaterials, able to synthetically mimic the natural protein presentation within the extracellular matrix.

Moreover, the combination of supramolecular hydrogels and droplet based microfluidics resulted in the fabrication of microgels. In comparison with bulk hydrogels, these microgels possess intriguing properties that make them favorable over bulk hydrogels for biomedical applications. Single keratocyte encapsulated microgels demonstrated the formation of porous microstructures, supporting migration and infiltration of the keratocytes. Due to their small size and reversible dynamic bonding these microgels possess a great potential towards minimally invasive therapies for corneal defects in the clinic.

In conclusion, the use of supramolecular microgels combined with the described variations in bioactivity hold a great potential as an artificial corneal stromal construct due to its injectability, and ability to support and/or recruit healthy corneal stromal keratocytes. Knowledge obtained within this dissertation is not confined solely to corneal developments, it can be translated towards other tissue-engineering applications based on cell-material interactions.
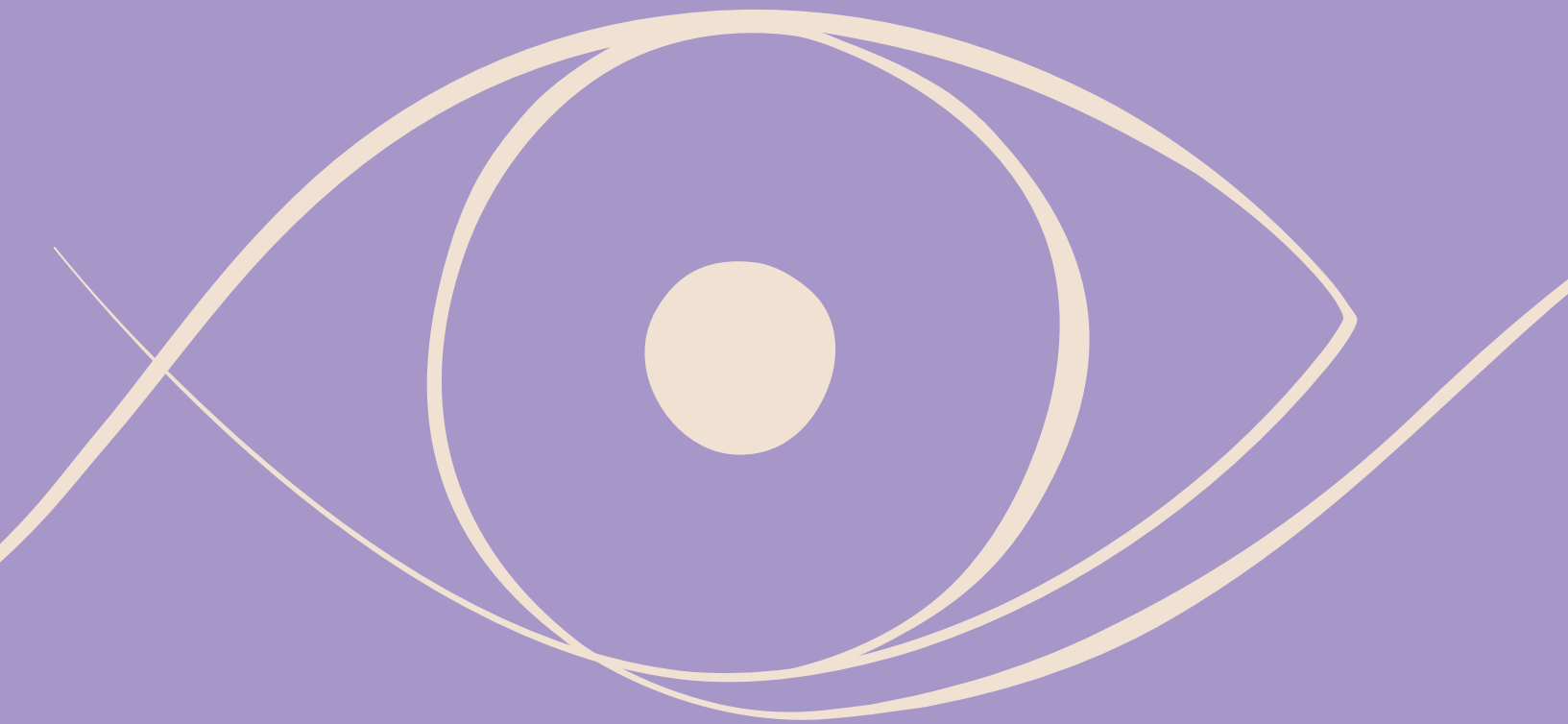
CHAPTER 1

A supramolecular approach to mimic
the corneal stromal microenvironment

1. ANATOMY AND STRUCTURE OF THE EYE, CORNEA & STROMA

The human eye

The principles of sight and visual perception all start with the human eye, which allows us to take in information from the environment and to analyze and interpret it. Herewith, complex structures and tissues are involved, each designed for a specific purpose and providing the eye with the ability to change light rays into a neural signal (**Figure 1**). The outermost layer of the human eye, the sclera, provides protection for the structures within the eye as well as resistance to the pressure of the fluids inside. At the anterior side of the eye, the sclera is covered with a transparent and avascular connective tissue called the cornea, providing a proper refractive surface for the eye.[1,2] Light rays entering the eye first pass the cornea, which already fulfills approximately two thirds of the total refraction power of the eye. The lens provides the additional refraction to accurately focus the light rays on the neural tissue of the retina. The retina is responsible for the translation of light into a signal, which is transmitted to various parts of the brain to be processed.[3] Within the interior of the eye both the anterior and posterior chamber hold aqueous humor produced by the ciliary body, providing the surrounding avascular tissues with nutrients.[2] Within this thesis the cornea will be the tissue of interest, due to its essential refractive properties.
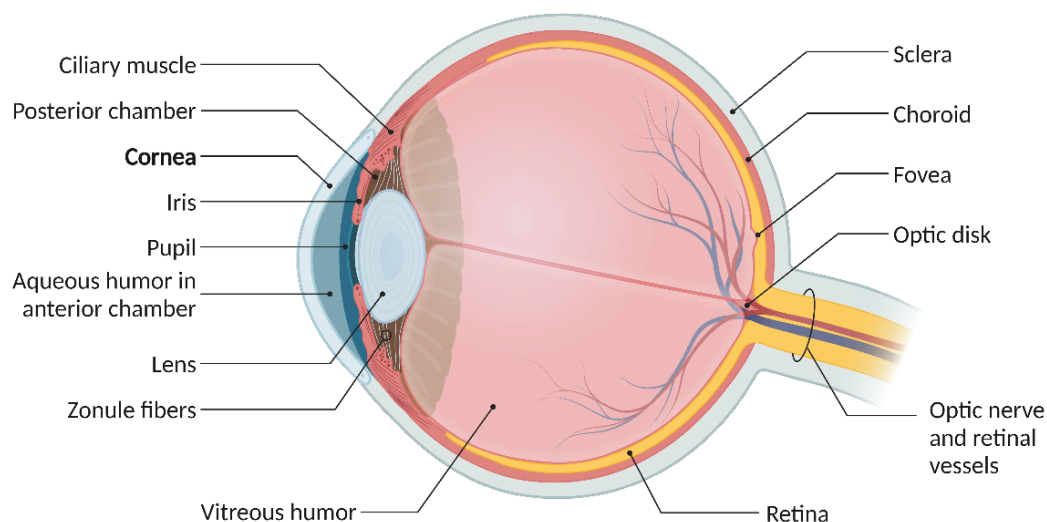
Figure 1. Schematic illustration of the anatomy of the eye globe, highlighting the cornea at the anterior side. Created with BioRender.com.

Corneal function and anatomy

Covered by the tear film, the cornea is positioned at the outermost part of the eye. It possesses the ability to protect the inner parts of the eye as well as to refract light from the external world towards the retina.[4] The cornea has a slightly oval shape, with a horizontal dimension of ~ 12 mm and a vertical dimension of ~ 11 mm. The thickness in the periphery of the cornea is approximately 650-700 μm and the thickness in the center of the cornea is approximately 500 μm.[2,5] The cornea consists of several layers (**Figure 2**), of which three cellular layers are separated from one another by two acellular layers. The first barrier with the outside environment is ~ 50 μm thick and created by 6-8 epithelial cell layers. The Bowman's layer, an acellular and dense fibrous sheet of interwoven collagen fibers with a total thickness of ~ 8-10 μm, separates the epithelium from the stroma. Inwards, the Descemet's membrane separates the stroma and the endothelium layer, being a ~ 10-12 μm thick basement membrane of laminin, fibronectin, collagen type IV, and collagen type VIII.[1,2,6] The final layer is the endothelium which is composed of hexagonally shaped endothelial cells with a diameter of ~ 5 μm. This layer controls the permeation of water, ions and metabolites to the rest of the cornea.[2,7]

With a thickness of ~ 500 μm the stroma comprises over 90% of the total thickness of the cornea. As such, the intrinsic characteristics of the stroma largely affect essential corneal properties, *i.e.* corneal transparency and strength.[1,2]

The stromal structure and extracellular matrix composition

Densely packed collagen type I lamellae in a heterodimeric complex with collagen type V and type VI create the highly organized structure of the corneal stroma. The distance between collagen fibrils is ~ 41.5 nm and the diameter of a single collagen fibril ranges between 22.5-35 nm. Collagen fibrils, which run parallel to one another, form flat bundles, called lamellae. Within the stroma about 200 sheets of these lamellae are arranged.[1,2] Successive lamellae of collagen fibrils are oriented in an orthogonal fashion, ensuring mechanical strength and transparency, which are both essential for the cornea to function properly.[8] Approximately ~ 71% of the corneal dry weight consists of collagen, being the most abundant extracellular matrix (ECM) protein of the stroma. Of the various collagen types being present within the stroma, about
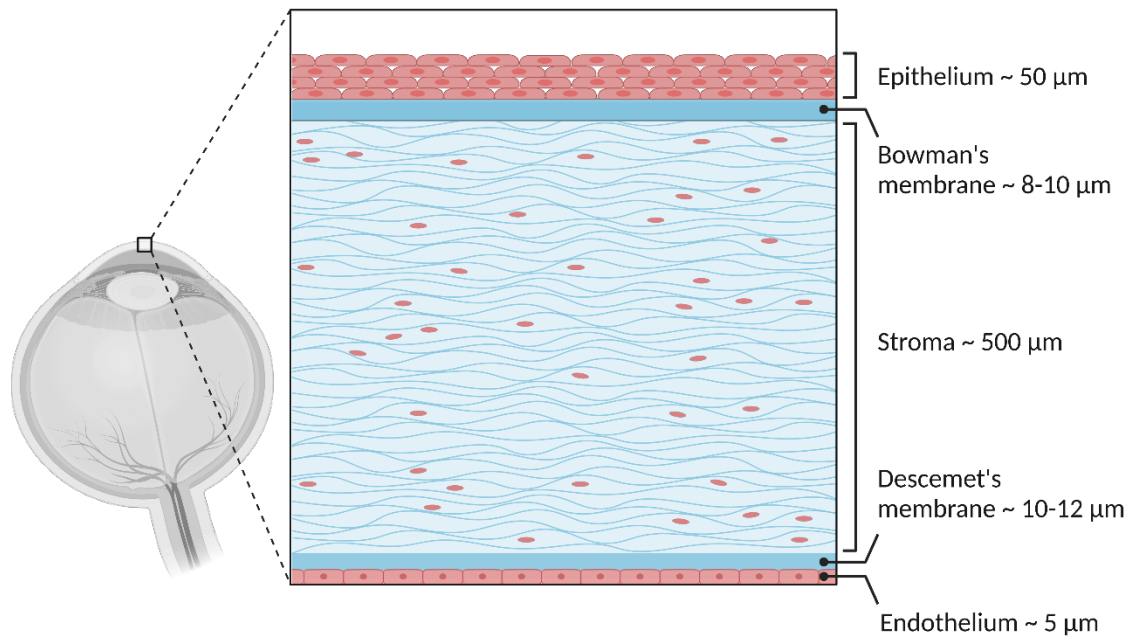
Figure 2. Anatomy of the cornea, showing the surface epithelium layer, the Bowman's membrane separating the epithelium from the stroma, the stroma, the Descemet's membrane separating the stroma from the single cell endothelium layer. Created with BioRender.com.

75% consists of collagen type I. Heterodimeric complexes are formed of a combination of collagen type I and collagen type V. Micro-fibrillar structures are composed of collagen type VI, taking in 17% of the total stromal collagen amount.[6,9] The presence of specialized leucine rich proteoglycans (PGs), *i.e.* keratocan, mimican, lumican, and decorin surround the collagen complexes. Together with negatively charged glycosaminoglycans (GAGs), like keratan sulfate, the leucine rich proteoglycans contribute to the high hydration of the stromal tissue, which contains ~ 78% water. The PGs as well as the GAGs function as ground substance and fill the areas between the fibrils and lamellae, therewith contributing to the organization of the stromal structure .[6,10]

The distribution of the lamellae within the stroma is not completely homogenous, as the lamellae in the anterior of the stroma, close to the Bowman's layer are more densely packed, drier, and stiffer compared with the lamellae in the posterior side of the cornea which are close to the aqueous humor. This difference in hydration is mainly responsible for the characteristic corneal curvature.[11] Both the Bowman's layer and the Descemet's membrane fulfill a barrier function to prevent excessive swelling of the cornea and associated loss of transparency.[12] Within the stroma a compression force is created by the anterior-to-posterior

flow, that has a flow rate of 20 μm/h from the posterior side towards the tear film where the fluid evaporates, and a flow rate of 40 μm/h in the opposite direction towards the aqueous humor.[12]

The cells hosted within the stroma are referred to as keratocytes, which account for ~ 5-10% of the total stromal volume. The distribution of the keratocytes in the stroma is not completely homogenous, as the keratocyte density on the anterior side is slightly higher compared with the posterior keratocyte density.[6,13] Via their long dendritic protrusions, keratocytes possess the ability to sense their surrounding local microenvironment. The microenvironment of the keratocytes is an organized combination of cellular elements (*i.e.* keratocytes, myofibroblast and immune cells), cell-cell interactions, ECM proteins, mechanical stimuli, and soluble factors (*i.e.* cytokines, oxygen gradients, and growth factors). As such, the stromal microenvironment influences the keratocyte cellular phenotype through physical, mechanical, and biochemical mechanisms. An import characteristic of the keratocytes is their ability to produce essential ECM components such as proteoglycans and matrix metalloproteinases (MMP). [6,13] Moreover, they continuously regenerate the collagen within the stroma.[14] Although this regeneration process seems to be quite slow, it is thought to assure the successful highly organized structure of the stroma.[15] A fast collagen production response often results in disorganized collagen deposition with associated scar formation and therewith loss of transparency.[15]

Disease or trauma to the corneal stroma

The ability of the cornea to ensure maximal focus of light on the retinal surface and to similarly minimize light scattering and transmission losses, is seriously hampered in case of a damaged or diseased cornea, resulting in visual impairment or even blindness.[4] Within a healthy cornea, the restorative process *in vivo* results in the regeneration of new, functional tissue that replaces the damaged or diseased components. However, in the case of larger stromal defects or diseases, healing often results in uncontrolled production of disorganized fibrotic tissue by keratocytes, resulting in loss of transparency and decreased visual performance. During this process, keratocytes can undergo metabolic activation, which provokes a change into a fibroblastic phenotype, leading to cell migration, proliferation and increased collagen production.[16,17] Unfortunately, the metabolic activation of keratocytes often ensues in an

irreversible transformation of the keratocytes into myofibroblasts, causing permanent scarring of the stroma.[18]

Pharmaceutical interventions in some cases slow disease progression, yet do not restore the patient's vision. A last remedy in otherwise untreatable patients is the use of an artificial cornea, a full thickness, completely artificial transparent material. This artificial cornea acts as a replacement of the injured or diseased cornea, aiming to maintain a minimum functionality of the cornea.[19–24] Still, this solution is far from ideal, neither restoring the pre-disease corneal function and structure, nor supporting self-regeneration of the native tissue. Moreover, artificial corneas often induce unwanted immune reactions, which sometimes are followed by rejection. Such reactions result in scar tissue at the implant border, causing a haze and sometimes even complete loss of the implant and eventually vision.[17,20,25,26] Thus, treatment options for patients with severe stromal disease or injury are very limited. Many patients at risk of blindness due to corneal disease or injury rely on corneal transplants from deceased human donors as the only available treatment. Unfortunately, there is a worldwide shortage of corneal graft tissue, with only 1 cornea available for 70 needed.[27]

2. TISSUE ENGINEERED CONSTRUCTS TO REGENERATE THE STROMA

In recent decades, ophthalmologists and bioengineers joined forces to engineer a living construct that is able to integrate with the patient's eye and to support the self-regeneration process of the native tissue, and subsequently successfully restoring the patient's vision. However, the cornea is a very complex tissue. Multiple materials properties, such as; transparency, biocompatibility, innervation and mechanical properties, all need to be considered when engineering a stromal construct. Hydrogels are defined as a three-dimensional interconnected network dispersed in an aqueous phase, comprising a viscoelastic nature and high water content. To this end, hydrogels often possess the most desirable material characteristics to closely mimic the natural environments of cells in various tissue types. A wide variety of hydrogel systems are currently used to recapitulate the most important features of the native ECM, ranging from completely natural to hybrid versions to fully synthetic. Although natural derived hydrogels are characterized by their powerful natural biochemical compositions, their stiffness is rather limited. The minimal concentration needed for complete

network formation and the maximum concentration to dissolve the natural-derived component, leave a narrow space to tune the stiffness. In contrast, a substantially larger range of stiffnesses is reached by synthetic hydrogels, yet these materials lack in bioactivity. To improve on these material limitations, hybrid hydrogels, where two gels with different properties are mixed, are being developed.
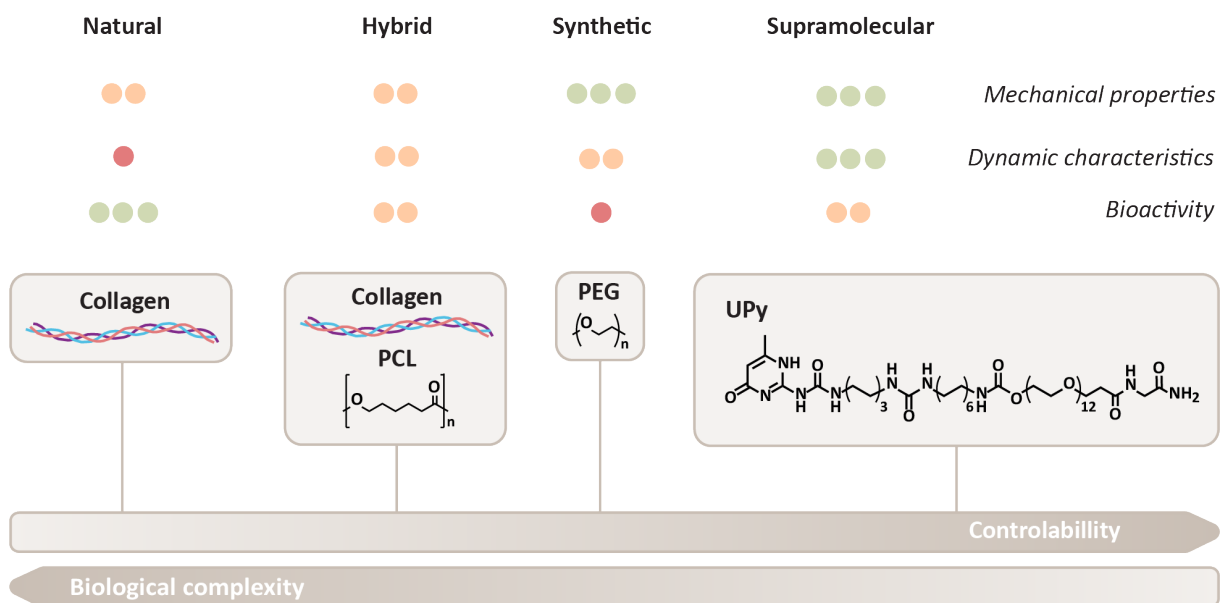
Figure 3. Overview of the ECM mimicking materials, classified as; natural, hybrid, synthetic covalent and synthetic supramolecular. Ranked by their biological complexity and material controllability, color rated by their mechanical, dynamic and bioactive characteristics. Adapted figure from Rijns *et al*. 2023.[103]

Hybrid hydrogels: the best of both worlds

Hybrid hydrogels combine the biological power of naturally derived hydrogels with the tunability of the synthetic hydrogels (**Figure 3**). The design of these hybrid hydrogels can be as simple as mixing a natural and synthetic network together, or complex, via introduction of smart synthetically modified natural polymers into the hydrogel.[28–32] Yet, due to the limited range of solvents, temperatures, and concentration, which allow dissolvability of the synthetic components without damaging the natural components, it is still challenging to combine natural and synthetic polymers within one hybrid hydrogel.[33]

Alginate is often used in hybrid hydrogels to impart processability and control the dynamic mechanical properties. Upon using different molecular weight polymers in combination with different crosslinking densities of calcium, which ionically crosslinks alginate,

the dynamic mechanical properties of the resulting hydrogels are modulated. By covalently coupling polyethylene glycol (PEG) to alginate, Chaudhuri *et al.* formed hydrogels with constant mechanical stiffness and alginate concentration, but varying stress relaxation and creep. This approach revealed that an enhanced substrate creep or stress relaxation led to increased cell spreading.[34,35] Double network alginate-PEG systems have also been developed, based on biocompatible polymers combining two cross-linking chemistries. This resulted in the formation of a dynamic network that allowed for self-healing and injectability, and of a static network that allowed improved stability on cell culture conditions. The combination of both networks led to a synergetic effect, enabling the formation of a tough injectable matrix.[36] Other hybrid gels based on PEG are developed by Trujillo *et al.* and include mixes of a fibronectin network consisting of 4-arm-PEG-maleimide, crosslinked with PEG-dithiol and thiolated protease-degradable peptides.[37] This design allows ECM proteins, like fibronectin, to bind growth factors such as VEGF and BMP2, herewith providing a highly controllable 3D environment to promote bone regeneration and vascularization.[37] The Seliktar lab mixed PEG with albumin, fibrinogen and gelatin, revealing that the PEG-proteins mixtures contain different degradation rates and mechanisms as compared to PEG only.[38]. PEG could also be mixed with fibrin to benefit from fibrin's bioactivity, while preventing the fast degradation of fibrin by increasing mechanical stability with PEG.[39]

Other hybrid hydrogels consisting of a covalently crosslinked bovine serum albumin (BSA) network, reinforced with non-covalently adsorbed polyelectrolytes, were studied by Khoury *et al.* Besides the reinforcement and large stiffening effect, the non-covalently attached polyelectrolytes can create and break local bonds, allowing the gels to heal any structural damage.[33] Another hybrid hydrogel is designed by the Kouwer lab and consists of Matrigel and polyisocyanide (PIC). PIC is the only synthetic polymer that exhibits stress stiffening: when subjected to mechanical stress, the polymer becomes stiffer and more resistant to deformation.[40] However, the limited bioactivity of PIC hampers its use in combination with cells. The hybrid combination of PIC and Matrigel results in a material that exhibits both stress stiffening properties and good bioactivity.[41]

Another class of hybrid hydrogels comprises MMP cleavable peptides, which function as interesting crosslinkers in synthetic materials contributing to a biomimetic degradation mechanism. Jha and coworkers studied the influence of degradation kinetics of MMP crosslinkers on biological outcomes of a cell laden hybrid hydrogel.[34] RGD functionalized

hyaluronic acid (HA), heparin and different MMP cleavable peptides were used to tune hydrogel degradation rate. Interestingly, the hydrogels crosslinked with the slow MMP-degradable peptides supported cardiac progenitor cell survival, proliferation, and endothelial cell differentiation.[34]

Collagen based hybrid hydrogels – towards a corneal construct

Biopolymers such as collagen, gelatin, silk, dextran, hyaluronic acid and decellularized stromal tissues are commonly studied as a potential hydrogel stromal construct. Despite the fact that these materials show great cell biocompatibility, they also pose a disease transmission risk, immunogenic concerns, scalability issues, and incompetent biomechanical properties.[42–45] The main stromal constituent is collagen, making collagen an obvious choice to mimic the native human stroma.[17] However there are some limitations to using solely collagen as a material, such as; inducing of immunogenicity upon the use of animal-derived collagen, low-density collagen in materials results in insufficient biomechanics, compression of collagen to remove water and therewith increase the biomechanics hampers in return the ability of cells to infiltrate, and crosslinking of collagen improves the strength, but reduces the biocompatibility.[44,46,47] The formation of collagen composites is an alternative approach to reinforce collagenous constructs without losing their biocompatibility.

For instance, Majumdar *et al.* fabricated robust, transparent cyclodextrin modulated type I collagen assembly with aligned fibers and lamellae (**Figure 4A**). During gelation, the cyclodextrins behave comparable to the small leucine-rich proteoglycans which regulate the fibril diameter and spacing via interactions with hydrophobic amino acids in collagen. The fabricated acellular and curved hydrogel implants created from this material integrated with the surrounding tissue and promoted re-epithelialization in an *in vivo* rabbit model. However, the potential of using cyclodextrin collagen gels in the clinic is limited due to its comprehensive preparation process, its inapplicability for irregularly sized cavities, and its pH and temperature conditions which may damage encapsulated cells.[48] In order to recapitulate a transparent native stromal structure, Kong *et al.* produced microfibrous poly(ε-caprolactone)-poly(ethylene glycol) grids via direct writing and infused the scaffolds with gelatin-methacryloyl. These composite hydrogels maintained the keratocyte-like phenotype of rat limbal stromal cells and supported keratocyte specific gene and protein expression. Furthermore, stromal matrix

synthesis and regeneration was demonstrated upon application of the implants in a rat intrastromal keratoplasty model.[49] Myung and coworkers introduced a bio-orthogonal copper-free form of click chemistry referred to as strain-promoted azide-alkyne cycloaddition (SPAAC), as a means to chemically crosslink collagen around cultured keratocytes.[50–52] To this end, collagen was modified with azide and dibenzocyclooctyne (DBCO) groups to enable the SPAAC reaction between azide-conjugated collagen and alkyne-conjugated collagen (**Figure 4B**). The clinical applicability of SPAAC is promising, since azides and alkynes do not react with functional groups on cells or tissues, the reaction produces no free radicals and side products, and the reaction can proceed in water under ambient conditions without the need for external catalysts. Primary corneal keratocytes were encapsulated within crosslinked collagen matrices. The collagen gels supported a co-culture of keratocytes within the bulk of the matrix and keratinocytes on their surface. Overall, the designed construct demonstrated to be a potential 3D in vitro model system for studying keratocyte-keratinocyte interactions within the corneal tissue.[50] Hereafter, SPAAC was used to create an interpenetrating polymer network hydrogel via mixing of thiolated hyaluronic acid, methacrylated hyaluronic acid, azido-modified collagen, and DBCO modified collagen at the same time. The collagen network supported cell adhesion, while hyaluronic acid improved the mechanical properties of the hydrogel. The combination of both networks demonstrated to be applicable for treatment of corneal defects. [51,52] Constructs based on a combination of collagen and chitosan stabilized by PEG, demonstrated improved stiffness of the material due to the addition of chitosan. Upon long-term *in vivo* implantation, these construct showed great physical and biological performance. During a 12-month study, the optical clarity of the chitosan-collagen composites showed even to be superior to human eye bank corneas.[53] Addition of electrospun polymers to collagen gels demonstrated to improve the saturability of stromal constructs. The aligned poly(lactic-co-glycolic acid (PLGA) electrospun fibers reinforced collagen hydrogels towards the mechanical requirements of the native tissue, aiming to reach the requirements for optical transparency.[54] Fernandes-Cunha *et al.* demonstrated an *in situ* forming approach to crosslink collagen using multi-arm PEG succinimidyl esters. These hybrid hydrogels supported corneal epithelial cells and keratocytes to proliferate when applied to corneal stromal defects, and maintained vision due to their transparency.[55]

A

I — Collagen → add CD and Buffer → Gelation (CD, early vitrification, Triple helix) → Micro-fibril assembly → further vitrification → Fibril growth (collagen microfibrils)

II — TEM: Collagen | β-cyclodextrin/collagen | β-cyclodextrin-suc/collagen | Cornea

B

I — Azide-PEG-collagen / Keratocyte / DBCO-collagen → Collagen crosslinking → Keratocyte encapsulation (SPAAC) → Keratinocyte → Co-culture keratinocyte on top keratocyte within matrix

II — Day 6, F-actin: Non-crosslinked gel | SPAAC gel 3.0 mg/mL | SPAAC gel 1.5 mg/mL

III — SPAAC gel - 1.5 mg/mL

C

I — (bioprinting schematic)

II — 3D Bio-printed lattice (Top view, Side view)

III — Brightfield | CAM | EthD-1; Day 0, Day 1, Day 7

IV — CSF viability over time; RLU; Day 0, Day 1, Day 7; Control, Pre-crosslinked; Alginate type
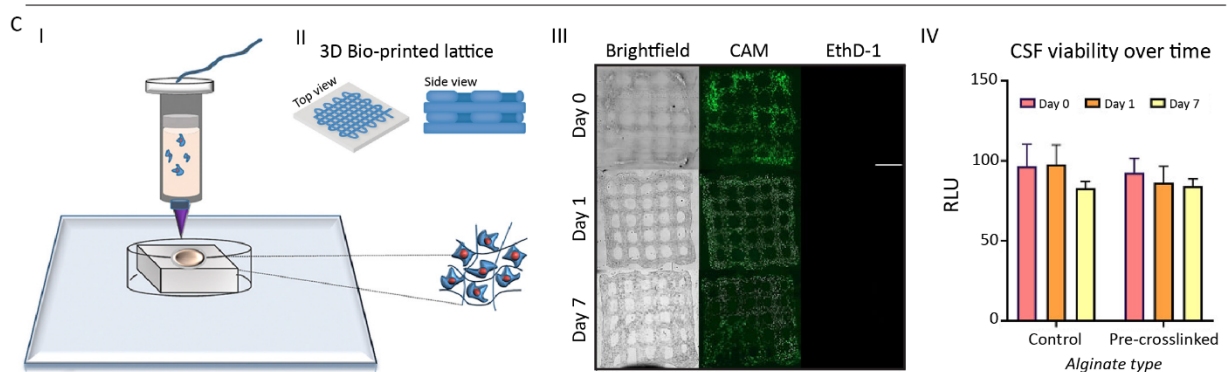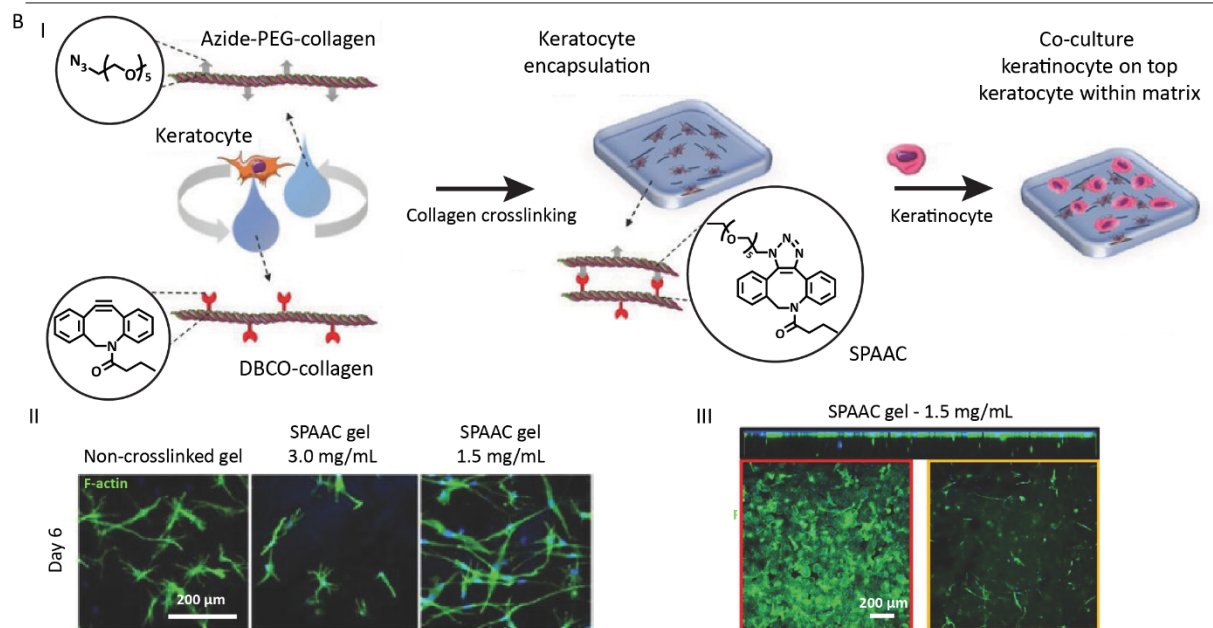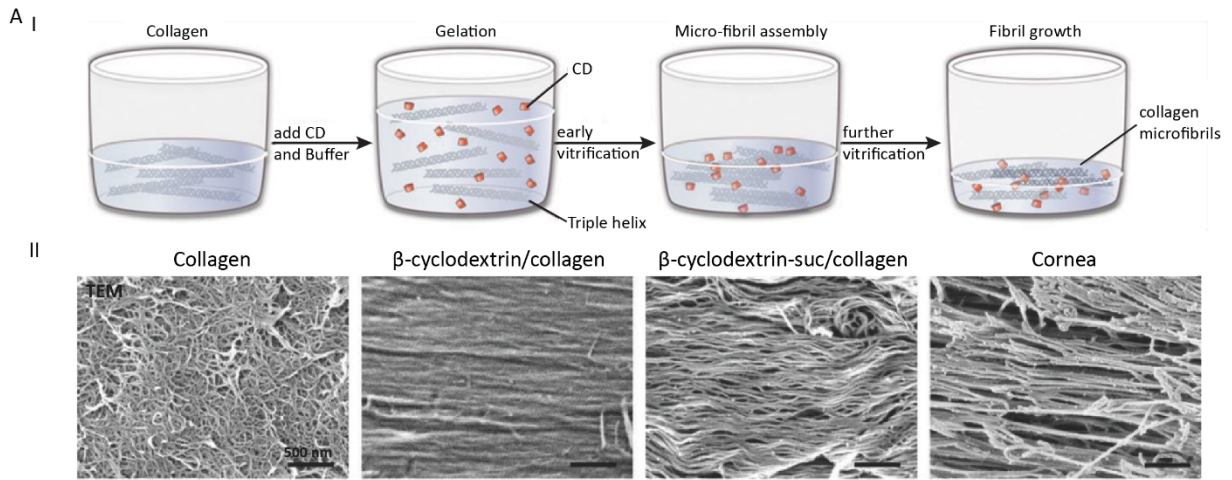
Figure 4. Examples of hybrid hydrogels used for corneal tissue engineering. **A)** Cyclodextrin modulate collagen assembly during vitrification, resulting in biomimetic fibril organization. I. Collagen vitrigels prepared by mixing equal volumes of collagen and CD-buffered solution. II. Transmission electron microscopy (TEM) to demonstrate the effect of CD functionality on collagen ultrastructure organization. Adapted from Majumdar *et al.* 2018.[48] **B)** Collagen gel matrix formation by strain-promoted azide-alkyne cycloaddition (SPAAC). I. Azide-PEG-conjugated collagen (Azide-PEG-collagen) and BCO-conjugated collagen (DBCO-collagen) were mixed with keratocytes to fabricate a corneal stroma tissue substitute. Keratinocytes were seeded on the collagen gel. II. F-actin staining showing the morphology of keratocytes encapsulated in the non-crosslinked and SPAAC gel at day 6. III. Confocal scans that show keratinocytes on the surface (red) and keratocytes within the gels (yellow). Adapted from Lee *et al.* 2018.[50] **C)** Studying the potential of pre-crosslinking low percentage alginate-based bio inks with CaSO4 as a useful strategy to improve bio-ink printability without having adverse effect on cell survival. I. Schematic representation of 3D bio-printed constructs. II. Schematic design of the 3D bio-printed lattices. III. Corneal stromal fibroblasts laden bio-inks were bio-printed and assessed for viability with live stain CAM and dead stain Ethd-1. IV. Metabolic activity of corneal stromal fibroblasts (CSF). Adapted from Kostenko *et al.* 2022.[60]

Collagen based hybrid corneal constructs – scaffold based

Some research groups focused on the development of scaffolds with aligned nanofibers, to mimic the organized structure of the collagen fibers within the cornea. An electrospun scaffold looks like a nanofibrous mat, which in dry conditions emits a solid behavior. Kim *et al.* generated a dome-shaped electrospun scaffold with radially aligned collagen-polycaprolactone (PCL) fibers possessing the ability to host cells, to minimize light scattering and to achieve a Young's modulus similar to the human cornea.[56] Other research groups focused on the design of collagen matrixes supplemented with proteoglycans or polysaccharides. For instance, Zhong *et al.* used electrospinning to create nanofibrous collagen-chondroitin sulfate scaffolds supplemented with GAGs, which were crosslinked by glutaraldehyde vapor. The collagen-GAG scaffold was constructed by electrospinning. A mixture of trifluoroethanol and water as solvent resulted in a nanofibrous and porous electrospun structure. The authors chose to use nano-fibrous-scaffolds, since this dimension provides a well-defined architecture with high surface area to volume ratio. Herewith, they proposed to promote guidance of cell growth and faster tissue regeneration compared to other dimensions.[57] Torbet *et al.* used magnetic orientation to create a corneal stroma-like scaffold, consisting of multiple intermeshed orthogonal layers of oriented collagen type I fibrils. The addition of proteoglycans improved the gel transparency by reducing the fibril diameter and eliminating lateral fusion of fibrils. In response to contact

guidance cues in and on the scaffold, human corneal keratocytes seeded onto the scaffolds aligned on the surface as well as within the bulk of the orthogonal collagen template.[58]

The technique of 3D bioprinting has gained notable interest for tissue engineering applications due to its ability to direct the hierarchical assembly of three-dimensional biological structures for tissue construction. As the corneal stroma contains a distinct arrangement of collagen lamellae, Connon and coworkers mainly focused on the feasibility of generating complex 3D bioprinted corneal stroma equivalents using pneumatic 3D extrusion bioprinting.[59] Sodium alginate and methacrylated collagen type I were initially used to prepare several low viscosity bio-inks. These bioinks were provided with the necessary stiffness to fabricate robust stromal constructs with precise control over the microarchitecture (**Figure 4C**). The encapsulation of keratocytes resulted in promising initial cell viability, showing a potential of using 3D bioprinting to design a stromal construct. Later on, pre-crosslinking with $CaSO_4$ of low percentage alginate-based bio-inks demonstrated to be a successful strategy to improve bio-ink printability without having a detrimental effect on cell survival.[60] Towards the clinical translation of 3D biofabrication, the suitability of the developed system for on-demand bioprinting and long-term culture of 3D bioprinted cell-laden constructs was explored, resulting in storable cell-laden bioinks.[61]

Pioneer within the field of engineered stromal constructs

One of the pioneering groups within the field of corneal tissue engineering is the group of Griffith and coworkers, who were the first to transplant recombinant human collagen type III constructs crosslinked by EDC/N-hydroxysuccinimide in patients in a phase I clinical trial.[62,63] These fabricated corneal constructs were transparent, robust, and cell-free. Within the first nine months regeneration of the epithelium was observed as well as subepithelial nerve formation and growth of stromal cells into the scaffolds. Longterm follow up studies confirmed that the implants remained stable and promoted regeneration of corneal tissue and nerves in all of the patients. Herewith, they showed the long term safety, efficacy, adaptability and modularity of collagen as building block for biomaterials in regeneration of human tissues.[62–66] However, biomaterials comprising full-length recombinant human collagen and extracted animal collagen provide only a limited number of functional groups applicable to chemical modification or crosslinking. To this end, the Griffith lab shifted their focus towards synthetic
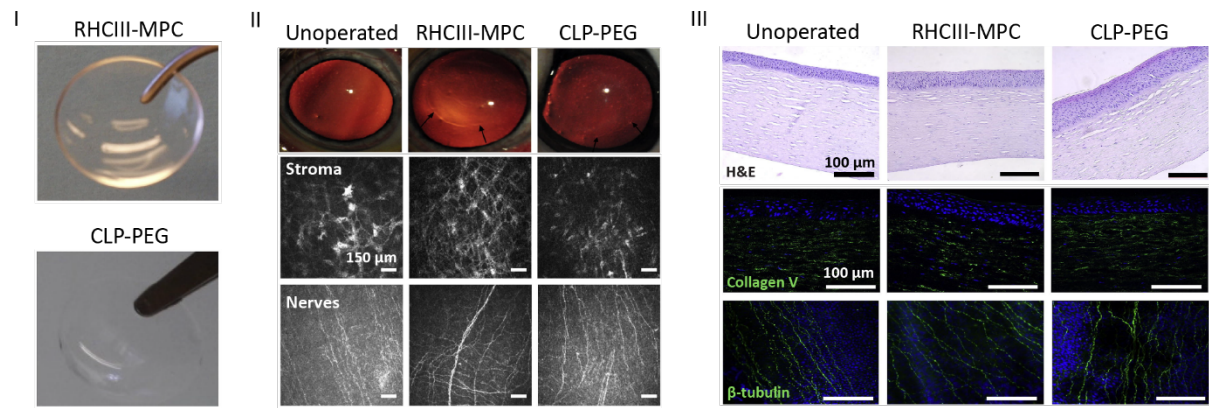
Figure 5. Examples of implants used for corneal tissue engineering fabricated by the Griffith lab. Fabrication of hydrogel implants based on short peptide analogs as alternatives to collagen. I. Control RHCIII-MPC implants and CLP-PEG implants are both optically clear as 500 μm thick implants. II. After 12 months of implantation in corneas of mini-pigs, the implants demonstrated to remain clear like the unoperated cornea. Arrows indicate the boundaries of the implants. In vivo confocal images show regeneration of stroma and epithelial nerves. III. H&E staining through a healthy cornea and corneas at 12 months after implantation. Stromal collagen type V is present and the sub-epithelial nerve plexus are stained with β-tubulin. Adapted from Jangamreddy *et al.* 2018.[67]

materials that can be readily scaled-up to broadly serve pre-clinical to clinical translation. Initially, short collagen-like peptides conjugated to multifunctional polyethylene glycol (CLP-PEG) were proposed as alternatives for full-length collagen use.[67] By conjugation of CLP to inert PEG, sufficiently robust and optically transparent hydrogel implants were produced (**Figure 5**). Compared with the previous designed RHCIII implants, the implants were not as tough. Yet, this was compensated for by being more elastic, which showed to be helpful during grafting of the implant for in-vivo studies. While the implants were able to promote regeneration, these solid-like implants require a complex surgical setting for implantation, involving higher costs with translation to the clinic.[67] Next the authors, combined the CLP-PEG with fibrinogen and generated a cell-free liquid hydrogel matrix to promote adhesion within corneal tissue defects.[68] This injectable hydrogel matrix with adhesive properties is referred to as LiQD cornea, which is designed as a sealant or filler of full-thickness corneal perforations.[68] Besides the development of synthetic alternatives for collagen, Haagdoorns *et al.* introduced the use of plant-derived type I collagen. The biocompatibility and efficacy of this plant-derived stromal construct were compared with the RHCIII hydrogel implants. The plant-derived RHCI is generated from genetically modified tobacco plants that allow the production of theoretically unlimited quantities of protein. Surprisingly, the RHCI implants demonstrated to be

biocompatible and promoted corneal regeneration in minipigs, opening doors for the use of plant-derived collagen as a collagen source for tissue engineering.[69]

3. SUPRAMOLECULAR HYDROGELS

In general, supramolecular chemistry is known as 'chemistry beyond the covalent bond'.[70] Supramolecular assemblies arise via chemical moieties within molecules, which selectively interact with each other via *e.g.* hydrogen bonding, hydrophobic interactions, van der Waals forces, electrostatic effects, and π-π interactions to form fiber-like structures, similar to materials in nature.[71,72] Compared to covalent bonds, these non-covalent bonds are relatively low-energy bonds that allow an easy breakage or reformation of the bonds, by which the supramolecular materials acquire their reversibility and associated dynamic properties.[71–73] Varying the formulation of these molecules allows for the formation of fibers, solid meshes, and hydrogels.[74]

In most tissues, the natural ECM is a dynamic hydrogel-like fibrous network generated by directed interactions between small and large molecules, resulting in the assembly of these molecules into supramolecular fibers or assemblies.[75] Synthetic supramolecular hydrogels possess the ability to closely mimic the natural ECM.[76,77] However, incorporation of bioactive cues to instruct cellular behavior is necessary to make these synthetic materials biocompatible.[78–82] To introduce function into these supramolecular materials, bioactive cues can be coupled to the monomeric building blocks and mixed into the supramolecular fibers.[83–85] Traditional synthetic hydrogels often depend on material degradability or large pore sizes to allow cellular activities such as spreading, proliferation and migration. Due to the reversibility of the non-covalent interactions, supramolecular hydrogels are very adaptable. Within the supramolecular hydrogels, this adaptability allows for matrix remodeling and supports cellular activities, without requiring hydrogel degradation or large pore sizes.[86–88]

Many research groups are exploring synthetic supramolecular biomaterials that allow the formation of fiber-like structures similar to materials in nature. Eventually, they aim to design supramolecular hydrogels that contain hierarchical complexes with synergistic functions, preserving all important properties of our native ECM. Various labs focused on the design, synthesis and characterization of supramolecular self-assembling structures, being

supramolecular protein-based biomaterials such as peptide amphiphiles (PAs), peptides, and engineered proteins.[87,89–92] The modularity and biocompatibility of these protein based biomaterials makes them good candidates for design of biomaterials in tissue engineering.[87,90,92] Another class of supramolecular biomaterials is based on the assembly of monomeric building blocks to form fiber-like structures. For instance, hydrogels based on complementary bis-urea motifs, in which the soft bending modes present in the bundles of bis-urea fibers lead to stress-stiffening behavior of the material.[93] Together with the ability to incorporate bioactive moieties via conjugation to a urea motif and mixing it into the material, these material properties allow for, the creation of hydrogels that closely mimic important characteristics of the ECM.[94]

Injectable, shear-thinning and self-healing hydrogels are highly favorable for biomedical applications and therefore often studied as a potential alternative for artificial corneas and corneal donor tissue.[95,96] Especially due to their scalability and possibility to use them in a minimal invasive and very precise manner to fill tissue defects or to introduce/recruit corneal cells and initiate self-regeneration. Here, we will focus on the design of corneal stromal microenvironments based on supramolecular ureido-pyrimidinone (UPy) based hydrogel as motivated below.

Ureido-pyrimidinone based hydrogels

An UPy-moiety allows for the formation of quadruple hydrogen bonding in a donor-donor-acceptor-acceptor fashion. These multiple directional hydrogen bonds induce the self-assembly into supramolecular polymers, which hold unique material properties such as adaptability, self-healing, stimuli responsiveness, and processibility.[97–99] To allow the assembly of elongated structures in aqueous media, hydrophobic spacers were attached onto the urea groups to shield the hydrogen bonding motifs from water and PEG chains were connected to the hydrophobic linkers as water-compatible units.[100,101] The effect of molecular exchange dynamics on the incorporation of bioactive motifs in supramolecular UPy-based hydrogels was thoroughly studied by Diba and coworkers.[102] Supramolecular hydrogels were formed by bifunctional and monofunctional molecules, containing UPy groups as supramolecular building blocks (**Figure 6**). To generate a bifunctional UPy-building block, a PEG chain with a molar weight of ~ 10 kDa is end-capped with two functional UPy-moieties. For the monofunctional

16

UPy-building block an oligo(ethylene glycol) (OEG) chain with a molar weight of 529 kDa is end-capped with a functional UPy-moiety at one end and a glycine-amide group at the other end. This way, the glycine-amide group is presented to the cells, while the OEG is shielded from exposure to minimize the non-fouling properties of the glycol. The monofunctional UPys allow for the formation of one-dimensional fibers, while the bifunctional UPys introduces interfiber crosslinks between the monofunctional UPys. The combination of monofunctional UPys and bifunctional UPys results in the formation of a transient network. By simply varying the ratio between the monofunctional and bifunctional UPys or by changing the concentration of the hydrogel, the mechanical and dynamic properties of the network can be tuned. With this comprehensive study, Diba *et al.* presented a novel supramolecular UPy hydrogel which allows for both 2D culture of cells as well as cell encapsulation and associated 3D cell culture. Furthermore, the system proved to acquire both dynamicity and tunability, allowing the incorporation of the cell adhesion ligand UPy-cRGD as well as other short peptide sequences conjugated to a UPy.[102]

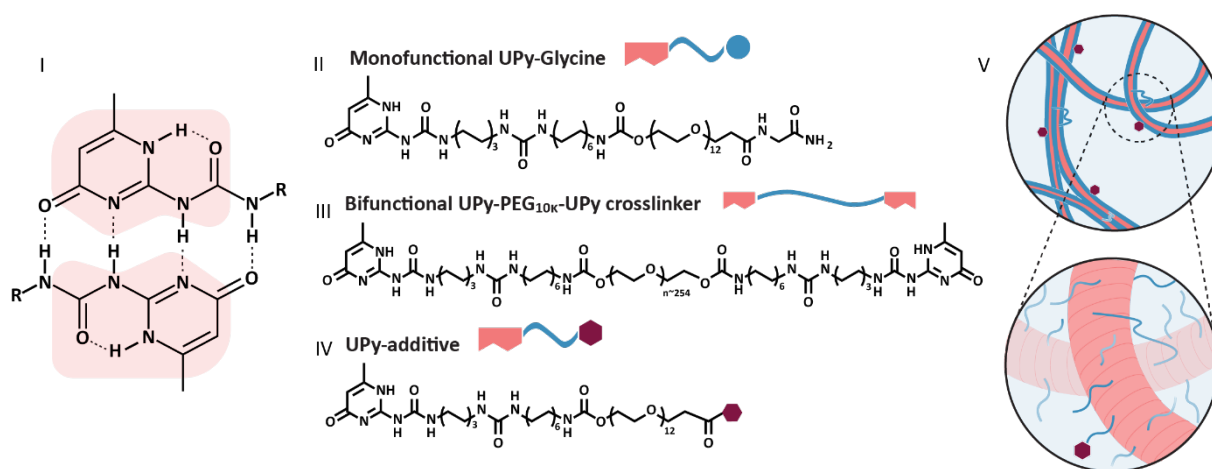**Figure 6.** Supramolecular system based on hydrogen bonding interactions. I. Dimerization of UPy keto tautomer's through quadruple hydrogen bonding. II. Chemical structures of UPy-Glycine (monofunctional UPy), III. UPy-PEG$_{10k}$-UPy (bifunctional UPy), IV. and UPy-additive. V. Schematic illustration of the supramolecular network. Blue linkages between fibers indicate interfiber cross-links formed by UPy-PEG$_{10k}$-UPy.

4. AIM AND OUTLINE OF THIS THESIS

In recent decades, significant scientific progress is made by ophthalmologists and bioengineers aiming to engineer biocompatible, implantable, and functional stromal constructs that induce self-regeneration of the compromised tissue. Despite their large investments and the presentation of diverse natural and synthetic materials as alternative implants, successful bioengineered constructs have not yet been integrated into clinical practice.[17,20,25,26] The aim of the research described in this thesis is to design a hydrogel based corneal stromal construct. The characteristics of the native stromal microenvironment determine the design criteria for the hydrogel. To this end we try to mimic the stromal microenvironments as closely as possible. A supramolecular approach is used to vary the bioactivity and mechanical properties of the supramolecular hydrogels, designing hydrogels that possess the needed biochemical cues and mechanical properties to support stromal keratocytes. In addition, the hydrogel design needs to be clinically applicable. For this purpose, the injectability of the various designed hydrogels was studied. First, the molecular building blocks of the hydrogels were varied, ranging from multiple bioactive peptide additives to various compositions of the building blocks. Second, full length natural collagen was mixed with UPy fibers to introduce bioactivity, creating a hybrid hydrogel. Then, diverse hydrogel networks were generated via the assembly of the introduced molecular building blocks in solution. As such, the studied hydrogel networks varied in biochemical cues and mechanical properties. The ability of the network to support the keratocytes, was used to define the success of the hydrogel based stromal construct. Finally, the supramolecular approach allowed for the formation of single cell encapsulated supramolecular microgels, providing an exciting new dimension to the application of our hydrogels.
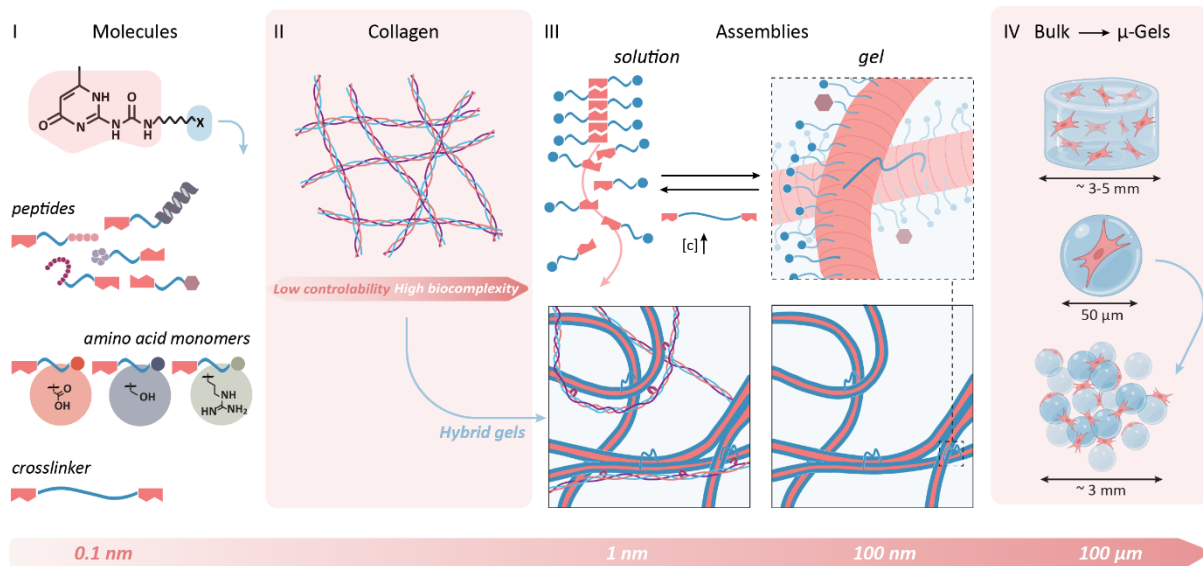
Figure 7. Length scales employed within this thesis. From left to right: I. Molecules being the supramolecular building blocks *i.e.* bioactive peptides, amino acid monomers, and the bifunctional crosslinker. II. Incorporation of natural collagen generating bioactive hybrid hydrogels. III. In solution the building blocks assemble into fibers which upon addition of a crosslinker start to form a transient network. IV. The introduced supramolecular approach allows for the formation of bulk hydrogels as well as microgels.

Chapter 2 describes the development of a fully synthetic corneal stromal construct via engineering of an injectable supramolecular hydrogel based on UPy-moieties with incorporated UPy-cRGD. The biological and mechanical performances of the synthetic hydrogel are compared with the performances of a developed hybrid hydrogel, consisting of UPy- and collagen type I fibers. The choice for a collagen based hybrid hydrogel is based on the significant function of collagen within the native stromal microenvironment.

In **chapter 3**, a collagen type I binding peptide additive is incorporated into the supramolecular UPy-stacks of the synthetic hydrogel, where it possess the ability to strengthen the interaction between the synthetic and natural compounds. Furthermore, various rheological and morphological analyses of a diverse set of hydrogel networks are performed, to explore the interactive and dynamic network generated by the synthetic matrix and the cells.

Chapter 4 demonstrates the development of a synthetic collagen mimicking hydrogel. Two collagen mimicking peptide additives are synthesized and incorporated into the supramolecular UPy-stacks of the synthetic hydrogel, being a UPy-GFOGER and UPy-DGEA peptide additive. Using analytical techniques, the ability of UPy-GFOGER to trimerize into a triple helix was

exposed. The biological performance, *i.e.* cell binding, cell spreading, and cell differentiation, of a synthetic hydrogel functionalized with either UPy-GFOGER, embracing a super structure, or UPy-DGEA, without a triple helix conformation, were investigated and compared.

In **chapter 5**, a library of supramolecular single polyaminoacids is introduced. Each supramolecular polyaminoacid consist of an amino acid monomer conjugated to a UPy-moiety. Besides studying the properties of all the polyaminoacids in solution the properties in hydrogels are studied as well, whereafter both 2D and 3D cell viability is evaluated. Excitingly, the supramolecular approach allowed for the formation of transient networks based on combinations of polyaminoacids, supporting 3D culture of cells. The influence of the diverse hydrogels on cellular behavior is explored via various analyses of cell function.

Chapter 6 describes the formation of single cell encapsulated supramolecular microgels. Various immunohistochemical analyses are used to investigate the micro stromal tissues and the underlying process of the microgel assembly. Upon assembly of the microgels, microporous scaffolds are generated which possess unique properties (*i.e.* stimulating cell migration and cell-cell interactions, introducing dynamic bonds between the microgels to allow remodeling), making them attractive for biomedical applications.

Finally, **chapter 7**, provides an epilogue with general discussion and future perspectives. The design criteria of the hydrogel based corneal stromal construct are evaluated, including the challenges that still remain. A perspective towards the clinical application of a synthetic stromal constructed is provided.

REFERENCES

1. DelMonte, D. W. & Kim, T. Anatomy and physiology of the cornea. *J Cataract Refract Surg* 37, 588–598 (2011).

2. Remington, L. A. *Clinical Anatomy and Physiology of the Visual System*. (Elsevier, 2012).

3. Meek, K. M. & Knupp, C. Corneal structure and transparency. *Prog Retin Eye Res* 49, 1–16 (2015).

4. Kong, B. *et al.* Fiber reinforced GelMA hydrogel to induce the regeneration of corneal stroma. *Nat Commun* 11, 1435 (2020).

5. Germundsson, J., Karanis, G., Fagerholm, P. & Lagali, N. Age-Related Thinning of Bowman's Layer in the Human Cornea In Vivo. *Investigative Opthalmology & Visual Science* 54, 6143 (2013).

6. Michelacci, Y. M. Collagens and proteoglycans of the corneal extracellular matrix. *Brazilian Journal of Medical and Biological Research* 36, 1037–1046 (2003).

7. Català, P. *et al.* Transport and Preservation Comparison of Preloaded and Pre-stripped-Only DMEK Grafts. *Cornea* 39, 1407–1414 (2020).

8. Mobaraki, M. *et al.* Corneal Repair and Regeneration: Current Concepts and Future Directions. *Front Bioeng Biotechnol* 7, (2019).

9. Newsome, D. A., Gross, J. & Hassell, J. R. Human corneal stroma contains three distinct collagens. *Invest Ophthalmol Vis Sci* 22, 376–81 (1982).

10. Schwend, T., Deaton, R. J., Zhang, Y., Caterson, B. & Conrad, G. W. Corneal Sulfated Glycosaminoglycans and Their Effects on Trigeminal Nerve Growth Cone Behavior In Vitro: Roles for ECM in Cornea Innervation. *Investigative Opthalmology & Visual Science* 53, 8118 (2012).

11. Ethier, C. R., Johnson, M. & Ruberti, J. Ocular Biomechanics and Biotransport. *Annu Rev Biomed Eng* 6, 249–273 (2004).

12. Formisano, N. *et al.* Mechanical Properties of Bioengineered Corneal Stroma. *Adv Healthc Mater* 10, 2100972 (2021).

13. Jester, J. V. & Ho-Chang, J. Modulation of cultured corneal keratocyte phenotype by growth factors/cytokines control in vitro contractility and extracellular matrix contraction. *Exp Eye Res* 77, 581–592 (2003).

14. Ziaei, M., Gokul, A., Vellara, H., Patel, D. & McGhee, C. N. Peripheral Cornea Crosslinking Before Deep Anterior Lamellar Keratoplasty. *Med Hypothesis Discov Innov Ophthalmol* 9, 127–134 (2020).

15. Wilson, S. L., El Haj, A. J. & Yang, Y. Control of Scar Tissue Formation in the Cornea: Strategies in Clinical and Corneal Tissue Engineering. *J Funct Biomater* 3, 642–687 (2012).

16. Garcia-Porta, N. *et al.* Corneal Biomechanical Properties in Different Ocular Conditions and New Measurement Techniques. *ISRN Ophthalmol* 2014, 1–19 (2014).

17. Matthyssen, S., Van den Bogerd, B., Dhubhghaill, S. N., Koppen, C. & Zakaria, N. Corneal regeneration: A review of stromal replacements. *Acta Biomater* 69, 31–41 (2018).

18. West-Mays, J. A. & Dwivedi, D. J. The keratocyte: Corneal stromal cell with variable repair phenotypes. *Int J Biochem Cell Biol* 38, 1625–1631 (2006).
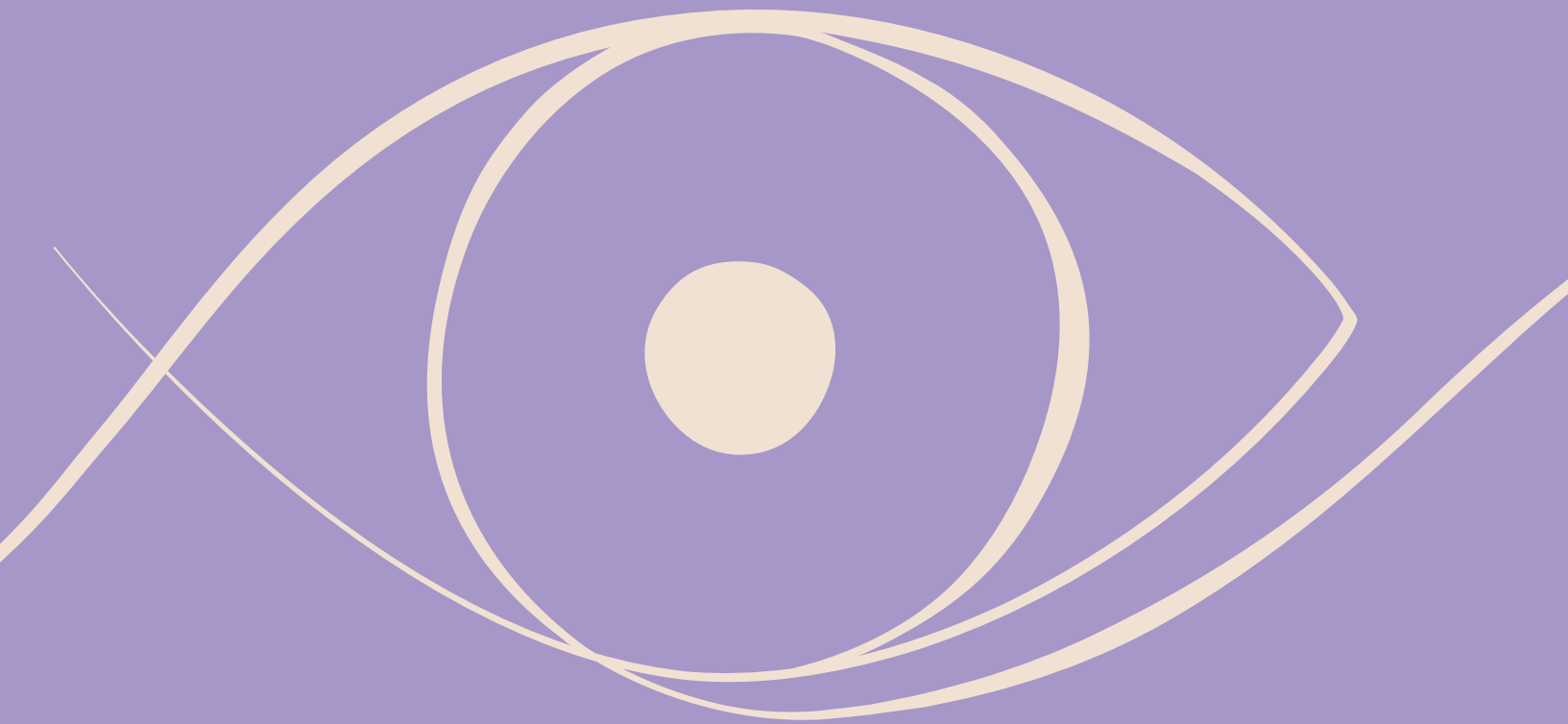
19. Lee, R. *et al.* Long-term Visual Outcomes and Complications of Boston Keratoprosthesis Type II Implantation. *Ophthalmology* 124, 27–35 (2017).

20. Kanu, L. N. *et al.* Predictive factors of Boston Type I Keratoprosthesis outcomes: A long-term analysis. *Ocul Surf* 18, 613–619 (2020).

21. Schrage, N., Hille, K. & Cursiefen, C. Aktuelle Versorgungsmöglichkeiten mit Keratoprothesen. *Der Ophthalmologe* 111, 1010–1018 (2014).

22. Cortina, M. & Cruz, J. *Keratoprostheses and Artificial Corneas*. (Springer Berlin Heidelberg, 2015). doi:10.1007/978-3-642-55179-6.

23. Avadhanam, V. S. *et al.* Detection of laminar resorption in osteo-odonto-keratoprostheses. *Ocul Surf* 17, 78–82 (2019).

24. Jirásková, N., Rozsival, P., Burova, M. & Kalfertova, M. AlphaCor artificial cornea: clinical outcome. *Eye* 25, 1138–1146 (2011).

25. Feiz, V. *et al.* Surface keratopathy after penetrating keratoplasty. *Trans Am Ophthalmol Soc* 99, 159–68; discussion 168-70 (2001).

26. Vannas, A., Holden, B. A. & Sweeney, D. F. Epithelial metabolism of the corneal graft is abnormal. *British Journal of Ophthalmology* 71, 593–597 (1987).

27. Gain, P. *et al.* Global Survey of Corneal Transplantation and Eye Banking. *JAMA Ophthalmol* 134, 167 (2016).

28. Goyal, R. *et al.* Development of hybrid scaffolds with natural extracellular matrix deposited within synthetic polymeric fibers. *J Biomed Mater Res A* 105, 2162–2170 (2017).

29. Setayeshmehr, M. *et al.* Hybrid and Composite Scaffolds Based on Extracellular Matrices for Cartilage Tissue Engineering. *Tissue Eng Part B Rev* 25, 202–224 (2019).

30. Faust, H. J. *et al.* A hyaluronic acid binding peptide-polymer system for treating osteoarthritis. *Biomaterials* 183, 93–101 (2018).

31. Singh, A. *et al.* Enhanced lubrication on tissue and biomaterial surfaces through peptide-mediated binding of hyaluronic acid. *Nat Mater* 13, 988–995 (2014).

32. Hezaveh, H. *et al.* Encoding Stem-Cell-Secreted Extracellular Matrix Protein Capture in Two and Three Dimensions Using Protein Binding Peptides. *Biomacromolecules* 19, 721–730 (2018).

33. Khoury, L. R. & Popa, I. Chemical unfolding of protein domains induces shape change in programmed protein hydrogels. *Nat Commun* 10, 5439 (2019).

34. Jha, A. K. *et al.* Matrix metalloproteinase-13 mediated degradation of hyaluronic acid-based matrices orchestrates stem cell engraftment through vascular integration. *Biomaterials* 89, 136–147 (2016).

35. Nam, S., Stowers, R., Lou, J., Xia, Y. & Chaudhuri, O. Varying PEG density to control stress relaxation in alginate-PEG hydrogels for 3D cell culture studies. *Biomaterials* 200, 15–24 (2019).

36. Aldana, A. A. *et al.* Biomimetic double network hydrogels: Combining dynamic and static crosslinks to enable biofabrication and control cell-matrix interactions. *Journal of Polymer Science* 59, 2832–2843 (2021).

37. Trujillo, S. *et al.* Engineered 3D hydrogels with full-length fibronectin that sequester and present growth factors. *Biomaterials* 252, 120104 (2020).

38. Berdichevski, A., Shachaf, Y., Wechsler, R. & Seliktar, D. Protein composition alters in vivo resorption of PEG-based hydrogels as monitored by contrast-enhanced MRI. *Biomaterials* 42, 1–10 (2015).

39. Benavides, O. M. *et al.* Capillary-Like Network Formation by Human Amniotic Fluid-Derived Stem Cells Within Fibrin/Poly(Ethylene Glycol) Hydrogels. *Tissue Eng Part A* 21, 1185–1194 (2015).

40. Kouwer, P. H. J. *et al.* Responsive biomimetic networks from polyisocyanopeptide hydrogels. *Nature* 493, 651–655 (2013).

41. Zhang, Y. *et al.* Tunable Hybrid Matrices Drive Epithelial Morphogenesis and YAP Translocation. *Advanced Science* 8, 2003380 (2021).

42. Ghezzi, C. E., Rnjak-Kovacina, J. & Kaplan, D. L. Corneal Tissue Engineering: Recent Advances and Future Perspectives. *Tissue Eng Part B Rev* 21, 278–287 (2015).

43. Brunette, I. *et al.* Alternatives to eye bank native tissue for corneal stromal replacement. *Prog Retin Eye Res* 59, 97–130 (2017).

44. Ahearne, M., Fernández-Pérez, J., Masterton, S., Madden, P. W. & Bhattacharjee, P. Designing Scaffolds for Corneal Regeneration. *Adv Funct Mater* 30, 1908996 (2020).

45. Matthyssen, S., Van den Bogerd, B., Dhubhghaill, S. N., Koppen, C. & Zakaria, N. Corneal regeneration: A review of stromal replacements. *Acta Biomater* 69, 31–41 (2018).

46. Sorushanova, A. *et al.* The Collagen Suprafamily: From Biosynthesis to Advanced Biomaterial Development. *Advanced Materials* 31, 1801651 (2019).

47. Kishore, V., Iyer, R., Frandsen, A. & Nguyen, T.-U. *In vitro* characterization of electrochemically compacted collagen matrices for corneal applications. *Biomedical Materials* 11, 055008 (2016).

48. Majumdar, S. *et al.* Cyclodextrin Modulated Type I Collagen Self-Assembly to Engineer Biomimetic Cornea Implants. *Adv Funct Mater* 28, 1804076 (2018).

49. Kong, B. *et al.* Fiber reinforced GelMA hydrogel to induce the regeneration of corneal stroma. *Nat Commun* 11, 1435 (2020).

50. Lee, H. J., Fernandes-Cunha, G. M., Na, K., Hull, S. M. & Myung, D. Bio-Orthogonally Crosslinked, In Situ Forming Corneal Stromal Tissue Substitute. *Adv Healthc Mater* 7, 1800560 (2018).

51. Chen, F., Le, P., Fernandes-Cunha, G. M., Heilshorn, S. C. & Myung, D. Bio-orthogonally crosslinked hyaluronate-collagen hydrogel for suture-free corneal defect repair. *Biomaterials* 255, 120176 (2020).

52. Chen, F., Le, P., Lai, K., Fernandes-Cunha, G. M. & Myung, D. Simultaneous Interpenetrating Polymer Network of Collagen and Hyaluronic Acid as an *In Situ*-Forming Corneal Defect Filler. *Chemistry of Materials* 32, 5208–5216 (2020).

53. Rafat, M. *et al.* PEG-stabilized carbodiimide crosslinked collagen–chitosan hydrogels for corneal tissue engineering. *Biomaterials* 29, 3960–3972 (2008).

54. Kong, B. *et al.* Tissue-engineered cornea constructed with compressed collagen and laser-perforated electrospun mat. *Sci Rep* 7, 970 (2017).

55. Fernandes-Cunha, G. M. *et al.* In situ-forming collagen hydrogel crosslinked via multi-functional PEG as a matrix therapy for corneal defects. *Sci Rep* 10, 1–13 (2020).

56. Kim, J. I., Kim, J. Y. & Park, C. H. Fabrication of transparent hemispherical 3D nanofibrous scaffolds with radially aligned patterns via a novel electrospinning method. *Sci Rep* 8, 3424 (2018).

57.	Zhong, S. P. *et al.* Development of a novel collagen–GAG nanofibrous scaffold via electrospinning. *Materials Science and Engineering: C* 27, 262–266 (2007).

58.	Torbet, J. *et al.* Orthogonal scaffold of magnetically aligned collagen lamellae for corneal stroma reconstruction. *Biomaterials* 28, 4268–4276 (2007).

59.	Isaacson, A., Swioklo, S. & Connon, C. J. 3D bioprinting of a corneal stroma equivalent. *Exp Eye Res* 173, 188–193 (2018).

60.	Kostenko, A., Swioklo, S. & Connon, C. J. Effect of Calcium Sulphate Pre-crosslinking on Rheological Parameters of Alginate Based Bio-Inks and on Human Corneal Stromal Fibroblast Survival in 3D Bio-Printed Constructs. *Front Mech Eng* 8, (2022).

61.	Kostenko, A., Connon, C. J. & Swioklo, S. Storable Cell-Laden Alginate Based Bioinks for 3D Biofabrication. *Bioengineering* 10, 23 (2022).

62.	Fagerholm, P. *et al.* A Biosynthetic Alternative to Human Donor Tissue for Inducing Corneal Regeneration: 24-Month Follow-Up of a Phase 1 Clinical Study. *Sci Transl Med* 2, (2010).

63.	Fagerholm, P. *et al.* Stable corneal regeneration four years after implantation of a cell-free recombinant human collagen scaffold. *Biomaterials* 35, 2420–2427 (2014).

64.	Lagali, N. *et al.* Innervation of Tissue-Engineered Recombinant Human Collagen-Based Corneal Substitutes: A Comparative In Vivo Confocal Microscopy Study. *Investigative Opthalmology & Visual Science* 49, 3895 (2008).

65.	Merrett, K. *et al.* Tissue-Engineered Recombinant Human Collagen-Based Corneal Substitutes for Implantation: Performance of Type I versus Type III Collagen. *Investigative Opthalmology & Visual Science* 49, 3887 (2008).

66.	Fagerholm, P., Lagali, N. S., Carlsson, D. J., Merrett, K. & Griffith, M. Corneal Regeneration Following Implantation of a Biomimetic Tissue-Engineered Substitute. *Clin Transl Sci* 2, 162–164 (2009).

67.	Jangamreddy, J. R. *et al.* Short peptide analogs as alternatives to collagen in pro-regenerative corneal implants. *Acta Biomater* 69, 120–130 (2018).

68.	McTiernan, C. D. *et al.* LiQD Cornea: Pro-regeneration collagen mimetics as patches and alternatives to corneal transplantation. *Sci Adv* 6, (2020).

69.	Haagdorens, M. *et al.* Plant Recombinant Human Collagen Type I Hydrogels for Corneal Regeneration. *Regen Eng Transl Med* 8, 269–283 (2022).

70.	Lehn, J.-M. Supramolecular chemistry: Where from? Where to? *Chem Soc Rev* 46, 2378–2379 (2017).

71.	Webber, M. J., Appel, E. A., Meijer, E. W. & Langer, R. Supramolecular biomaterials. *Nat Mater* 15, 13–26 (2016).

72.	Hutin, M., Burakowska-Meise, E., Appel, W. P. J., Dankers, P. Y. W. & Meijer, E. W. From Molecular Structure to Macromolecular Organization: Keys to Design Supramolecular Biomaterials. *Macromolecules* 46, 8528–8537 (2013).

73.	Webber, M. J. Engineering responsive supramolecular biomaterials: Toward smart therapeutics. *Bioeng Transl Med* 1, 252–266 (2016).

74.	Bakker, M. H. & Dankers, P. Y. W. Supramolecular biomaterials based on ureidopyrimidinone and benzene-1,3,5-tricarboxamide moieties. in *Self-assembling Biomaterials* 177–204 (Elsevier, 2018).

75. Burla, F., Mulla, Y., Vos, B. E., Aufderhorst-Roberts, A. & Koenderink, G. H. From mechanical resilience to active material properties in biopolymer networks. *Nature Reviews Physics* 1, 249–263 (2019).

76. Tibbitt, M. W. & Anseth, K. S. Hydrogels as extracellular matrix mimics for 3D cell culture. *Biotechnol Bioeng* 103, 655–663 (2009).

77. Cruz-Acuña, R. *et al.* Synthetic hydrogels for human intestinal organoid generation and colonic wound repair. *Nat Cell Biol* 19, 1326–1335 (2017).

78. Lutolf, M. P. & Hubbell, J. A. Synthetic biomaterials as instructive extracellular microenvironments for morphogenesis in tissue engineering. *Nat Biotechnol* 23, 47–55 (2005).

79. DeForest, C. A. & Tirrell, D. A. A photoreversible protein-patterning approach for guiding stem cell fate in three-dimensional gels. *Nat Mater* 14, 523–531 (2015).

80. Gjorevski, N. *et al.* Designer matrices for intestinal stem cell and organoid culture. *Nature* 539, 560–564 (2016).

81. Prince, E. & Kumacheva, E. Design and applications of man-made biomimetic fibrillar hydrogels. *Nat Rev Mater* 4, 99–115 (2019).

82. Kratochvil, M. J. *et al.* Engineered materials for organoid systems. *Nat Rev Mater* 4, 606–622 (2019).

83. Baker, M. B. *et al.* Exposing Differences in Monomer Exchange Rates of Multicomponent Supramolecular Polymers in Water. *ChemBioChem* 17, 207–213 (2016).

84. Dankers, P. Y. W., Harmsen, M. C., Brouwer, L. A., Van Luyn, M. J. A. & Meijer, E. W. A modular and supramolecular approach to bioactive scaffolds for tissue engineering. *Nat Mater* 4, 568–574 (2005).

85. Spaans, S. *et al.* Supramolecular surface functionalization via catechols for the improvement of cell–material interactions. *Biomater Sci* 5, 1541–1548 (2017).

86. Wang, H. & Heilshorn, S. C. Adaptable Hydrogel Networks with Reversible Linkages for Tissue Engineering. *Advanced Materials* 27, 3717–3736 (2015).

87. Madl, C. M. *et al.* Maintenance of neural progenitor cell stemness in 3D hydrogels requires matrix remodelling. *Nat Mater* 16, 1233–1242 (2017).

88. Tang, S. *et al.* Adaptable Fast Relaxing Boronate-Based Hydrogels for Probing Cell–Matrix Interactions. *Advanced Science* 5, 1800638 (2018).

89. von Gröning, M., de Feijter, I., Stuart, M. C. A., Voets, I. K. & Besenius, P. Tuning the aqueous self-assembly of multistimuli-responsive polyanionic peptide nanorods. *J Mater Chem B* 1, 2008 (2013).

90. Sun, F., Zhang, W.-B., Mahdavi, A., Arnold, F. H. & Tirrell, D. A. Synthesis of bioactive protein hydrogels by genetically encoded SpyTag-SpyCatcher chemistry. *PNAS* 111, 11269–11274 (2014).

91. Hartgerink, J. D., Beniash, E. & Stupp, S. I. Peptide-amphiphile nanofibers: A versatile scaffold for the preparation of self-assembling materials. *PNAS* 99, 5133–5138 (2002).

92. Lampe, K. J., Antaris, A. L. & Heilshorn, S. C. Design of three-dimensional engineered protein hydrogels for tailored control of neurite growth. *Acta Biomater* 9, 5590–5599 (2013).

93. Fernandez-Castano Romera, M. *et al.* Strain Stiffening Hydrogels through Self-Assembly and Covalent Fixation of Semi-Flexible Fibers. *Angewandte Chemie International Edition* 56, 8771–8775 (2017).

94. van Gaal, R. C. *et al.* Functional peptide presentation on different hydrogen bonding biomaterials using supramolecular additives. *Biomaterials* 224, 119466 (2019).

95. Diba, M. *et al.* Self-Healing Biomaterials: From Molecular Concepts to Clinical Applications. *Adv Mater Interfaces* 5, 1800118 (2018).

96. Madl, A. C. & Myung, D. Supramolecular Host–Guest Hydrogels for Corneal Regeneration. *Gels* 7, 163 (2021).

97. Sijbesma, R. P. *et al.* Reversible Polymers Formed from Self-Complementary Monomers Using Quadruple Hydrogen Bonding. *Science (*1979*)* 278, 1601–1604 (1997).

98. Chebotareva, N., Bomans, P. H. H., Frederik, P. M., Sommerdijk, N. A. J. M. & Sijbesma, R. P. Morphological control and molecular recognition by bis-urea hydrogen bonding in micelles of amphiphilic tri-block copolymers. *Chemical Communications* 4967 (2005).

99. Lightfoot, M. P., Mair, F. S., Pritchard, R. G. & Warren, J. E. New supramolecular packing motifs: π-stacked rods encased in triply-helical hydrogen bonded amide strands. *Chemical Communications* 1945–1946 (1999).

100. Bastings, M. M. C. *et al.* A Fast pH-Switchable and Self-Healing Supramolecular Hydrogel Carrier for Guided, Local Catheter Injection in the Infarcted Myocardium. *Adv Healthc Mater* 3, 70–78 (2014).

101. Dankers, P. Y. W. *et al.* Hierarchical Formation of Supramolecular Transient Networks in Water: A Modular Injectable Delivery System. *Advanced Materials* 24, 2703–2709 (2012).

102. Diba, M. *et al.* Engineering the Dynamics of Cell Adhesion Cues in Supramolecular Hydrogels for Facile Control over Cell Encapsulation and Behavior. *Advanced Materials* 33, 2008111 (2021).

103. Rijns, L. *et al.* Using chemistry to recreate the complexity of the extracellular space: from natural to fully synthetic matrices utilizing supramolecular biomaterials - *in preparation* .

CHAPTER **2**

Development of a fully synthetic corneal stromal construct via supramolecular hydrogel engineering

Recent advances in the field of ophthalmology show great potential in the design of bioengineered constructs to mimic the corneal stroma. Hydrogels based on synthetic supramolecular polymers, are attractive synthetic mimics of the natural highly hydrated corneal stroma. Here, a fully synthetic corneal stromal construct is developed via engineering of an injectable supramolecular hydrogel based on ureido-pyrimidinone (UPy) moieties. The hydrogel displays a dynamic and tunable behavior, which allows for control of biochemical and mechanical cues. Two hydrogels are developed, a fully synthetic hydrogel functionalized with an UPy-cRGD additive, and a hybrid hydrogel based on UPy-moieties mixed with collagen type I fibers. Both hydrogels supported cell encapsulation and associated cellular deposition of extracellular matrix (ECM) proteins after 21 days. Excitingly, the hydrogels support the activation of isolated primary keratocytes into stromal fibroblasts as well as the differentiation toward more quiescent corneal stromal keratocytes, demonstrated by their characteristic long dendritic protrusions and a substantially diminished cytokine secretion. Furthermore, cells survive shear stresses during an injectability test. Together, these findings highlight the development of an injectable supramolecular hydrogel as a synthetic corneal stromal microenvironment able to host primary keratocytes.

INTRODUCTION

The cornea is located at the outermost of the eye fulfilling two main functions; protecting the inner parts of the eye and allowing for vision by refracting light from the external world toward the retina. The cornea is responsible for two-thirds of the refractive power of the eye, by maximizing light focusing on the retina and minimizing light scattering losses. These properties turn the cornea in a crucial tissue to ensure a clear vision. Disease or injury can result in a damaged cornea, and eventually cause visual regression or even blindness.[1,2] The corneal tissue exists of five layers; epithelial cells, the acellular Bowman's layer, stroma, the acellular Descemet's membrane and endothelial cells.[3] About 90% of the cornea is composed of the corneal stroma, which predominantly affects the corneal function. The corneal stroma is a highly hydrated and organized tissue. It consists of condensed collagen type I lamellae in heterodimeric complex with collagen type V and VI, surrounded by specific proteoglycans. Collagen fibrils within sequential lamellae are oriented in an orthogonal fashion. The high level of organization together with the hydration results in a specific mechanical strength and the ability to refract light.[4–6] Cells in the cornea comprise 5-10% of the stromal volume and are referred to as corneal keratocytes, characterized by long dendritic protrusions. Corneal keratocytes slowly regenerate the collagen in the stroma and produce extracellular matrix (ECM) components, such as collagen type I and proteoglycans. In case of trauma or disease keratocytes can undergo metabolic activation and change into a fibroblastic phenotype, resulting in cell migration, proliferation, and upscaled collagen production.[7,8]

The *in vivo* regeneration process of patients with severe stromal disease or injury often results in uncontrollable production of disorganized fibrotic tissue due to an irreversible transformation of the keratocytes into myofibroblasts. This process often results in permanent scarring and further aggravation of the patient's visual performance.[9] Treatment options for patients with severe stromal disease or injury are very limited. Many patients at risk of blindness rely on corneal transplants from deceased human donors as the only effective available treatment. Unfortunately, there is a worldwide shortage of corneal graft tissue, with only one cornea available for seventy needed.[10] In recent decades, ophthalmologists and bioengineers together are dedicated to engineer a construct, which allows to integrate into the patient's eye. Desirably, this artificial construct should support the self-regeneration process of the native tissue, and successfully restore the patient's vision. Due to the complexity of the

stromal tissue, multiple material properties such as; transparency, biocompatibility, innervation, and the biomechanics need to be considered, while engineering a stromal construct.

Due to the viscoelastic nature and high water content, injectable hydrogels are proposed to be an attractive alternative for artificial corneas and corneal donor tissue.[11,12] Within the field of corneal tissue engineering there is an urgent need for readily available tissue substitutes that can precisely fill corneal defects in a minimal invasive manner.[12] Very common biopolymers such as collagen, gelatin, silk, dextran, hyaluronic acid and decellularized stromal tissues are studied as potential hydrogel stromal constructs. Despite the fact that these materials show great cellular compatibility, they also pose some limitations, *i.e.* risk of disease transmission, immunogenic concerns, scalability issues, and incompetent biomechanical properties.[8,13–15]

A solution to these disadvantages is to design a stromal construct via synthetic hydrogels based on supramolecular moieties, allowing for material tunability and selectivity by the incorporation of bioactive additives into the material to provide the needed biochemical cues.[11,16] Previously, 3D encapsulation of cells in supramolecular hydrogels was demonstrated by using a two component system containing molecules with complementary ureido-pyrimidinone (UPy) groups as supramolecular building blocks.[18] Via fourfold hydrogen bonding these UPy groups dimerize and form lateral stacks. In solution, these stacks assemble into fibers and transient networks are formed.

The aim of this work is to develop a hydrogel based on supramolecular chemistry that closely mimics the stromal microenvironment and induces self-regeneration of the damaged tissue. To this end, the hydrogel design should meet some important criteria, *i.e.* a mechanically stable environment and allowing flow of nutrients to encapsulate keratocytes.[17] To achieve our aim, the biological and mechanical characteristics of two hydrogels are thoroughly studied and compared, namely; (1) a fully synthetic hydrogel-based stromal construct based on UPy-fibers and functionalized with a bioactive cyclic arginine-glycine-aspartate (cRGD) additive, and (2) a hybrid hydrogel-based stromal construct composed of a combination of UPy-fibers and natural collagen type I fibers (**Figure 1A**). Two variations of keratocytes are used to explore the cellular biocompatibility of both hydrogel constructs, being a SV40-immortalised human corneal keratocyte cell line (HCK) and human donor derived primary keratocytes (PKs). HCKs are more robust compared with the PKs, yet significantly less representative (**Figure 1B**). The HCKs are

assumed to impose an irreversible phenotype of myofibroblast. Two treatments are used for the PKs. To mimic the quiescent native keratocytes, the cells are treated with culture medium supplemented with high glucose and low serum. To mimic metabolic activation of keratocytes and the transformation into fibroblasts, the PKs are treated with culture medium supplemented with high serum.

The fundament of the two supramolecular hydrogels is based on two variations of molecules with complementary UPy-groups (**Figure 2A**). An alkyl spacer is incorporated to shield the hydrogen bonds in water, creating a hydrophobic pocket upon assembly of UPy-dimers into 1D stacks. Hydrogen bonding of flanking urea groups implements further stabilization of the formed stacks, and further assembly occurs by bundling of the stacks into fibers (**Figure 2B**).[11,18] The monofunctional hydrogelator, consists of a 528 Da oligo(ethylene glycol) (OEG) chain end-capped with a functional UPy-moiety at one end and a glycine-amide group at the other end. Due to this molecular design of the monofunctional molecule it is expected that the glycols' non-fouling properties are shielded from exposure, while the glycine-amide groups are assumed to be presented to the cells. Upon addition of a bifunctional 10 kDa poly(ethylene glycol) (PEG) chain end-capped with two functional UPy-moieties, interfiber cross-links are formed.[18] To introduce bioactivity into the synthetic hydrogel, a cell adhesive supramolecular additive is used based on a monofunctional molecule functionalized with an integrin-binding cRGD ligand. Both the synthetic (+UPy-cRGD) and the hybrid (+collagen) hydrogel are thoroughly studied in this work via various analyses of the biological and mechanical performances of both hydrogels.

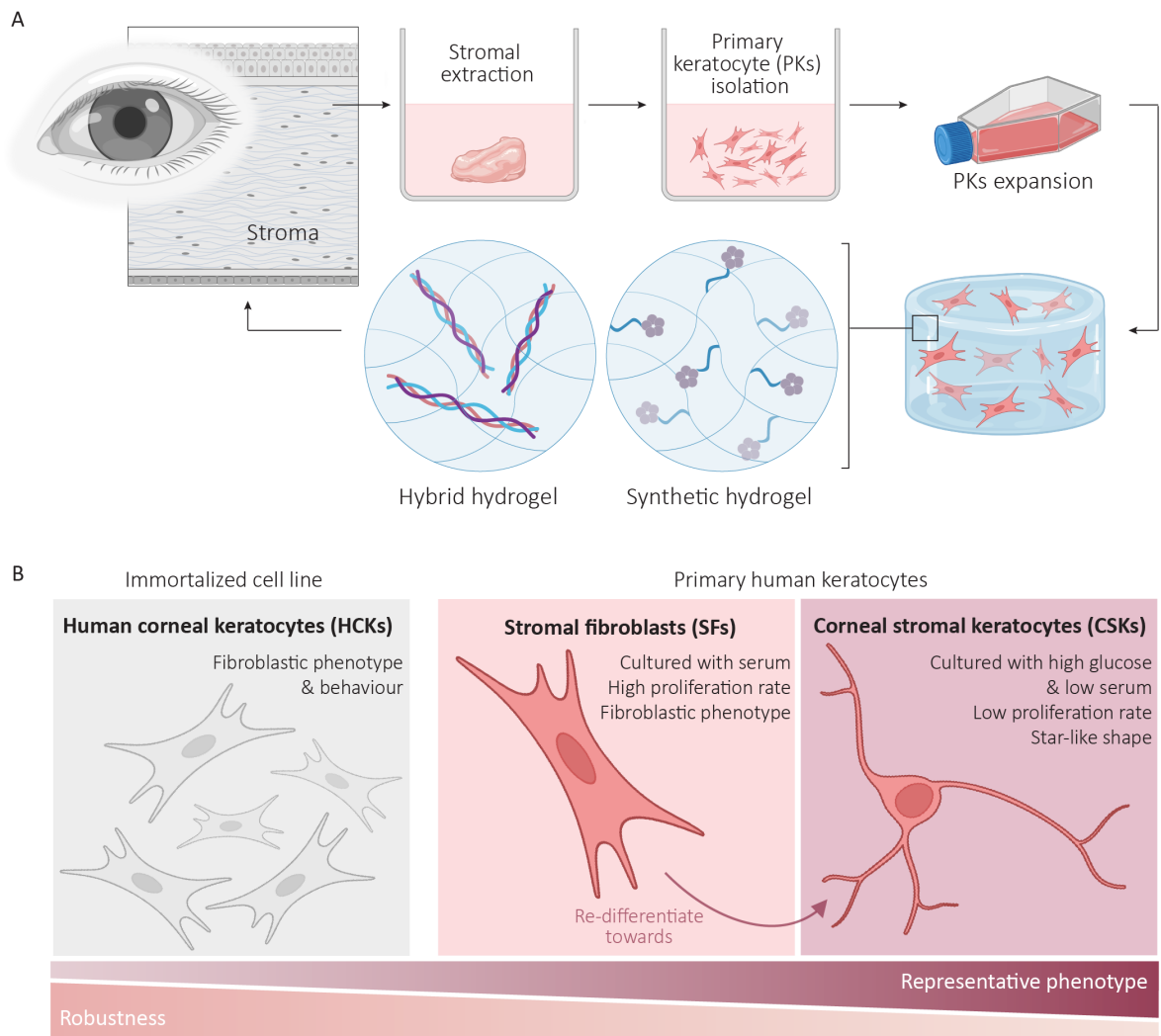**Figure 1.** Overview of this study. **A)** The design of a supramolecular hydrogel as a stromal construct and the concept of the two hydrogel systems used in this study. **B)** Overview of the cells used in this study, the robust SV40-immortalized human corneal keratocyte cell line and isolated human primary keratocytes activated towards stromal fibroblasts (SFs) or differentiated towards corneal stromal keratocytes (CSKs).

RESULTS AND DISCUSSION

Formulation and mechanical properties of synthetic & hybrid hydrogels

Both the bifunctional building block and the monofunctional building block (with or without additive) are received as a powder, and dissolved separately in aqueous solutions (**Figure 2C**). Via fourfold hydrogen bonding between the functional UPy groups the monofunctional building blocks start to dimerize and form lateral stacks, assembling into fibers. The solution of the bifunctional building blocks and the solution of the monofunctional building blocks are both diluted with cell culture medium to provide the cells with some nutrients during gelation. To encapsulate cells within the hydrogel, cells are supplemented to the bifunctional building block solution. Addition of the dissolved bifunctional molecules to the monofunctional fibers in solution introduces interfiber crosslinks, resulting in the formation of a transient network.

A pristine hydrogel (no additives, solely monofucntional and bifunctional molecules), a synthetic hydrogel (+UPy-cRGD additive) and a hybrid hydrogel (+collagen) were engineered via the above mentioned preparation method. Rheological measurements showed a solid-like behavior (*i.e.*, G' > G") for all the hydrogel networks when formulated with 2.5 wt/v% of bifunctional and monofunctional molecules in each composition. A complete gelation of all the hydrogels resulted in a storage modulus of ~ 11 kPa for both the pristine hydrogel and the synthetic UPy-cRGD hydrogel and a storage modulus of ~ 8 kPa for the hybrid hydrogel, respectively (Experimental section, Figure 9). For successful cell encapsulation and to perform extended cell cultures it is necessary to embed the hydrogels in cell culture medium. This prevents desiccation of the gel and provides nutrients for the cells. Rheological measurements of pre-formed hydrogels, incubated with medium for 24 hours prior to the measurement, showed a decrease in storage moduli compared with the final storage moduli of the formation measurements. Measurements of the pre-formed gels, which were embedded in medium, resulted in similar storage moduli of 2577 ±185 Pa for the pristine hydrogel, 2445 ±430 Pa for the synthetic hydrogel and 2410 ±464 Pa for the hybrid hydrogel, respectively (**Figure 2D**). Furthermore, the results showed similar needed critical strain and viscoelastic behavior for all the hydrogels.
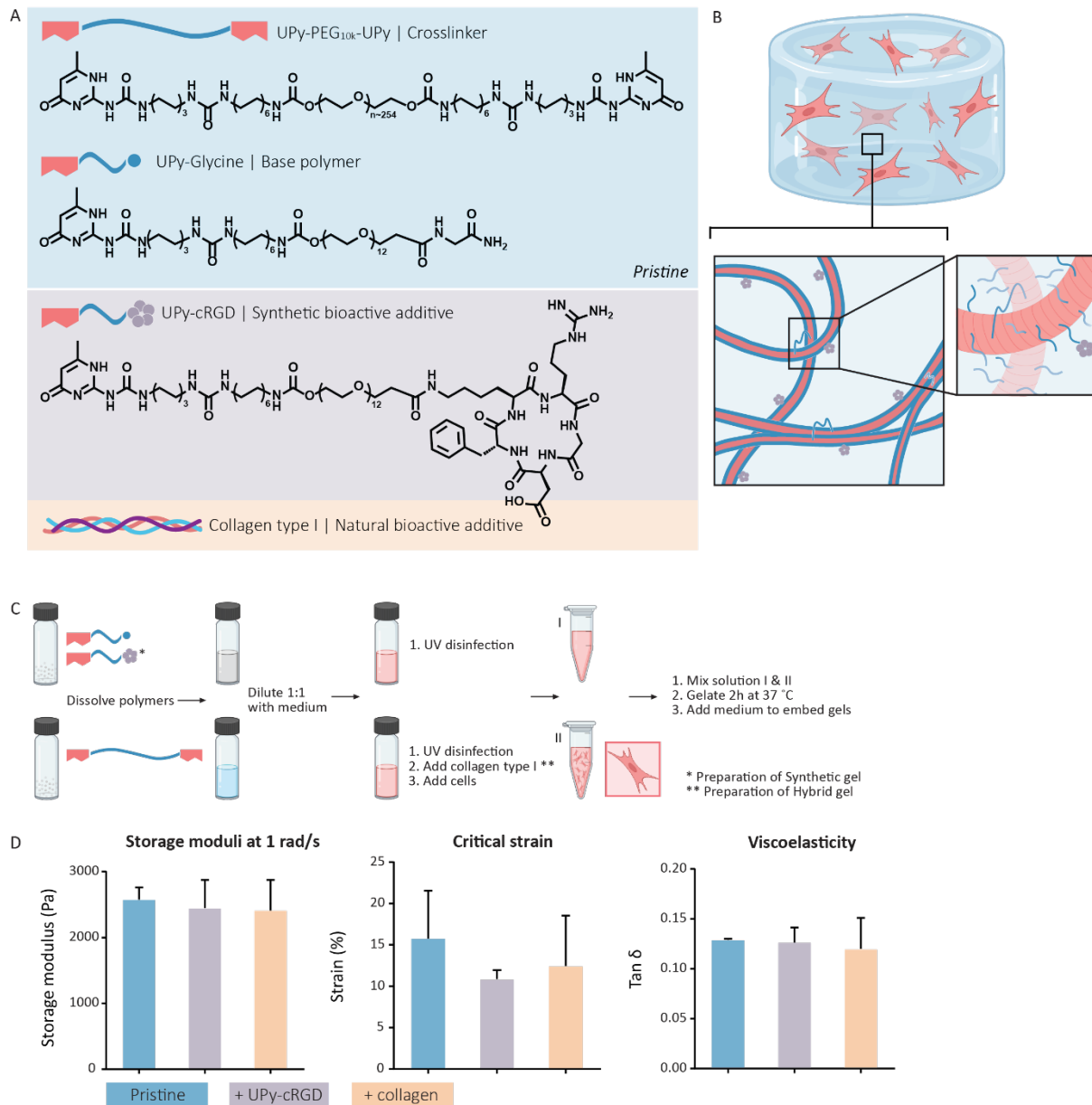
Figure 2. Overview of the chemical properties of the hydrogel, the formulation method of the hydrogel and rheological measurements of the three formulated hydrogels. **A)** The chemical structures of the hydrogelator UPy-glycine (monofunctional molecule), the crosslinker UPy-PEG$_{10K}$-UPy (bifunctional molecule), and the bioactive additive UPy-cRGD and schematic illustration of collagen type I. **B)** Schematical illustration of the supramolecular network. Blue linkages between fibers indicate interfiber cross-links formed by UPy-PEG$_{10K}$-UPy. **C)** Hydrogel formulation method for 3D cell encapsulation. **D)** Mechanical properties of a pristine, synthetic and hybrid hydrogel measured after described preparation of the gels. G', critical strain and tan(delta) values of hydrogels measured at 1 rad s^{-1} and 1% strain, sample size n=3, mean ± standard deviation presented.

Supramolecular hydrogels support human corneal keratocyte encapsulation and ECM protein deposition

A SV40-immortalised human corneal keratocyte cell line (HCK) was used as a simplified cell model to explore the possibilities of the supramolecular hydrogels.[19,20] At first the HCKs were encapsulated within the synthetic and hybrid hydrogel and cultured for 14 days. As a control the cells were also encapsulated within a pristine hydrogel (without cell adhesive additives) and a hybrid hydrogel functionalized with UPy-cRGD (**Figure 3A**). After a 14-day culture, HCKs encapsulated within the synthetic and the hybrid hydrogel, showed the expected elongated morphology of the HCKs. Proliferation marker Ki-67 marked proliferating HCKs in both systems, suggesting the cells are still proliferating after 14 days of encapsulation. Furthermore, collagen type I protein deposition was supported by the synthetic hydrogel and the results indicated a homogenous mixed-in collagen type I for the hybrid hydrogel. Based on these results, no differences in biological performance between the synthetic and hybrid hydrogel were observed. A round-shaped cell morphology was observed for the HCKs encapsulated within the pristine hydrogel. In addition the cells clustered together, forming cell clumps instead of a homogenous distribution of spreaded cells throughout the gel. These observations demonstrated the need to provide essential biochemical cues within the hydrogels, to allow the keratocytes to maintain their healthy morphology. The hybrid hydrogel functionalized with UPy-cRGD did not improve the biological performances of the hydrogel. These results demonstrated that the incorporation of both additives did not led to a reinforcement of the hydrogels biological performance.

To further analyze the biological performance of the synthetic hydrogel, the HCKs were encapsulated and cultured for 7, 14 and 21 days to perform some additional immunohistochemical analyses (**Figure 3B**). During culture, an increase in cellular deposition of collagen type V and collagen type VI was observed between day 7 and day 21. At all the timepoints, some cells expressed proliferation marker Ki-67, indicating a continuous proliferation of the cells.
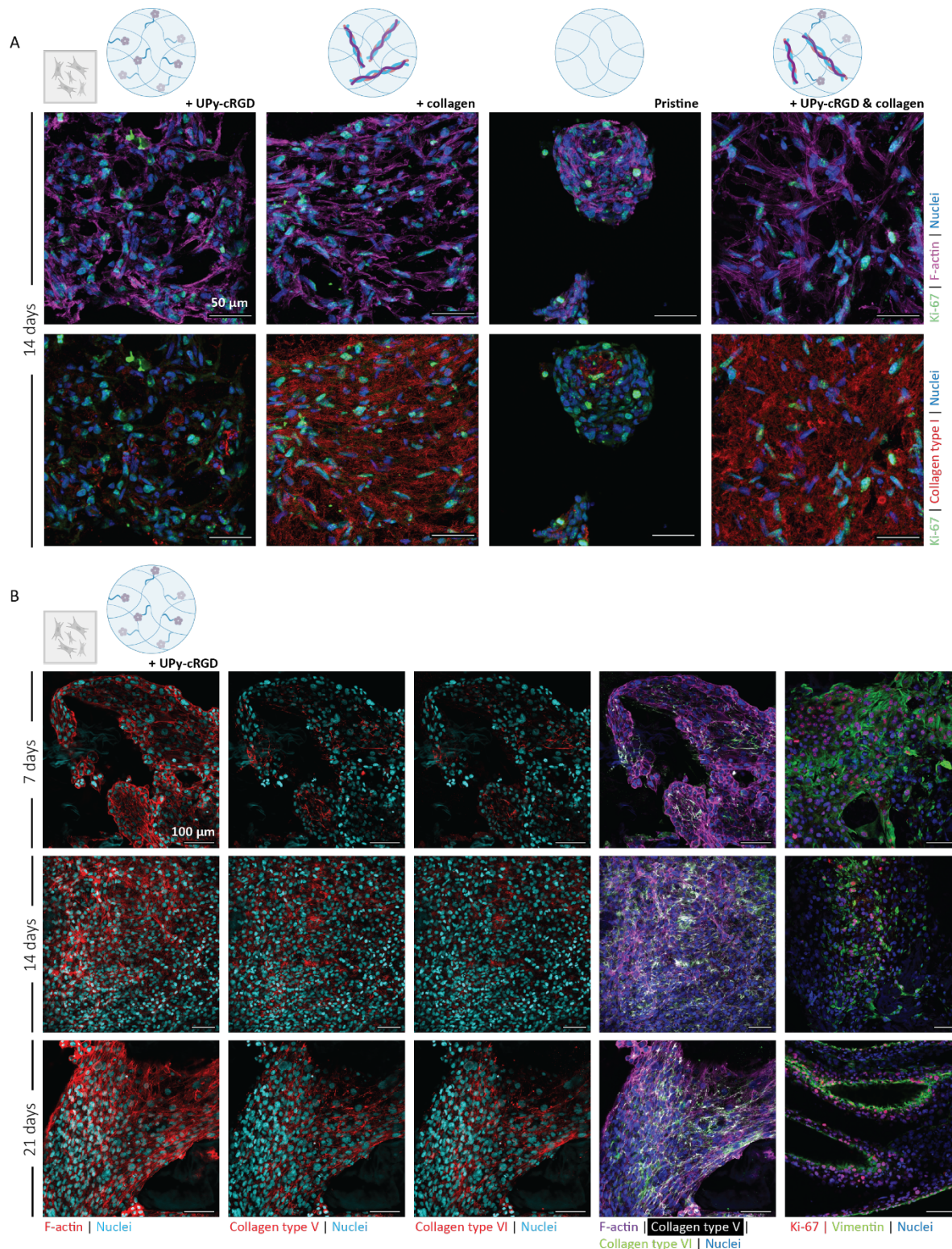
Figure 3. Human corneal keratocytes encapsulated and cultured for 7, 14 and 21 days in supramolecular hydrogels are able to spread, proliferate and deposit ECM proteins. **A)** HCKs encapsulated and cultured for 14 days in the synthetic UPy-cRGD hydrogel and in the hybrid collagen hydrogel. The pristine hydrogel and a hybrid hydrogel functionalized with UPy-cRGD are used as a control. Stained for Ki67 (green), F-actin (purple), collagen type I (red) and the nuclei (blue). Scale bar represents 50 μm, n=2 (two hydrogels per staining). **B)** HCKs encapsulated and cultured in the synthetic hydrogel for 7, 14 and 21 days. Stained for F-actin, collagen type V, collagen type VI, Ki-67 and vimentin. Scale bar represents 100 μm, n=2 (two hydrogels per staining).

37

Primary keratocyte encapsulation and steering of phenotype

Human primary keratocytes (PKs) are isolated from human donor corneal stroma and expanded *in vitro*. The PKs are successfully encapsulated into the synthetic and hybrid system (day 0). Subsequently, after one day of culture (day 1) the PKs are treated in two manners; (1) with serum towards stromal fibroblasts (SFs) or (2) with low serum and high glucose towards quiescent corneal stromal keratocytes (CSKs).[21] The cellular encapsulation was prolonged to 21 days to allow successful (re-)differentiation of the PKs (**Figure 4**).

PKs encapsulated within the synthetic and hybrid hydrogel, treated with high serum, attain a fibroblastic phenotype and exhibit a higher proliferation rate (**Figure 5A, B**). A substantial different cellular visualization is observed for the encapsulated PKs treated with high glucose and low serum. The results demonstrated hydrogels loaded with fewer cells compared with the high serum treated PKs (Experimental section, Figure 10B). The keratocytes show long dendritic protrusions that allow them to sense the surrounding matrix and other cells. Especially, the cells encapsulated within the synthetic hydrogel possess long protrusions of ~ 300-350 µm (**Figure 5C, D**). Multicolored images show the differences in cell height. As expected for cells cultured in a 3D environment, these results demonstrated the ability of the cells to spread and migrate towards all directions. Without the addition of bioactive additives the PKs were not able to adhere to the hydrogel, only a few cell clumps existing of small rounded cells were observed on day 7. At culture day 21, rheological measurements were performed on hydrogels loaded with encapsulated cells.
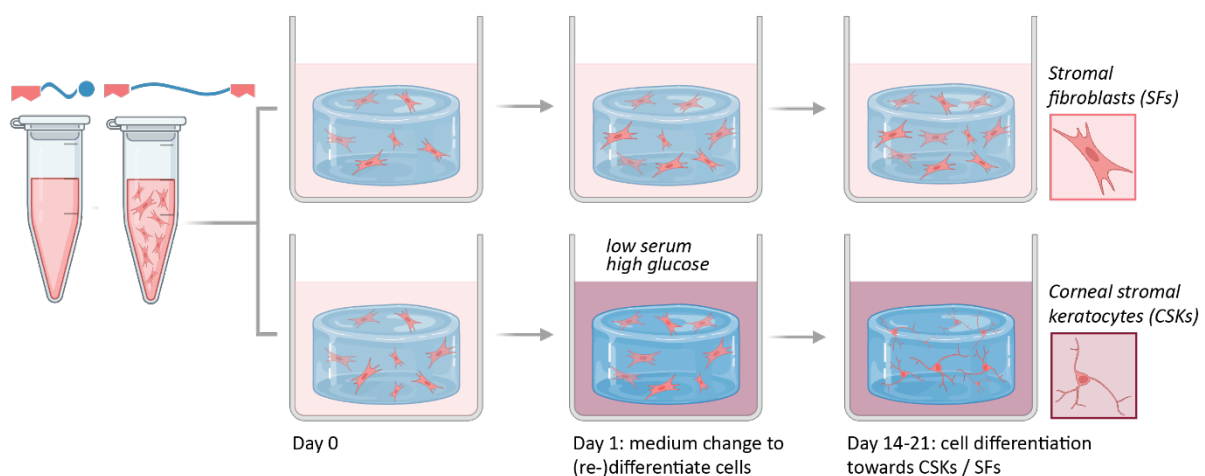
Figure 4. Experimental set up and timeline of human primary keratocytes (PKs) encapsulated and cultured for 21 days in supramolecular hydrogels.

Due to the variation in bioactive additive as well as the provided supplements in the cell culture medium, these measurements were performed to explore any signs of differences in cellular rearrangement of the hydrogel-networks. However, the rheological measurements demonstrate that the storage moduli, critical strain and viscosity of the pristine, synthetic and hybrid hydrogel are all within a similar range to each other (**Figure 5E, F, G**). The rheological measurements were also repeated with PKs derived from another donor, again the results were all in similar range to each other and comparable to the first dataset (Appendix, Figure 13 and 14).
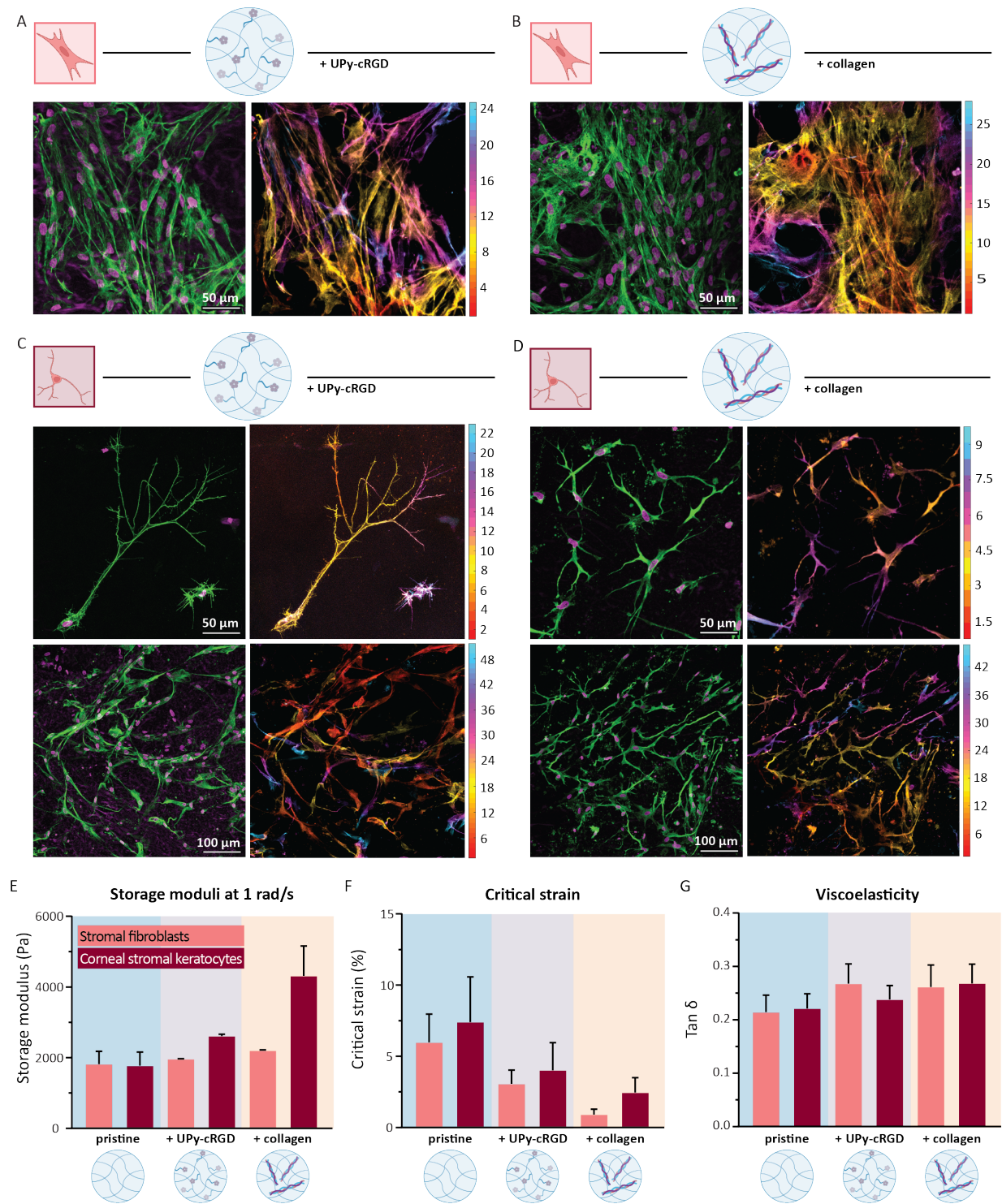
Figure 5. Human primary keratocytes (PKs) encapsulated and cultured for 21 days in supramolecular hydrogels, n=2 (two hydrogels per condition). Fluorescent confocal images of PKs stained for vimentin (green) and nuclei (blue), and multicolored images show the cell heights. Scale is in μm. Are provided of the various conditions. **A)** PKs treated with serum towards stromal fibroblasts encapsulated within the synthetic gel. **B)** PKs treated with serum towards stromal fibroblasts encapsulated within the hybrid gel. **C)** PKs treated with high glucose and low serum towards corneal stromal keratocytes encapsulated in the synthetic hydrogel. **D)** PKs treated with high glucose and low serum towards corneal stromal keratocytes encapsulated in the hybrid hydrogel. **E)** Storage moduli at 1 rad/s, mean ± standard deviation presented. **F)** Critical strain, mean ± standard deviation presented. **G)** Viscoelastic behavior, mean ± standard deviation presented.

PKs slightly experience mechanotransduction when encapsulated in supramolecular hydrogels

PKs encapsulated within the synthetic and hybrid hydrogel, treated with high glucose and low serum, experience a surrounding gel-matrix with a stiffness of ~ 2-4 kPa. Mechanotransduction allows cells to sense and adapt to external forces by cytoskeleton remodeling or activating specific genetic programs.[22] To explore the interaction between the cells and the material in more detail, an analysis of yes-associated-protein (YAP) is implemented in this study. YAP is a mechanosensitive transcriptional regulator, which is on a mechanical level regulated by mechanical cues such as ECM rigidity, strain or adhesive area.[23] Pathways involving YAP translocation to the nucleus, allow the cells to perceive ECM mechanics and to spread.[24] At first, the metabolic activity of the CSKs was measured via a resazurin assay. These results demonstrated metabolic active CSKs on day 17 (**Figure 5A**). Furthermore, the results of the synthetic hydrogel demonstrated the ability of both hydrogels to support the elongated keratocyte morphology as well as the cellular deposition of collagen type I. A homogenous distribution of the mixed-in collagen type I and a similar elongated cell morphology were observed for the keratocytes cultured within the hybrid hydrogel (**Figure 5B**). A custom-made cell profiler pipeline was used to quantify the intensity of YAP expression inside the cytoplasm and inside the nuclei. The ratios between nuclear YAP intensity and YAP intensity within the cytoplasm of the CSKs encapsulated within the synthetic and hybrid hydrogel are both above 1 (**Figure 6C, D**). In addition, the nuclei eccentricity value of the CSKs encapsulated in both hydrogel systems is also within the same range of ~ 0.8-1.0, suggesting that the nuclei are oval-shaped instead of round-shaped (**Figure 6E**). Both the higher nuclear YAP intensity as well as the oval-shaped nuclei suggest that the cells do experience mechanotransduction.

Yet, between the synthetic and hybrid hydrogel there is no difference in mechanotransduction sensed by the encapsulated PKs.
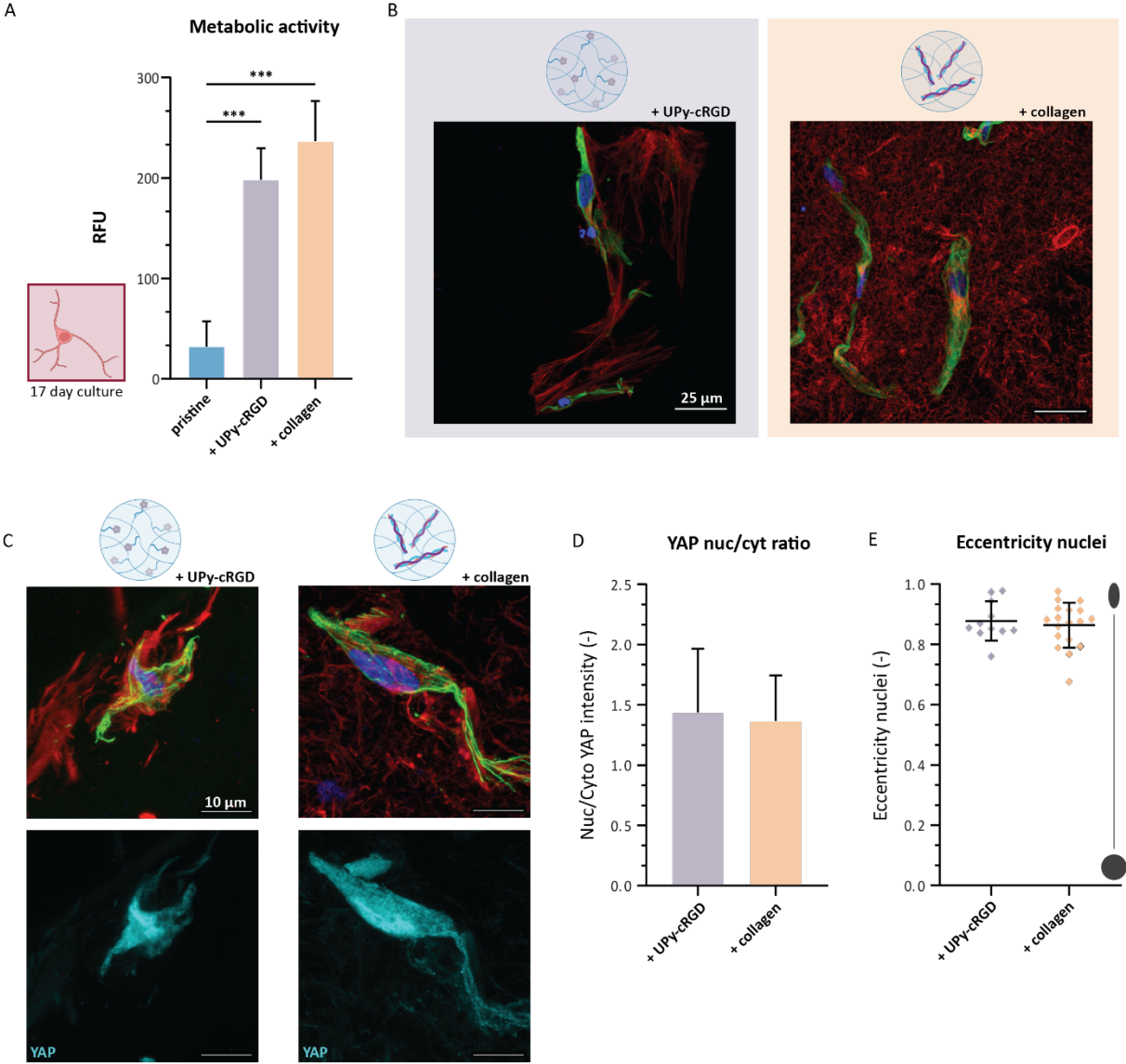
Figure 6. Encapsulated PKs treated towards CSKs sensed similar mechanotransduction when encapsulated in the synthetic or hybrid hydrogel and cultured for 17 days. **A)** Metabolic activity measured after 17-day culture showing almost no activity for the cells in the pristine hydrogel, n=3, *** p < 0.0005, ± standard deviation. **B)** Immunohistochemical staining of F-actin (green), collagen type I (red) and nuclei (blue). Scale bar represents 25 μm. **C)** Immunohistochemical staining of F-actin (green), collagen type I (red) and nuclei (blue), top row. And YAP signal (cyan), bottom row. Scale bar represents 10 μm. **D)** YAP nucleus/cytoplasm ratio, for both gels around 1.4, mean ± standard deviation presented, n=3. **E)** Nucleus eccentricity, for both hydrogels between 0.8 and 1.0, mean ± standard deviation presented, n=3.

(Re-)differentiation of primary keratocytes into corneal stromal keratocytes

During the 21-day cell culture of encapsulated cells, small amounts of cell culture medium were stored to perform an enzyme-linked-immunosorbent assay (ELISA). From literature it is known that SFs secrete several cytokines, *i.e.* Interleukin-8 (IL-8), Interleuking-15 (IL-15) and RANTES/CCL5. All of these cytokines are pro-inflammatory molecules, being important for neutrophil recruitment and T-cell activation. In contrast, quiescent CSKs hardly secrete these cytokines. To this end, an ELISA to measure IL-8 secretion was used to analyze the cellular (re-)differentiation during 3D cell culture of 21 days within the synthetic and hybrid hydrogel.[25] PKs encapsulated within the synthetic and hybrid hydrogel, treated with high serum towards SFs, secreted >2600 pg/mL IL-8. While, PKs encapsulated within the synthetic and hybrid hydrogel, treated with low serum and high glucose towards CSKs, secreted <415 pg/mL IL-8. These results indicate a substantial difference in cellular processes and behavior between the PKs treated towards SFs and the PKs treated towards CSKs (**Figure 7A**). Cellular IL-8 secretion was not affected by the different bioactive additives within the two hydrogels, for both the synthetic and the hybrid hydrogel the results demonstrated a substantial decrease in IL-8 secretion for PKs treated towards CSKs. The analysis of IL-8 secretion at various time points during the cell culture of 21 days, demonstrated a progressive decrease of IL-8 secretion by the PKs treated towards CSKs (**Figure 7B**). In contrast, the PKs treated towards SFs, demonstrated a progressive increase of cellular IL-8 secretion during culture. This behavior was expected for the SFs, since these cells are highly proliferative, resulting in an increase of cells during culture and associated an increase in cellular cytokine secretion. The cellular secretion of IL-8 at various time points in the cell culture demonstrated a change in the cellular behavior of the PKs treated towards CSKs. The cellular secretion of IL-8 by the PKs treated towards CSK is significantly lower compared with the secreted IL-8 by the PKs treated towards SFs. This differences could be caused by the difference in cell proliferation and associated cell numbers, however dividing the IL-8 concentration by the cell concentration demonstrated a rather limited influence of cell proliferation (Experimental section, Figure 10C). The experiment was repeated with PKs of another donor and the same trend in IL-8 secretion was observed for these cells (Experimental section, Figure 11). Healthy human keratocytes do also express crystallin proteins that reduce light scattering and enhance the optical performance of the stromal tissue. One of these proteins is the enzyme aldehyde dehydrogenase 3 Family member A 1 (ALDH3A1), which is

assumed to be a specific marker for keratocytes. Here, immunohistochemical staining showed the expression of ALDH3A1 in PKs differentiated towards CSKs (**Figure 7C**), suggesting that the encapsulated PKs successfully differentiated into CSKs.
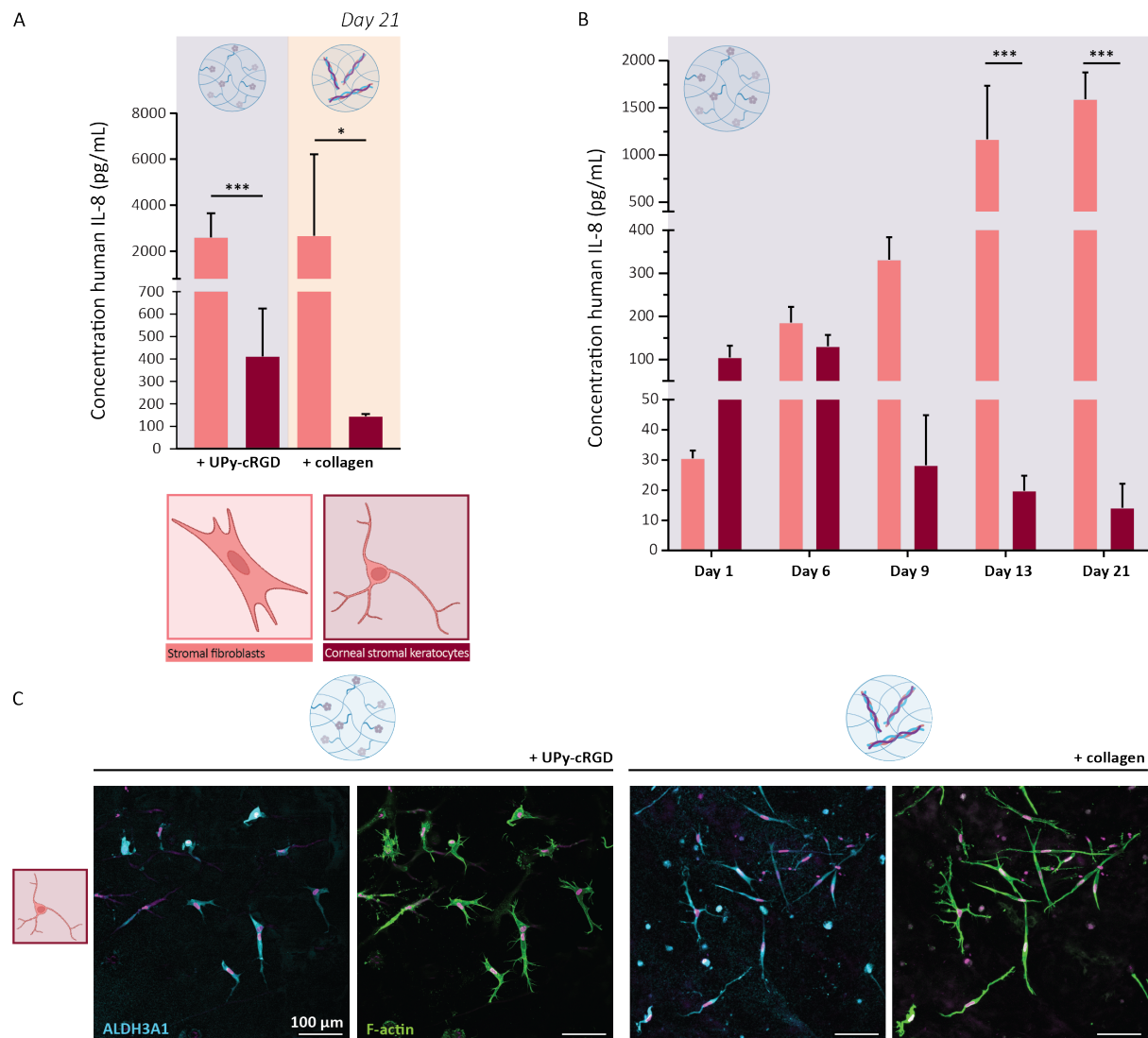
Figure 7. PKs (re)differentiated towards stromal fibroblasts and corneal stromal keratocytes when encapsulated and cultured in the synthetic and the hybrid hydrogel, sample size n=3. **A)** Interleukin 8 (IL-8) secretion by PKs encapsulated in the synthetic and hybrid hydrogel at culture day 21, mean ± standard deviation presented, *** $p < 0.0005$, * $p < 0.05$. Controls of this experiment can be found in Figure 11A. **B)** IL-8 secretion of PKs cultured in the synthetic UPy-cRGD hydrogel at day 1, 6, 9, 13 and 21, mean ± standard deviation presented, *** $p < 0.0005$. Control of this experiment can be found in Figure 11B. **C)** Immunofluorescent staining of ALDH3A1 (cyan), F-actin (green) and nuclei (magenta). Scale bar represents 100 μm.

Cells survived shear stresses during injectability test

Above mentioned results are all obtained by using standard pipette tips and precise mixing of the polymer solutions per well. To eventually turn the supramolecular artificial stromal construct into an attractive tool for biomedical applications, we here focused on the clinical applicability of the hydrogel. for this purpose, the injectability of the stromal construct was explored. A needle with a diameter of 0.16 mm was used to study the injectability. Two days post the encapsulation of cells in the injected synthetic hydrogel, a live-viability staining showed cell survival. After 7 days of culture, immunohistochemical staining indicated that the cells survived and slowly were able to attain their healthy morphology (**Figure 8A, D**). Expression of YAP is clearly observed inside the nuclei, and analysis of the YAP expression showed a mean ratio of ~ 2.5 between nuclear YAP intensity and YAP intensity within the cytoplasm (**Figure 8B**). A nuclear eccentricity of ~ 0.75 indicates the nuclei are oval-shaped instead of round-shaped (**Figure 8C**). Together these results demonstrated that the cells do experience mechanotransduction. It is proposed that, this increase in YAP nuclear/cytoplasm ratio could be triggered by the experienced shear stress during the injection through the needle. However, the cells were able to survive and spread, prolonged cell culture is necessary to increase knowledge about the long term impact of the injection procedure on cellular behavior.
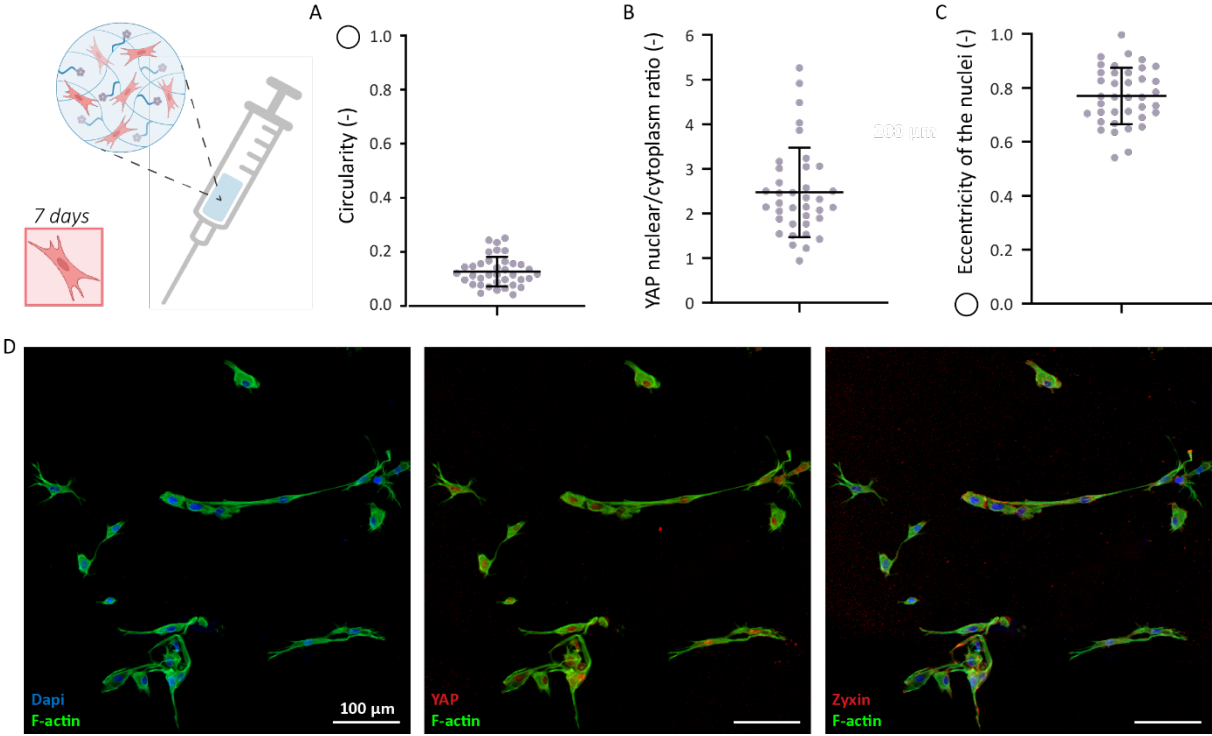
Figure 8. Exploring the injectability of the hydrogels resulted in properly formed gels containing spreaded PKs, n=3. Bar graphs all presented as mean ± standard deviation. **A)** Cell morphology expressed in circularity, towards 1 indicates a round-shaped cell and towards 0 indicates a spreaded cell. **B)** YAP nuclei/cytoplasm ratio, around ~ 2.5. **C)** Nuclei eccentricity of ~ 0.75. **D)** After 7 days Immunofluorescent staining was performed, the cells were stained for F-actin (green), nuclei (blue), and YAP / zyxin (red). Scale bar represents 100 μm.

CONCLUSION

This work demonstrates the successful engineering of a fully synthetic corneal stromal construct via supramolecular hydrogel engineering. Here, we compared the differences in rheological properties, cell encapsulation, cell culture and cell differentiation between a fully synthetic hydrogel and a hybrid hydrogel, and demonstrated no substantial differences between both hydrogels. This is surprising, due to the substantial differences in bioactivity between the presence of small bioactive UPy-cRGD additives within the synthetic hydrogel, and the presence of full length collagen type I fibers within the hybrid hydrogel. The fully synthetic hydrogel showed to be an attractive candidate as a fully synthetic stromal ECM mimicking material, suitable to encapsulate PKs. Encapsulation and culture of representative PKs, which were treated towards CSKs, showed long dendritic protrusions, expressed the keratocyte specific marker ALDH3A1 and demonstrated a lower cell concentration indicating a slower proliferation rate. Moreover, 3D cultured PKs treated towards CSKs hardly secreted any cytokines. Taken together, these cellular characteristics demonstrated the (re)differentiation of PKs encapsulated and cultured within the fully synthetic hydrogel. Towards clinical use of the synthetic hydrogel, injectability properties were studied. PKs survived the shear stresses during the injection trial, demonstrating the ability of using the synthetic stromal hydrogel construct as an attractive minimal invasive tool to fill tissue defects or to introduce corneal cells and initiate self-regeneration. In conclusion, the synthetic stroma has shown to be a functional and mechanically stable microenvironment, allowing inflow of nutrients to successfully encapsulate native keratocytes.

EXPERIMENTAL SECTION

Preparation of hydrogels

Both the bifunctional building blocks as well as the monofunctional building blocks were received as powders. Bifunctional molecules (UPy-PEG$_{10K}$-UPy) were dissolved at 70 °C in an neutral PBS solution for 1.5 hours. Monofunctional molecules (UPy-Glycine or UPy-Glycine + UPy-cRGD) were dissolved at 70 °C in an alkaline PBS solution (containing 160 mM NaOH) for 20 minutes. After the powders were completely dissolved, the solutions were cooled down to room temperature. A specific volume of HCl solution (2 M) was added to the monofunctional solution to reach neutral pH. For hybrid hydrogel preparation collagen type I (Gibco, Collagen I bovine, A1064401) was added to the bifunctional molecule solution, 20 µL was added per 100 µL complete gel (0.1 wt/v%). Upon addition of the bifunctional molecule solution to the monofunctional molecule solutions gelation was initiated, resulting in hydrogel formation. Incubation of the hydrogels at 37 °C allowed a proper gelation of the, and after 1 hour the hydrogels were embedded in PBS to prevent dehydration.

Rheological measurements

A discovery hybrid rheometer (DHR-3, TA Instruments) was used for all the rheological measurements of supramolecular solutions (formations measurements in SI) and pre-formed hydrogels.

Measuring pre-formed hydrogels without cells

Hydrogels were made via above mentioned protocol inside a polystyrene 96 well F-bottom cell culture microplate (Greiner bio-one, 655180). After formation, the gels were left 24 hours incubated in PBS at 37 °C. For measurement, gels were transferred onto the peltier plate and a flat stainless-steel plate-plate geometry (diameter = 8 mm) was used. The geometry was slowly lowered, to prevent sample damage, until the sample completely filled the geometry, resulting in a gap height of 625 – 1050 µm. Low viscosity oil (47 V 100, RHODORSIL®) was applied to seal the gap around the hydrogel to minimize evaporation or drying during the measurements performed on 37 °C.

Measuring pre-formed hydrogels with cells

Hydrogels were made via the below mentioned cell encapsulation protocol, inside a polystyrene 96 well F-bottom cell culture microplate (Greiner bio-one, 655180). Prior to the measurement, during cell culture, the gels were stored embedded in medium inside a cell culture incubator at 37 °C, 21% O_2 and 5% CO_2 for 17 or 21 days, respectively. On the day of the measurement the medium on top

of the gels was removed and the gels were washed 1x with PBS. Subsequently the gels were transferred to the rheometer and a flat stainless-steel plate-plate geometry (diameter = 8 mm) was used. The geometry was slowly lowered, to prevent sample damage, until the sample completely filled the geometry, resulting in a gap height of 625 – 1050 µm. Low viscosity oil (47 V 100, RHODORSIL®) was applied to seal the gap around the hydrogel to minimize evaporation or drying during the measurements performed on 37 °C.

Measuring rheological characteristics

Strain sweep measurements (1-1000% strain, 1 rad s^{-1}) were performed to determine the linear viscoelastic region of hydrogels. Frequency sweeps were measured with frequencies ranging from 100 to 0.1 rad s^{-1}, at a constant strain of 1%. Time sweeps were measured at a constant frequency and a constant strain of 1 rad s^{-1} and 1%. Stress relaxation experiments were performed by applying a strain of 7.5%, and measuring the generated stress for 1000 seconds. The data were normalized using the stress generated after 1 s.
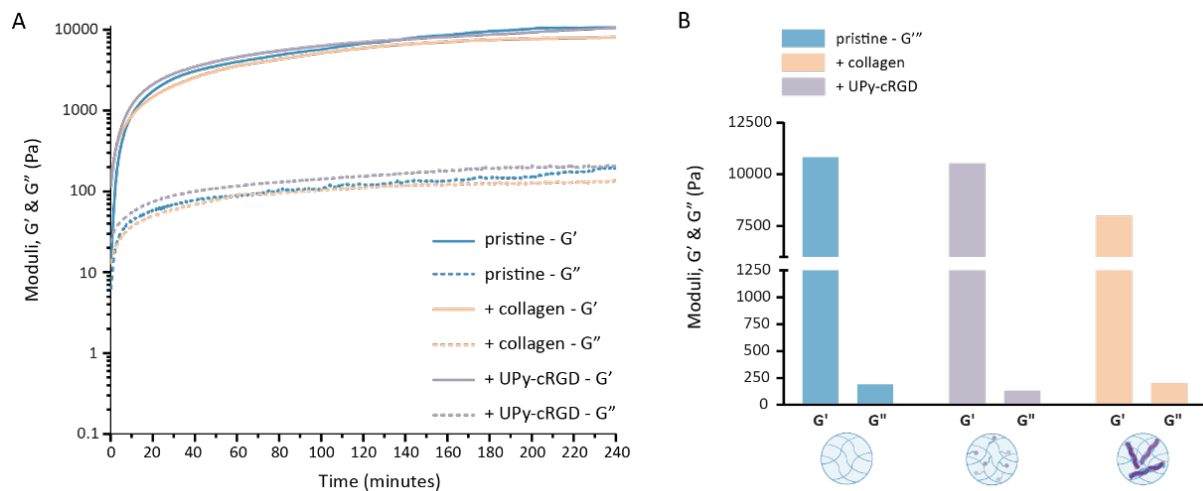

Figure 9. Rheological properties of the pristine, synthetic and hybrid hydrogel after mixing the hydrogelators on top of the rheometer plate. Hydrogel formation and measurements at 37 °C. **A)** Time-sweep measured over a time span of 4 hours, **B)** the storage (G') and loss (G") moduli after 4 hour formation.

Human corneal keratocyte (HCK) cell culture

Human corneal keratocyte (HCK) cell lines were obtained as a kind gift from Dr. Zorn-Kruppa (University Medical Center Hamburg). The HCK cell line was derived from the human corneal stroma and immortalized through SV-40 transfection, and has been previously demonstrated to mimic both the phenotype and the response to growth factor stimulations of their primary precursors.[19,28] HCK cells were cultured in Dulbecco's Modified Eagle's Medium (DMEM, Sigma-Aldrich) supplemented with 5% FBS (Biochrom), and 1% penicillin/streptomycin at 37 °C, 21% O_2 and 5% CO_2 until ±80% confluency was reached. Due to activation of the cells by the FBS supplementation, the HCK cells can be considered activated keratocytes, resembling a fibroblastic phenotype. Cells were passaged twice a week, and cells between passages #5 and #10 were used for the experiments described.

Primary keratocyte (PK) cell culture

Primary human keratocytes were isolated from leftover human corneoscleral transplant material from Descemet Membrane Endothelial Keratoplasty surgery, which were obtained from the Cornea Department of the ETB-BISLIFE Multi-Tissue Center (Beverwijk, the Netherlands). The keratocytes were cultured in expansion medium (1:1 mixture of Dulbecco's modified Eagle's medium/F-12 supplemented with GlutaMAX (DMEM/F12 (Ham) + GlutaMAXTM, 10565-018; Gibco), 5% Fetal Bovine Serum (FBS, Biochrom AG), 1% penicillin/streptomycin (P/S, Biochrom AG), and 1 mM L-ascorbic acid 2-phosphate sesquimagnesium salt hydrate (Vitamin C, Sigma A8960)) at 37 °C, 21% O_2 and 5% CO_2 until ±80% confluency. Since the medium contained FBS, keratocytes were considered to be activated matrix-producing cells, referred to as stromal fibroblasts (SFs). To initiate cell (re-)differentiation towards corneal stromal keratocytes, another medium composition was used: differentiation medium (Dulbecco's modified Eagle's medium supplemented with GlutaMAX (GlutaMAXTM, 11880-028; Gibco), 1% penicillin/streptomycin (P/S, Biochrom AG), and 1 mM L-ascorbic acid 2-phosphate sesquimagnesium salt hydrate (Vitamin C, Sigma A8960), 1x ITS (Sigma, I3146), 2 mg/mL D-glucose (Invitrogen, 15023021), 2.5 mg/mL D-mannitol (Fluka, 63560)).[21] Cells were cultured with medium changes every 3 days, keratocytes from multiple donors were used up to passage #3. TrypLE Express Enzyme (1x), no phenol red (12604013, Gibco) was used to detach the cells from the culture flask and use them for experiments.

Cell encapsulation in hydrogels

Both the bifunctional as well as the monofunctional building blocks were received as powders. The bifunctional molecules (UPy-PEG$_{10K}$-UPy) were dissolved at 70 °C in an neutral PBS solution for 1.5 hours. Monofunctional molecules (UPy-Glycine or UPy-Glycine + UPy-cRGD) were dissolved at 70

°C in an alkaline PBS solution (containing 160 mM NaOH) for 20 minutes. After completely dissolving the powders of the bifunctional and monofunctional building blocks, the solutions were cooled down to room temperature. A specific volume of HCl solution (2 M) was added to the solution of monofunctional molecules to reach a neutral pH. Cell culture medium was added to both solutions 1:1, to provide the cells already with some nutrients during the gelation process later on in the procedure. Afterwards, both solutions are transferred from a glass vial to a sterile Eppendorf tube, from this step onwards a safety cabinet is used to guarantee a sterile work environment. The solutions were disinfected by exposing them to UV-light for 20 minutes. Subsequently, the cells were prepared and counted, the following cell concentrations were used during the experiments:

HCKs: 100 cells/mL

Primary keratocytes treated towards SFs: 100 cells/µL

Primary keratocytes treated towards CSKs: 200 cells/µL

The cells needed for encapsulation were suspended in the correct amount of medium and this cell suspension was added to the solution of bifunctional molecules. Due to the addition of the cells suspension, the bifunctional molecules were diluted. To correct for this extra dilution step, the initial concentration of the bifunctional molecules was slightly higher (0.78 wt/v% instead of 0.52 wt/v%). For every experiment the bifunctional molecules were diluted with 1/3 of cell suspension, resulting in a final 0.52 wt/v% of bifunctional molecules. All the gels were prepared in wells of a non-adhesive 96-well plate (Fisher Scientific, Nunclon Sphera-Treated, U-Shaped-Bottom plate 15227905).

Synthetic hydrogel:

First 40 µL monofunctional molecules in solution were added to a well. Meanwhile, the cells were added to the solution of bifunctional molecules and mixed thoroughly. Second, 40 µL of bifunctional molecules / cell mixture were added to the 40 µL solution of monofunctional molecules inside the well. The molecules were mixed by carefully pipetting up and down (at least 3x per well), any air bubbles were removed by using a needle.

Pristine hydrogel:

First 40 µL monofunctional molecules in solution were added to a well. Instead of adding the cells, only medium was added to the solution of bifunctional molecules and mixed thoroughly. Second, 40 µL of bifunctional molecules / medium mixture were added to the 40 µL solution of monofunctional molecules inside the well. The molecules were mixed by carefully pipetting up and down (at least 3x per well), any air bubbles were removed by using a needle.

Hybrid hydrogel:

For hybrid hydrogel preparation collagen type I (Gibco, Collagen I bovine, A1064401) was added to the solution of the bifunctional molecules, 20 μL was added per 100 μL complete gel (0.1 Wt/v%). Initially, the bifunctional molecules were dissolved at a higher wt/v% compared with the bifunctional molecules used for the synthetic or pristine hydrogel, to correct for this extra dilution step with the collagen. At first, 40 μL solution of monofunctional molecules was added to a well. The cells and the collagen were added to the solution of bifunctional molecules and mixed thoroughly. Second, 40 μL of bifunctional molecules / cell / collagen mixture were added to the 40 μL solution of monofunctional molecules inside the well. The molecules were mixed by carefully pipetting up and down (at least 3x per well), any air bubbles were removed by using a needle.

For the exact hydrogel compositions, see **table 1**. All the hydrogels were placed in the incubator at 37 °C, 21% O_2 and 5% CO_2 for 1 hour to allow for proper gelation. After 1 hour, medium was carefully added to the wells to embed the gels, and the hydrogels with encapsulated cells were placed back in the incubator at 37 °C, 21% O_2 and 5% CO_2. After 1 day the cell culture medium to embed the hydrogel was refreshed and for the PKs treated towards CSKs the expansion medium was replaced by the differentiation medium. Encapsulation of the PKs within the pristine hydrogel was not successful (**Figure 10A**). Only a few clusters of round-shaped cells were observed on day 7 of the culture.
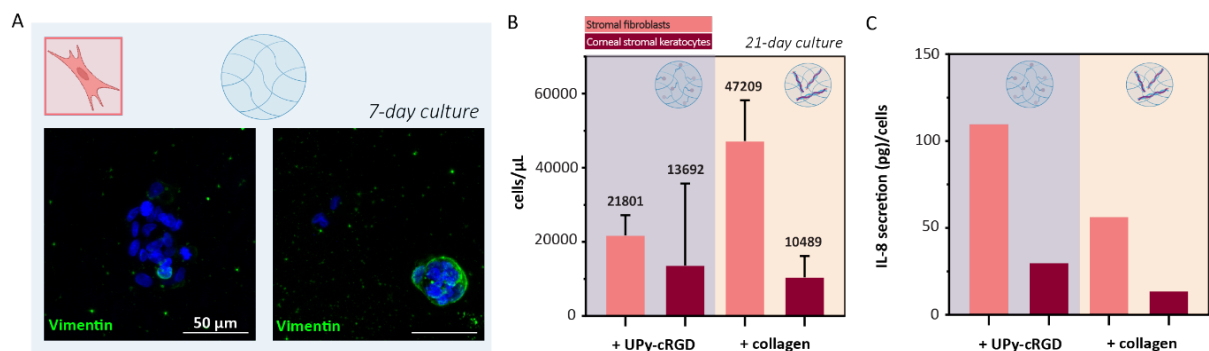
Figure 10. A) Primary keratocytes encapsulated and cultured in a pristine hydrogel for 7 days, treated with serum towards stromal fibroblast. **B)** Quantification of the number of cells within a hydrogel. Six images used per hydrogel, counted cells were corrected for the volume of the z-stack. Initially started with 100 cells/μL for the gels loaded with PKs treated towards SFs and 200 cells/μL for the gels loaded with PKs towards CSKs, mean ± standard deviation presented. **C)** Concentration of cellular secreted IL-8 divided by the cell concentration.

Table 1. Overview of the three studied hydrogel compositions; pristine hydrogel, synthetic hydrogel and hybrid hydrogel. Calculations were made for one complete hydrogel with a volume of 80 μL.

Hydrogel compositions

Pristine hydrogel (no additives)					
Building block / additive	*Ratio*	*μmol*	*mM*	*wt/v %*	
UPy-PEG$_{10K}$-UPy	1	0.02	0.234	0.26	
UPy-Glycinamide	80	1.5	18.75	2.24	
Synthetic hydrogel (+UPy-cRGD					
Building block / additive	*Ratio*	*μmol*	*mM*	*wt/v %*	
UPy-PEG$_{10K}$-UPy	1	0.02	0.234	0.26	
UPy-Glycinamide	67.2	1.26	15.75	1.88	
UPy-cRGD	12.8	0.24	3.0	0.52	
Hybrid hydrogel (+collagen)					
Building block / additive	*Ratio*	*μmol*	*mM*	*wt/v %*	*Concentration (mg/ml)*
UPy-PEG$_{10K}$-UPy	1	0.02	0.234	0.26	
UPy-Glycinamide	80	1.5	18.75	2.24	
Collagen				0.1	1

Cell staining and Imaging

Before immunohistochemical stainings were carried out, the hydrogels were washed 3x with PBS (5 min per wash). All cells encapsulated within the hydrogels were fixated for 20 minutes at room temperature using 3.7% paraformaldehyde (formalin 37%, 104033.1000, Merck). After washing with PBS, samples were permeabilized for 15 minutes with 0.5% Triton X-100 in PBS. Followed by adding a blocking solution of 10% donkey or goat serum in 0.05% Triton X-100 in PBS for 30 minutes. Next, the cells were incubated with the primary antibodies diluted in 2% donkey serum in 0.05% Triton X-100 in PBS overnight at 4 °C. Thereafter, the cells were washed thoroughly with 0.05% Triton X-100 in PBS, including wash waiting steps of 5-10 min. Next, the cells were incubated with the secondary antibodies and phalloidin at room temperature for 2 hours. Finally, the cells were stained with DAPI at a dilution of 1:250 for 10 min and washed thoroughly with PBS (including was waiting steps of 5-10 min). During imaging, complete/intact hydrogels were place on a thin coverslip (24x69 mm, VWR 631-1575) immerged in mowiol 4-88 (Sigma Aldrich, 81381) and imaged using Leica TCS SP8 X inverted confocal microscope (Leica Microsystems) using HC PL APO CS2 objectives

(20x/0.75, 40x/0.95).). Images were processed in ImageJ to create a max-projection image of the original z-stack. See **table 2** for the primary and secondary antibodies used within this study.

Metabolic activity

Prior to the YAP-analysis a resazurin assay was performed to check the metabolic activity. Primary keratocytes (PKs) of passage #2 were encapsulated with a cell density of 30.000 cells per 100 μL hydrogel. The PKs were cultured for 17 days using high glucose and low serum differentiation medium, which was refreshed every 2-3 days. On day 17, at first a resazurin assay was performed, afterwards the hydrogels were thoroughly washed and 1 gel of each condition was used for rheological measurements, the other ones were fixated for immunohistochemical staining.

First, the gels were washed with PBS. Afterwards the gels were transferred to a new 24 well plate (each gel in a separate well). To each well 500 μL of 44 μM resazurin in medium was added and incubated at 37 °C for 3 hours. Subsequently, 2x 200 μL of the incubated resazurin/medium was collected and transferred to a black 96-well plate to measure fluorescence (excitation: 530/25 and emission: 590/35) with the plate reader (Synergy HTX, BioTek).

To test the significant differences in metabolic activity, a Shapiro-Wilk test was performed to prove a normal distribution of the data, n=3. An one way Anova and Tukey's multiple comparisons test was performed with Graphpad Prism. Differences were considered significant for p-values <0.05. Values are presented as an average ± standard deviation, *** $p < 0.0005$ (0.0004). The YAP and eccentricity analyses are not significant.

Table 2. Overview of the used dyes, primary-, and secondary antibodies.

Antibody / dye	Company / reference #	Dilution
4',6-diamidino-2-phenylindole dihydrochloride (DAPI)	Sigma-Aldrich, D9542	1:250
Phalloidin 488	Sigma-Aldrich	1:300
Phalloidin 555	Sigma-Aldrich	1:300
Anti-Collagen type I	C2456, Sigma	1:250
Anti-Collagen type V	1350-01, Southem Biotech	1:250
Anti-Collagen type VI	70R-CR009x, Fitzgerald	1:250
Anti-Vimentin	Ab20346, Abcam	1:300
Anti-Ki-67	Rb1510-P0, Thermo Scientific	1:200
Anti- tubulin β3	801202, BioLegend	1:100
Anti-YAP1	Ab52771, Abcam	1:100
Anti-ALDH3A1	Ab76976, Abcam	1:100
Anti-ZYX	HPA004835, Atlas antibodies	1:100
Secondary antibodies		
Anti-mouse IgG1 (goat) 555	A21127, Molecular Probes	1:250
Anti-mouse IgG1 (goat) 488	A21121, Molecular Probes	1:250
Anti-goat IgG (donkey) 488	A11055, Molecular Probes	1:250
Anti-rabbit IgG (donkey) 555	A31572, Molecular Probes	1:250
Anti-rabbit IgG (donkey) 488	A21206, Molecular Probes	1:250
Anti-rabbit IgG (donkey) 647	711-605-152 Jackson	1:250
Anti-rabbit IgG (goat) 647	A21244, Molecular Probes	1:250
Anti-rabbit IgG (goat) 555	A211428, Molecular Probes	1:250
Anti-mouse IgG2a (goat) 555	A21137, Molecular Probes	1:250
Anti-mouse IgM (goat) 488	A21042, Molecular Probes	1:250
Anti-mouse IgM (goat) 555	A21426, Molecular Probes	1:250

All stainings were performed with a combination of solely donkey or goat secondary antibodies. Donkey serum was used for a combination of solely donkey based secondary antibodies, goat serum was used for a combination of solely goat based secondary antibodies.

Enzyme-linked immunosorbent assay (ELISA)

On various days during the 3D cell culture, medium was refreshed and all medium surrounding the sample was collected in separate small Eppendorf tubes and stored at -80 °C. All ELISA experiments were executed with n=3, and all the standards as well as the samples are ran in duplicate. The following IL-8 concentrations were used for the standard curve of IL-8:

1000 pg/mL, 500 pg/mL, 250 pg/mL, 125 pg/mL, 62.5 pg/mL, 31.3 pg/mL, 15.6 pg/mL.

Uncoated Nunc™MaxiSorp™ ELISA plates (BioLegend, 423501) were used, these plates were coated with capture antibody diluted in 1x coating buffer one day prior to running the ELISA (overnight incubation at 4°C). See **table 3** for all the compositions of the used reagents. On the experiment day all the samples, the plates and the ELISA MAX™ Deluxe Set components (BioLegend®) were brought to room temperature. All the washing steps were executed in a similar manner, namely: 4 times with at least 300 µL wash buffer (0.05% Tween-20 in PBS) per well and residual buffer was blotted by firmly tapping the plate upside down on absorbent paper. After incubation with the capture antibody the plate was washed and blocked with 1x assay diluent A at room temperature for 1 hour with shaking (500 rpm) to minimize non-specific binding and reduce background. During this incubation, the samples for the standard curve were prepared and every well plate comprised a standard. After blocking, the wells were washed and incubated with 100 µL of the samples and standards at room temperature for 2 hours with shaking (500 rpm), all samples were diluted 4x in 1x assay diluent (25 µL sample, 75 µL 1x assay diluent). Thereafter, the wells were washed and 100 µL of detection antibody solution was added to each well, and incubated at room temperature for 1 hour with shaking (500 rpm). The wells were washed again and incubated with 100 µL of diluted Avidin-HRP solution at room temperature for 30 min with shaking (500 rpm). Subsequently, the wells were washed 5x thoroughly with wash buffer, and soaked in buffer for 1 minute for each wash to minimize background. Then, 100 µL of substrate solution C was added and incubated in the dark for 15 minutes. During this step, positive wells turned blue in color. To stop the reaction, 100 µL Stop Solution for TMB Substrate (BioLegend, 4230021) was added to each well. All the positive wells turned from blue to yellow during this step. After adding the stop solution to the wells, the plate was softly tapped to the table a few times to proper mix the solutions and immediately the absorbance at 450 nm was measured with the plate reader (Synergy HTX, BioTek). In addition the absorbance at 570 nm was measured, this absorbance could be subtracted from the 450 nm absorbance. The standard curve for each ELISA was plotted in excel and polynomial curve-fitting software with order 3 or 4 was used to determine the best fit. Using this formula together with the

measured absorbance value, resulted in the calculation of the amount of cytokine secretion.

Positive controls were performed, by taken the medium of PKs cultured in normal polystyrene cell culture plates (**Figure 11A, B**). Additionally, the ELISA to measure IL-8 secretion by the PKs encapsulated within the hydrogels was repeated by using PKs derived from another human donor (**Figure 11C, D**).

To test the significant differences of the results of the Elisa assay, a Shapiro-Wilk test was performed to prove a normal distribution of the data, n=3. An unpaired t-test was performed with Graphpad Prism. Differences were considered significant for p-values <0.05. Values are presented as an average ± standard deviation. *** p < 0.0005 (0.0003), * p < 0.05 (0.0378).

Table 3. Reagents used to perform an ELISA with 2x a complete 96-well plate

4 mL Coating Buffer A (5x)	16 mL of Deionized Water
100 µL of Capture Antibody (200x)	20 mL of 1x Coating Buffer
12 mL of Assay Diluent A (5x)	48 mL of PBS
100 µL of Detection Antibody (200x)	20 mL of 1x Assay Diluent A
20 µL of Avidin-HRP (1000x)	20 mL of 1x Assay Diluent A
Substrate Solution C	-
Used ELSIA set: *ELISA MAX™ Deluxe Set Human IL-8 (BioLegend, 431504)*	

3D Height indication cell images

A custom MatLab script was written to pair a specific height of the cell within the obtained z-stack image to a specific color. Image stacks obtained from channels corresponding to the DAPI (nuclei) and phalloidin (F-actin) were used to create these 3D height indication cell images. LAS X Life Science Microscope Software was used to calculate the original µm distance in the z-direction from the original *lif* file. *The custom MatLab script was written by Mark C. van Turnhout.*

Figure 11. Additional data of IL-8 secretion by PKs. **A)** Positive control of data shown in figure 7A, IL-8 secretion on day 21 of PKs cultured on normal culture treated polystyrene, mean ± standard deviation presented. **B)** Positive control of data shown in figure 7B. IL-8 secretion on day 1, 9 and 21 of PKs cultured on normal culture treated polystyrene. **C)**. IL-8 secretion of PKs cultured in the synthetic hydrogel at day 1, 9 and 21 (another donor), n=3, mean ± standard deviation presented. **D)** Positive control of data shown in figure 11C, mean ± standard deviation presented.

Injection of Hydrogel

Initially this protocol is similar to the preparation of hydrogels protocol. The proper dissolved and neutral solutions of monofunctional molecules and the bifunctional molecules are placed on ice in separate Eppendorf tubes. A clean Eppendorf tube, small syringe and a 30G needle were placed on ice as well. At first, both molecule solutions were mixed 1:1 together in the clean and pre-cooled Eppendorf tube and afterwards the tube was placed back on ice. Subsequently, the needle and syringe were used to collect the molecule mixture and to inject the mixture in an empty petri dish/well (Figure S9). The injected hydrogel is placed in the incubator at 37 °C to form properly. After 1 hour, surrounding medium was added and it was observed that the gel stayed intact,

suggesting a proper formation. The following cell concentrations were used; 200 cells/µL gel and 400 cells/µL gel. Live staining was carried out according to the manufacturers protocol (Thermo Fisher Scientific) using calcein-AM to stain for live cells on day 2 of the culture. Afterwards on day 7, immunohistochemical staining was carried out as described above and cell image analyses was carried out as described below.

Cell Image Analyses

All image analyses were analyzed from maximum-intensity z-projections of confocal image stacks. Cell count (Figure S2) was analyzed from images obtained after nuclei staining. To this end, ImageJ software was used to determine the number of nuclei per image. To determine the localization of YAP, z-projections of images were obtained from channels corresponding to the DAPI (nuclei), phalloidin (F-actin) and anti-YAP antibody staining (YAP). Afterwards CellProfiler™ (cell image analyses software) was used to design a pipeline that determined the nuclear areas and cytoplasmic areas (**Figure 12**). The mean intensity was determined in those respective areas and the ratio between the concentration present in nuclear and cytoplasmic regions of cell was then used as a measure of YAP nuclear translocation. The same pipeline was also used to determine the nuclear eccentricity and the cell circularity (4π x (cell area / perimeter of the cell^2)).
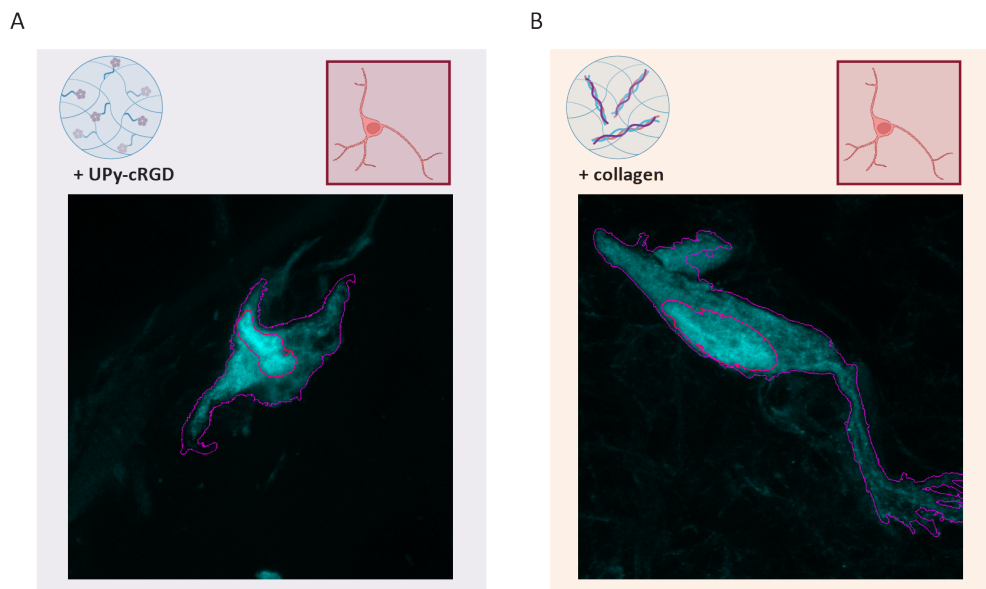
Figure 12. Additional data supporting Figure 6. Cellprofiler™ was used to determine the intensity of YAP signal in the cytoplasm (magenta) and the YAP intensity in the nucleus (red). YAP signal in cyan. **A)** Cell encapsulated and cultured for 17 days in the synthetic hydrogel. **B)** Cell encapsulated and cultured for 17 days in the hybrid hydrogel.

APPENDIX
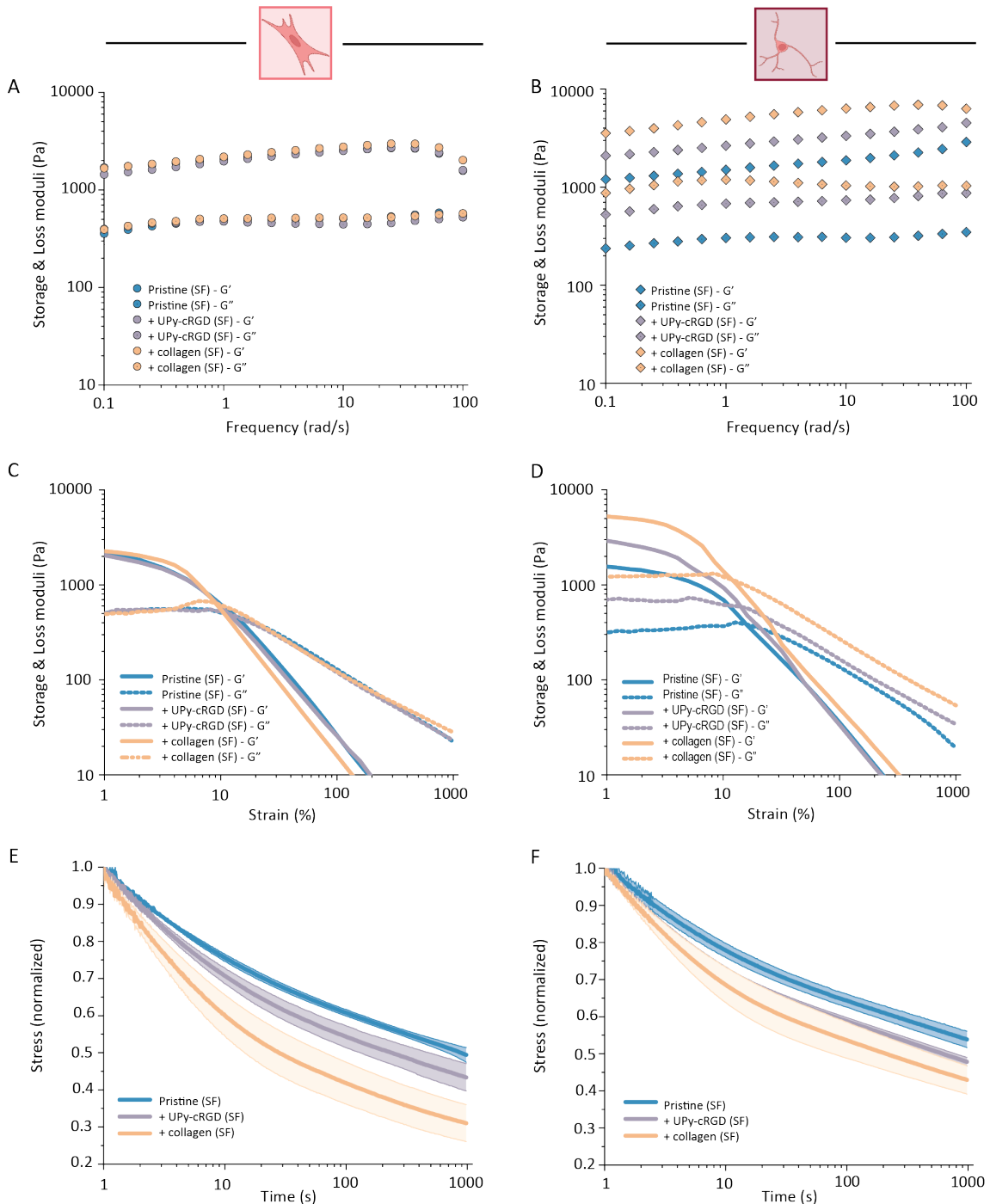
Figure 13. Additional graphs of main text figure 5. The mechanical properties of the pristine, synthetic and hybrid hydrogel with primary keratocytes encapsulated and cultured for 21 days. Measured at 37 °C, n=3. Showing **A)** the frequency sweep comparing the hydrogels for the PKs treated as stromal fibroblasts, **B)** the frequency sweep comparing the hydrogels for the PKs treated as stromal keratocytes, **C)** the strain-sweep comparing the hydrogels for the PKs treated as stromal fibroblasts, **D)** the strain-sweep comparing the hydrogels for the PKs treated as stromal keratocytes, **E)** stress-relaxation at 1% strain, measured over a time span of 1000 s, comparing the hydrogels for the PKs treated as stromal fibroblasts, **F)** the stress-relaxation at 1% strain, measured over a time span of 1000 s, comparing the hydrogels for the PKs treated as stromal keratocytes.
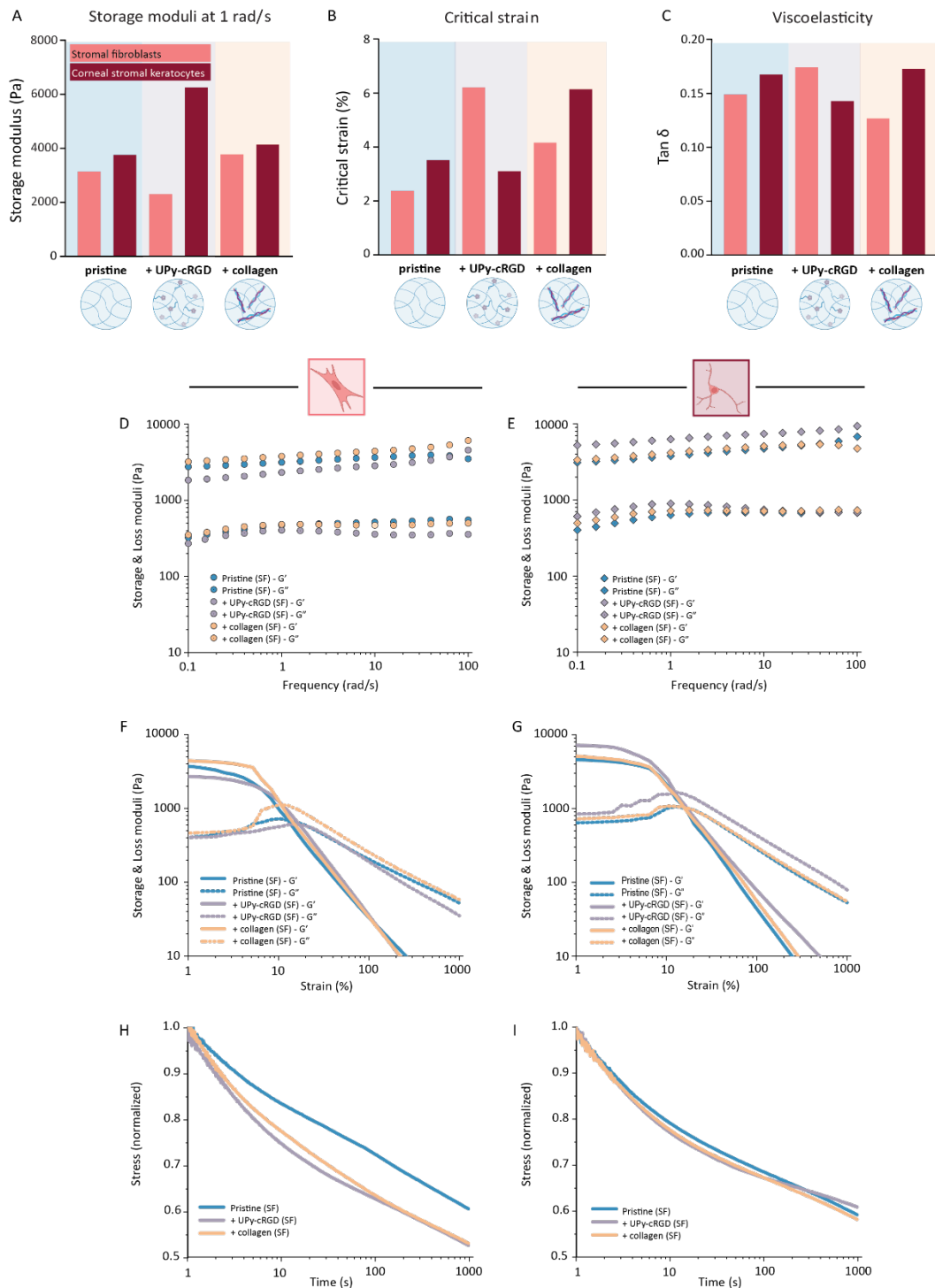
Figure 14. The mechanical properties of the pristine, synthetic and hybrid hydrogel with primary keratocytes encapsulated and cultured for 21 days. Measured at 37 °C, n=3. Showing **A)** the storage moduli at 1 rad/s, **B)** the critical strain, **C)** the viscoelasticity, **D)** the frequency sweep comparing the hydrogels for the PKs treated as stromal fibroblasts, **E)** the frequency sweep comparing the hydrogels for the PKs treated as stromal keratocytes, **F)** the strain-sweep comparing the hydrogels for the PKs treated as stromal fibroblasts, **G)** the strain-sweep comparing the hydrogels for the PKs treated as stromal keratocytes, **H)** the stress-relaxation at 1% strain, measured over a time span of 1000 s, comparing the hydrogels for the PKs treated as stromal fibroblasts, **I)** the stress-relaxation at 1% strain, measured over a time span of 1000 s, comparing the hydrogels for the PKs treated as stromal keratocytes.

REFERENCES

1. Kong, B. *et al.* Fiber reinforced GelMA hydrogel to induce the regeneration of corneal stroma. *Nat Commun* 11, 1435 (2020).

2. DelMonte, D. W. & Kim, T. Anatomy and physiology of the cornea. *J Cataract Refract Surg* 37, 588–598 (2011).

3. Germundsson, J., Karanis, G., Fagerholm, P. & Lagali, N. Age-Related Thinning of Bowman's Layer in the Human Cornea In Vivo. *Investigative Opthalmology & Visual Science* 54, 6143 (2013).

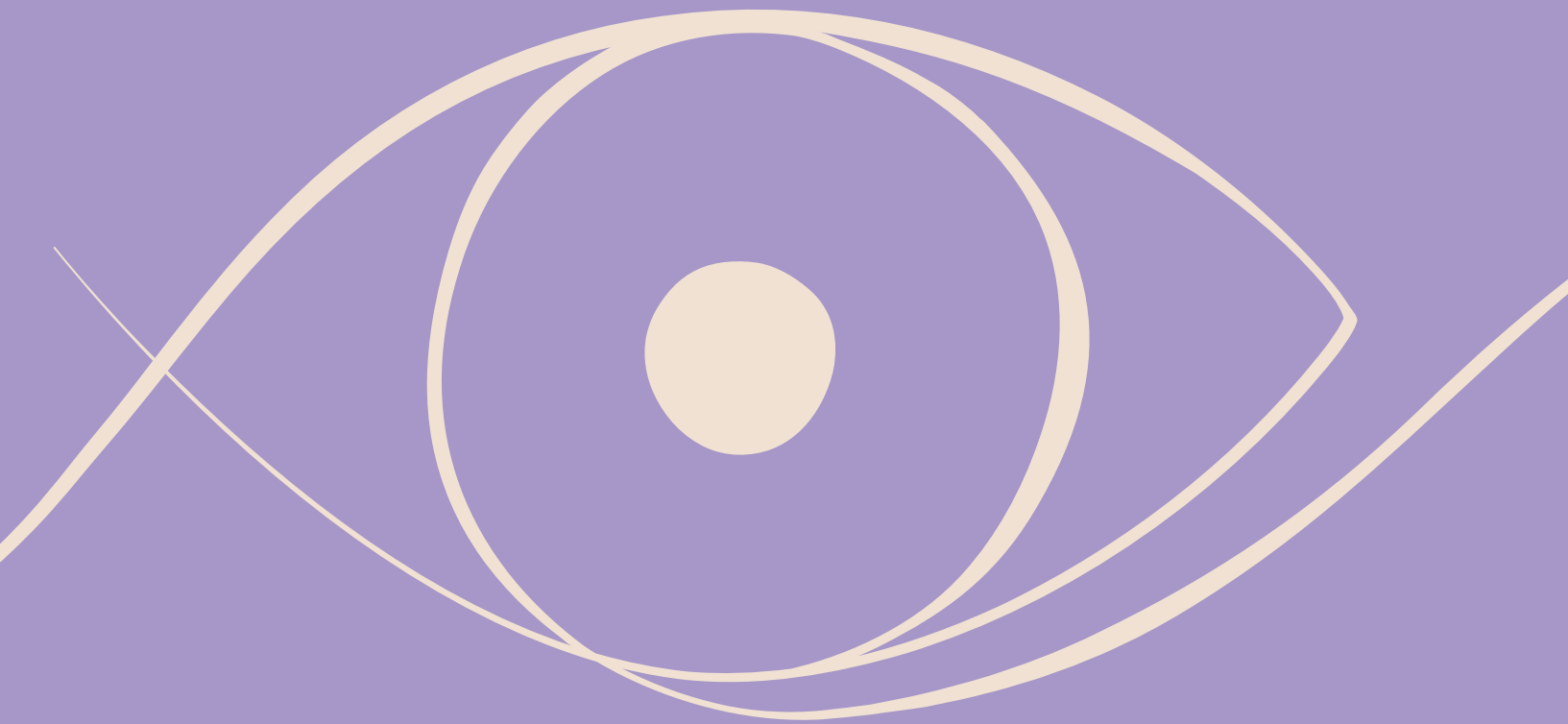4. Mobaraki, M. *et al.* Corneal Repair and Regeneration: Current Concepts and Future Directions. *Front Bioeng Biotechnol* 7, (2019).

5. Michelacci, Y. M. Collagens and proteoglycans of the corneal extracellular matrix. *Brazilian Journal of Medical and Biological Research* 36, 1037–1046 (2003).

6. Meek, K. M. & Knupp, C. Corneal structure and transparency. *Prog Retin Eye Res* 49, 1–16 (2015).

7. Garcia-Porta, N. *et al.* Corneal Biomechanical Properties in Different Ocular Conditions and New Measurement Techniques. *ISRN Ophthalmol* 2014, 1–19 (2014).

8. Matthyssen, S., van den Bogerd, B., Dhubhghaill, S. N., Koppen, C. & Zakaria, N. Corneal regeneration: A review of stromal replacements. *Acta Biomater* 69, 31–41 (2018).

9. West-Mays, J. A. & Dwivedi, D. J. The keratocyte: Corneal stromal cell with variable repair phenotypes. *Int J Biochem Cell Biol* 38, 1625–1631 (2006).

10. Gain, P. *et al.* Global Survey of Corneal Transplantation and Eye Banking. *JAMA Ophthalmol* 134, 167 (2016).

11. Diba, M. *et al.* Self-Healing Biomaterials: From Molecular Concepts to Clinical Applications. *Adv Mater Interfaces* 5, 1800118 (2018).

12. Madl, A. C. & Myung, D. Supramolecular Host–Guest Hydrogels for Corneal Regeneration. *Gels* 7, 163 (2021).

13. Ghezzi, C. E., Rnjak-Kovacina, J. & Kaplan, D. L. Corneal Tissue Engineering: Recent Advances and Future Perspectives. *Tissue Eng Part B Rev* 21, 278–287 (2015).

14. Brunette, I. *et al.* Alternatives to eye bank native tissue for corneal stromal replacement. *Prog Retin Eye Res* 59, 97–130 (2017).

15. Ahearne, M., Fernández-Pérez, J., Masterton, S., Madden, P. W. & Bhattacharjee, P. Designing Scaffolds for Corneal Regeneration. *Adv Funct Mater* 30, 1908996 (2020).

16. Dankers, P. Y. W., Harmsen, M. C., Brouwer, L. A., Van Luyn, M. J. A. & Meijer, E. W. A modular and supramolecular approach to bioactive scaffolds for tissue engineering. *Nat Mater* 4, 568–574 (2005).

17. Formisano, N. *et al.* Mechanical Properties of Bioengineered Corneal Stroma. *Adv Healthc Mater* 10, 2100972 (2021).

18. Diba, M. *et al.* Engineering the Dynamics of Cell Adhesion Cues in Supramolecular Hydrogels for Facile Control over Cell Encapsulation and Behavior. *Advanced Materials* 33, 2008111 (2021).

19. Zorn-Kruppa, M. *et al.* A Human Corneal Equivalent Constructed from SV40-immortalised Corneal Cell Lines. *Alternatives to Laboratory Animals* 33, 37–45 (2005).

20.   Manzer, A. K. SV40-Transformed Human Corneal Keratocytes: Optimisation of Serum-free Culture Conditions. *ALTEX* 33–39 (2009)

21.   Foster, J. W., Gouveia, R. M. & Connon, C. J. Low-glucose enhances keratocyte-characteristic phenotype from corneal stromal cells in serum-free conditions. *Sci Rep* 5, 10839 (2015).

22.   Dupont, S. *et al.* Role of YAP/TAZ in mechanotransduction. *Nature* 474, 179–183 (2011).

23.   Elosegui-Artola, A. *et al.* Force Triggers YAP Nuclear Entry by Regulating Transport across Nuclear Pores. *Cell* 171, 1397-1410.e14 (2017).

24.   Nardone, G. *et al.* YAP regulates cell mechanics by controlling focal adhesion assembly. *Nat Commun* 8, 15321 (2017).

25.   Yam, G. H.-F. *et al.* Nerve regeneration by human corneal stromal keratocytes and stromal fibroblasts. *Sci Rep* 7, 45396 (2017).

26.   Jester, J. V. Corneal crystallins and the development of cellular transparency. *Semin Cell Dev Biol* 19, 82–93 (2008).

27.   Jester, J. V. *et al.* The cellular basis of corneal transparency: evidence for 'corneal crystallins'. *J Cell Sci* 112, 613–622 (1999).

28.   Manzer, A. K. *et al.* SV40-transformed human corneal keratoeytes: Optimisation of serum-free culture conditions. *ALTEX* 26, 33–39 (2009).

CHAPTER 3

A collagen binding peptide additive to biofunctionalize supramolecular hydrogels

Cells and their surrounding matrix form a dynamic and interactive network. This interaction is essential for tissues to remain in a healthy state or to remodel and adapt to new situations. This work focuses on the complex and dynamic cell-matrix interplay. Previously, hydrogels were often treated as static environments with the focus merely on a certain cellular outcome. Here, we demonstrated the ability of cells to actively probe their surrounding matrix, suggesting a cell induced rearrangement of the network. To this end, a collagen binding peptide additive is presented, aiming to introduce an interaction between the synthetic and the natural components within a hydrogel. After successful synthesis, conjugation to an ureido-pyrimidinone (UPy) moiety allowed the incorporation of the collagen type I binding peptide additive (UPy-C1B) into the supramolecular UPy-stacks of the transient network. Two approaches are used to study the affinity of UPy-C1B for collagen. First, UPy-C1B was introduced within the hybrid hydrogel based on collagen- and UPy-fibers. Instead of just mixing both fibers, the additive was used to introduce an additional crosslink between the natural and synthetic fibers. Second, the UPy-C1B additive was introduced in a fully synthetic hydrogel, to study its binding affinity for cellular produced collagens. Incorporation of UPy-C1B into the hybrid hydrogel resulted in substantial morphological and mechanical changes of the network, indicating an interaction between the synthetic UPy-fibers and the natural collagen fibers.

INTRODUCTION

Biophysical properties of the extracellular matrix (ECM), *i.e.* mechanics and dynamics, are important parameters to control cell migration, spreading and proliferation.[1,2] Due to the continuous interplay between cells and their surrounding matrix, the ECM requires to be a dynamic interactive network.[3,4] The specific properties of the ECM polymers, *i.e.* the stress stiffening behavior of collagen, fibrin, *etc.*, can be exploited by cells to change the mechanical properties of their cytoskeleton.[5–7] In return, the tractions generated by cells cause a change in the physical parameters of the extracellular matrix. This in turn, is sensed by other cells in the matrix, changing their behavior and cell fate. This shows the complex interplay underlying the cell-matrix interaction and behavior.[8–11] Over the years, both natural and synthetic hydrogels proved to be good candidates to mimic the ECM.[12–15] Natural based hydrogels have great bioactive properties, yet they often have limited control over physical parameters. In contrast, synthetic hydrogels offer good control over the physical aspects, but integration of bioactive cues can be difficult and limited. In this respect, natural and synthetic polymers are often combined, exploiting the advantages of both systems to obtain a wider range of different properties and greater complexity, similar to the natural ECM. Chaudhuri *et al.* combined polyethylene glycol (PEG)-based networks with alginate to create networks with tunable dynamic properties and to control cell adhesion and spreading.[16] Trujillo *et al.* designed PEG based hydrogels combined with fibronectin, which outperformed fully synthetic PEG hydrogels, showing the advantages of more complex hybrid networks.[17] Some other groups started to design peptides that can bind ECM proteins, which are incorporated within hybrid or synthetic hydrogels. The presence of these ECM-binding peptides in the network ensures both cellular remodeling of the matrix as well as recruitment of specific cell-secreted ECM proteins towards the matrix.[18–20]

To design a successful hydrogel applicable within the tissue engineering field, we aim (1) to provide the necessary biochemical cues within the hydrogel to create cellular anchor ligands as well as to support cellular matrix production, (2) to control the physical parameters as well as the bioactive properties of the hydrogel upon combining synthetic and natural polymers. To achieve both characteristics, a supramolecular hydrogel was biofunctionalized with a collagen type I binding peptide additive (**Figure 1A**). Previously, collagen binding phages were identified from commercially available phage libraries by Helms *et al.*, discovering a

monovalent H_2N-HVWMQAPGGGK(biotin)-NH_2 construct that possessed the ability to bind to collagen type I.[21] This knowledge was used to synthesize a GCGGPAQMWVH peptide, which was conjugated to an ureido-pyrimidinone (UPy) moiety to generate a supramolecular collagen binding peptide additive (UPy-C1B). Conjugation to the UPy-moiety allows the incorporation of the peptide additive into supramolecular UPy-stacks of the hydrogel network, where it reinforces an interaction between the synthetic and natural components (**Figure 1B**).

Within this study various hydrogel compositions based on supramolecular chemistry are explored. Due to the supramolecular approach, all the hydrogels possess tunable mechanical and dynamic properties, while incorporation of various functional moieties is relatively straightforward. The base hydrogel consists of two variations of molecules with complementary UPy-groups. Monofunctional molecules, with one functional UPy building block, form dimers due to fourfold hydrogen bonds. These UPy-dimers assemble into 1D stacks, which bundle into UPy-fibers (**Figure 1F**). A transient network is generated upon addition of a bifunctional UPy molecule, UPy-PEG$_{10K}$-UPy, forming inter-fiber crosslinks. In addition, a hybrid hydrogel is fabricated, based on a mixture of UPy-fibers and natural collagen type I fibers. In this hybrid hydrogel construct the added collagen provides the biochemical cues to support the encapsulated cells (**Figure 1E**).Variations of the synthetic base hydrogel and hybrid hydrogel are made via the incorporation of multiple additives, *i.e.* the novel UPy-C1B which is hypothesized to interact with the collagen produced by encapsulated cells and/or the commercial collagen used to introduce bioactivity in the hybrid hydrogel (**Figure 1B**), the well-known UPy-cRGD which supports cellular adhesion (**Figure 1C**), and UPy-Cy5 which visualizes the network (**Figure 1D**).

The cornea is a soft tissue at the front of the eye, responsible for transmitting and refracting light rays, predominantly consists of collagen type I.[22,23,24] To increase our knowledge about the design of corneal stromal microenvironments based on supramolecular hydrogels, corneal cells were used to encapsulate and culture within various hydrogels. Next, multiple material characteristics, such as; the biophysical properties, network morphology, and bioactive properties of several variations from the synthetic and hybrid hydrogel, were explored (**Figure 1G**). In addition to the results obtained on the binding affinity of the introduced UPy-C1B with collagen, the results provided interesting insights into the interplay between cell and matrix. For this reason, we also investigated the ability of cells to actively probe their surrounding matrix, resulting in a cell induced rearrangement of the network.
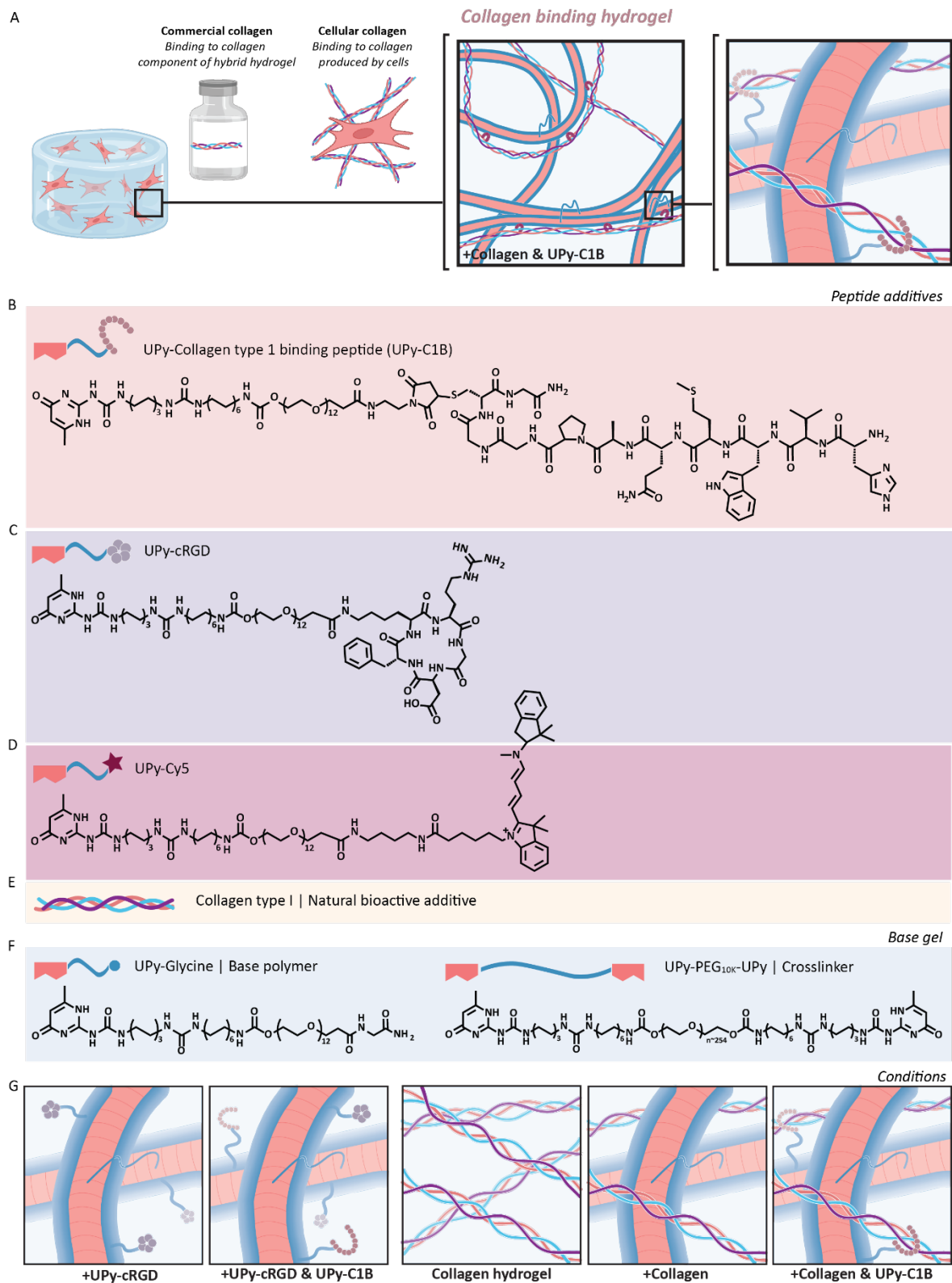
Figure 1. Schematical conceptual figure including the chemical structures of the molecules and schematic representation of the studied conditions. **A)** Conceptual figure. **B)** Chemical structure of UPy-C1B. **C)** Chemical structure of UPy-cRGD. **D)** Chemical structure of UPy-Cy5. **E)** Schematic representation of collagen type I, used within the hybrid hydrogel. **F)** Chemical structures of the used hydrogelators, the UPy-Glycine and the crosslinker UPy-PEG$_{10K}$-UPy. **G)** The schematic representation of the fiber assembly of the studied conditions.

RESULTS AND DISCUSSION

Synthesis of collagen type I binding peptide (C1B) additive and conjugation to a UPy-moiety

The GCGGPAQMWVH peptide was synthesized using standard Fmoc solid phase peptide synthesis (SPPS) on a rink amide resin, with a propargyl glycine at the N-terminus and an introduced cysteine on the C-terminus to enable coupling to the UPy-moiety. The Fmoc-protected GC(Trt)GGPAQ(Trt)MW(tBu)VH(Trt) peptide was deprotected using piperidine as a base, resulting in a primary amine. Thereafter, the peptide was deprotected and removed from the resin using trifluoroacetic acid (TFA) and ultrapure water mixed with triisopropylsilane (TIS) to simultaneously remove the side-protective groups on the amino acids (**Scheme 1**). Upon using TFA, highly reactive cationic species were generated from the protecting groups that
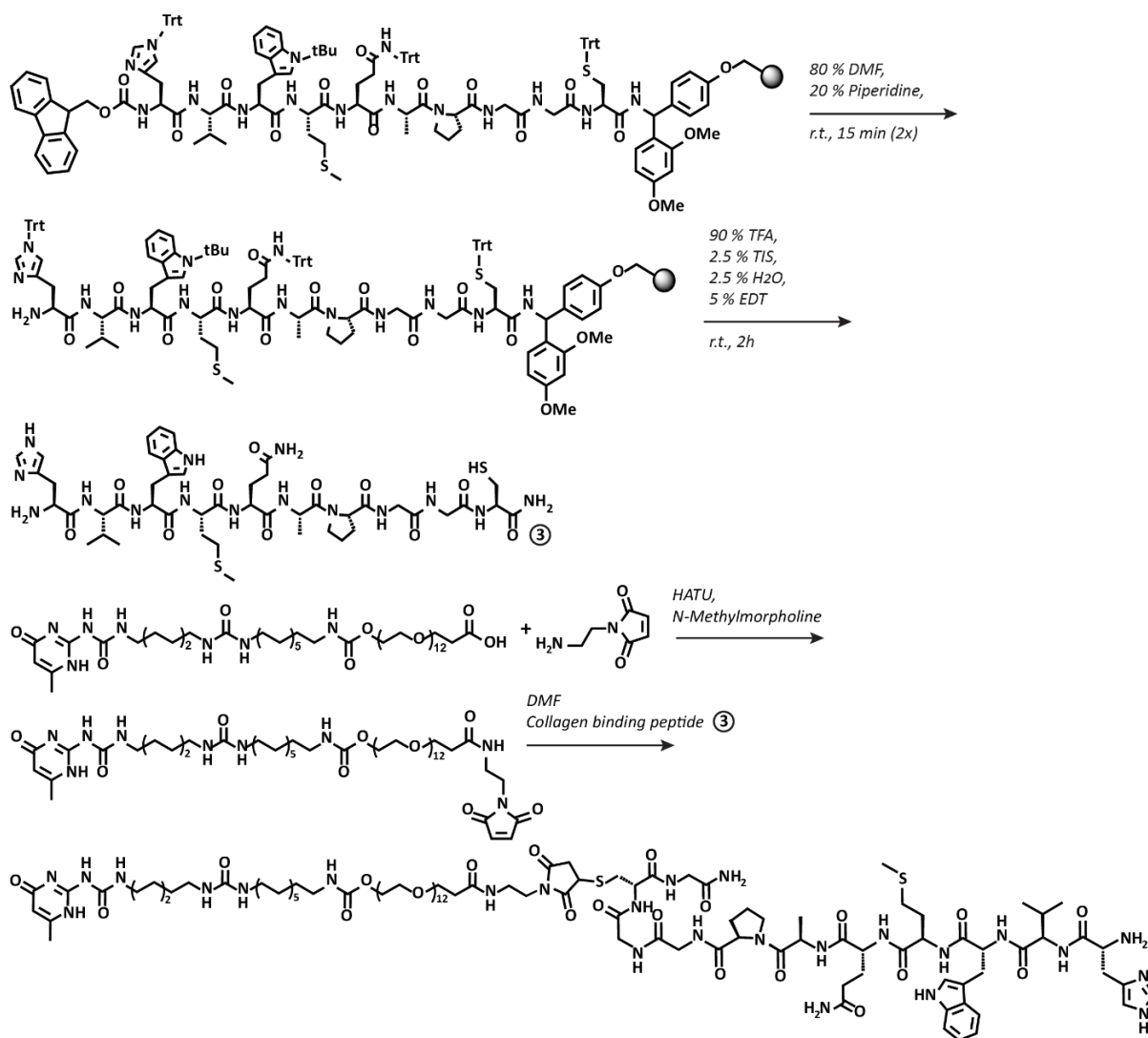
Scheme 1. Conjugation of Fmoc SPPS GCGGPAQMWVH to a UPy-moiety via maleimide-thiol chemistry, resulting in the supramolecular bioactive additive UPy-GCGGPAQMWVH (referred to as UPy-C1B).

could react with the nucleophilic group of the cystine. To this end, the scavenger ethanedithiol (EDT) was added to quench these ions. Residual unreacted peptides were removed through purification with preparative reverse-phase liquid chromatography-mass spectrometry (RP-LCMS). To this end, the peptide was gained with a yield of 91% in high purity (> 95%). The GCGGPAQMWVH peptide was attached to the UPy-moiety via maleimide-thiol chemistry, where Tris(2-carboxyethyl)phosphine (TCEP) was used to cleave the sulfide bonds and therewith activate the thiol in the cysteine to react with the maleimide. The UPy-GCGGPAQMWVH was gained with a yield of 76% in high purity (>98%).

Comparison of mechanical, morphological, and biological properties upon introducing UPy-C1B peptide into the hybrid hydrogel

A hybrid hydrogel functionalized with the UPy-C1B peptide additive was formulated to study the binding affinity of UPy-C1B to the collagen fibers of the hybrid hydrogel network. The incorporation of the UPy-C1B within the hybrid hydrogel network was expected to introduce additional crosslinks between the UPy-fibers and the collagen fibers. For this purpose, the storage moduli of both the hybrid hydrogel and the hybrid hydrogel functionalized with UPy-C1B were measured and compared (**Figure 2A**). In addition, to study the impact of the incorporation of various peptide additives on the rheological properties of the hydrogels in general, the storage moduli of other hydrogel variations were measured as well. The results showed an average storage modulus of 2410±464 Pa for the hybrid hydrogel and an average storage modulus of 2846±705 Pa for the hybrid hydrogel functionalized with UPy-C1B. However, an average storage modulus of 2984±289 Pa was measured for the hydrogel functionalized with UPy-C1B without collagen, indicating no difference in storage moduli of the hydrogels with or without Upy-C1B and with or without collagen. Furthermore, comparable average storage moduli were measured for the pristine hydrogel, synthetic hydrogel functionalized with UPy-cRGD, and the hybrid hydrogel functionalized with UPy-cRGD, being 2577±185 Pa, 2445±430 Pa, and 3089±1025 Pa, respectively. Next the morphological properties of the hybrid hydrogel network as well as the UPy-C1B functionalized hybrid hydrogel network were explored. Collagen adhesion protein 35 (CNA35) was used to visualize the collagen network (**Figure 2B**). The collagen fibers within the UPy-C1B functionalized hybrid hydrogel seemed to form a slightly less dense network with increased distances between the

collagen fibers, compared with the collagen fibers within the hybrid hydrogel without UPy-C1B. This increased distance between the collagen fibers could be explained by a pulling effect between the peptide incorporated within the UPy-fibers and the collagen fibers within the hybrid hydrogel. Due to an interaction between the collagen fibers and the peptide, collagen fibers are 'captured' and 'pulled' towards the UPy-network. However, the obtained results do not provide enough information to prove this assumption. The observed differences are rather small and the obtained images were not sufficient for quantification of the data.

Primary keratocytes were encapsulated within the hybrid hydrogel functionalized with UPy-C1B to study the bioactivity of the additive. The cells were cultured in 3D for 21 days. Immunohistochemical staining of collagen type I demonstrated a homogenous distribution of collagen type I for the hybrid hydrogel functionalized with UPy-C1B. The hybrid hydrogel functionalized with UPy-C1B supported an elongated and healthy cell morphology of the encapsulated keratocytes. The primary keratocytes were simultaneously encapsulated within the synthetic hydrogel functionalized with UPy-cRGD, acting as a positive control. The observed cell density within the hybrid hydrogel functionalized with UPy-C1B corresponds with the cell density observed within the synthetic hydrogel (**Figure 2C**). Only a minimal deposition of intracellular collagen type VI was observed for the cells encapsulated in both hydrogels.

Investigating the interaction between UPy-C1B and collagen produced by encapsulated cells

Hydrogels are functionalized with peptide additives for various purposes. Here, the UPy-cRGD is used as a synthetic ligand to induce cell binding to the biomaterial. The synthesized UPy-C1B is hypothesized to bind to collagen type I fibers produced and deposited by the cells. Due to this interaction between the hydrogel network and the cellular collagen we aimed to create a hydrogel with an enhanced ability to maintain the cellular produced collagen, contributing to the formation of their own native microenvironment. To study the binding affinity of the UPy-C1B peptide additive to the cellular collagen fibers, human corneal keratocytes (HCKs) were encapsulated within a synthetic hydrogel functionalized with UPy-cRGD and UPy-C1B. The HCKs need several days to deposit collagen fibers, for this purpose the cellular collagen production was monitored on day 7, 14, and 21 during culture. Similar cell densities and cell morphologies were observed for HCKs cultured in both the synthetic hydrogel functionalized with UPy-cRGD (**Figure 3A**), acting as a control, and the synthetic hydrogel functionalized with both UPy-cRGD

and UPy-C1B (**Figure 3B**). Immunohistochemical staining was used to visualize the deposited collagen type I, type V, and type VI. The results of both hydrogels demonstrated an increase in deposition of cellular collagens from day 7 to day 21. However, the cellular collagen deposition within the hydrogel functionalized with solely UPy-cRGD and the cellular collagen deposition within the hydrogel functionalized with both UPy-cRGD and UPy-C1B showed to be very similar. Therewith, these results did not provide enough information to indicate an interaction between the used UPy-C1B peptide additive and the collagen fibers produced by the cells.
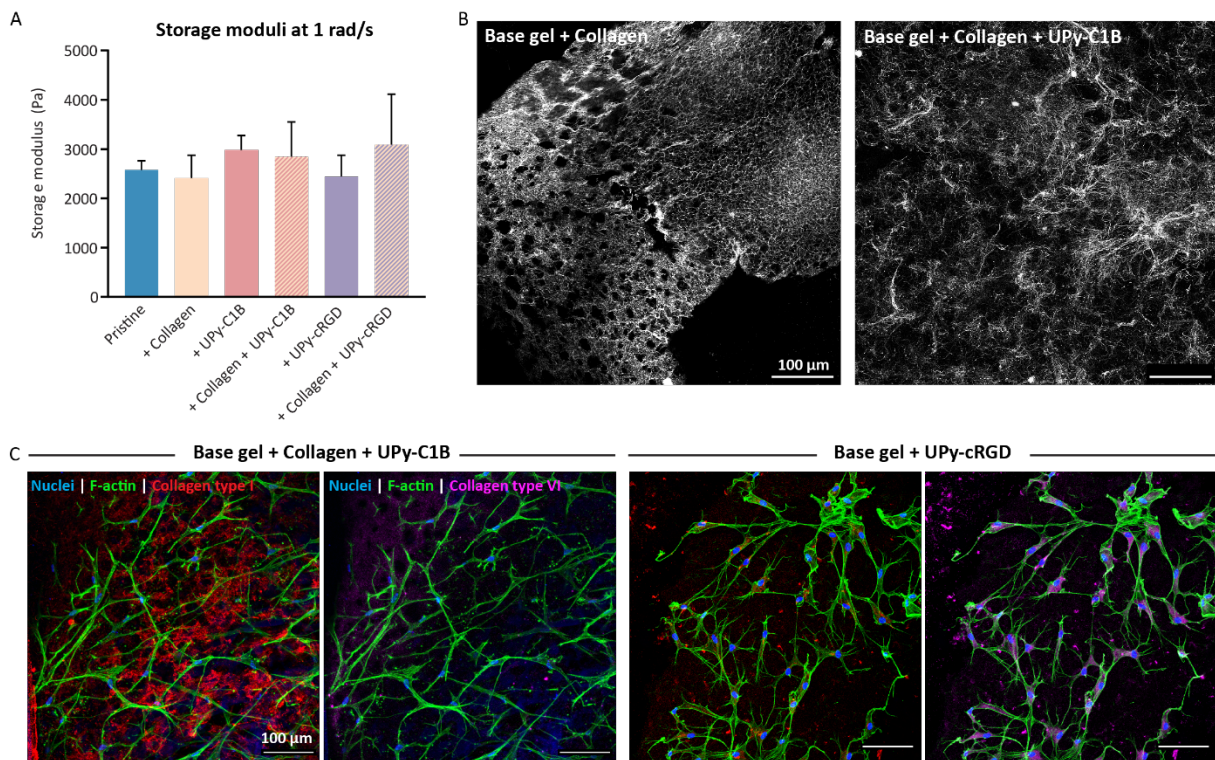
Figure 2. Mechanical, morphological, and biological properties of various hydrogels of 2.5 wt/v%. **A)** Storage moduli at 1 rad/s, sample size n=3, mean ± standard deviation presented. **B)** Confocal image of the collagen network within the studied hydrogels, stained with CNA35. **C)** Confocal image of immunohistochemical staining of the nuclei (blue), F-actin (green), collagen type I (red), and collagen type VI (purple). An elongated cell morphology is observed for the keratocytes encapsulated within the hybrid hydrogel functionalized with UPy-C1B and the synthetic hydrogel functionalized with UPy-cRGD. Keratocytes were cultured for 21 days.
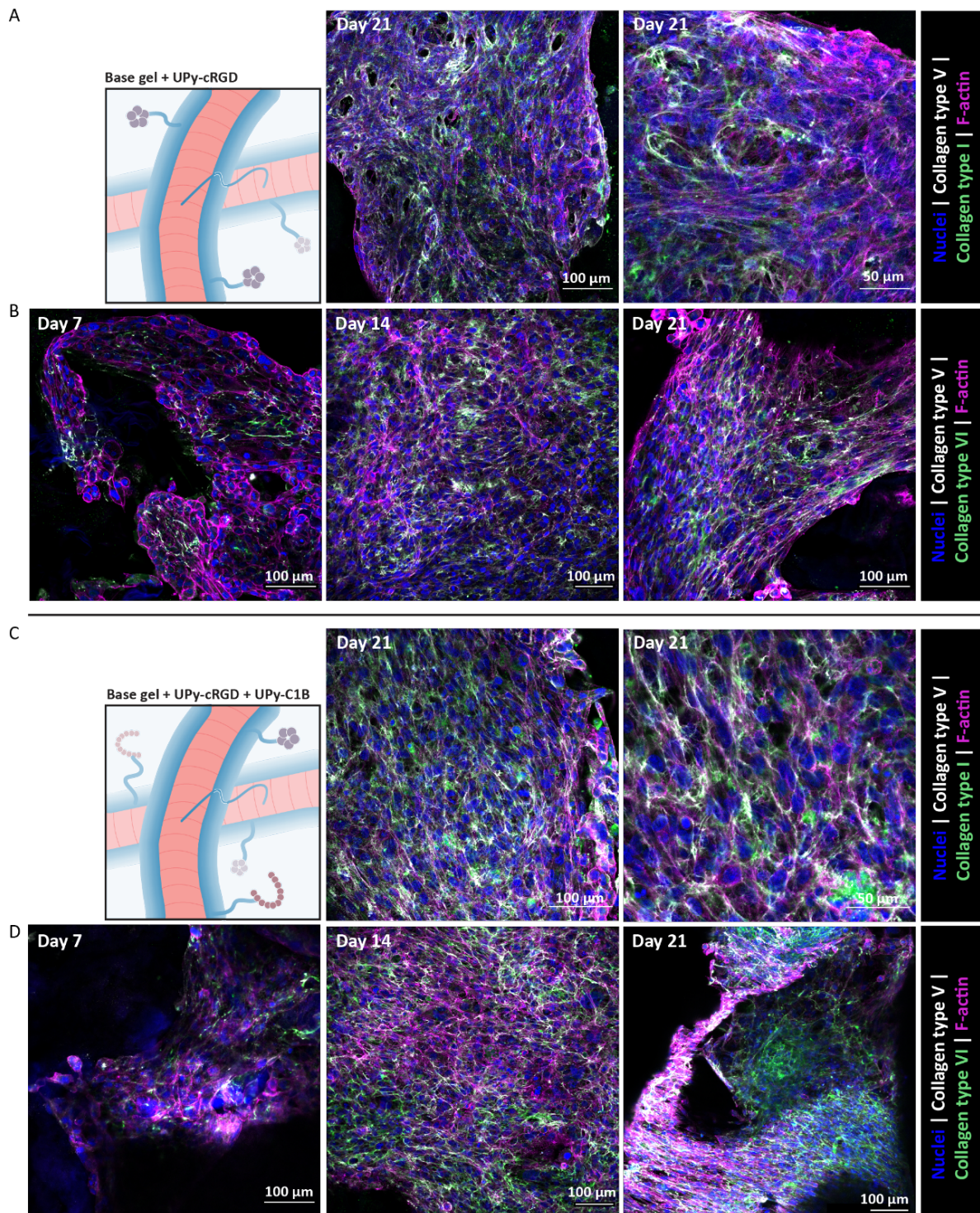
Figure 3. Similar collagen type I, V, and VI deposition upon encapsulation and 21-day 3D culture of human corneal keratocytes within synthetic hydrogels functionalized with or without UPy-C1B. **A)** Hydrogel functionalized with UPy-cRGD, nuclei in blue, collagen type V in white, collagen type I in green, F-actin in magenta. **B)** Hydrogel functionalized with UPy-cRGD, nuclei in blue, collagen type V in white, collagen type VI in green, F-actin in magenta. **C)** Hydrogel functionalized with UPy-cRGD and UPy-C1B, nuclei in blue, collagen type V in white, collagen type I in green, F-actin in magenta. **D)** Hydrogel functionalized with UPy-cRGD and UPy-C1B, nuclei in blue, collagen type V in white, collagen type VI in green, F-actin in magenta.

Comparison of mechanical, morphological, and biological properties upon introducing UPy-C1B peptide into a lower weight per volume percentage (wt/v%) hybrid hydrogel

Both the experiments described above were executed with hydrogels at a weight per volume percentage of ~ 2.5%. With storage moduli ranging between 2410 ±464 Pa and 3089 ±1025 Pa, it was assumed that the hydrogels were too stiff to measure any affinity of the UPy-C1B peptide additive with collagen fibers. During the following experiments, UPy-C1B was incorporated within lower weight per volume percentage hydrogels, aiming to observe an affinity of the UPy-C1B peptide with collagen fibers. As a control, to study and compare the morphological properties of the various hydrogels, a full collagen based hydrogel was implemented in this study. Upon heating to physiological conditions, the full collagen based hydrogel formed a soft viscoelastic network with a storage modulus of 56 ±2 Pa (**Figure 4A**). By lowering the weight per volume percentage to 0.3 wt/v% it was achieved to generated a synthetic hydrogel functionalized with UPy-cRGD with a similar storage modulus. Interestingly, when UPy-cRGD was replaced with collagen, a small enhancement in the storage modulus was observed, resulting in a storage modulus of 84 ±18 Pa. This indicates a small cooperative effect between the synthetic and natural component in this hybrid network. Incorporation of UPy-C1B enhanced the storage modulus of the hybrid network, resulting in a storage modulus of 111 ±3 Pa. Remarkably, initial UPy-C1B functionalization of the hydrogel significantly weakened the hydrogel, resulting in a much lower storage modulus of 20 ±0.5 Pa. Only, upon combining the UPy-C1B with collagen a large increase in the storage modulus was observed, showing the strong cooperative interaction between the natural and synthetic components that was achieved here.

For visualization, collagen was stained with CNA35, while UPy-Cy5 was incorporated into the bundles to visualize the UPy-network, taking advantage of the supramolecular nature of the system. The full collagen hydrogel formed a thin fiber-like network, while the pristine UPy-based hydrogel formed a network with thicker bundles and larger pores (**Figure 4B, C**). For the hybrid hydrogel, mixing UPy and collagen, both morphologies remained present, showing formation of a double network where UPy and collagen seemed to form their own network morphology, independently of one-another but also not hindering the network formations (**Figure 4D**). Morphological differences were observed once the UPy-C1B was incorporated in the network (**Figure 4E**). While the collagen network maintained its heterogenous mesh-like

structure with thin fibers, the UPy-fibers were thicker and more clustered alongside the collagen network, showing a large effect from the additional linker between the networks.

Primary keratocytes were encapsulated and cultured in 3D for three days to allow the cells to adhere to the hydrogel and to study the biocompatibility of the soft hydrogels. Keratocytes with a round-shaped morphology were observed in the natural full collagen hydrogels (**Figure 5A**), while elongated cell morphologies were observed in both the synthetic hydrogel functionalized with UPy-cRGD and the hybrid hydrogel functionalized with UPy-C1B (**Figure 5B, C**).
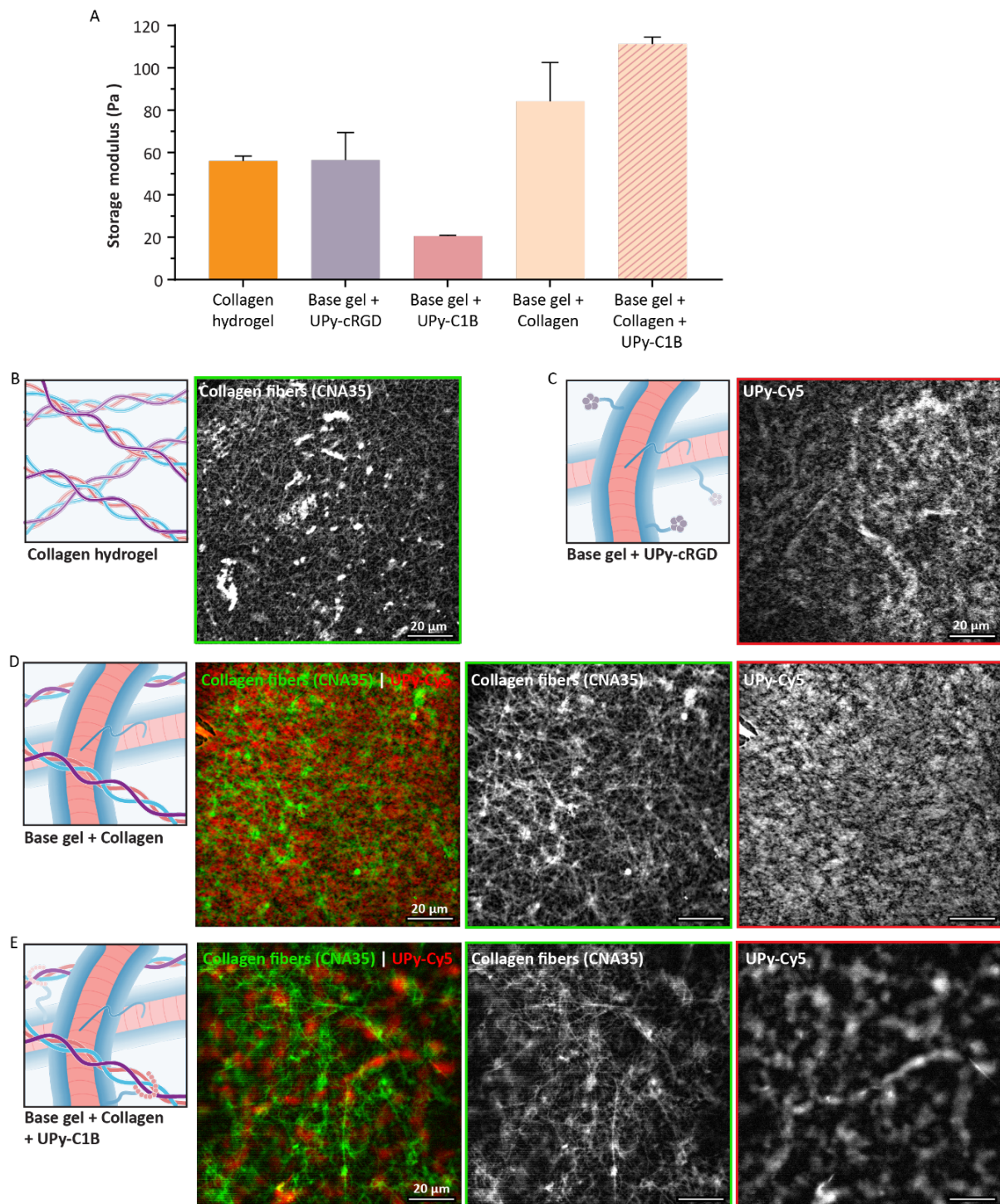
Figure 4. Mechanical and morphological properties of various hydrogels of 0.3 wt/v%. **A)** Storage moduli, sample size n=2, mean ± standard deviation presented. **B)** Confocal image of the collagen based hydrogel stained with CNA35, showing a thin fiber-like network. **C)** Confocal image of the hydrogel functionalized with UPy-cRGD, showing a mesh-like hydrogel with thicker bundles and larger pores compared to collagen. **D)** Merged and single channel images of the hybrid hydrogel, with collagen in green and UPy in red, showing formation of a double network with a homogenous distribution of UPy and collagen. **E)** Merged and single channel images of the hybrid hydrogel functionalized with UPy-C1B, showing formation of an interactive network, in which the UPy fibers are more clustered around the collagen network.
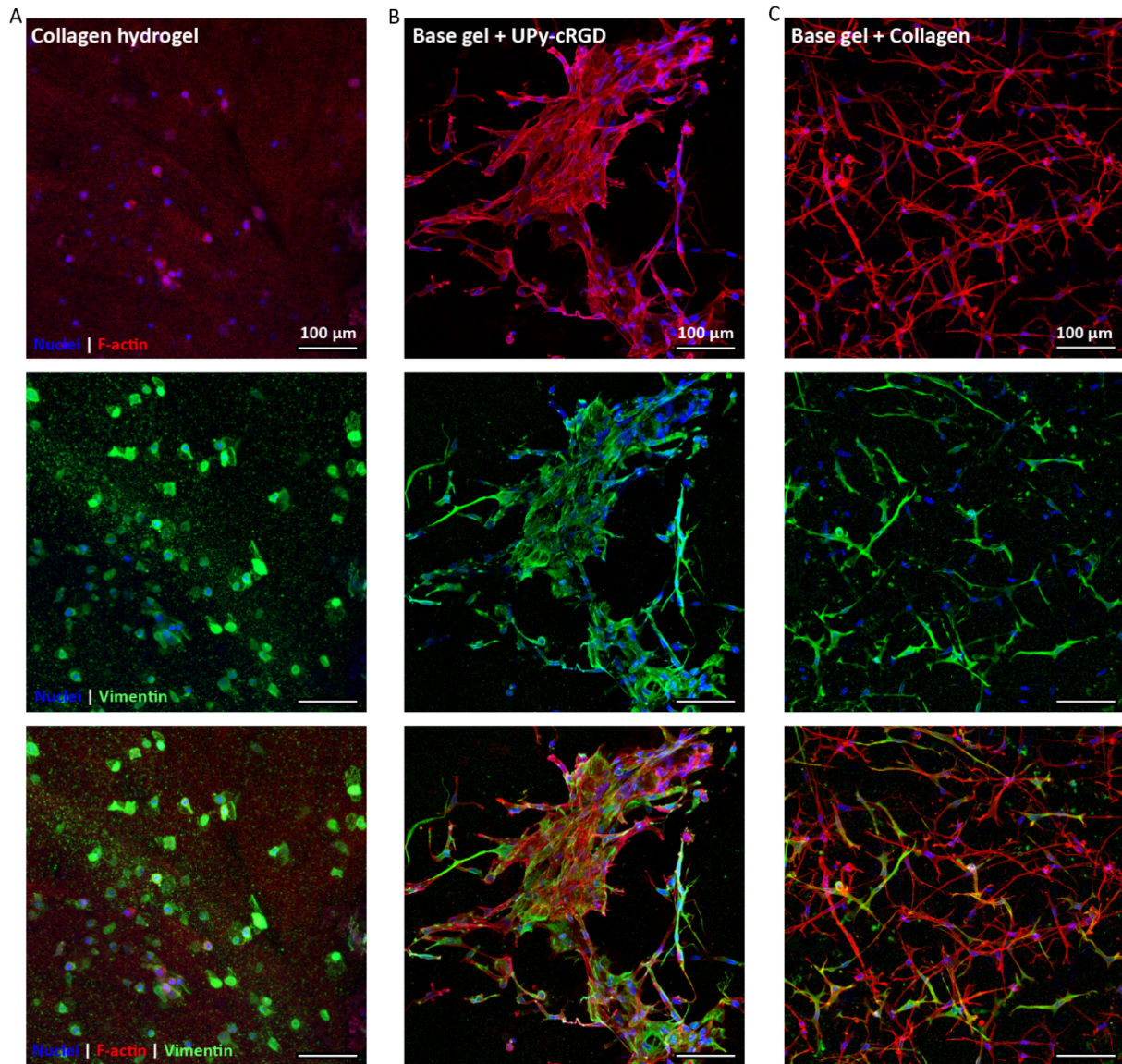
Figure 5. Immunohistochemical staining of the nuclei (blue), F-actin (red), and vimentin (green) showing a round-shaped keratocytes when encapsulated within the full collagen hydrogel, while observing an elongated cell morphology for the keratocytes encapsulated within the synthetic hydrogel functionalized with UPy-cRGD and the hybrid hydrogel functionalized with UPy-C1B. Keratocytes were cultured for 3 days. **A)** Cell images of keratocytes encapsulated within full collagen gel. **B)** Cell images of keratocytes encapsulated within synthetic hydrogel functionalized with UPy-cRGD. **C)** Cell images of keratocytes encapsulated within hybrid hydrogel functionalized with UPy-C1B.

Cell-gel interactions mimic complex cell-matrix behavior

Since active cell spreading and a healthy morphology of the keratocytes were only observed for the synthetic and the hybrid hydrogels, only these hydrogels were used during the succeeding experiments. To investigate the influence of cells on the mechanical properties of the hydrogels, the hydrogels including the encapsulated cells were transferred to the rheometer after a 3-days cell culture. Although spreaded cells were still observed in the synthetic hydrogel functionalized with UPy-cRGD, no significant increase in storage modulus was observed for this pure synthetic matrix (**Figure 6A**). The hybrid network without the additional crosslink, showed an increase of 47% in stiffness (**Figure 6B**). Similarly, the stiffest hydrogel network, *i.e.* the hybrid hydrogel functionalized with UPy-C1B showed a significant stiffening effect during culture (**Figure 6C**). The spreaded cells actively increased the storage modulus with 33%, showing the active role of cellular behavior on the mechanical properties of these matrices. Interestingly, the presence of cells within both the hybrid hydrogel as well as the hybrid hydrogel functionalized with UPy-C1B resulted in similar stiffnesses of the cell/hydrogel constructs. These results imply a possible rearrangement of the network in presence of cells, rendering the additional crosslink less relevant over prolonged time periods, in which cells rearrange the network. Overall, these results showed a complex interplay between cells and the gel, were cell adhesion and spreading actively changed bulk mechanical properties in a reciprocal interplay, mimicking the complex *in vivo* cell-ECM interplay.

The hybrid hydrogel induced the largest increase in storage modulus, for this purpose this condition was analyzed in more detail by analyzing the expression of yes-associated-protein (YAP) in the cells. YAP is a mechanosensitive transcriptional regulator, which is on a mechanical level regulated by mechanical cues such as matrix rigidity, strain or adhesive area.[25] The results of the hybrid hydrogel, showing the largest increase in stiffness after a cell culture of 3 days, demonstrated an increase of YAP expression in the nuclei compared with the overall YAP expression in the cytoplasm of the keratocytes (**Figure 6E**). Pathways involving YAP translocation to the nucleus are known to allow the cells to perceive ECM mechanics and to spread.[26] The results demonstrated the presence of mechanotransduction within the hybrid hydrogel, which was translated into the rearrangement of the mechanical properties due to an interactive interplay between the cells and the gel resulting in a 47% increased storage modulus.
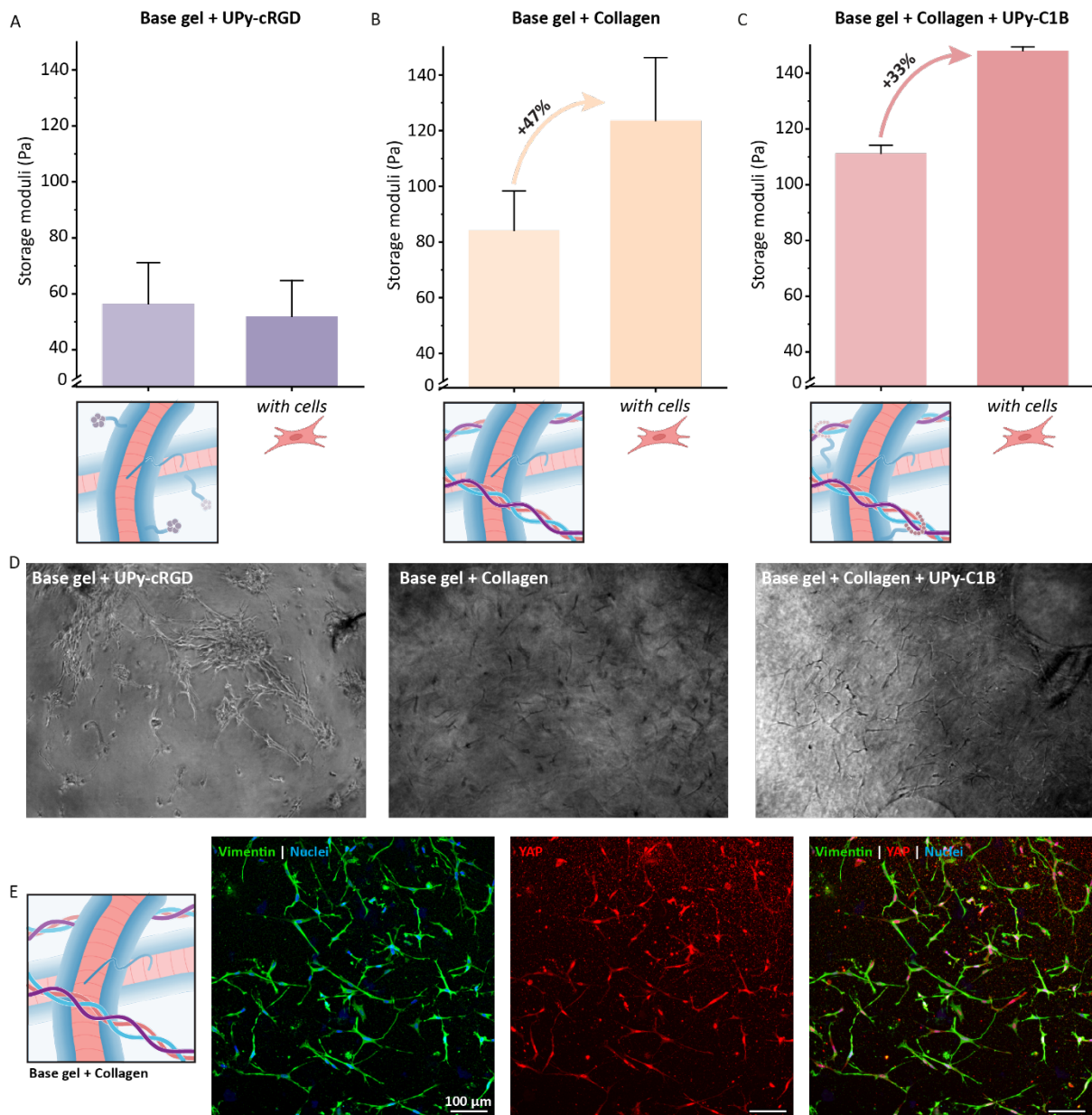
Figure 6. Effects of cellular tractions on the mechanical properties after three days of 3D culture. **A)** Obtained storage modulus of the synthetic hydrogel functionalized with UPy-cRGD in the absence and presence of cells, showing no significant difference in storage moduli, mean ± standard deviation presented. Even although cells were still able to spread (Brightfield image below, taken just before measurement). **B)** Storage modulus of the hybrid hydrogel in the absence and presence of cells, where addition of cells enhanced the stiffness with 47%, attributed to the presence of spreaded cells, mean ± standard deviation presented (Brightfield image below, taken just before measurement). **C)** Storage modulus of the hybrid hydrogel functionalized with UPy-C1B in the absence and presence of cells, showing that addition of cells increased the stiffness with 33%, mean ± standard deviation presented (Brightfield image below showing spreaded cells, taken just before measurement). **D)** Brightfield images of the cells taken just before the measurement. **E)** Immunohistochemical staining of keratocytes cultured for 3 days within the hybrid hydrogel (without UPy-C1B), vimentin in green, YAP in red, and nuclei in blue.

The ability of keratocytes to influence the dynamic properties of their surrounding synthetic or hybrid microenvironment.

Previously we focused on the influence of cells on the storage moduli of the hydrogels, here we focus on the ability of the cells to influence the dynamics of the hydrogel networks. Stress relaxation measurements were used to determine the network dynamics; an initial strain was applied, and the stress decay was followed over time. The obtained relaxation curves were fitted with a continuous relaxation spectrum, which provided insights into the underlying relaxation mechanisms. Samples with and without cells were compared to study the effects of cell induced changes on the network dynamics. Previously, no significant changes in stiffness of the synthetic hydrogel functionalized with UPy-cRGD were observed. The analysis of the relaxation mechanisms again highlights the similarity in the hydrogel networks with and without cells (**Figure 7A**). Interestingly, the relaxation spectra of the hybrid hydrogels showed the presence of two clear relaxation mechanisms (**Figure 7B**), in contrast to the single relaxation mechanism showed by the synthetic network. These spectra indicate the formation of an interactive network with a more complex relaxation pattern. Incorporation of UPy-C1B as an additional link between the natural and synthetic systems even further increased the complexity of the mechanisms, resulting in a much more complicated spectrum of various mechanisms underlying the formation of a complicated interactive network (**Figure 7C**). A substantial change in the relaxation spectrum was observed upon the presence of cells within the hybrid hydrogel network functionalized with UPy-C1B. The interaction between cells and the hydrogel network resulted in a shift of the spectrum towards two clear distinct mechanisms. These two mechanisms are remarkably at the same time scales as the hybrid network without UPy-C1B, yet with the faster relaxation mechanism being slightly more dominant compared to the spectra of the hybrid network without UPy-C1B. Together, these results showed the complex cell-gel interactions, in which cells actively change the mechanics and dynamics of their surroundings via the rearrangement of certain crosslinks (*i.e.* UPy-C1B). Due to the substantial influence of the cells on the gel network, the additional links induced by UPy-C1B became less relevant.
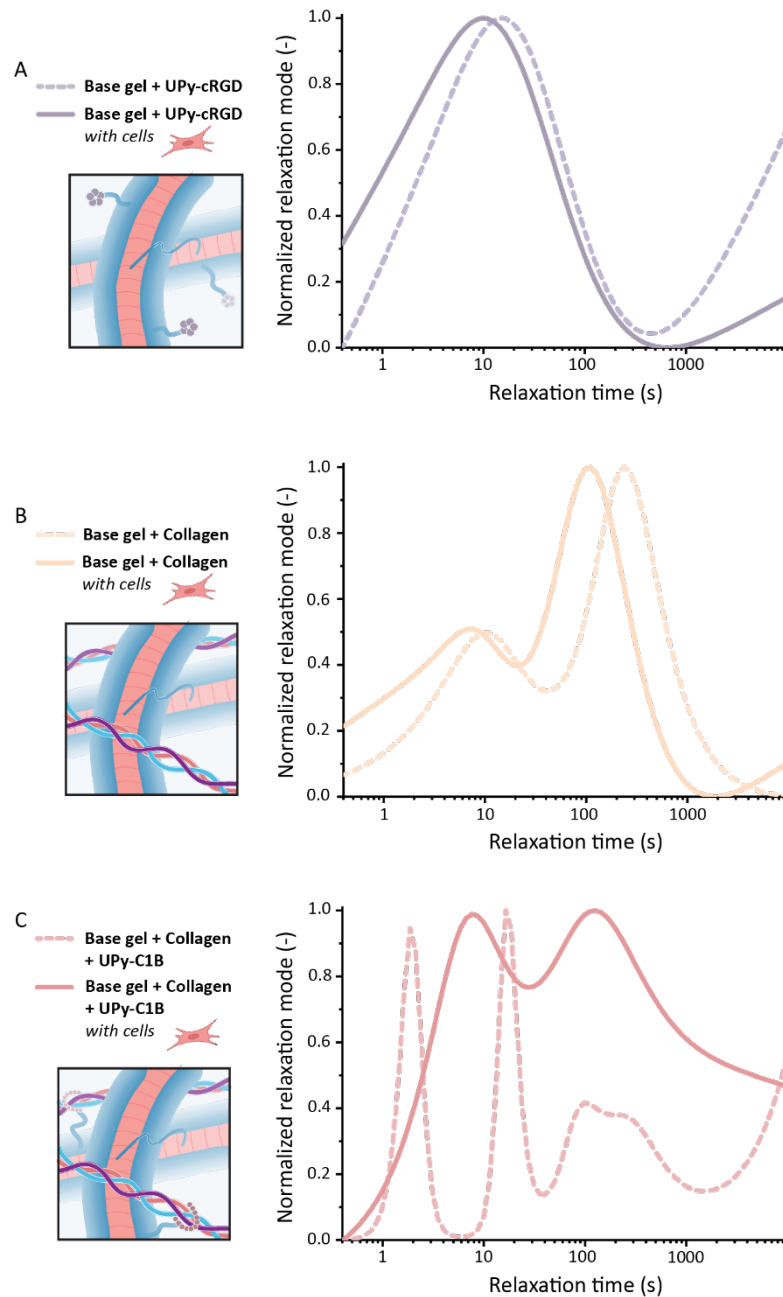
Figure 7. Dynamical changes of cell-matrix induced by cells. **A)** Obtained relaxation spectra form the hydrogel functionalized with UPy-cRGD in the absence and presence of cells, were short time scales were dominant. **B)** Obtained relaxation spectra for the hybrid hydrogel, showing that in the presence of cells, relaxation mechanisms shifted to shorter time scales while an additional longer relaxation mechanism is suggested (> 1000s). **C)** Relaxation spectrum of the hybrid hydrogel functionalized with UPy-C1B, showing a complete change in the presence of cells, with only two peaks present instead of four.

CONCLUSIONS

Here, we introduced a collagen binding peptide additive to functionalize supramolecular hydrogels, and to strengthen the interaction within a hydrogel between the synthetic UPy-fibers and natural collagen fibers, which are either manually added or produced by cells. Incorporation of the UPy-C1B into the hybrid hydrogel resulted in an increase of the storage modulus as well as morphological changes of the network, indicating a strong interaction between the synthetic components of the UPy-stacks and the natural collagen fibers of the hybrid hydrogel. Moreover, this work demonstrates the ability of cells to actively probe their surrounding gel matrix by altering the initial properties of the gel. Within both the hybrid hydrogel without additives and the hybrid hydrogel functionalized with UPy-C1B the interaction between the encapsulated cells and the gel resulted in increased storage moduli of both hydrogel networks. These results demonstrate the impact of cells on the mechanical properties of the hydrogels, indicating the capability of cells to rearrange their surrounding matrix. Herewith, we achieved to mimic the complex *in vivo* cell-matrix interplay within the hybrid hydrogel construct with or without UPy-C1B incorporation. Overall, via incorporation of a collagen binding peptide additive, we introduced a promising and novel hybrid hydrogel construct, comprising a great bioactivity as well as controlled physical properties.

EXPERIMENTAL SECTION

Synthesis of UPy- GCGGPAQMWVH peptide additive via maleimide-thiol conjugation

The Gly-Cys-Gly-Gly-Pro-Ala-Gln-Met-Trp-Val-His peptide was synthesized using standard Fmoc solid-phase peptide synthesis on a rink amide resin at 0.1 mmol scale. The Fmoc-group was removed using 20 v/v% piperidine in DMF for 2x15 minutes, while still on the rink amide resin. Subsequently, the peptide was cleaved from the resin in a 90:2.5:2.5:5 v/v% TFA:TIS:H_2O:EDT for 2 hours. The cleavage mixture was precipitated 6x in ice-cold Et_2O. Preparative reverse phase LC-MS on a C18 column using a gradient of 20-25% of acetonitrile in H_2O, containing 0.1% TFA was used to purify the crude compound. The GCGGPAQMWVH peptide was attached to the UPy-moiety via maleimide-thiol chemistry, where Tris(2-carboxyethyl)phosphine (TCEP) is used to cleave the sulfide bonds and therewith activate the thiol in the cysteine to react with the maleimide. *Jingyi Huang performed the conjugation of GCGGPAQMWVH to the UPy-maleimide.*

Human corneal keratocyte (HCK) cell culture

Human corneal keratocyte (HCK) cell lines were obtained as a kind gift from Dr. Zorn-Kruppa (University Medical Center Hamburg). The HCK cell line was derived from the human corneal stroma and immortalized through SV-40 transfection, and has been previously demonstrated to mimic both the phenotype and the response to growth factor stimulations of their primary precursors.[27,28] HCK cells were cultured in Dulbecco's Modified Eagle's Medium (DMEM, Sigma-Aldrich) supplemented with 5% FBS (Biochrom), and 1% penicillin/streptomycin at 37 °C, 21% O_2 and 5% CO_2 until ±80% confluency was reached. Due to activation of the cells by the FBS supplementation, the HCK cells can be considered activated keratocytes, resembling a fibroblastic phenotype. Cells were passaged twice a week, and cells between passages 5 and 10 were used for the experiments described.

Primary keratocyte (PK) cell culture

Primary human keratocytes were isolated from leftover human corneoscleral transplant material from Descemet Membrane Endothelial Keratoplasty surgery, which were obtained from the Cornea Department of the ETB-BISLIFE Multi-Tissue Center (Beverwijk, the Netherlands). The keratocytes were cultured in expansion medium (1:1 mixture of Dulbecco's modified Eagle's medium/F-12 supplemented with GlutaMAX (DMEM/F12 (Ham) + GlutaMAXTM, 10565-018; Gibco), 5% Fetal Bovine Serum (FBS, Biochrom AG), 1% penicillin/streptomycin (P/S, Biochrom AG), and 1 mM L-ascorbic acid 2-phosphate sesquimagnesium salt hydrate (Vitamin C, Sigma A8960)) at 37 °C, 21% O_2 and 5% CO_2 until ±80% confluency. Since the medium contained FBS, keratocytes were

considered to be activated matrix-producing cells, referred to as stromal fibroblasts (SFs). To initiate cell (re-)differentiation towards corneal stromal keratocytes, another medium composition was used: differentiation medium (Dulbecco's modified Eagle's medium supplemented with GlutaMAX (GlutaMAXTM, 11880-028; Gibco), 1% penicillin/streptomycin (P/S, Biochrom AG), and 1 mM L-ascorbic acid 2-phosphate sesquimagnesium salt hydrate (Vitamin C, Sigma A8960), 1x ITS (Sigma, I3146), 2 mg/mL D-glucose (Invitrogen, 15023021), 2.5 mg/mL D-mannitol (Fluka, 63560)).[29] Cells were cultured with medium changes every 3 days, keratocytes from multiple donors were used up to passage #3. TrypLE Express Enzyme (1x), no phenol red (12604013, Gibco) is used to detach the cells from the culture flask and use them for experiments.

Preparation of 2.5 wt/v% hydrogels for rheology and cell encapsulation

Both the bifunctional as well as the monofunctional building blocks were received as powders. The bifunctional molecules (UPy-PEG$_{10K}$-UPy) were dissolved at 70 °C in an neutral PBS solution for 1.5 hours. Monofunctional molecules (UPy-Glycine or UPy-Glycine + UPy-cRGD) were dissolved at 70 °C in an alkaline PBS solution (containing 160 mM NaOH) for 20 minutes. After completely dissolving the powders of the bifunctional and monofunctional building blocks, the solutions were cooled down to room temperature. A specific volume of HCl solution (2 M) was added to the solution of monofunctional molecules to reach a neutral pH. Cell culture medium is added to both solutions 1:1, to provide the cells already with some nutrients during the gelation process later on in the procedure. Afterwards, both solutions are transferred from a glass vial to a sterile Eppendorf tube, from this step onwards a safety cabinet is used to guarantee a sterile work environment. The solutions were disinfected by exposing them to UV-light for 20 minutes. Subsequently, the cells were prepared and counted, the following cell concentrations were used during the experiments:

HCKs: 100 cells/mL | Primary keratocytes: 100 cells/µL

The cells needed for encapsulation were suspended in the correct amount of medium and this cell suspension was added to the solution of bifunctional molecules. Due to the addition of the cells suspension, the bifunctional molecules were diluted. To correct for this extra dilution step, the initial concentration of the bifunctional molecules was slightly higher (0.78 wt/v% instead of 0.52 wt/v%). For every experiment the bifunctional molecules were diluted with 1/3 of cell suspension, resulting in a final 0.52 wt/v% of bifunctional molecules. All the gels were prepared in wells of a non-adhesive 96-well plate (Fisher Scientific, Nunclon Sphera-Treated, U-Shaped-Bottom plate 15227905).

Hydrogels used for rheology:

At first 50 μL monofunctional molecules (pristine: only UPy-Glycine, +collagen: only UPy-Glycine, +C1B: UPy-Glycine and UPy-C1B, +collagen +C1B: UPy-Glycine and UPy-C1B, +cRGD: UPy-Glycine and UPy-cRGD, +RGD +collagen: UPy-Glycine and UPy-cRGD) solution were added to a well, than only medium was added to the solution of the bifunctional molecules and mixed thoroughly. Secondly 50 μL of this mixture was added to the 50 μL monofunctional molecules solution inside the well. The molecules were mixed by carefully pipetting up and down (at least 3x per well), any air bubbles were removed by using a needle. All the hydrogels were incubated at 37 °C, 21% O_2 and 5% CO_2 for 1 hour to allow for proper gelation. After 1 hour, phosphate buffered saline (PBS) to embed the gels was carefully added to the wells, and the hydrogels were placed back in the incubator at 37 °C, 21% O_2 and 5% CO_2 for ~ 24h before rheological measurements were performed.

Synthetic hydrogel (+UPy-additives):

First 50 μL monofunctional molecules in solution were added to a well. Meanwhile, the cells were added to the solution of bifunctional molecules and mixed thoroughly. Second, 50 μL of bifunctional molecules / cell mixture were added to the 50 μL solution of monofunctional molecules inside the well. The molecules were mixed by carefully pipetting up and down (at least 3x per well), any air bubbles were removed by using a needle.

Hybrid hydrogel functionalized with UPy-C1B:

For hybrid hydrogel preparation collagen type I (Gibco, Collagen I bovine, A1064401) was added to the solution of the bifunctional molecules, 20 μL was added per 100 μL complete gel (0.1 Wt/v%). Initially, the bifunctional molecules were dissolved at a higher wt/v% compared with the bifunctional molecules used for the synthetic or pristine hydrogel, to correct for this extra dilution step with the collagen. At first, 50 μL solution of monofunctional molecules was added to a well. The cells and the collagen were added to the solution of bifunctional molecules and mixed thoroughly. Second, 50 μL of bifunctional molecules / cell / collagen mixture were added to the 50 μL solution of monofunctional molecules inside the well. The molecules were mixed by carefully pipetting up and down (at least 3x per well), any air bubbles were removed by using a needle.

For the exact hydrogel compositions, see **table 1**. All the hydrogels were placed in the incubator at 37 °C, 21% O_2 and 5% CO_2 for 1 hour to allow for proper gelation. After 1 hour, medium to embed the gels was carefully added to the wells, and the hydrogels with encapsulated cells were placed back in the incubator at 37 °C, 21% O_2 and 5% CO_2. After 1 day, the cell culture medium to embed the hydrogel was refreshed, and during the 21-day culture the medium was refreshed every 2-3 days.

Table 1. Overview of the hydrogel compositions of the 2.5 wt/v% hydrogels studied. Calculations were made for one complete hydrogel of 100 μL.

Building block / additive	Ratio	μmol	mM	Wt/v %	Concentration (mg/ml)
Pristine hydrogel (no additives)					
UPy-PEG$_{10K}$-UPy	1	0.023	0.234	0.26	
UPy-Glycinamide	80	1.88	18.75	2.24	
+ collagen (hybrid hydrogel)					
UPy-PEG$_{10K}$-UPy	1	0.023	0.234	0.26	
UPy-Glycinamide	80	1.88	18.75	2.24	
Collagen				0.1	1
+ UPy-C1B					
UPy-PEG$_{10K}$-UPy	1	0.023	0.234	0.26	
UPy-Glycinamide	75.6	1.77	17.72	2.12	
UPy-C1B	4.4	0.103	1.03	0.25	
+ collagen + UPy-C1B (hybrid hydrogel functionalized with UPy-C1B)					
UPy-PEG$_{10K}$-UPy	1	0.023	0.234	0.26	
UPy-Glycinamide	75.6	1.77	17.72	2.12	
UPy-C1B	4.4	0.103	1.03	0.25	
Collagen				0.1	1
+ UPy-cRGD (synthetic hydrogel)					
UPy-PEG$_{10K}$-UPy	1	0.023	0.234	0.26	
UPy-Glycinamide	75.6	1.77	17.72	2.12	
UPy-cRGD	4.4	0.103	1.03	0.18	
+ collagen + UPy-cRGD (synthetic hydrogel functionalized with UPy-C1B)					
UPy-PEG$_{10K}$-UPy	1	0.023	0.234	0.26	
UPy-Glycinamide	75.6	1.77	17.72	2.12	
UPy-cRGD	4.4	0.103	1.03	0.18	
Collagen				0.1	1
+ UPy-cRGD + UPy-C1B (synthetic hydrogel)					
UPy-PEG$_{10K}$-UPy	1	0.023	0.234	0.26	
UPy-Glycinamide	71.2	1.67	16.69	1.99	
UPy-cRGD	4.4	0.103	1.03	0.18	
UPy-C1B	4.4	0.103	1.03	0.25	

Preparation of 0.3 wt/v% hydrogels for rheology and cell encapsulation

Hydrogels were prepared with the similar procedure as described above (2.5 wt/v% hydrogels). Except for the gelation time, the 0.3 wt/v% hydrogels were incubated for 2 hours (instead of 1 hour) at 37 °C to allow proper gelation. Upon encapsulation of cells within the 0.3 wt/v% hydrogels, the well plates were turned up-side-down during the gelation time. See **table 2** for the compositions. The full collagen hydrogel was prepared according to the provided procedure of the manufacturer (Gibco, Collagen I bovine, A1064401).

Table 2. Overview of the hydrogel compositions of the 0.3 wt/v% hydrogels studied. Calculations were made for one complete hydrogel of 100 μL.

Building block / additive	Ratio	μmol	mM	Wt/v %	Concentration (mg/ml)
+ collagen (hybrid hydrogel)					
UPy-PEG$_{10K}$-UPy	1	0.003	0.03	0.005	
UPy-Glycinamide	82	0.24	2.40	0.29	
Collagen				0.1	1
+ UPy-C1B					
UPy-PEG$_{10K}$-UPy	1	0.023	0.03	0.005	
UPy-Glycinamide	69.3	0.203	2.03	0.24	
UPy-C1B	12.8	0.04	0.37	0.09	
+ collagen + UPy-C1B (hybrid hydrogel functionalized with UPy-C1B)					
UPy-PEG$_{10K}$-UPy	1	0.023	0.03	0.005	
UPy-Glycinamide	69.3	1.77	17.72	0.24	
UPy-C1B	12.8	0.103	1.03	0.09	
Collagen				0.1	1
+ UPy-cRGD (synthetic hydrogel)					
UPy-PEG$_{10K}$-UPy	1	0.03	0.03	0.005	
UPy-Glycinamide	69.3	0.203	2.03	0.24	
UPy-cRGD	12.8	0.03	0.37	0.065	

Martin G.T.A. prepared many solvents to generate the hydrogels and prepared some of the pre-formed hydrogels used during rheological measurements as well.

Rheological measurements

A discovery hybrid rheometer (DHR-3, TA Instruments) was used for all the rheological measurements.

Measuring pre-formed hydrogels without cells

Hydrogels were made via above mentioned protocol inside a polystyrene 96 well F-bottom cell culture microplate (Greiner bio-one, 655180). After formation, the gels were left 24 hours incubated in PBS at 37 °C. For measurement, gels were transferred onto the peltier plate and a flat stainless-steel plate-plate geometry (diameter = 8 mm) was used. The geometry was slowly lowered, to prevent sample damage, until the sample completely filled the geometry, resulting in a gap height of 625 – 1050 μm. Low viscosity oil (47 V 100, RHODORSIL®) was applied to seal the gap around the hydrogel to minimize evaporation or drying during the measurements which were performed on 37 °C.

Measuring pre-formed hydrogels with cells

To determine mechanical changes on a longer time scale (72h), gels were formed in a 96 well plate at 37 °C and after 1 hour overlayed with cell medium. During the 72h, the gels were stored inside a cell incubator at 37°C, 21% O_2 and 5% CO_2. After 3 days, gels were transferred to a DHR3 rheometer (37 °C), equipped with a 8 mm stainless steel plate-plate geometry. The geometry was slowly lowered until the gel made full contact with the top plate (gap: ~ 500 um). Silicon oil (47 V 100, RHODORSIL®) was used around the gel to prevent sample drying during the measurement. All subsequent measurements were performed at 37 °C. Frequency sweeps were measured with frequencies ranging from 100 to 0.1 rad s-1, at a constant strain of 1%. Amplitude sweeps were measured with strain ranging from 0.1 to 100 %, at a constant frequency of 1 rad/s. Stress relaxation experiments were performed by applying a strain of 7.5 % (strain rise time: 0.9 s), and measuring the generated stress for 1000 seconds. The data were normalized using the stress generated after 2 s. Continuous time relaxation spectra were calculated by averaging two stress relaxation spectra between 4 s and 1000 s. The resulting G(t) was then fitted via the rheology TRIOS software using:

$$G(t) = G_e + \int_{-\infty}^{+\infty} Hln(\tau)e^{-t/\tau}d\ln\tau$$

The obtained H_i values were then plotted vs τ and normalized using the highest and lowest H_i value.

Martin G.T.A. Rutten performed all the rheological measurements presented in this study and analyzed the data including all the necessary calculations.

Staining of the collagen network using CNA35

The hydrogels stained with CNA35 were prepared similarly as the hydrogels without cells, used for rheology measurements. At first a CNA35-mcherry staining solution was made with 1:50 dilution. The PBS was replaced with the CNA35 staining solution and incubated for 1.5 hours. Afterwards the hydrogels were washed 3x 5 minutes with PBS. During imaging, complete/intact hydrogels were placed on a thin coverslip (24x69 mm, VWR 631-1575) immerged in mowiol 4-88 (Sigma Aldrich, 81381) and imaged using Leica TCS SP8 X inverted confocal microscope (Leica Microsystems) using HC PL APO CS2 objectives (20x/0.75, 40x/0.95, 63x/1.4). Images were processed in ImageJ. *Some of the images shown in this work were acquired by Martin G.T.A. Rutten.*

Cell staining and Imaging

Before immunohistochemical stainings were carried out, the hydrogels were washed 3x with PBS (5 min per wash). All cells encapsulated within the hydrogels were fixated for 20 minutes at room temperature using 3.7% paraformaldehyde (formalin 37%, 104033.1000, Merck). After washing with PBS, samples were permeabilized for 15 minutes with 0.5% Triton X-100 in PBS. Followed by adding a blocking solution of 10% donkey or goat serum in 0.05% Triton X-100 in PBS for 30 minutes. Next, the cells were incubated with the primary antibodies diluted in 2% donkey serum in 0.05% Triton X-100 in PBS overnight at 4 °C. Thereafter, the cells were washed thoroughly with 0.05% Triton X-100 in PBS, including wash waiting steps of 5-10 min. Next, the gels were incubated with the secondary antibodies and phalloidin at room temperature for 2 hours. Finally, the cells were stained with DAPI at a dilution of 1:250 for 10 min and washed thoroughly with PBS (including was waiting steps of 5-10 min). During imaging, complete/intact hydrogels were place on a thin coverslip (24x69 mm, VWR 631-1575) immerged in mowiol 4-88 (Sigma Aldrich, 81381) and imaged using Leica TCS SP8 X inverted confocal microscope (Leica Microsystems) using HC PL APO CS2 objectives (20x/0.75, 40x/0.95). Images were processed in ImageJ to create a max-projection image of the original z-stack. See **table 3** for the primary and secondary antibodies used within this study.

Table 3. Overview of the used dyes, primary-, and secondary antibodies.

Antibody / dye	Company / reference #	Dilution
4',6-diamidino-2-phenylindole dihydrochloride (DAPI)	Sigma-Aldrich, D9542	1:250
Phalloidin 488	Sigma-Aldrich	1:300
Phalloidin 555	Sigma-Aldrich	1:300
Anti-Collagen type I	C2456, Sigma	1:250
Anti-Collagen type V	1350-01, Southem Biotech	1:250
Anti-Collagen type VI	70R-CR009x, Fitzgerald	1:250
Anti-Vimentin	Ab20346, Abcam	1:300
Anti-YAP1	Ab52771, Abcam	1:100
Secondary antibodies		
Anti-mouse IgG1 (goat) 555	A21127, Molecular Probes	1:250
Anti-mouse IgG1 (goat) 488	A21121, Molecular Probes	1:250
Anti-goat IgG (donkey) 488	A11055, Molecular Probes	1:250
Anti-rabbit IgG (donkey) 555	A31572, Molecular Probes	1:250
Anti-rabbit IgG (donkey) 488	A21206, Molecular Probes	1:250
Anti-rabbit IgG (donkey) 647	711-605-152 Jackson	1:250
Anti-rabbit IgG (goat) 647	A21244, Molecular Probes	1:250
Anti-rabbit IgG (goat) 555	A211428, Molecular Probes	1:250
Anti-mouse IgM (goat) 488	A21042, Molecular Probes	1:250

All stainings were performed with a combination of solely donkey or goat secondary antibodies. Donkey serum was used for a combination of solely donkey based secondary antibodies, goat serum was used for a combination of solely goat based secondary antibodies.

REFERENCES

1. Discher, D. E., Janmey, P. & Wang, Y. Tissue Cells Feel and Respond to the Stiffness of Their Substrate. *Science (1979)* 310, 1139–1143 (2005).

2. Engler, A. J., Sen, S., Sweeney, H. L. & Discher, D. E. Matrix Elasticity Directs Stem Cell Lineage Specification. *Cell* 126, 677–689 (2006).

3. Miller, C. J. & Davidson, L. A. The interplay between cell signalling and mechanics in developmental processes. *Nat Rev Genet* 14, 733–744 (2013).

4. Bril, M., Fredrich, S. & Kurniawan, N. A. Stimuli-responsive materials: A smart way to study dynamic cell responses. *Smart Mater Med* 3, 257–273 (2022).

5. Storm, C., Pastore, J. J., MacKintosh, F. C., Lubensky, T. C. & Janmey, P. A. Nonlinear elasticity in biological gels. *Nature* 435, 191–194 (2005).

6. Piechocka, I. K., Bacabac, R. G., Potters, M., MacKintosh, F. C. & Koenderink, G. H. Structural Hierarchy Governs Fibrin Gel Mechanics. *Biophys J* 98, 2281–2289 (2010).

7. Chaudhuri, O. Viscoelastic hydrogels for 3D cell culture. *Biomater Sci* 5, 1480–1490 (2017).

8. Jansen, K. A., Bacabac, R. G., Piechocka, I. K. & Koenderink, G. H. Cells Actively Stiffen Fibrin Networks by Generating Contractile Stress. *Biophys J* 105, 2240–2251 (2013).

9. Yuan, H. *et al.* Synthetic fibrous hydrogels as a platform to decipher cell–matrix mechanical interactions. *Proceedings of the National Academy of Sciences* 120, (2023).

10. Solon, J., Levental, I., Sengupta, K., Georges, P. C. & Janmey, P. A. Fibroblast Adaptation and Stiffness Matching to Soft Elastic Substrates. *Biophys J* 93, 4453–4461 (2007).

11. Mitrossilis, D. *et al.* Real-time single-cell response to stiffness. *Proceedings of the National Academy of Sciences* 107, 16518–16523 (2010).

12. Lee, K. Y. & Mooney, D. J. Hydrogels for Tissue Engineering. *Chem Rev* 101, 1869–1880 (2001).

13. Chaudhary, S. & Chakraborty, E. Hydrogel based tissue engineering and its future applications in personalized disease modeling and regenerative therapy. *Beni Suef Univ J Basic Appl Sci* 11, 3 (2022).

14. Blache, U. *et al.* Engineered hydrogels for mechanobiology. *Nature Reviews Methods Primers* 2, 98 (2022).

15. Drury, J. L. & Mooney, D. J. Hydrogels for tissue engineering: scaffold design variables and applications. *Biomaterials* 24, 4337–4351 (2003).

16. Chaudhuri, O. *et al.* Hydrogels with tunable stress relaxation regulate stem cell fate and activity. *Nat Mater* 15, 326–334 (2016).

17. Trujillo, S. *et al.* Engineered 3D hydrogels with full-length fibronectin that sequester and present growth factors. *Biomaterials* 252, 120104 (2020).

18. Singh, A. *et al.* Enhanced lubrication on tissue and biomaterial surfaces through peptide-mediated binding of hyaluronic acid. *Nat Mater* 13, 988–995 (2014).

19. Faust, H. J. *et al.* A hyaluronic acid binding peptide-polymer system for treating osteoarthritis. *Biomaterials* 183, 93–101 (2018).

20. Hezaveh, H. *et al.* Encoding Stem-Cell-Secreted Extracellular Matrix Protein Capture in Two and Three Dimensions Using Protein Binding Peptides. *Biomacromolecules* 19, 721–730 (2018).

21. Helms, B. A. *et al.* High-Affinity Peptide-Based Collagen Targeting Using Synthetic Phage Mimics: From Phage Display to Dendrimer Display. *J Am Chem Soc* 131, 11683–11685 (2009).

22. Zhou, H.-Y., Cao, Y., Wu, J. & Zhang, W.-S. Role of corneal collagen fibrils in corneal disorders and related pathological conditions. *Int J Ophthalmol* (2017)

23. Meek, K. M. Corneal collagen—its role in maintaining corneal shape and transparency. *Biophys Rev* 1, 83–93 (2009).

24. Morishige, N., Takagi, Y., Chikama, T., Takahara, A. & Nishida, T. Three-Dimensional Analysis of Collagen Lamellae in the Anterior Stroma of the Human Cornea Visualized by Second Harmonic Generation Imaging Microscopy. *Investigative Opthalmology & Visual Science* 52, 911 (2011).

25. Elosegui-Artola, A. *et al.* Force Triggers YAP Nuclear Entry by Regulating Transport across Nuclear Pores. *Cell* 171, 1397-1410.e14 (2017).

26. Nardone, G. *et al.* YAP regulates cell mechanics by controlling focal adhesion assembly. *Nat Commun* 8, 15321 (2017).

27. Zorn-Kruppa, M. *et al.* A Human Corneal Equivalent Constructed from SV40-immortalised Corneal Cell Lines. *Alternatives to Laboratory Animals* 33, 37–45 (2005).

28. Manzer, A. K. *et al.* SV40-transformed human corneal keratoeytes: Optimisation of serum-free culture conditions. *ALTEX* 26, 33–39 (2009).

29. Foster, J. W., Gouveia, R. M. & Connon, C. J. Low-glucose enhances keratocyte-characteristic phenotype from corneal stromal cells in serum-free conditions. *Sci Rep* 5, 10839 (2015).

CHAPTER 4

Collagen type I mimicking peptide additives to functionalize synthetic supramolecular hydrogels

Small bioactive peptide sequences derived from extracellular matrix proteins possess the ability to interact with specific cell receptors. As such, these peptide additives are excellent mimics to develop materials for 3D cell culture. Here, two types of supramolecular modified collagen type I mimicking peptide additives are presented; UPy-GFOGER (39 amino acids), which has a novel superstructure, and the short and more simplistic designed UPy-DGEA (7 amino acids). Our aim is to study the impact of both collagen type I mimicking peptide additives, connected to the conformational difference between both peptide additives, on their biological performances. Various analyzing techniques demonstrated the ability of the supramolecular UPy-GFOGER to self-assemble into short nanofibers with brush-like outer features, suggesting trimerization into a triple helix. Compared with UPy-GFOGER, UPy-DGEA is a short, relatively easy to synthesize additive without a complex structure. Since, collagen type I is a major component of the human corneal stroma, primary keratocytes (PKs) are encapsulated within the functionalized hydrogels to provide insights in the induced bioactivity of both additives. Incorporation of UPy-GFOGER supported a spreaded morphology and (re-)differentiation of the encapsulated PKs, while tiny round-shaped cells were observed within the hydrogels functionalized with UPy-DGEA. This difference in biological success between UPy-GFOGER and UPy-DGEA indicates the difficulty of using short peptide additives without a complex structure to mimic the complex structure of natural collagen.

INTRODUCTION

Via various receptors a cell is continuously interacting with its own specific native microenvironment, the extracellular matrix (ECM).[1] Collagens are the most abundantly present proteins within the ECM, forming supramolecular assemblies that participate in cell-matrix interactions. Based on their supramolecular assemblies collagens can be subdivided into various subfamilies such as fibrils, beaded filaments, anchoring fibrils, and networks. The human cornea is located at the outermost part of the eye, covering the tear film. The thickest layer within the cornea is the stroma, which due to its size substantially affects the corneal functions. An important characteristic of the stroma is its very specific and highly organized structure of packed collagen type I fibrils. These fibrils are surrounded by specialized proteoglycans, resulting in a highly hydrated tissue.[2,3] A collagen type I molecule consists of a typical $(Gly-X-Y)_n$ repeating sequence with the variable amino acids often being a proline or hydroxyproline. This specific repeating sequence induces a triple-helical conformation.[4–6] Via cis- or trans peptide bonds between the proline residues polyprolines are known to from either a right-handed polyproline I helix or a left-handed polyproline II helix.[7–9] Three α chains of collagen type I in a left-handed polyproline II-helix conformation coil around each other to assemble into a right-handed triple helix.[4,8,10–12] The self-assembly of collagen into a triple helix conformation is stabilized through hydrogen bonding between N-H groups of the glycines and C=O groups of the prolines or hydroxyprolines.[8,10,13] Cell-matrix interactions are initiated via short bioactive sequences of amino acids, derived from various ECM proteins in the microenvironment surrounding the cells that enable binding to cellular receptors.[14–18] Via solid-phase peptide synthesis (SPPS) it is possible to synthesize these short amino acid sequences, whereafter they can be used to functionalize biomaterials. Previously, various short collagen mimicking peptides have been generated, *i.e.* RGDS (present in laminin, collagen I and IV)[19,20], DGEA (present in collagen I and IV)[21,22], GTPGPQGIAGQRGVV (linear peptide derived from the α1 helix of collagen I)[23], RADA16-GG-FPGERGVEGPGP (derived from collagen I)[24], GGYGGGPC(GPP)5-GFOGER-(GPP)$_5$GPC (derived from collagen I)[25], and $(PKG)_4(POG)_4(QOG)_4$ (derived from collagen I).[26] In addition, some studies demonstrated the need of a triple-helical conformation of GFOGER-like additives to allow improved bioactivity upon usage in biomaterials. The GFOGER sequence is often flanked by Gly-Pro-Pro (GPP) repeating units to induce trimerization into a triple-helical conformation.[10,27–30]

The incorporation of peptide additives into a supramolecular system allows the material to mimic the dynamic and reconfigurable nature of the ECM. For instance, the use of peptide amphiphiles (PA), which possess the ability to interact with cells through a high density of surface signals. Cell encapsulation within the three-dimensional supramolecular network of PA nanofibers is achieved via the presentation of a bioactive epitope on the nanofiber surface. Various short peptide sequences have been used as bioactive epitope, such as the laminin derived IKVAV sequence or VEGF-mimetic peptide sequences.[31–33] Besides PAs, supramolecular hydrogels are also formed from molecules with bifunctional or monofunctional fourfold hydrogen bonding designs. The use of bifunctional and monofunctional molecules containing ureido-pyrimidinone (UPy) groups as supramolecular building blocks was studied by Diba *et al*., demonstrating dynamic hydrogels functionalized with cyclic integrin-binding arginine-glycine-aspartate (cRGD) ligands to enhance cell spreading.[34] To effectively present the cRGD ligand to the cells a UPy-moiety was modified with cRGD to allow incorporation into the monofunctional fiber. While non-modified cRGD additives showed to be ineffective to promote cell attachment, since the molecules were prone to burst release.[34] Previous studies focusing on the peptide presentation within a UPy-network demonstrated the need of peptides conjugated to UPy-moieties as well. Together, these studies resulted in an amphiphilic design, in which a short oligo(ethylene glycol)(OEG) spacer was introduced.[35–41] UPy-dimers self-assemble into 1D stacks, using π-π interactions stabilized by hydrogen bonds from a flanking urea group, which allow these stacks to turn into a bundle.[34,36,42,43] Conjugation of the synthesized peptides to a supramolecular UPy-moiety allows, due to the modularity of supramolecular materials, the formation of a stable bulk material functionalized with these peptide additives, acting as biochemical cues to induce cell adhesion, cell spreading, or even more complex cell-material interactions.[35,37–41,44–46]

Here, a collagen type I mimicking polypeptide GGG-GPP$_5$-GFOGER-GPP$_5$ (GFOGER) (**Figure 1A**) and a short GCGDGEA (DGEA) peptide (**Figure 1B**) are synthesized, conjugated to an UPy-moiety and studied for their bioactivity when incorporated within an UPy-based hydrogel. The supramolecular UPy-based hydrogel comprises of a 528 Da oligo(ethylene glycol) (OEG) chain end-capped with a UPy moiety at one end and a glycine-amide group at the other end (UPy-Glycine) and a 10 kDa poly(ethylene glycol) (PEG) chain, end-capped with two functional UPy-moieties (UPy-PEG$_{10K}$-UPy) acting as a crosslinker (**Figure 1C**).[34] Two control hydrogels were incorporated in this study as a reference, namely a synthetic UPy hydrogel

functionalized with UPy-cRGD (**Figure 1D**) and a hybrid hydrogel based on a mixture of UPy molecules and collagen type I (**Figure 1E**). While both peptide additives are designed to mimic collagen type I, we assume only the UPy-GFOGER additive will fold into a supramolecular aggregate comprising a triple-helical conformation. This assumption is based on the presence of GPP repetition units within the UPy-GFOGER, and the absence of these units within the UPy-DGEA. Within this study we will investigate the influence of this conformational difference between the additives on their bioactivity, when both are individually used to functionalize a synthetic hydrogel (**Figure 1F**). Since collagen type I is major component of the human corneal stroma, primary corneal keratocytes are encapsulated and cultured within UPy-GFOGER and UPy-DGEA functionalized hydrogels to provide insights about the induced bioactivity of both additives.[47,48]

RESULTS AND DISCUSSION

Synthesis of the bioactive GFOGER additive and conjugation to a UPy-moiety

N- or C-terminus modifications of the collagen type I-mimicking peptide GGG-GPP$_5$-GFOGER-GPP$_5$ (GFOGER) with additional supramolecular moieties, e.g. aromatic, metal-coordinating or electrostatic groups, allowed for the generation of exciting higher-ordered structures.[5,11,49–52] Here, a UPy-moiety was conjugated to the GFOGER polypeptide N-terminus (UPy-GFOGER) whereafter the self-assembly behavior with respect to triple helix formation and fiber formation was explored.

Standard Fmoc SPPS on a rink amide resin was performed for the synthesis of the GFOGER polypeptide. After each amino acid coupling an acetylation step was performed to prevent the growing of unreacted peptide chains that lack one or more amino acids. The Fmoc protecting the N-terminus of the polypeptide was removed by using the base piperidine (**Scheme 1**). Subsequently, the polypeptide was deprotected and removed from the resin using a cleaving mixture of trifluoroacetic acid (TFA) and ultrapure water, mixed with triisopropylsilane (TIS). Due to the growth of peptide chains that did not react during an amino acid coupling step on the resin, synthesizing polypeptides in high purity using SPPS was considered to be challenging.
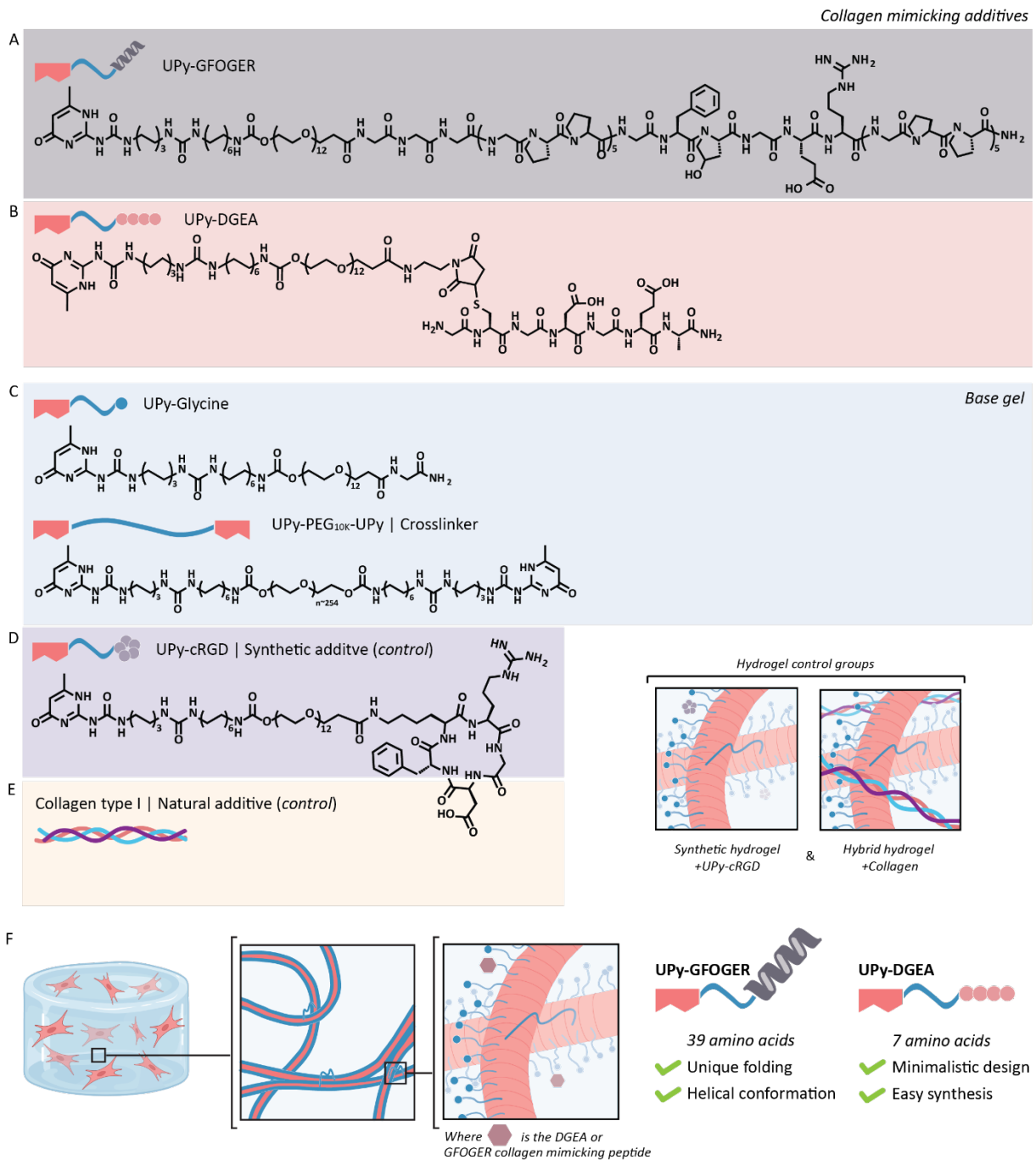
Figure 1. Chemical structures of the molecules and schematic representation of the studied conditions. **A)** The chemical structure of UPy-GFOGER. **B)** The chemical structure of UPy-DGEA. **C)** The chemical properties of the hydrogelators and a schematic representation of the fiber assembly and hydrogel formation. **D)** The chemical structure of UPy-cRGD. **E)** Schematic representation of collagen type I, used within the hybrid hydrogel. **F)** Schematic illustration of the supramolecular network. Blue linkages between fibers indicate interfiber cross-links formed by UPy-PEG$_{10K}$-UPy. The collagen mimicking additives UPy-GFOGER and UPy-DGEA are used to functionalize a synthetic supramolecular hydrogel.

Here as well, some impurities are detected after cleaving the peptide from the resin, whereafter the GFOGER polypeptide was purified using preparative RP-LCMS. To this end, the polypeptide was gained with a yield of 19% in high purity (> 95%).

A UPy-synthon with a UPy-C6-U-C12-Uret-mOEG12-C2-COOH molecular design was used to modify the N-terminus of the GFOGER polypeptide, creating a supramolecular collagen mimicking bioactive additive. The use of HATU and DIPEA activated the carboxylic acid group, which reacted with the primary amine located at the N-terminus of the GFOGER polypeptide. Residual UPy-synthon was removed by running a preparative RP-LCMS, which decreased the final yields due to the affinity of the OEG-segment for the silica column. Yet, UPy-GFOGER is successfully synthesized and gained with a yield of 13% in high purity (> 95%).
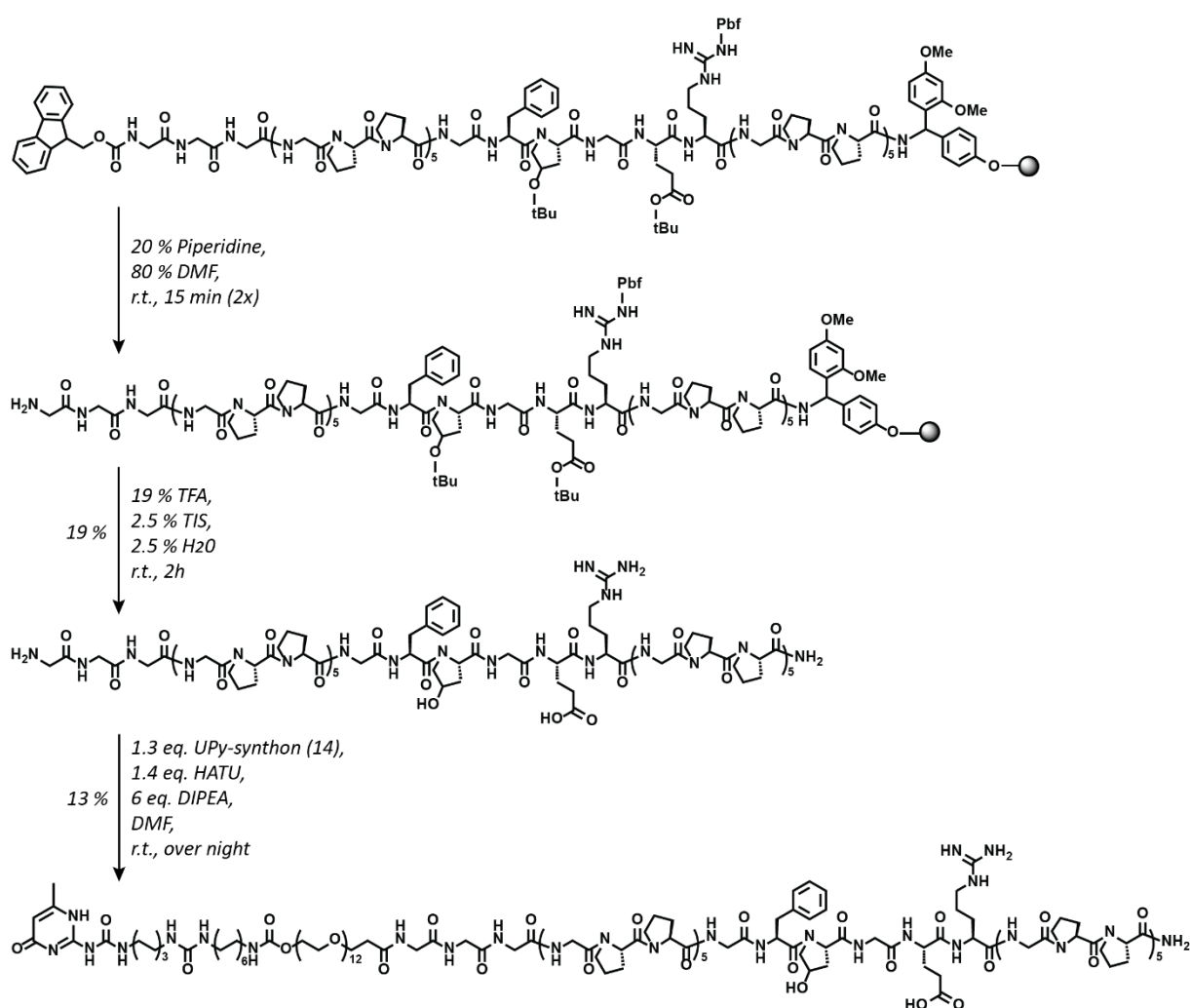
Scheme 1 Synthesis of GGG-GPP$_5$-GFOGER-GPP$_5$ polypeptide and the conjugation to a UPy-moiety via the N-terminus of the polypeptide, resulting in the supramolecular bioactive additive UPy-GGG-GPP$_5$-GFOGER-GPP$_5$ (referred to as UPy-GFOGER).

Synthesis of the bioactive GCGDGEA additive and conjugation to a UPy-moiety

The GCGDGEA peptide was synthesized using standard Fmoc solid phase peptide synthesis (SPPS) on a rink amide resin, with a propargyl glycine at the N-terminus and an introduced cysteine on the C-terminus to enable coupling to the UPy-moiety. The Fmoc-protected GCGD(tBU)GE(tBU)A peptide was deprotected using piperidine as a base, resulting in a primary amine. Thereafter, the peptide was deprotected and removed from the resin using TFA and ultrapure water mixed with TIS to simultaneously remove the side-protective groups on the amino acids (**Scheme 2**). Upon using TFA, highly reactive cationic species were generated from the protecting groups that could react with the nucleophilic group of the cystine, the scavenger ethanedithiol (EDT) was added to quench these ions. Residual unreacted peptides were removed through purification with preparative reverse-phase liquid chromatography-mass spectrometry (RP-LCMS). The GCGDGEA peptide was attached to the UPy-moiety via maleimide-thiol chemistry, where Tris(2-carboxyethyl)phosphine (TCEP) was used to cleave the sulfide bonds and therewith activate the thiol in the cysteine to react with the maleimide. The UPy-GCGDGEA was gained with a yield of 54% in high purity (> 96%).

The ability of UPy-GFOGER to self-assemble: the effects of diluting and mixing on triple helix formation

The combination of the dihedral bond angle in the repeating glycine-proline-proline pattern of the GFOGER polypeptide, together with the intermolecular hydrogen bonding between the amide groups induces trimerization into a triple helix conformation in an aqueous environment.[5] The unique triple helix conformation associates with a specific optical activity, allowing circular dichroism (CD) spectroscopy to investigate the presence of a helical formation.[53] GFOGER, the UPY-GFOGER conjugate, and UPy-Glycine (functioning as a control) were deprotonated and dissolved in alkaline PBS and afterwards neutralized to a pH of ~ 7.4 with HCl solution. Overnight molecular assembly was allowed at 4 °C to ensure triple helix formation, and optical activity was measured at 37 °C. As expected, UPy-Glycine did not show any CD (**Figure 2A**). Yet, both GFOGER as well as UPy-GFOGER exhibited spectral features characteristic of a triple helix, showing maxima around 225 nm, a crossover around 220 nm,

and a broad negative peak near 205 nm.[53] These results indicate that the CD behavior of UPy-

GFOGER is caused by the polypeptide segment.
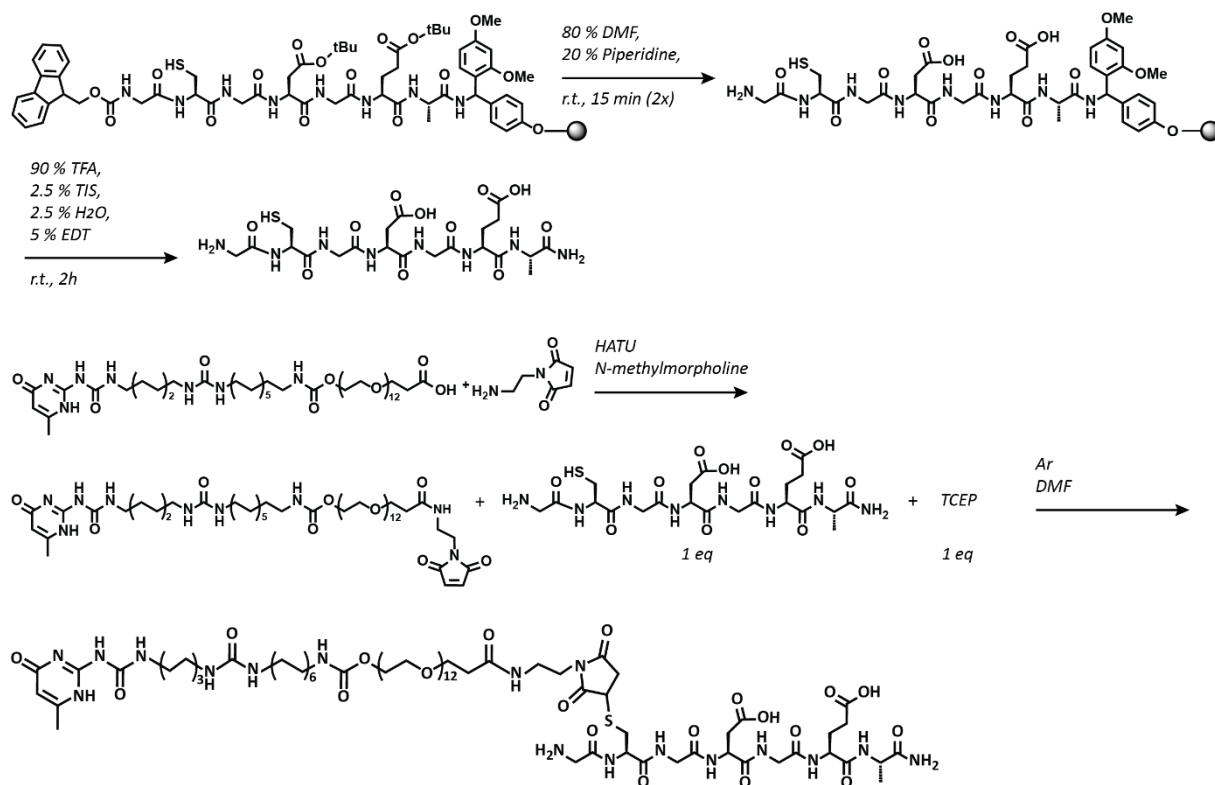
Scheme 2. Conjugation of Fmoc SPPS GCGDGEA to a UPy-moiety via maleimide-thiol chemistry, resulting in the supramolecular bioactive additive UPy-GCGDGEA (referred to as UPy-DGEA).
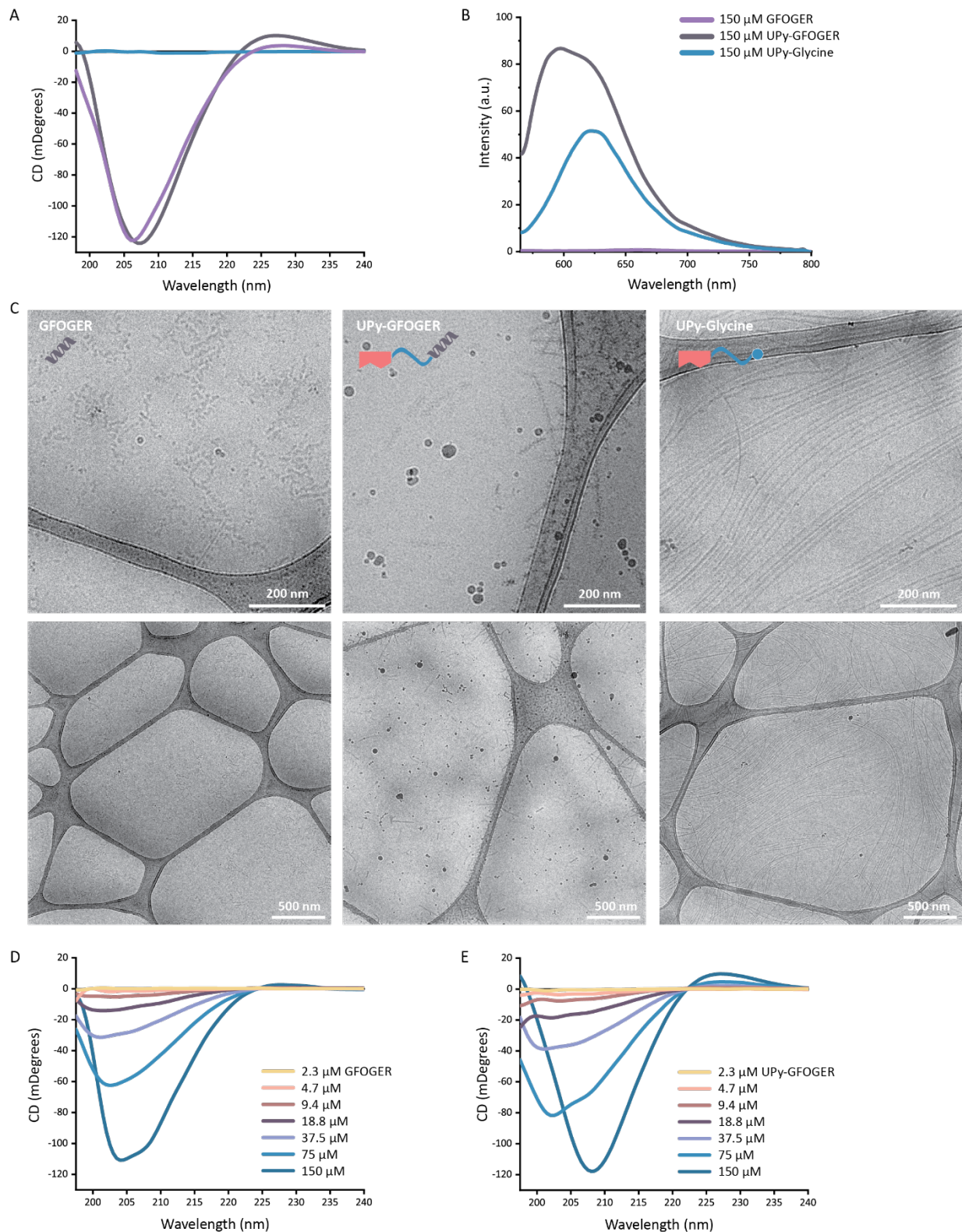
Figure 2. Morphological analysis of supramolecular assemblies containing triple helix forming regions. **A)** CD spectra of GFOGER, UPy-GFOGER, and UPy-Glycine at a concentration of 150 µM at 37 °C. **B)** Fluorescent emission spectra of Nile red dye (7.5 µM) in GFOGER, UPy-GFOGER, and UPy-Glycine solutions (150 µM) at 37 °C. **C)** Cryogenic transmission electron micrographs of supramolecular assemblies of GFOGER, UPy-GFOGER, and UPy-Glycine. **D)** CD spectra of dilution series of GFOGER at 37 °C. **E)** CD spectra of dilution series of UPy-GFOGER at 37 °C.

The observed fiber-like morphology within the UPy-GFOGER assemblies could be caused by stacking of UPy-dimers. To investigate this scenario, a Nile red dye, which only fluoresces in a hydrophobic environment, is used. Nile red has an excitation wavelength of 485 nm, while the emission wavelength is mainly dependent on the polarity of the environment. If the lipophilic dye incorporates as a guest molecule into the hydrophobic core of a self-assembled UPy-fiber, a fluorescent signal can be observed.[54,55] UPy-Glycine showed a distinct fluorescent emission spectrum with a peak at a wavelength of 620 nm (**Figure 2B**), indicating a hydrophobic pocket in the UPy-fiber for the Nile red dye to incorporate into. The fluorescent emission spectrum of UPy-GFOGER showed a blue shift as well as a broader shoulder between 600 – 625 nm, indicating an increase in hydrophobicity of the environment for the Nile red dye and stacking of the UPy-GFOGER molecules.[54,55]

Visualization of the morphologies of the self-assembled structures of GFOGER, UPy-GFOGER, and UPy-Glycine are demonstrated by cryo-TEM images (**Figure 2C**). In aqueous environment, the GFOGER polypeptide formed small aggregates with coiled features. A quite different visualization was observed for the UPy-GFOGER molecules that assembled into small nanofibers with a distinct brush-like morphology, showing a preference for localization around the carbon grid. Similar to previous work, UPy-Glycine molecules aggregated into very long nanofibers with a smooth appearance compared to the brush-like UPy-GFOGER aggregates.[34] These results suggest that the brush-like structures observed around the UPy-GFOGER fibers originate from triple helices formed by the GFOGER polypeptide segments.

Two segments within UPy-GFOGER allow for self-assembly of the molecule: the dimerizing UPy-moiety (1), and the trimerizing GFOGER polypeptide region (2). To study if one of these two segments dominates the assembly behavior of UPy-GFOGER, dilution series were prepared of GFOGER and UPy-GFOGER ranging from 2.3 µM to 150 µM, and analyzed by CD spectroscopy. The GFOGER dilutions (**Figure 2D**) show CD spectra characteristics of a triple helix in the range of 9.4 – 150 µM, while the UPy-GFOGER dilutions (**Figure 2E**) show CD spectra characteristics of a triple helix in the range of 18.8 – 150 µM. These results suggest a slightly enhanced stabilization of the triple helix formation for the GFOGER polypeptide compared with the conjugated UPy-GFOGER.

The impact of mixing UPy-Glycine and UPy-GFOGER on triple helix formation

To allow the incorporation of the supramolecular collagen mimicking UPy-GFOGER additive into a synthetic UPy-based hydrogel it was necessary to mix UPy-Glycine with UPy-GFOGER. For this purpose, it was considered to be interesting to study the effect on triple helix formation by dilution of the GFOGER segment. To this end, stock solutions were prepared in alkaline PBS buffer both at a concentration of 150 µM of UPy-GFOGER and 150 µM of UPy-Glycine. The stock solutions were mixed at desired ratios, neutralized with HCl solution, and allowed to equilibrate overnight. Except for the pure UPy-Glycine, all the mixtures showed a CD effect (**Figure 3A**). The CD spectra of the mixtures showed a decreased CD single upon dilution of the GFOGER segment by an increased addition of UPy-Glycine. At a UPy-GFOGER mol content of less than a third, the characteristic CD spectrum, which refers to a triple helix, was lost. Yet, the CD spectra of the mixtures with even lower content of UPy-GFOGER still showed optical activity. To this end, a mixture with only 5 mol% UPy-GFOGER (referring to the 19:1 mixture) was visualized through cryo-TEM to investigate the morphologies of the supramolecular assemblies. Long nanofibers were observed within the mixture via the obtained cryo-TEM images. These nanofibers lacked the brush-like morphology, which was assumed to be characteristic for the UPy-GFOGER (**Figure 3B**). Taken together, dilution by addition of UPy-Glycine resulted in a change of the polypeptide segment in UPy-GFOGER, from a triple helix into a random coil conformation. Furthermore, these results indicated that the assembly behavior is mainly dominated by the dimerizing UPy-moieties instead of by the polypeptide GFOGER segment.
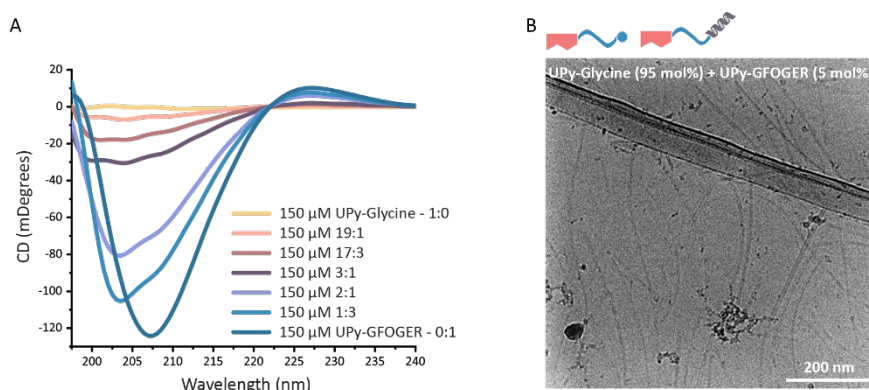

Figure 3. Conformational change of UPy-GFOGER upon mixing and dilution by UPy-Glycine. **A)** CD spectra of UPy-GFOGER and UPy-Glycine mixtures at various concentration ratios at 37 °C. **B)** Cryogenic transmission electron micrograph of supramolecular assemblies of UPy-GFOGER and UPy-Glycine at a 19:1 mol ratio (orange graph in CD spectra).

3D culture of human primary keratocytes encapsulated in synthetic collagen mimicking hydrogels

After successful synthesis of the collagen mimicking UPy-GFOGEA and a thorough characterization of the conformational properties of UPy-GFOGER, both the UPy-GFOGER and the UPy-DGEA additive were used to generate full synthetic hydrogels, allowing for 3D cell culture of primary keratocytes. Donor derived human primary keratocytes (PK) were encapsulated within hydrogels functionalized with either the UPy-GFOGER or the UPy-DGEA and cultured up to 21-days. The +UPy-GFOGER functionalized hydrogel supported the PKs to attain their healthy spreaded morphology (**Figure 4A**). The +UPy-DGEA functionalized hydrogel was not able to support the healthy morphology of the encapsulated PKs, resulting in clusters of round-shaped cells (**Figure 4B**). Both the synthetic hydrogel functionalized with UPy-cRGD as well as the hybrid hydrogel mixed with natural collagen type I (thoroughly studied in chapter 2) were used as reference hydrogels. Multicolored images show the various heights of the cells within the z-direction of the hydrogel, demonstrating the ability of the cells to spread and grow in the provided 3D environment. The results of the +UPy-cRGD (**Figure 4C**) and +collagen (**Figure 4D**) control showed a high density of spreaded and elongated cells, similar to the previous results of these two hydrogel conditions. Together, these results demonstrated a novel synthetic hydrogel functionalized with UPy-GFOGER, which supports PKs to adhere and to adapt to their healthy spreaded morphology in a similar fashion as the +UPy-cRGD and +Collagen functionalized hydrogels. The +UPy-DGEA hydrogel showed to be less suitable for the encapsulation of keratocytes, yet this hydrogel could be useful for cell types with a preference for cell-cell interactions above cell-matrix interactions, *i.e.* organoids.

Mechanotransduction allows cells to sense and adapt to external forces by cytoskeleton and focal adhesion (FA) remodeling or activating specific genetic programs.[56] To explore the interaction between the cells and the material in more detail, an analysis of yes-associated-protein (YAP) was implemented in this study. The immunohistochemical images of PKs encapsulated and cultured in the various hydrogels showed the expression of YAP within the cytoplasm and/or nuclei. For the +UPy-GFOGER (**Figure 5A**), the +UPy-DGEA hydrogel (**Figure 5B**) and the +UPy-cRGD hydrogel (**Figure 5C**) it was difficult to observe a difference in YAP expression between the cytoplasm and the nuclei. On the contrary, nuclear YAP seemed to be expressed in the majority of the PKs encapsulated within the hybrid hydrogel (+collagen)

(**Figure 5D**). These variations could be explained by the difference in cell density. Compared with the sparse spreaded cells present within the +UPy-GFOGER hydrogel, the hybrid hydrogels demonstrated a more dense cell network, favoring cell-cell interactions that affect the activation and expression of YAP within the nuclei.[57]
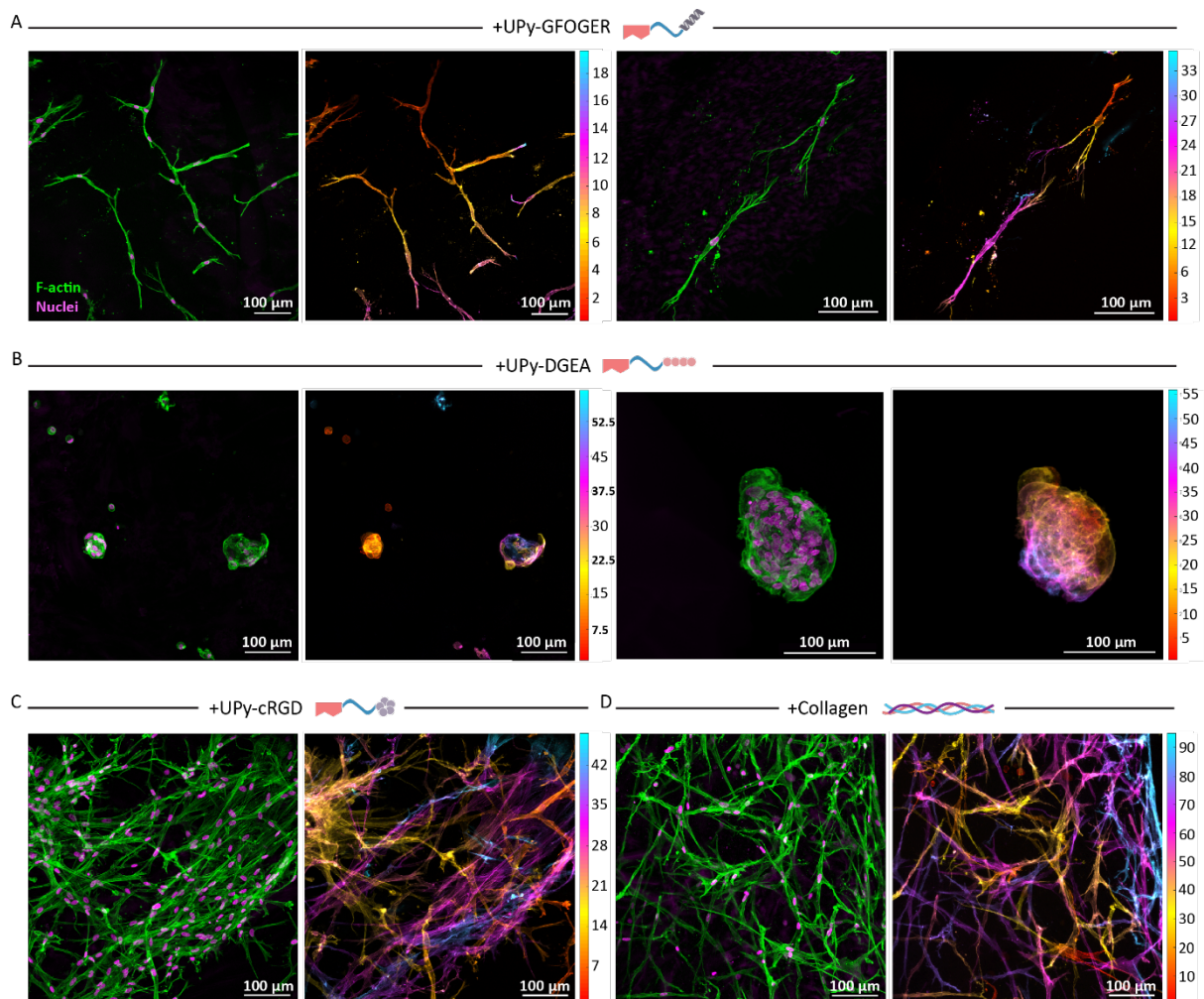
Figure 4. UPy-GFOGER and UPy-DGEA functionalized hydrogels allow for 3D encapsulation and culture of PKs. For all the images accounts the following: F-actin is in green, nuclein are in magenta and the scale bars represent 100 μm. The scale of the height images is in μm. **A)** The cellular results of the synthetic UPy-GFOGER. **B)** The cellular results of the synthetic UPy-DGEA. **C)** The cellular results of the synthetic 'golden standard' control UPy-cRGD. **D)** The cellular results of the hybrid collagen type I hydrogel.
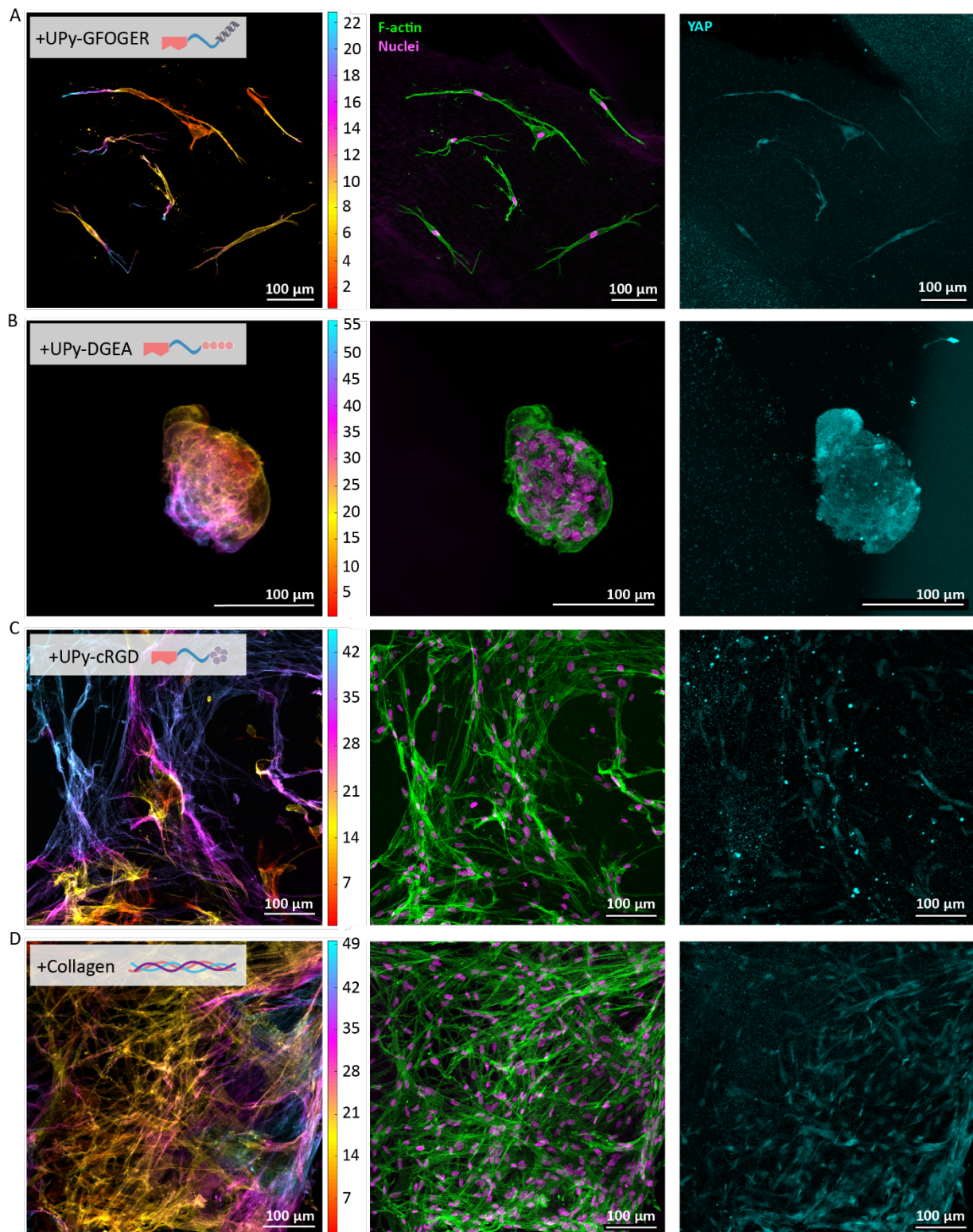
Figure 5. Encapsulated PKs sensed similar mechanotransduction when encapsulated in the synthetic +UPy-GFOGER and +UPy-DGEA hydrogels, compared with the +UPy-cRGD and hybrid hydrogel control when cultured for 21 days. Height images are in µm scale, F-actin is in green, nuclei are in magenta and YAP is in cyan. Scale bars represent 100 µm. **A)** The results of the synthetic +UPy-GFOGER hydrogel. **B)** The results of the synthetic +UPy-DGEA hydrogel. **C)** The results of the synthetic +UPy-cRGD hydrogel. **D)** The results of the hybrid +collagen hydrogel.

Differentiation of primary keratocytes encapsulated in synthetic collagen mimicking hydrogels

After a successful encapsulation of the PKs within the hydrogels functionalized with collagen mimicking peptides, the PKs were treated in two manners; (1) with serum towards stromal fibroblasts (SFs) or (2) with low concentration of serum and high concentration of glucose towards quiescent corneal stromal keratocytes (CSKs).[58] At first all the hydrogels were embedded in medium with serum to allow adherence of the PKs to the material. On culture day 1, the medium is changed to low serum and high glucose medium, allowing the PKs to (re-)differentiate towards CSKs during the 21-day culture.

Healthy human keratocytes do express crystallin proteins, which reduce light scattering and enhance the optical performance of the stromal tissue. One of these proteins is the enzyme aldehyde dehydrogenase 3 Family member A1 (ALDH3A1), which is often used as a specific marker for keratocytes.[59,60] Here, immunohistochemical staining showed the expression of ALDH3A1 in PKs treated towards CSKs (**Figure 6A**). Within the cell clusters formed by the PKs encapsulated and cultured within the hydrogel functionalized with UPy-DGEA, a less clear ALDH3A1 expression was observed. In contrast, the PKs encapsulated and cultured within the hydrogels functionalized with UPy-GFOGER, UPy-cRGD and collagen all showed a distinct ALDH3A1 expression, indicating that the PKs start to comprise specific keratocyte behavior.

During this 21-day cell culture, small amounts of cell culture medium were stored to perform an enzyme-linked-immunosorbent assay (ELISA). From literature it is known that SFs secrete among others the cytokine Interleukin-8 (IL-8), which is a pro-inflammatory molecule responsible for neutrophil recruitment and T-cell activation. Since, CSKs barely secrete the cytokine IL-8 an ELISA based on IL-8 secretion was used to analyze the cellular (re-)differentiation possibilities of PKs encapsulated and cultured within hydrogels functionalized with collagen mimicking peptides.[61] PKs treated with high serum towards SFs and encapsulated within the +UPy-GFOGER, +UPy-DGEA, +UP-cRGD, and +collagen hydrogel secreted; 6562 ±979 pg/mL, 867 ±349 pg/mL, 7429 ±160 pg/mL, and 3262 ±889 pg/mL IL-8, respectively (**Figure 6B**). While, PKs treated with low serum and high glucose towards CSKs encapsulated within the +UPy-GFOGER, +UPy-DGEA, +UP-cRGD, and +collagen hydrogel secreted; 111 ±105 pg/mL, 27 ±4 pg/mL, 204 ±58 pg/mL, and 29 ±2 pg/mL IL-8, respectively (**Figure 6C**). Significant differences were observed between the secreted IL-8 by PKs treated towards SFs or CSKs, while being encapsulated within the UPy-GFOGER functionalized hydrogel. These results also corresponded

with the results of the two controls. Solely, the secreted IL-8 concentration by PKs treated towards SFs or CSKs while encapsulated within the hydrogel functionalized with UPy-DGEA, showed no significant differences. Furthermore, the results demonstrated a significant increase in secreted IL-8 concentration for the PKs treated towards SFs between day 7 and day 21. On the contrary, the results demonstrated a significant decrease in secreted IL-8 concentration for the PKs treated towards CSKs between day 7 and day 21. The increase in IL-8 concentration for the PKs treated towards SFs and the decrease in IL-8 concentration for the PKs treated towards CSK accounts for all the hydrogels, except the +UPy-DGEA functionalized hydrogel. Taken together, both the increase in ADLH3A1 expression as well as the significant decrease of secreted IL-8, demonstrated that the hydrogel functionalized with UPy-GFOGER allows the PKs to (re-)differentiate into CSKs.
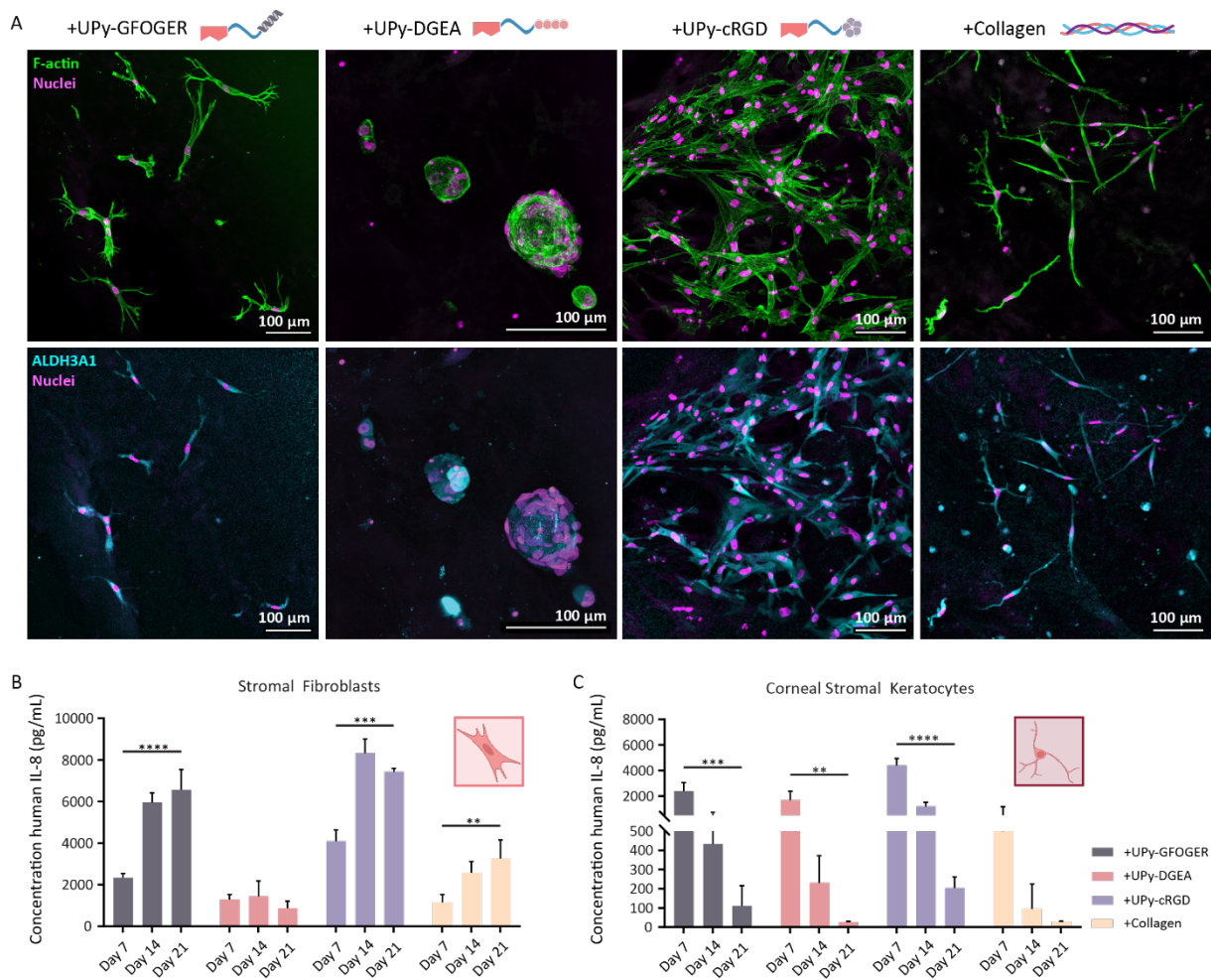
Figure 6. PKs (re)differentiated towards stromal fibroblasts and corneal stromal keratocytes when encapsulated and cultured in the synthetic hydrogels functionalized with either UPy-GFOGER or UPy-DGEA, n=3. **A)** Immunofluorescent staining of F-actin (green), nuclei (magenta) and ALDH3A1 (cyan). Scale bar represents 100 μm. **B)** Interleukin 8 (IL-8) secretion on culture day 7, 14, and 21 by PKs encapsulated within the various hydrogels and treated towards stromal fibroblasts. Sample size n=3, ** $p < 0.01$, *** $p < 0.001$, **** $p < 0.0001$, mean ± standard deviation presented. **C)** Interleukin 8 (IL-8) secretion on culture day 7, 14, and 21 by PKs encapsulated within the various hydrogels and treated towards corneal stromal keratocytes. Sample size n=3, ** $p < 0.01$, *** $p < 0.001$, **** $p < 0.0001$, mean ± standard deviation presented.

CONCLUSION

Here, both UPy-GFOGER and UPy-DGEA are introduced as two supramolecular modified collagen type I mimicking peptides. Both circular dichroism (CD) spectroscopy as well as cryogenic transmission electron microscopy (cryo-TEM) demonstrated the self-assembly behavior with respect to the triple-helical formation of UPy-GFOGER, resulting in a novel superstructure. Encapsulation and culture of PKs within a hydrogel functionalized with either UPy-GFOGER or UPy-DGEA demonstrated distinct differences in cellular behavior. Round-shaped cells and cell clumps were observed for the PKs cultured within the hydrogel functionalized with UPy-DGEA, while the UPy-GFOGER functionalized hydrogel allowed the PKs to attain an elongated morphology. Moreover, PKs encapsulated and cultured within UPy-GFOGER functionalized hydrogels started to (re-)differentiate into CSKs, demonstrated by expression of keratocyte marker ALDH3A1 and a significant decrease in cellular IL-8 secretion.

While the synthesis of UPy-DGEA is easier and faster compared with the synthesis of UPy-GFOGER, the induced bioactivity of the short additive is not sufficient compared with the bioactivity of the UPy-GFOGER functionalized gels. Herewith, the obtained results indicate the need of a complex structure of the collagen mimicking peptide additive to provide the desired biochemical cues for the cells. With this novel UPy-GFOGER molecule we designed a collagen type I mimicking bioactive additive, which allows the formation of a synthetic stromal microenvironment, mimicking closely the natural ECM.

EXPERIMENTAL SECTION

Synthesis of GGG-GPP5-GFOGER-GPP5 (GFOGER) peptide

Standard Fmoc solid-phase peptide synthesis on a rink resin at 0.150 mmol scale was used to synthesize the Gly-Gly-Gly-(Gly-Pro-Pro)$_5$-Gly-Phe-Hyp-Gly-Glu-Arg-(Gly-Pro-Pro)$_5$ polypeptide. The F-moc group was removed from Fmoc-Gly-Gly-Gly-(Gly-Pro-Pro)$_5$-Gly-Phe-Hyp(tBu)-Gly-Glu(OtBu)-Arg-(Gly-Pro-Pro)$_5$ (567 mg, 0.3 mmol) using 20 v/v% piperidine in DMF for 2 x 15 minutes, while still on the rink amide resin. A cleaving mixture of 95:2.5:2.5 v/v% TFA:TIS:H$_2$O for 2 hours was used to cleave the peptide from the resin. To yield a whit fluffy solid, the cleavage mixture was precipitated 5x in ice-cold Et$_2$O and subsequently freeze-dried. Preparative reverse phase LC-MS on a C18 column using a gradient of 20-25% of acetonitrile in H$_2$O, containing 0.1% TFA was used to purify the crude compound. After purification, the final yield was 107 mg GFOGER peptide (19%), which had a purity of > 95%. *The synthesis and characterization of GFOGER and UPy-GFOGER described in this chapter was in close collaboration with Johnick F. van Sprang.*

Synthesis of UPy-GFOGER

The GFOGER polypeptide (84 mg; 0.025 mmol) was dissolved in 4 mL DMF. The UPy-synthon was synthesized as previously reported.[62] The UPy-synthon (37 mg; 0.32 mmol) was dissolved in 3 mL DMF. DIPEA (26 μL; 0.15 mmol) and HARU (13.3 mg; 0.035 mmol) were dissolved in 2 mL DMF and added to the UPy-synthon solution, whereafter the complete mixture was stirred for 15 min at room temperature. After pre-activation the reaction mixture was added to the GFOGER polypeptide solution and reacted overnight under shaking conditions at room temperature. To yield a white fluffy solid, the cleavage mixture was precipitated 5x in ice-cold Et$_2$O and subsequently freeze-dried. Preparative reverse phase LC-MS on a C18 column using a gradient of 30-35% of acetonitrile in H$_2$O, containing 0.1% TFA was used to purify the crude compound. After purification, the final yield was 16 mg GFOGER peptide (13%), which had a purity of > 5%.

Synthesis of UPy-GCGDGEA peptide additive via maleimide-thiol conjugation

The Gly-Cys-Gly-Asp-Gly-Glu-Ala peptide was synthesized using standard Fmoc solid-phase peptide synthesis on a rink amide resin at 0.1 mmol scale. The Fmoc-group was removed using 20 v/v% piperidine in DMF for 2 x 15 minutes, while still on the rink amide resin. Subsequently, the peptide was cleaved from the resin in a 90:2.5:2.5:5 v/v% TFA:TIS:H$_2$O:EDT for 2 hours. The cleavage mixture was precipitated 6x in ice-cold Et$_2$O. Preparative reverse phase LC-MS on a C18 column using a gradient of 20-25% of acetonitrile in H$_2$O, containing 0.1% TFA was used to purify the crude

compound. The GCGDGEA peptide was attached to the UPy-moiety via maleimide-thiol chemistry, where Tris(2-carboxyethyl)phosphine (TCEP) is used to cleave the sulfide bonds and therewith activate the thiol in the cysteine to react with the maleimide.

Jingyi Huang performed the conjugation of GCGDGEA to the UPy-maleimide.

Circular dichroism spectroscopy

Stock solutions (300 µM) were prepared by dissolving GFOGER, UPy-GFOGER, and UPy-Glycine in alkaline pBS solutions (containing 80 mM NaOH in PBS) and heated to 70 °C for 1 hour. For the preparations of the mixtures the stock solutions were diluted 2x in alkaline PBS solution and mixed in the desired ratios, followed by neutralization by using 1 M HCl. Afterwards the samples were left overnight at 4 °C to allow assembly. Samples were measured at a scan speed of 100 nm per min, with a data pitch of 0.25 nm, a response time of 0.5 seconds, and a bandwidth of 2 nm. A suprasil® quartz cuvette was used with a pathlength of 1 mm, and a chamber volume of 350 µL (Hellma Analytics). The spectra were measured from 400 to 170 nm at 37 °C. Graphs are shown from 197.5 to 240 nm, due to noise observed below 200 nm due to wavelength absorption of water.

The samples for the CD experiments were prepared in collaboration with Johnick F. van Sprang, the CD experiments were performed together with Maaike J.G. Schotman.

Nile red assay

150 µM stock solutions with a volume of 1 mL were prepared by dissolving GFOGER, UPy-GFOGER, and UPy-Glycine at 70 °C in alkaline PBS solutions (containing 80 mM of NaOH) for 1 hour. After cooling down to room temperature, 1.5 µL of 5 mM Nile red stock was added to each solution, and the solutions were neutralized with 1 M HCl. The solutions were left overnight at 4 °C to equilibrate before the measurements were performed. A Varian Fluorescence spectrophotometer was used to measure the Nile red assays. After excitation of the samples the fluorescence emission scans were recorded from 560 to 800 nm at a fixed temperature of 37 °C. the excitation and emission slits were fixed at 5 nm, and the scan rate used was 600 nm per min, PMT detector voltage was set to 1000 V. *Both the sample preparation for the Nile red assay as well as the actual measurement was performed in collaboration with Johnick F. van Sprang.*

Cryogenic transmission electron microscopy

150 µM stock solutions were prepared by dissolving GFOGER, UPy-GFOGER, and UPy-Glycine at 70 °C in alkaline PBS solutions (containing 80 mM of NaOH) for 1 hour. After cooling down, the desired mixtures were made and the, if necessary, and then the solutions were mixed thoroughly and

neutralized with 1 M HCl. Lacey carbon film grids (200 mesh, 50 μm hole size; Electron Microscopy Sciences) were surface plasma treated at 5 mA for 40 seconds using a Cressington 208 carbon coater, and each dispersion (3 μL) was applied onto each grid. Using an automated vitrification robot (FEI Vitrobot Mark III), excess sample was removed through blotting with filter paper for 3 seconds at -3 mm. Thin films of dipsersions were vitrified by plunging the grids into liquid ethane, which is just above its freezing point. A FEI-Titan TEM equipped with a field emission gun operating at 300 kV was used to carry out imaging. Samples were imaged using a post-column Gatan energy filter and a 2048x2048 Gatan CCD camera. Micrographs were recorded at low dose conditions, using a defocus setting of -10 μm at 25.000x magnification.

Maaike J.G. Schotman performed all the cryo-TEM experiments.

Primary keratocyte (PK) cell culture

Primary human keratocytes were isolated from leftover human corneoscleral transplant material from Descemet Membrane Endothelial Keratoplasty surgery, which were obtained from the Cornea Department of the ETB-BISLIFE Multi-Tissue Center (Beverwijk, the Netherlands). The keratocytes were cultured in expansion medium (1:1 mixture of Dulbecco's modified Eagle's medium/F-12 supplemented with GlutaMAX (DMEM/F12 (Ham) + GlutaMAXTM, 10565-018; Gibco), 5% Fetal Bovine Serum (FBS, Biochrom AG), 1% penicillin/streptomycin (P/S, Biochrom AG), and 1 mM L-ascorbic acid 2-phosphate sesquimagnesium salt hydrate (Vitamin C, Sigma A8960)) at 37 °C, 21% O_2 and 5% CO_2 until ± 80% confluency. Since the medium contained FBS, keratocytes were considered to be activated matrix-producing cells, referred to as stromal fibroblasts (SFs). To initiate cell (re-)differentiation towards corneal stromal keratocytes, another medium composition was used: differentiation medium (Dulbecco's modified Eagle's medium supplemented with GlutaMAX (GlutaMAXTM, 11880-028; Gibco), 1% penicillin/streptomycin (P/S, Biochrom AG), and 1 mM L-ascorbic acid 2-phosphate sesquimagnesium salt hydrate (Vitamin C, Sigma A8960), 1x ITS (Sigma, I3146), 2 mg/mL D-glucose (Invitrogen, 15023021), 2.5 mg/mL D-mannitol (Fluka, 63560)).[58] Cells were cultured with medium changes every 3 days, keratocytes from multiple donors were used up to passage #3. TrypLE Express Enzyme (1x), no phenol red (12604013, Gibco) is used to detach the cells from the culture flask and use them for experiments.

Cell encapsulation in hydrogels

Both the bifunctional as well as the monofunctional building blocks were received as powders. The bifunctional molecules (UPy-PEG$_{10K}$-UPy) were dissolved at 70 °C in an neutral PBS solution for 1.5 hours. Monofunctional molecules (UPy-Glycine + UPy-cRGD or UPy-Glycine + UPy-GFOGER or UPy-

Glycine + UPy-DGEA) were dissolved at 70 °C in an alkaline PBS solution (containing 160 mM NaOH) for 20 minutes. After completely dissolving the powders of the bifunctional and monofunctional building blocks, the solutions were cooled down to room temperature. A specific volume of HCl solution (2 M) was added to the solution of monofunctional molecules to reach a neutral pH. Cell culture medium is added to both solutions 1:1, to provide the cells already with some nutrients during the gelation process later on in the procedure. Afterwards, both solutions are transferred from a glass vial to a sterile Eppendorf tube, from this step onwards a safety cabinet is used to guarantee a sterile work environment. The solutions were disinfected by exposing them to UV-light for 20 minutes. Subsequently, the cells were prepared and counted, the following cell concentrations were used during the experiments:

HCKs: 100 cells/mL

Primary keratocytes treated towards SFs: 100 cells/μL

Primary keratocytes treated towards CSKs: 200 cells/μL

The cells needed for encapsulation were suspended in the correct amount of medium and this cell suspension was added to the solution of bifunctional molecules. Due to the addition of the cells suspension, the bifunctional molecules were diluted. To correct for this extra dilution step, the initial concentration of the bifunctional molecules was slightly higher (0.78 wt/v% instead of 0.52 wt/v%). For every experiment the bifunctional molecules were diluted with 1/3 of cell suspension, resulting in a final 0.52 wt/v% of bifunctional molecules. All the gels were prepared in wells of a non-adhesive 96-well plate (Fisher Scientific, Nunclon Sphera-Treated, U-Shaped-Bottom plate 15227905).

Synthetic hydrogels:

First 40 μL monofunctional molecules in solution were added to a well. Meanwhile, the cells were added to the solution of bifunctional molecules and mixed thoroughly. Second, 40 μL of bifunctional molecules / cell mixture were added to the 40 μL solution of monofunctional molecules inside the well. The molecules were mixed by carefully pipetting up and down (at least 3x per well), any air bubbles were removed by using a needle.

Hybrid hydrogel (control hydrogel):

For hybrid hydrogel preparation collagen type I (Gibco, Collagen I bovine, A1064401) was added to the solution of the bifunctional molecules, 20 μL was added per 100 μL complete gel (0.1 Wt/v%). Initially, the bifunctional molecules were dissolved at a higher wt/v% compared with the bifunctional molecules used for the synthetic or pristine hydrogel, to correct for this extra dilution

step with the collagen. At first, 40 µL solution of monofunctional molecules was added to a well. The cells and the collagen were added to the solution of bifunctional molecules and mixed thoroughly. Second, 40 µL of bifunctional molecules / cell / collagen mixture were added to the 40 µL solution of monofunctional molecules inside the well. The molecules were mixed by carefully pipetting up and down (at least 3x per well), any air bubbles were removed by using a needle.

For the exact hydrogel compositions, see **table 1**. All the hydrogels were placed up-side down in the incubator at 37 °C, 21% O_2 and 5% CO_2 for 1 hour to allow for proper gelation. After 1 hour, medium to embed the gels was carefully added to the wells, and the hydrogels with encapsulated cells were placed back in the incubator at 37 °C, 21% O_2 and 5% CO_2. After 1 day, the cell culture medium, surrounding the hydrogel is refreshed and for the PKs treated towards CSKs the expansion medium is replaced by the differentiation medium.

Table 1. Overview of the four hydrogel compositions used within this study. Calculations were made for one complete hydrogel with a volume of 80 µL.

Hydrogel compositions

Synthetic hydrogel (+UPy-cRGD)					
Building block / additive	*Ratio*	*µmol*	*mM*	*Wt/v %*	*Total Wt/v %*
UPy-PEG$_{10K}$-UPy	1	0.0094	0.117	0.13	
UPy-Glycinamide	73.6	0.69	8.63	1.03	1.29
Additive	6.4	0.06	0.75	0.13	
Synthetic hydrogel (+UPy-GFOGER)					
Building block / additive	*Ratio*	*µmol*	*mM*	*Wt/v %*	*Total Wt/v %*
UPy-PEG$_{10K}$-UPy	1	0.0094	0.12	0.13	
UPy-Glycinamide	75.6	0.71	8.85	1.06	1.42
Additive	4.4	0.04	0.52	0.23	
Synthetic hydrogel (+UPy-DGEA)					
Building block / additive	*Ratio*	*µmol*	*mM*	*Wt/v %*	*Total Wt/v %*
UPy-PEG$_{10K}$-UPy	1	0.0094	0.12	0.13	
UPy-Glycinamide	73.6	0.69	8.63	1.03	1.3
Additive	6.4	0.06	0.75	0.14	
Hybrid hydrogel (+collagen)					
Building block / additive	*Ratio*	*µmol*	*mM*	*Wt/v %*	*Total Wt/v %*
UPy-PEG$_{10K}$-UPy	1	0.0094	0.12	0.13	
UPy-Glycinamide	83.3	0.75	9.38	1.12	1.25
Collagen		0.1 Wt/v%			

Cell staining and Imaging

Before immunohistochemical stainings were carried out, the hydrogels were washed 3x with PBS (5 min per wash). All cells encapsulated within the hydrogels were fixated for 20 minutes at room temperature using 3.7% paraformaldehyde (formalin 37%, 104033.1000, Merck). After washing with PBS, samples were permeabilized for 15 minutes with 0.5% Triton X-100 in PBS. Followed by adding a blocking solution of 10% donkey or goat serum in 0.05% Triton X-100 in PBS for 30 minutes. Next, the cells were incubated with the primary antibodies diluted in 2% goat serum in 0.05% Triton X-100 in PBS overnight at 4 °C. Thereafter, the cells were washed thoroughly with 0.05% Triton X-100 in PBS, including wash waiting steps of 5-10 min. Next, the cells were incubated with the secondary antibodies and phalloidin at room temperature for 2 hours. Finally, the cells were stained with DAPI at a dilution of 1:250 for 10 min and washed thoroughly with PBS (including was waiting steps of 5-10 min). During imaging, complete/intact hydrogels were place on a thin coverslip (24x69 mm, VWR 631-1575) immerged in mowiol 4-88 (Sigma Aldrich, 81381) and imaged using a Leica TCS SP8 X inverted confocal microscope (Leica Microsystems) using HC PL APO CS2 objectives (20x/0.75, 40x/0.95). Images were processed in ImageJ to create a max-projection image of the original z-stack. See **table 2** for the primary and secondary antibodies used within this study.

Table 2. Overview of the used dyes, primary-, and secondary antibodies.

Antibody / dye	Company / reference #	Dilution
4',6-diamidino-2-phenylindole dihydrochloride (DAPI)	Sigma-Aldrich, D9542	1:250
Phalloidin 488	Sigma-Aldrich	1:300
Phalloidin 555	Sigma-Aldrich	1:300
Anti-YAP1	Ab52771, Abcam	1:100
Anti-ALDH3A1	Ab76976, Abcam	1:100
Secondary antibody		
Anti-rabbit IgG (goat) 647	A21244, Molecular Probes	1:250

Enzyme-linked immunosorbent assay (ELISA)

On various days during the 3D cell culture, medium was refreshed and all medium surrounding the sample was collected in separate small Eppendorf tubes and stored in -80 °C upon use. All ELISA experiments were executed with n=3, and all the standards as well as the samples are ran in duplicate. The following IL-8 concentrations were used for the standard curve of IL-8: 1000 pg/mL, 500 pg/mL, 250 pg/mL, 125 pg/mL, 62.5 pg/mL, 31.3 pg/mL, 15.6 pg/mL.

Uncoated Nunc™MaxiSorp™ ELISA plates (BioLegend, 423501) were used, and coated with capture antibody diluted in 1x coating buffer one day prior to running the ELISA (overnight incubation at 4 °C). See **table 3** for all the compositions of the used reagents. On the experiment day all the samples, the plates and the ELISA MAX™ Deluxe Set components (BioLegend®) were brought to room temperature. All the wash steps were executed in a similar manner, namely: 4 times with at least 300 µL wash buffer (0.05% Tween-20 in PBS) per well and residual buffer was blotted by firmly tapping the plate upside down on absorbent paper. After incubation with the capture antibody the plate was washed and blocked with 1x assay diluent A at room temperature for 1 hour with shaking (500 rpm) to minimize non-specific binding and reduce background. During this incubation, the samples for the standard curve were prepared and every well plate comprised a standard. After blocking, the wells were washed and incubated with 100 µL of the samples and standards at room temperature for 2 hours with shaking (500 rpm), all samples were diluted 4x in 1x assay diluent (25 µL sample, 75 µL 1x assay diluent). Thereafter, the wells were washed and 100 µL of detection antibody solution was added to each well, and incubated at room temperature for 1 hour with shaking (500 rpm). The wells were washed again and incubated with 100 µL of diluted Avidin-HRP solution at room temperature for 30 min with shaking (500 rpm). Subsequently, the wells were washed 5x thoroughly with wash buffer, and soaked in buffer for 1 minute for each wash to minimize background. Then, 100 µL of substrate solution C was added and incubated in the dark for 15 minutes. During this step, positive wells turned blue in color. To stop the reaction, 100 µL Stop Solution for TMB Substrate (BioLegend, 4230021) was added to each well. All the positive wells turned from blue to yellow during this step. After adding the stop solution to the wells, the plate was softly tapped to the table a few times to proper mix the solutions and immediately the absorbance at 450 nm was measured with the plate reader (Synergy HTX, BioTek). In addition the absorbance at 570 nm was measured, this absorbance could be subtracted from the 450 nm absorbance. The standard curve for each ELISA was plotted in excel and polynomial curve-fitting software with order 3 or 4 was used to determine the best fit. Using this formula together with the measured absorbance value, resulted in the calculation of the amount of cytokine secretion.

Graphpad Prism was used to perform statistical analysis. A 2-way Anova combined with a Sídák's multiple comparisons test demonstrated significant differences between the cellular IL-8 secretion of cells treated as stromal fibroblasts or cells treated towards corneal stromal keratocytes between day 7 and 21 for all the hydrogels, except the hydrogel functionalized with UPy-DGEA.

Table 3. Reagents used to perform an ELISA with 2x a complete 96-well plate

4 mL Coating Buffer A (5x)	16 mL of Deionized Water
100 µL of Capture Antibody (200x)	20 mL of 1x Coating Buffer
12 mL of Assay Diluent A (5x)	48 mL of PBS
100 µL of Detection Antibody (200x)	20 mL of 1x Assay Diluent A
20 µL of Avidin-HRP (1000x)	20 mL of 1x Assay Diluent A
Substrate Solution C	-
Used ELSIA set: *ELISA MAX™ Deluxe Set Human IL-8 (BioLegend, 431504)*	

3D Height indication cell images

A custom MatLab script was written to pair a specific height of the cell within the obtained z-stack image to a specific color. Image stacks obtained from channels corresponding to the DAPI (nuclei) and phalloidin (F-actin) were used to create these 3D height indication cell images. LAS X Life Science Microscope Software was used to calculate the original µm distance in the z-direction from the original *lif* file. *The custom MatLab script was written by Mark C. van Turnhout.*
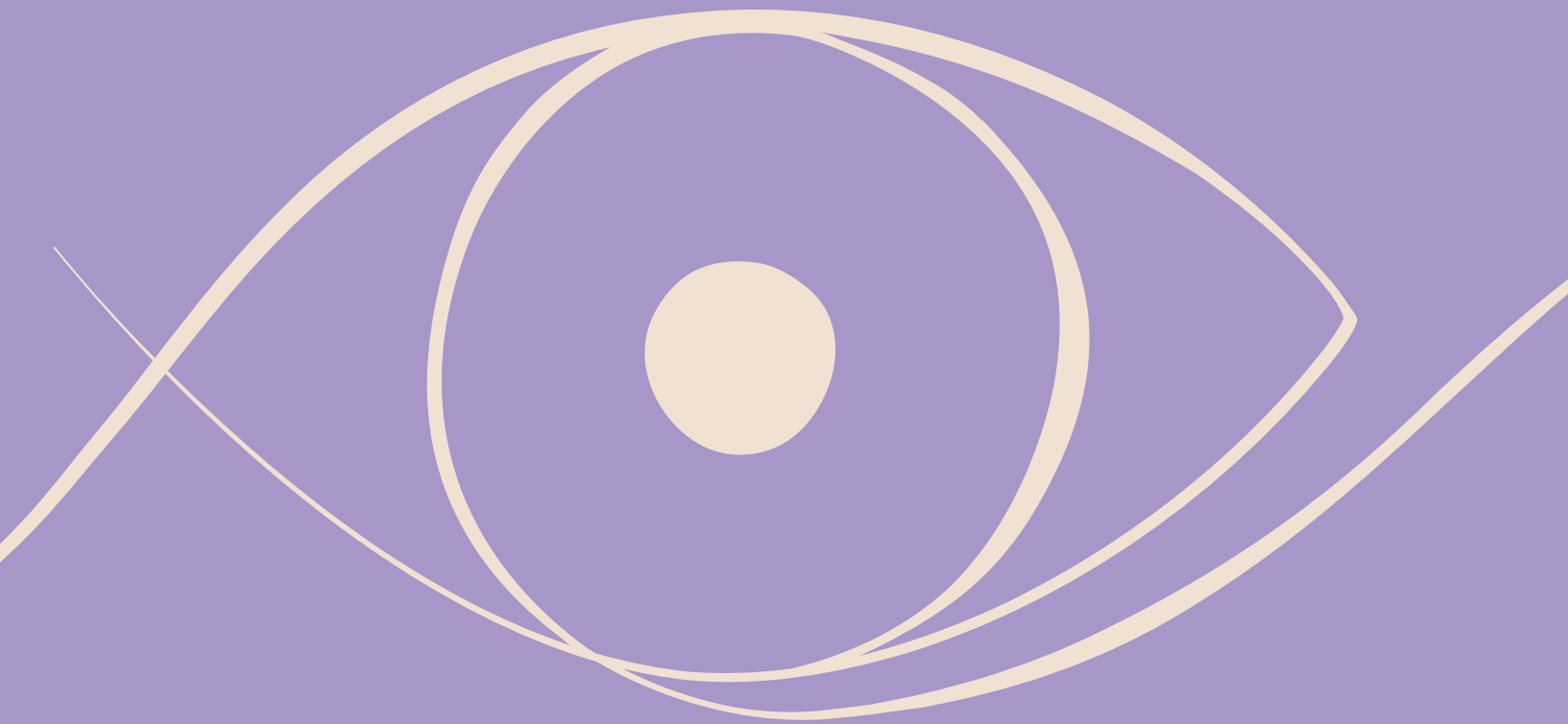
REFERENCES

1. Schwartz, M. A. Transmembrane signalling by integrins. *Trends Cell Biol* 2, 304–308 (1992).

2. Mobaraki, M. *et al.* Corneal Repair and Regeneration: Current Concepts and Future Directions. *Front Bioeng Biotechnol* 7, (2019).

3. Formisano, N. *et al.* Mechanical Properties of Bioengineered Corneal Stroma. *Adv Healthc Mater* 10, 2100972 (2021).

4. Walker, K. T. *et al.* Non-linearity of the collagen triple helix in solution and implications for collagen function. *Biochemical Journal* 474, 2203–2217 (2017).

5. Luo, J. & Tong, Y. W. Self-Assembly of Collagen-Mimetic Peptide Amphiphiles into Biofunctional Nanofiber. *ACS Nano* 5, 7739–7747 (2011).

6. Emsley, J., Knight, C. G., Farndale, R. W. & Barnes, M. J. Structure of the Integrin α2β1-binding Collagen Peptide. *J Mol Biol* 335, 1019–1028 (2004).

7. Bochicchio, B. & Tamburro, A. M. Polyproline II structure in proteins: Identification by chiroptical spectroscopies, stability, and functions. *Chirality* 14, 782–792 (2002).

8. Brodsky, B. & Persikov, A. V. Molecular Structure of the Collagen Triple Helix. in 301–339 (2005). doi:10.1016/S0065-3233(05)70009-7.

9. Horng, J.-C. Stereoelectronic effects on polyproline conformation. *Protein Science* 15, 74–83 (2006).

10. Reyes, C. D. & García, A. J. Engineering integrin-specific surfaces with a triple-helical collagen-mimetic peptide. *J Biomed Mater Res A* 65A, 511–523 (2003).

11. Luo, T. & Kiick, K. L. Collagen-Like Peptide Bioconjugates. *Bioconjugate Chemistry* vol. 28 816–827

12. Yamazaki, C. M. *et al.* A collagen-mimetic triple helical supramolecule that evokes integrin-dependent cell responses. *Biomaterials* 31, 1925–1934 (2010).

13. Creamer, T. P. & Campbell, M. N. Determinants of the polyproline II helix from modeling studies. in 263–282 (2002).

14. Hynes, R. O. Integrins. *Cell* 110, 673–687 (2002).

15. Luo, B.-H., Carman, C. V. & Springer, T. A. Structural Basis of Integrin Regulation and Signaling. *Annu Rev Immunol* 25, 619–647 (2007).

16. Diamond, M. S. & Springer, T. A. The dynamic regulation of integrin adhesiveness. *Current Biology* 4, 506–517 (1994).

17. Giancotti, F. G. & Ruoslahti, E. Integrin Signaling. *Science (1979)* 285, 1028–1033 (1999).

18. Huettner, N., Dargaville, T. R. & Forget, A. Discovering Cell-Adhesion Peptides in Tissue Engineering: Beyond RGD. *Trends Biotechnol* 36, 372–383 (2018).

19. Hersel, U., Dahmen, C. & Kessler, H. RGD modified polymers: biomaterials for stimulated cell adhesion and beyond. *Biomaterials* 24, 4385–4415 (2003).

20. Pierschbacher, M. D. & Ruoslahti, E. Cell attachment activity of fibronectin can be duplicated by small synthetic fragments of the molecule. *Nature* 309, 30–33 (1984).

21.   Staatz, W. D. *et al.* Identification of a tetrapeptide recognition sequence for the alpha 2 beta 1 integrin in collagen. *J Biol Chem* 266, 7363–7 (1991).

22.   Anderson, J. M. *et al.* Osteogenic differentiation of human mesenchymal stem cells synergistically enhanced by biomimetic peptide amphiphiles combined with conditioned medium. *Acta Biomater* 7, 675–682 (2011).

23.   Hennessy, K. M. *et al.* The effect of collagen I mimetic peptides on mesenchymal stem cell adhesion and differentiation, and on bone formation at hydroxyapatite surfaces. *Biomaterials* 30, 1898–1909 (2009).

24.   Bradshaw, M. *et al.* Designer self-assembling hydrogel scaffolds can impact skin cell proliferation and migration. *Sci Rep* 4, 6903 (2014).

25.   Wojtowicz, A. M. *et al.* Coating of biomaterial scaffolds with the collagen-mimetic peptide GFOGER for bone defect repair. *Biomaterials* 31, 2574–2582 (2010).

26.   O'Leary, L. E. R., Fallas, J. A., Bakota, E. L., Kang, M. K. & Hartgerink, J. D. Multi-hierarchical self-assembly of a collagen mimetic peptide from triple helix to nanofibre and hydrogel. *Nat Chem* 3, 821–828 (2011).

27.   Bezerra, K. S. *et al.* Computational investigation of the $\alpha_2\beta_1$ integrin–collagen triple helix complex interaction. *New Journal of Chemistry* 42, 17115–17125 (2018).

28.   Knight, C. G. *et al.* The Collagen-binding A-domains of Integrins α1β1 and α2β1Recognize the Same Specific Amino Acid Sequence, GFOGER, in Native (Triple-helical) Collagens. *Journal of Biological Chemistry* 275, 35–40 (2000).

29.   Khew, S. T. & Tong, Y. W. The Specific Recognition of a Cell Binding Sequence Derived from Type I Collagen by Hep3B and L929 Cells. *Biomacromolecules* 8, 3153–3161 (2007).

30.   Shekaran, A. & Garcia, A. J. Nanoscale engineering of extracellular matrix-mimetic bioadhesive surfaces and implants for tissue engineering. *Biochimica et Biophysica Acta (BBA) - General Subjects* 1810, 350–360 (2011).

31.   Hendricks, M. P., Sato, K., Palmer, L. C. & Stupp, S. I. Supramolecular Assembly of Peptide Amphiphiles. *Acc Chem Res* 50, 2440–2448 (2017).

32.   Silva, G. A. *et al.* Selective Differentiation of Neural Progenitor Cells by High-Epitope Density Nanofibers. *Science (1979)* 303, 1352–1355 (2004).

33.   Webber, M. J. *et al.* Supramolecular nanostructures that mimic VEGF as a strategy for ischemic tissue repair. *Proceedings of the National Academy of Sciences* 108, 13438–13443 (2011).

34.   Diba, M. *et al.* Engineering the Dynamics of Cell Adhesion Cues in Supramolecular Hydrogels for Facile Control over Cell Encapsulation and Behavior. *Advanced Materials* 33, 2008111 (2021).

35.   Dankers, P. Y. W., Harmsen, M. C., Brouwer, L. A., Van Luyn, M. J. A. & Meijer, E. W. A modular and supramolecular approach to bioactive scaffolds for tissue engineering. *Nat Mater* 4, 568–574 (2005).

36.   Dankers, P. Y. W. *et al.* Hierarchical Formation of Supramolecular Transient Networks in Water: A Modular Injectable Delivery System. *Advanced Materials* 24, 2703–2709 (2012).

37.   Dankers, P. Y. W. *et al.* Bioengineering of living renal membranes consisting of hierarchical, bioactive supramolecular meshes and human tubular cells. *Biomaterials* 32, 723–733 (2011).

38.   van Gaal, R. C. *et al.* Functional peptide presentation on different hydrogen bonding biomaterials using supramolecular additives. *Biomaterials* 224, 119466 (2019).

39. van Gaal, R. C. *et al.* Biomaterial screening of protein coatings and peptide additives: towards a simple synthetic mimic of a complex natural coating for a bio-artificial kidney. *Biomater Sci* 9, 2209–2220 (2021).

40. Mollet, B. B. *et al.* A modular approach to easily processable supramolecular bilayered scaffolds with tailorable properties. *J. Mater. Chem. B* 2, 2483–2493 (2014).

41. Spaans, S. *et al.* Supramolecular surface functionalization via catechols for the improvement of cell–material interactions. *Biomater Sci* 5, 1541–1548 (2017).

42. Kautz, H., Van Beek, D. J. M., Sijbesma, R. P. & Meijer, E. W. Cooperative end-to-end and lateral hydrogen-bonding motifs in supramolecular thermoplastic elastomers. *Macromolecules* vol. 39 4265–4267

43. Ramaekers, M. *et al.* Self-Assembly of Chiral Supramolecular Ureido-Pyrimidinone-Based Poly(ethylene glycol) Polymers via Multiple Pathways. *Macromolecules* 47, 3823–3828 (2014).

44. van Almen, G. C. *et al.* Development of Non-Cell Adhesive Vascular Grafts Using Supramolecular Building Blocks. *Macromol Biosci* 16, 350–362 (2016).

45. Goor, O. J. G. M., Brouns, J. E. P. & Dankers, P. Y. W. Introduction of anti-fouling coatings at the surface of supramolecular elastomeric materials via post-modification of reactive supramolecular additives. *Polym Chem* 8, 5228–5238 (2017).

46. Ippel, B. D., Arts, B., Keizer, H. M. & Dankers, P. Y. W. Combinatorial functionalization with bisurea-peptides and antifouling bisurea additives of a supramolecular elastomeric biomaterial. *J Polym Sci B Polym Phys* 57, 1725–1735 (2019).

47. Michelacci, Y. M. Collagens and proteoglycans of the corneal extracellular matrix. *Brazilian Journal of Medical and Biological Research* 36, 1037–1046 (2003).

48. Meek, K. M. & Knupp, C. Corneal structure and transparency. *Prog Retin Eye Res* 49, 1–16 (2015).

49. Cejas, M. A. *et al.* Collagen-Related Peptides: Self-Assembly of Short, Single Strands into a Functional Biomaterial of Micrometer Scale. *J Am Chem Soc* 129, 2202–2203 (2007).

50. Rele, S. *et al.* D-periodic collagen-mimetic microfibers. *J Am Chem Soc* 129, 14780–7 (2007).

51. Kar, K. *et al.* Aromatic Interactions Promote Self-Association of Collagen Triple-Helical Peptides to Higher-Order Structures. *Biochemistry* 48, 7959–7968 (2009).

52. Pires, M. M. & Chmielewski, J. Self-assembly of Collagen Peptides into Microflorettes via Metal Coordination. *J Am Chem Soc* 131, 2706–2712 (2009).

53. Fields, G. B. & Prockop, D. J. Perspectives on the synthesis and application of triple-helical, collagen-model peptides. *Biopolymers* 40, 345–357 (1996).

54. Fowler, S. D. & Greenspan, P. *The Journal of Histochemistry and Cytochemistry Application of Nile Red, a Fluorescent Hydrophobic Probe, for the Detection of Neutral Lipid Deposits in Tissue Sections: Comparison with Oil Red 0'*. vol. 33 (1985).

55. Bastings, M. M. C. *et al.* Quantifying Guest-Host Dynamics in Supramolecular Assemblies to Analyze Their Robustness. *Macromol Biosci* 19, 1800296 (2019).

56. Dupont, S. *et al.* Role of YAP/TAZ in mechanotransduction. *Nature* 474, 179–183 (2011).

57. Kwon, H., Kim, J. & Jho, E. Role of the Hippo pathway and mechanisms for controlling cellular localization of YAP/TAZ. *FEBS J* 289, 5798–5818 (2022).

58. Foster, J. W., Gouveia, R. M. & Connon, C. J. Low-glucose enhances keratocyte-characteristic phenotype from corneal stromal cells in serum-free conditions. *Sci Rep* 5, 10839 (2015).

59. Jester, J. V. Corneal crystallins and the development of cellular transparency. *Semin Cell Dev Biol* 19, 82–93 (2008).

60. Jester, J. V. *et al.* The cellular basis of corneal transparency: evidence for 'corneal crystallins'. *J Cell Sci* 112, 613–622 (1999).

61. Yam, G. H.-F. *et al.* Nerve regeneration by human corneal stromal keratocytes and stromal fibroblasts. *Sci Rep* 7, 45396 (2017).

62. de Feijter, I. *et al.* Solid-Phase-Based Synthesis of Ureidopyrimidinone–Peptide Conjugates for Supramolecular Biomaterials. *Synlett* 26, 2707–2713 (2015).

CHAPTER 5

Creating a hydrogel library based on protein mimicking supramolecular polyaminoacids

Amino acids are the essential building blocks of proteins, and determine the sequence controlled supramolecular folding into three dimensional protein structures. Inspired by the impact of amino acids in natural processes, amino acids are often used as building blocks to design functional biomaterials. Here, our goal is to create an exciting library of supramolecular amino acid monomers via the conjugation of an ureido-pyrimidinone (UPy) moiety to single amino acids. In solution, the supramolecular amino acid monomers assemble into supramolecular polyaminoacids, showing some small differences in fiber morphology and zeta potential. The introduction of a crosslinker to the supramolecular polyaminoacids resulted in the formation of transient networks, which enabled to study the influence of the various networks on cellular behavior. Both 2D cell culture, on top of the single polyaminoacids hydrogels, as well as 3D cell culture, encapsulation within the hydrogels, supported the cells to attain their spreaded morphology, to migrate, and to (re-)differentiate during culture. Excitingly, via mixing of multiple supramolecular amino acid monomers, our supramolecular approach allows for the formation of transient networks presenting various amino acids to the cells. Together, this work presents a library of supramolecular polyaminoacids as a novel design tool to generate a library of functional biomaterials able to synthetically mimic the natural protein presentation within the extracellular matrix.

INTRODUCTION

Within all biological processes proteins fulfill essential functions, acting as important and all-round macromolecules in living systems. The essential building blocks of proteins comprise of a variety of twenty amino acids, which are responsible for the sequence controlled supramolecular folding into three dimensional protein structures. This specific tertiary structure provides versatility to proteins, allowing them to possess numerous functions, *e.g.* acting as a catalysts, providing mechanical support, generating movement, contributing to tissue growth and cell differentiation.[1] Synthetic polyaminoacids, composed of one or more amino acids, have been widely studied for biological applications, resulting in various peptidomimetic materials with promising biological functionalities and easy metabolization processes of the degradation products.[2–4] For instance ε-poly(lysine), a cationic polymer which possesses promising biodegradability and biocompatibility.[5,6] Synthetic polymers conjugated to polyaminoacids introduced new functional materials, expanding the range of material properties.[4,7] For instance, Lin and coworkers synthesized various hybrid peptidomimetic polymers with the ambition to gain control over the material properties via reconstruction and manipulation of the secondary protein structure.[8–10] To this end, Lu *et al.* demonstrated a series of poly(L-glutamate) analogues with extended hydrophobic side chains that proved to be the driving force behind the formation of water-soluble helical structures.[9] Another approach to gain control over composition and architecture is the use of controlled ring-opening polymerization of amino acid N-carboxyanhydride (NCA), shown by Song *et al.,* who synthesized well-defined polypeptides via NCAs.[10]

Besides covalently based polymers, the use of supramolecular assemblies is an often used approach to mimic the biological function of proteins. A very diverse class of hydrogels is represented by self-assembling peptide hydrogels, combining the advantages of both natural and synthetic hydrogels. Recently, self-assembling peptide hydrogels are gaining interest within the tissue engineering field due to their versatile bottom-up design, biocompatibility, and functionalization possibilities. With the twenty natural amino acids available as library of building blocks, several researchers have designed peptide sequences that self-assemble into nanofibrous microenvironments. These nanofibrous microenvironments mimic the native extracellular matrix (ECM) and allow for the generation of self-assembling peptide hydrogels suitable for drug delivery and screening, tissue regeneration, and injectable cell therapy

applications.[11–34] For instance, Stupp and coworkers focus on peptide amphiphiles (PAs), where a typical fiber-forming PA molecule consist of a hydrophobic domain, typically a long alkyl tail, a short peptide sequence, capable of forming intermolecular hydrogen bonding, charged amino acids, to allow good solubility in water, and a bioactive epitope. Formation of hydrogen bonds between the peptide segments induces the formation of filamentous assemblies, which allow the use of PAs as functional biomaterials, whereafter incorporation of short peptide sequences like RGDS, IKVAV, and VEGF allowed the PAs to interact with cells.[35–39] In addition, Cui *et al.* produced various one-dimensional morphologies by changing the amino acids order within an tetrapeptide amphiphile, therewith demonstrating to control the morphology of one-dimensional nanostructures through rational choices of amino acid sequences.[40] Another supramolecular approach is based on the self-assembly of Fmoc-dipeptides, driven by hydrogen bonding and the attractive interactions between π electrons in the aromatic fluorenyl rings. Jayawarna *et al.* studied a library of Fmoc-dipeptides and demonstrated the spontaneous assembly of various Fmoc-dipeptides into fibrous bioactive hydrogels suitable for 2D and 3D culture of different cell lines. The structure and physical properties of these gels relied on the amino acid sequences of the peptide building blocks.[11,13,41] Zhou *et al.* showed another minimalistic approach to use Fmoc-di-/tri-peptides instead of longer peptides and derivatives, by demonstrating a mixture of Fmoc-RGD and Fmoc-FF (Fluorenyl-methoxycarbonyl-diphenylalanine) self-assembled into RGD-displaying peptides, providing a highly hydrated, stiff nanofibrous network able to promote fibroblast viability.[14,41]

Here, via the conjugation of a supramolecular ureido-pyrimidinone (UPy) moiety to single amino acids, we introduce an exciting library of supramolecular amino acid monomers. Due to the UPy-groups these supramolecular monomers dimerize via fourfold hydrogel bonding, resulting in lateral stacking and the assembly into supramolecular polyaminoacid fibers (**Figure 1A**). Herewith a library of functional hydrogels based on supramolecular polyaminoacids is generated, mimicking the protein presentation within the ECM via the design of a novel synthetic and minimalistic supramolecular approach. The introduction of a crosslinker, poly(ethylene glycol)(PEG) chain, end-capped with two functional UPy moieties (UPy-PEG$_{10K}$-UPy), to the supramolecular polyaminoacids allowed the transition from fibers in solution towards transient networks (**Figure 1B**). The formation of supramolecular polyaminoacid hydrogels allowed to study the influence of the various transient networks on cellular behavior via both 2D cell culture, on top of the hydrogels, as well as 3D cell culture,

encapsulation of cells within the hydrogels. Eventually mixtures of various single supramolecular polyaminoacids within one supramolecular hydrogel complex are studied as well. These mixtures allow for the presentation of various amino acids to the cells, mimicking the natural protein presentation within the ECM (**Figure 1C**).

RESULTS AND DISCUSSION

Properties of supramolecular polyaminoacid fibers in solution

The design of these supramolecular single polyaminoacids consists of oligo(ethylene glycol) (OEG) monomers, which are end-capped with a UPy moiety at one end and a single amino acid group at the other end (UPy-AA). The UPy-AA were subdivided into five different groups (**Figure 1A**), being the UPy-AA with charged positive side chains: UPy-Arginine (UPy-Arg), UPy-Histidine (UPy-His), UPy-Lysine (UPy-Lys), charged negative side chain: UPy-Aspartic acid (UPy-Asp), UPy-Glutamic acid (UPy-Glu), polar uncharged side chains: UPy-Serin (UPy-Ser), UPy-Threonine (UPy-Thr), UPy-Asparagine (UPy-Asn), UPy-Glutamine (UPy-Glu), special cases: UPy-Cysteine (UPy-Cys), UPy-Glycine (UPy-Gly), UPy-Proline (UPy-Pro), and hydrophobic side chains: UPy-Alanine (UPy-Ala), UPy-Valine (UPy-Val), UPy-Isoleucine (UPy-Ile), UPy-Leucine (UPy-Leu), UPy-Methionine (UPy-Met), UPy-Tyrosine (UPy-Tyr). Some of the UPy-AA showed to be a bit turbid and not completely transparent after dissolving in the neutral or basic conditions, being UPy-Thr, UPy-Asn, UPy-Gln, UPy-Leu, UPy-Met, UPy-Tyr. Yet, these UPy-AA were dissolved enough to be used for or follow-up experiments. Two UPy-AA were left out of the study due to poor solubility, being UPy-Phenylalanine (UPy-Phe) and UPy-Tryptophan (UPy-Trp).

To explore the effect of the amino acid functionality on the self-assembly of the UPy units, monofunctional UPy units functionalized with the single amino acids were dissolved in alkaline PBS (pH ~ 12) at elevated temperature. Due to high pH, crosslinks are disrupted by deprotonation of the UPy molecule, resulting in the optimal solubility of the UPy-AA compounds.[43] To neutralize the UPy-AA compounds, 1 M HCl was used and the assembling behavior of the UPy-AA was characterized using cryogenic transmission electron microscopy (cryo-TEM) (**Figure 2A**), from which the fiber diameter was determined (**Figure 2B**). Furthermore, the zeta-potential was measured (**Figure 2C**), determining the net surface charge of the UPy-AA in solution.
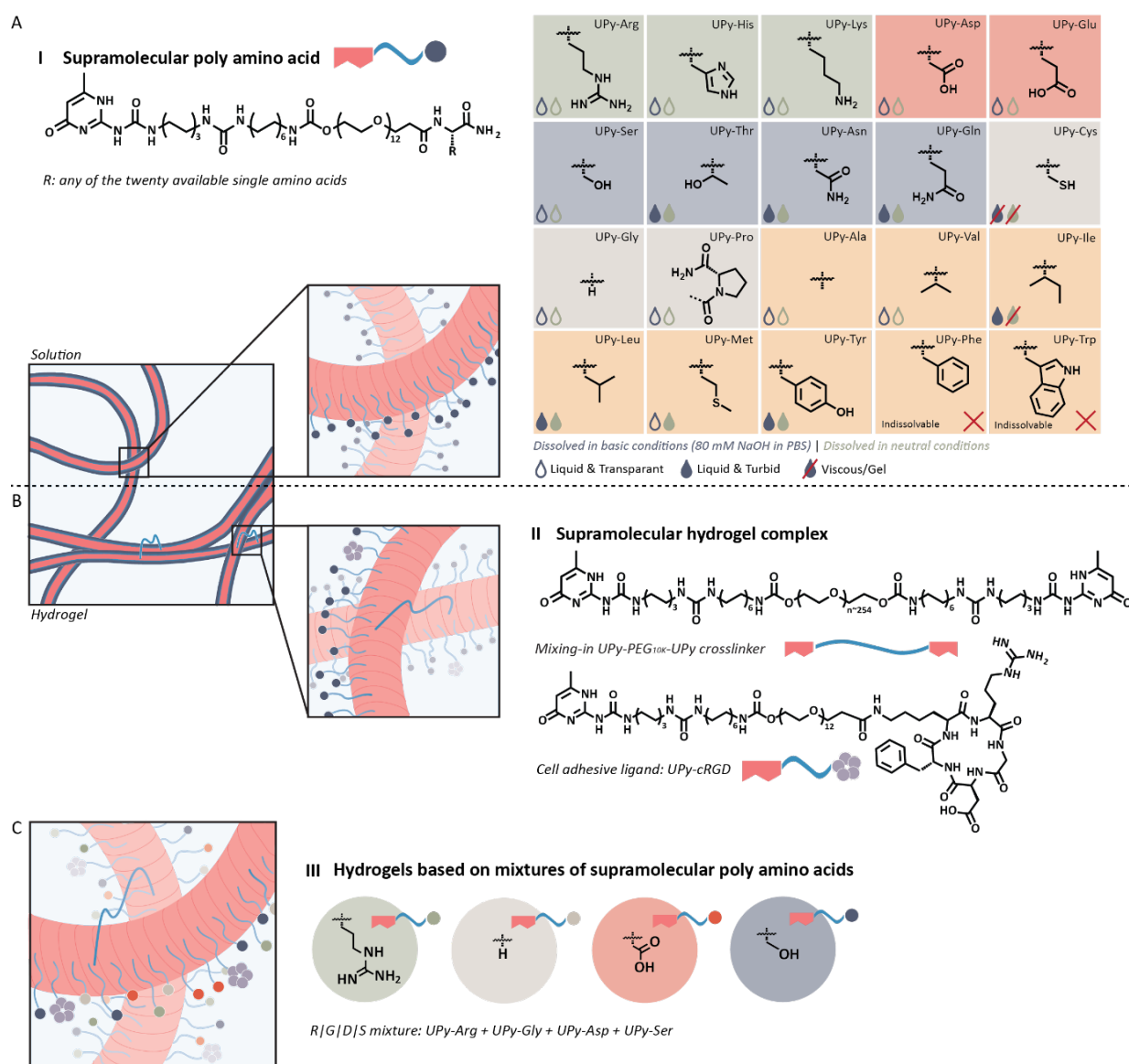
Figure 1. Conceptual overview of the work described in this study. **A)** Schematic representation of the synthesized supramolecular polyaminoacid. The UPy-based molecules self-assemble into fibers through dimerization via quadruple hydrogel bonds and lateral stacking (still a solution). Including an overview of the monofunctional UPy-moieties with different amino acid functionalities, *i.e.* positively charged UPy-AA (green), negatively charged UPy-AA (red), polar UPy-AA (blue), special cases (grey), and hydrophobic UPy-AA (orange). Dissolved at a concentration of 19 mM in basic and neutral conditions, respectively. UPy-Phe and UPy-Trp are unable to be dissolved. **B)** Addition of the bifunctional UPy-PEG$_{10K}$-UPy will lead to the formation of a transient network, with the UPy-PEG$_{10K}$-UPy acting as a crosslinker. The bioactive UPy-cRGD introduces ligands into the hydrogel system to allow cell adhesion. **C)** Desired mixtures of supramolecular polyaminoacids can be introduced into the hydrogel system, resulting in long fibers, which present various amino acids to the cells.

UPy-Arg (diameter size 6.1 ±0.6 nm) and UPy-Lys (diameter size 5.8 ±0.4 nm) show to form long flexible nanofibers that tend to cluster and entangle randomly, both displaying a positive charge of 37.6 ±4 mV and 39.2 ±2, respectively. Surprisingly, these are the only UPy-AA that display clustering tendency as well as being the only UPy-AA containing a positive charged side chain at neutral pH. Part of the amine side chains of UPy-Arg and UPy-Lys could be shielded by the negatively charged phosphates in PBS, neutralizing the charge. This salt shielding could result in a hydrophobic nonpolar side chains, which are favorable for hydrophobic clusters.[44] Despite UPy-His belongs to the same sub-group as UPy-Arg and UPy-Lys, its assembly behavior showed to be different. UPy-His (diameter size 4.6 ±0.5 nm) shows long fibril assembly that appear to be bundling with some occasional shorter fibers, displaying a neutral charge of 0.20 ±1 mV. UPy-Asp and UPy-Glu have a relatively short, polar, negatively-charged side group. For UPy-Asp, highly structured fiber bundling assembly along with thick long fibers (diameter size 6.1 ±0.4 nm) were observed together with a negative charge of -49.6 ±5 mV. UPy-Glu shows as well long fibers, yet the structured fiber bundling of UPy-Asp is less abundantly present. Perhaps this is related to the slightly thicker fibers (diameter size 6.8 ±0.6 nm) and slightly less negative charge of -34 ±1 mV. The polar UPy-Ser (diameter size 4.4 ±0.4 nm), UPy-Thr (diameter size 5.4 ±0.4 nm), and UPy-Gln (diameter size 5.4 ±0.4 nm) show long flexible fiber assembly. Slightly more fiber bundling is observed for UPy-Ser and UPy-Thr, displaying a negative charge of -23.6 ±2.5 mV and -15 ±2 mV, respectively. UPy-Asn (diameter size 6.3 ±0.9) deviated from the other UPy-AA within this sub group, displaying a negative charge of -43.6 ±3.4 mV and showing more thick and even a bit belt-like fibril morphologies. UPy-Gly (diameter size 4.6 ±0.3 nm) displaying a negative charge of -29.6 ±2.5 mV differs slightly from UPy-Pro (diameter size 5.8 ±0.6 nm) displaying a less negative charge of -8.5 ±1 mV. Long fiber formation can be observed for UPy-Gly, while UPy-Pro assembles into long undisrupted fibers along with shorter fibers, ranging from approximately 50-400 nm. The proline side chain could be responsible for these disruptions. Although the fiber thickness and negative charge of UPy-Cys (diameter size 5.0 ±0.6 nm, -25.1 ±3 mV) are comparable with UPy-Gly, the observed fiber morphology deviates heavily from the long UPy-Gly fiber morphology. Apparently the cysteine side chain influences the fibril formation substantially, resulting in a truncated fiber morphology existing of fibers with a length varying from 10-300 nm. The UPy-AA with a hydrophobic amino acid functionality all showed to have a quite similar, slightly negative charge, with being -16 ±2 mV (UPy-Ala), -8.2 ±0.4 mV (UPy-Val), -7.1 ±0.5 mV (UPy-Ile), -12.1 ±1 mV (UPy-Leu), -15.1 ±1 mV (UPy-Met) and
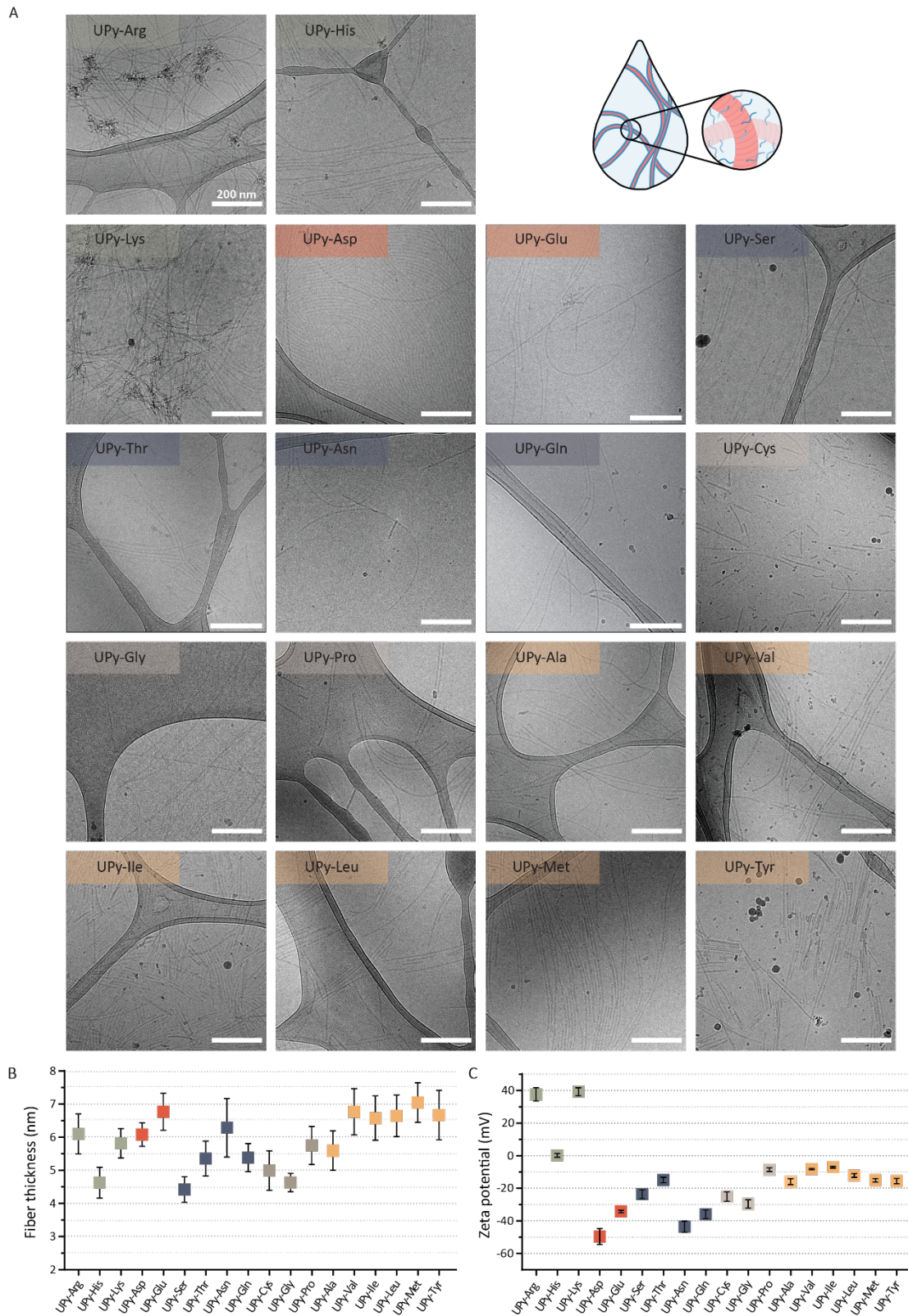
Figure 2. Properties in solution. **A)** Cryogenic transmission electron microscopy images of the diluted UPy-AA (80 µM, ~ 0.1 mg/mL) in neutralized PBS, scale bar represents 200 nm. **B)** Calculated fiber thickness from the cryogenic transmission electron microscopy images, calculated from 3 images per UPy-AA, 6 fibers per image, ± standard deviation. **C)** Zeta-potential measurements of UPy-amino acids in solution at a concentration of 0.4 mM in 0.1x PBS, ± standard deviation.

-15.6 ±1 mV (UPy-Tyr). Elongated, long, belt-like fiber formation was noticed for UPy-Ala (diameter size 5.6 ±0.6 nm), which deviated this UPy-AA from the other UPy-AA within the hydrophobic subgroup. For UPy-Val (diameter size 6.8 ±0.7 nm), UPy-Leu (diameter size 6.6 ±0.6 nm) and UPy-Met (diameter size 7.0 ±0.6 nm) showed elongated long fibers formation and bundling assembly. UPy-Tyr (diameter size 6.7 ±0.7 nm) and UPy-Ile (diameter size 6.6 ±0.7 nm) showed short fiber formation that clustered in bundles. Noteworthy, is the observed difference in fiber length between UPy-Ile and UPy-Leu, which is the isomer of UPy-Ile.

These results demonstrated substantial differences between the assembly in solution of the various supramolecular polyaminoacid monomers into supramolecular polyaminoacid fibers, *e.g.* fiber length, fiber diameter, and charge. Even rather small differences in the R-group of the amino acids provoked changes in the fiber morphology, as seen with the isomers UPy-Ile and UPy-Leu.

Formation and rheological properties of supramolecular polyaminoacid hydrogels

The fundament of the supramolecular hydrogel consists of bifunctional and monofunctional molecules, both containing functional hydrogen bonding UPy groups as supramolecular building blocks. Addition of low contents bifunctional UPy-PEG, a 10 kDa poly(ethylene glycol) (PEG) chain end-capped with two functional UPy moieties, acting as a crosslinker between the monofunctional fibers of the UPy-AA, led to the formation of transient networks (**Figure 3A**).[42] Integrin-binding cyclic arginine-glycine-aspartate (cRGD) ligands are introduced into the hydrogel system to design a fully synthetic hydrogel, allowing cell hosting. A monofunctional molecule is functionalized with a UPy-cRGD end group, fulfilling the role as a cell-adhesive supramolecular additive (**Figure 3B**). Visualization of the transient network was realized by introducing a fluorescent label into the hydrogel system. A monofunctional molecule is functionalized with a sulfonated cyanine dye (UPy-Cy5) end group, fulfilling the role as a fluorescent supramolecular additive.

The presented supramolecular hydrogel system allows for both 2D cell culture, on top of the hydrogels, as well as 3D cell culture via cell encapsulation within the hydrogel (**Figure 3C**). Both methods start identically, by dissolving the bifunctional UPy-PEG separately from the monofunctional UPy-AA (including additives). For 2D cell culture, the bifunctional and
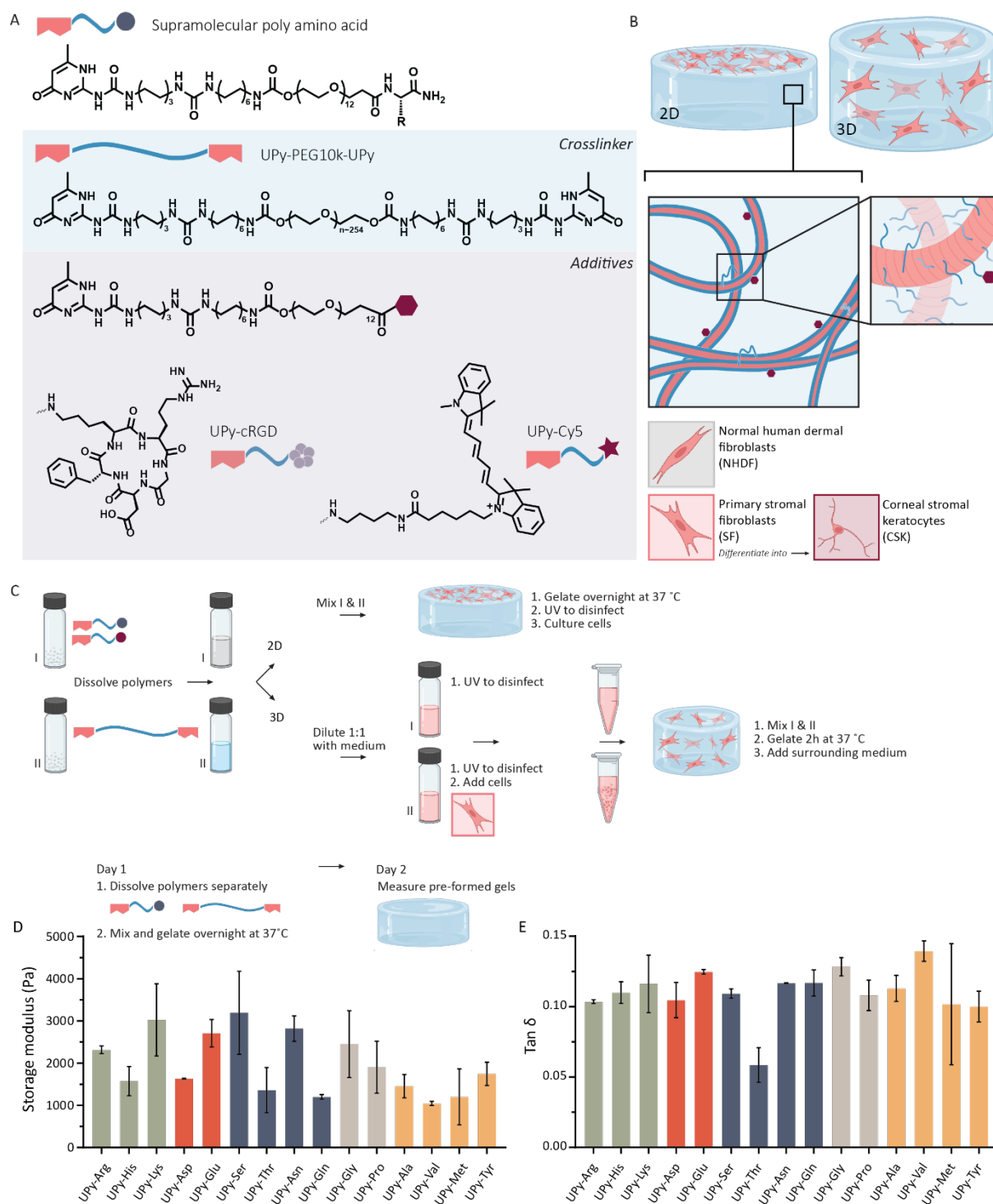
Figure 3. Hydrogel formulation and overview of this study. **A)** Overview of the bifunctional UPy-moiety acting as a crosslinker, the monofunctional UPy-moiety with variable R group, the UPy-cRGD used to add bioactivity to the system and the UPyCy5 used to visualize the network. **B)** Both 2D and 3D cell cultures are performed with two cell types; normal human dermal fibroblasts (NHDF) cell line and primary keratocytes treated towards stromal fibroblasts (SFs) or treated towards corneal stromal keratocytes (CSKs). **C)** Hydrogel formulation method. **D)** The storage modulus of the various pre-formed UPy-AAs are shown at a frequency of 1 rad/s, 1% strain, at a concentration of 18.7 mM UPy-AA combined with 0.23 mM UPy-PEG in 1x PBS, mean ± standard deviation presented. **E)** The loss tangent showing the viscoelastic behavior of the gels, mean ± standard deviation presented.

monofunctional molecules are mixed together and left for overnight gelation. To realize 3D cell culture, the cells need to be encapsulated within the hydrogel. To this end the bifunctional and monofunctional molecules are both diluted with cell culture medium to provide the cells with some nutrients during gelation. Cells are supplemented to the bifunctional molecules in solution and afterwards the bifunctional and monofunctional molecules are mixed together and left 2 hours for proper gelation before cell culture medium was added to the cells.

The effect of the UPy-AA at increased concentration (~ 18.7 mM) crosslinked with bifunctional UPy-PEG (0.23 mM) was examined by rheology measurements. The mechanical properties of these gels were measured, determining the storage modulus (**Figure 3D**) and viscoelastic behavior by means of tangent delta (tan δ) (**Figure 3E**). Cells are known to be responsive towards material stiffness, with loss of cytoskeletal tension on soft substrates, leading to a rounded morphology. In contrast, stiff substrates can withstand higher traction forces from the cells, inducing an increase of the tensile state of the cytoskeleton resulting in a spreaded cellular morphology.[45] Due to the impact of material stiffness on cellular behavior, the rheological properties of hydrogels are important to examine. Unfortunately, UPy-Cys, UPy-Ile, and UPy-Leu were left out for the hydrogel studies due to poor solubility at high concentrations, resulting in highly turbid or semi-gelated solutions. The storage moduli varied for the UPy-AA hydrogels from 1045 ±50 Pa for UPy-Val to 3195 ±983 Pa for UPy-Ser. For the positively charged UPy-AA both UPy-Arg 2315 ±92 Pa and UPy-Lys 3025 ±856 Pa showed a somewhat higher storage moduli compared with UPy-His 1575 ±346 Pa. Perhaps the differences in fiber morphology observed with the cryo-TEM do have an influence on the storage moduli, while both UPy-Arg and UPy-Lys demonstrated an enhanced stiffness and previously the cryo-TEM demonstrated their tendency to cluster. The negatively charged UPy-Asp 1635 ±7 showed a lower stiffness compared with UPy-Glu 2710 ±325. This difference in stiffness could be related to the more abundantly present structured fiber bundling of UPy-Asp observed in the cryo-TEM. These bundle formations can sterically hinder the bifunctional UPy-PEG molecules in some extent to form supramolecular interactions, lowering the supramolecular crosslinks between the UPy-Asp and bifunctional UPy-PEG. For the polar UPy-AA both UPy-Ser and UPy-Asn 2820 ±297 Pa showed similar stiffnesses. Noteworthy are the substantially lower stiffnesses for UPy-Thr 1362 ±535 and UPy-Gln 1200 ±57 within the polar UPy-AA sub group. No motivation for these differences can be found in the previous data of the cryo-TEM and related fiber thickness nor the zeta potential. Both UPy-Gly and UPy-Pro

showed similar stiffnesses of 2450 ±792 Pa and 1905 ±615 Pa, respectively. Apparently the differences observed in fiber morphology between the UPy-AA within the hydrophobic subgroup did not lead to any substantial differences in the stiffness, *i.e.* UPy-Ala 1455 ±276, UPy-Met 1202 ±662 and UPy-Tyr 1745 ±276. A subtle difference in storage moduli is observed between the different groups, with the hydrophobic UPy-AA (UPy-Ala, UPy-Val, UPy-Met, UPy-Tyr) displaying a trend towards a lower storage modulus, and the positively charged (UPy-Arg, UPy-His, UPy-Lys), negatively charged (UPy-Asp, UPy-Glu) and polar UPy-AA (UPy-Ser, UPy-Thr, UPy-Asn, UPy-Gln) show a trend towards a higher storage modulus. This effect could be due to the diminished solubility and mobility of the hydrophobic amino acids, which to some extend lowers the supramolecular crosslink formation. No substantial differences were observed in viscoelastic behavior between the UPy-AA. Overall, these results demonstrated storage moduli ranging between 1000-3000 Pa with no substantial differences between the storage moduli of the various UPy-AA hydrogels.

Culture of keratocytes on top of supramolecular polyaminoacid hydrogels (2D)

To examine the cellular compatibility and adhesive properties of the hydrogels, isolated human primary keratocytes (PKs) were cultured on top of the hydrogels for three days and stained for F-actin to visualize the cytoskeleton (**Figure 4A**). Nuclei visualization was used to perform a nuclei count, which provided the amount of nuclei per mm^2 (**Figure 4B**), the visualized cytoskeleton was used to calculate the cellular surface coverage of the hydrogel (**Figure 4C**). Additionally, after 7 days of culture another set of hydrogels was used to perform a metabolic activity assay (**Figure 4D**). Keratocytes cultured on top of the positively charged UPy-Arg and UPy-Lys hydrogels demonstrated a spreaded morphology, and high values of the nuclei count and surface coverage percentages as well. These results indicated the ability of UPy-Arg and UPy-Lys to support a healthy cellular behavior. Similar trends were observed in other studies, in which positive coatings[46] and positively-charged hydrogels[47,48] often showed to support cellular adhesion. This is mediated by the interaction between polyanionic cell surface and polycationic surface or hydrogel. The UPy-His hydrogels show a similar spreaded morphology, yet a substantial higher nuclei count and surface coverage. Though the histidine contains a neutral charge at neutral pH (confirmed by the zeta-potential measurements), the histidine side-chain shows to have a positive effect regarding the cellular spreading. Both UPy-Asp and

UPy-Glu supported cells to adhere the hydrogels and to spread. Noteworthy is the tendency of the cells to form cell clusters, resulting in a diminished nuclei count compared to the positively charged hydrogels. Negatively charged surfaces induce binding to polar functionalities on the cell membrane and mediate protein binding with proteins containing polyelectrolytic charges.[49] Bet *et al.* stated an improved cellular adhesion due to the polarity of the negative charge, influencing the wettability to a level suitable for cell adhesion.[50] This principle can induce an increase of cellular adhesion between negative charged hydrogels and cell membrane, leading to a spreaded morphology of the cells. Furthermore, the DAPI stain, which contains two amidine side groups with a positive charge, stained the fibril structure of the UPy-Asp and UPy-Glu transient network, which further strengthens the hypothesis of proteins being absorbed on the negatively charged hydrogels. High variability was observed for the UPy-AA hydrogels within the polar amino acid sub group, showing different cellular morphologies as well as a large variation in the nuclei count and surface coverage. UPy-Ser and UPy-Gln showed high cellular adhesion with spreaded cellular morphologies and also both a high nuclei count and surface coverage. UPy-Thr and UPy-Asn showed a lower cellular adhesion, diminished spreaded cellular morphology and increased tendency for cell clustering. Both UPy-Gly and UPy-Pro showed similar high cellular adhesion and spreaded cellular morphology. Moreover, the keratocytes showed a small preference for the formation of cell sheets instead of separated spreaded cells, resulting in the highest number of nuclei/mm^2 and surface coverage. UPy-Ala showed to behave as an exception within the hydrophobic UPy-AA sub group. In addition to the fiber thickness, and zetapotential results, the cellular results of UPy-Ala are also very comparable with the results of UPy-Gly and UPy-Pro. With a single methyl group as side-chain, the hydrophobic character of UPy-Ala is lower in comparison to the other hydrophobic UPy-AA. To this end, the other hydrophobic UPy-AA, *i.e.* UPy-Val, UPy-Ile, UPy-Leu, UPy-Met, UPy-Tyr, showed a lower cellular adhesion with small single cells or small clusters of cells. The combination of an average number of nuclei/mm^2 together with a low cell surface coverage, indicates that the adhering cells are smaller in size. The somewhat less spreaded cellular morphology could be influenced by the increase in hydrophobic side-chains. This increase could lead to a more collapsed state of the side chains, which can entrap the ligand moieties present in the hydrogel and render them less available for cellular attachment. Overall, the metabolic activity of the cells cultured on the different substrates did not deviate substantially between the UPy-AA hydrogels.
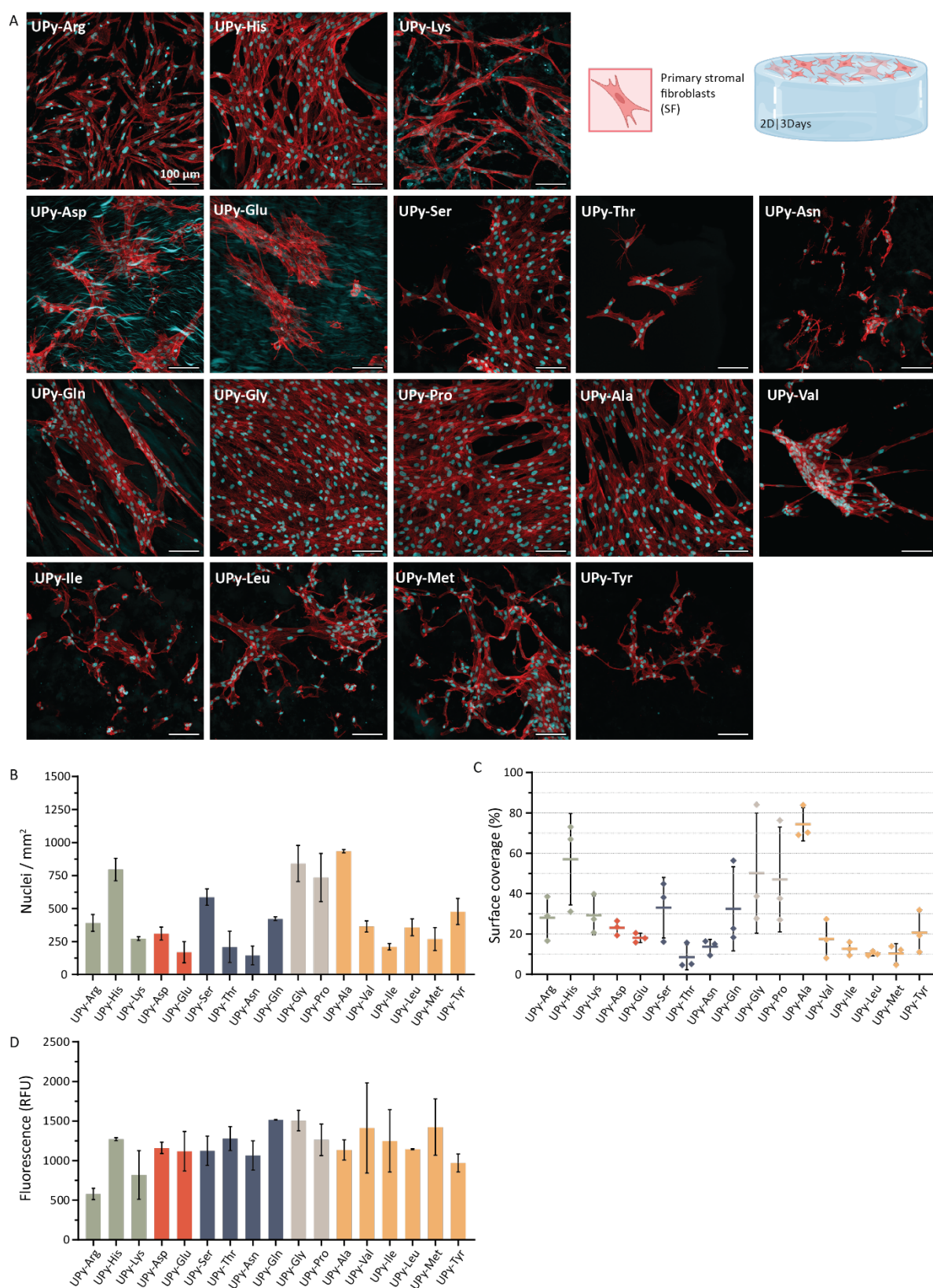
Figure 4. PKs cultured on top of the AA hydrogels containing 1 mM UPy-cRGD (2D). **A)** Immunofluorescent staining of f-actin (red) and nuclei (cyan). 3-day culture, scale bars are 100 μm. **B)** Average number of nuclei per mm² of fixated PKs quantification after 3 days of culture, data derived from two replicates, mean ± standard error of the mean presented. **C)** Surface coverage of the cells in percentage. **D)** Metabolic activity of PKs after 7 days of culture, data derived from two replicates, mean ± standard error of the mean presented.

An additional experiment was performed with another cell type, namely normal human dermal fibroblasts, which were also cultured for 3 days on top of a selection of UPy-AA hydrogels (**Figure 9**). Despite the difference in cell type, similar cell adhesion and cellular morphologies were observed for the UPy-AA hydrogels. To examine the need for the adhesive ligand (UPy-cRGD), some of the hydrogels were prepared without incorporation of a UPy-cRGD (**Figure 10**). Only a few cells adhered to these hydrogels, and these cells were not able to exhibit a spreaded morphology. These results indicated that the addition of the adhesive ligand is necessary for all the studied UPy-AA hydrogels to support cell adhesion.

Culture of keratocytes on top of UPy-Cy5 functionalized supramolecular polyaminoacid hydrogels (2D)

To gain more information on how the cells do adhere to the UPy-AA hydrogels, monofunctional UPy moieties functionalized with Cy5 were used to visualize the transient network. For this experiment, only a selection of UPy-AA hydrogels were studied, being the positively charged UPy-Lys, the negatively charged UPy-Glu, and the neutral UPy-Gly. Primary keratocytes (PKs) were cultured on top of these hydrogels for 7 days, and afterwards the cell-hydrogel constructs were analyzed by using a confocal microscope (**Figure 5A**). All three UPy-AA hydrogels allowed the cells to adhere and a spreaded morphology of the cells was observed. The use of UPy-Cy5 revealed a striking network visualization of UPy-Lys, instead of a homogenous fluorescent hydrogel, short fibers with a length of ~ 8 µm as well as very bright fluorescent clusters of fibers were observed. The previously observed cryo-TEM results demonstrated as well long flexible nanofibers, with the tendency to cluster. However, the merged images provided no indication of an interaction between these short fibers and the cells. For UPy-Glu a very homogenous material is visualized without any short fibers or fluorescent clusters present. It seems that the cells do feel the curves of the material, as the cells tend to grow and spread alongside the material curves. The results of UPy-Gly are quite similar to the results of UPy-Glu, a homogenous material, without any short fibers or clusters. Compared with UPy-Glu, fiber like structures are a bit more abundant. The 3D visualization of each hydrogel showed as well a distinct difference between UPy-Lys and the other two UPy-AA hydrogels (**Figure 5B**). The projection of UPy-Glu and UPy-Gly showed a homogenous material, without holes or clusters of fibers. On the contrary, the projection of UPy-Lys showed a mix of clustered fibers,

alternately with holes. Compared with UPy-Gly and UPy-Glu, the network of UPy-Lys can be described as hydrogel with a mesh-like structure. Some additional rheological measurements were performed, to examine if these differences in network formation influence the rheological properties during the hydrogel formation. However, no substantial differences were observed with these measurements.

Due to the substantial difference in network formation, some extra cell analysis were performed. To examine if this mesh-like structure of the UPy-Lys also influence the migration and spreading of the cells. Although the PKs are cultured on top of the hydrogels (2D), it seems that the cells do not only spread on top of the hydrogels but the hydrogels also allows them to spread or migrated slightly into the hydrogel. Multicolored images visualize the original height of the cells in the obtained confocal image (**Figure 5C**). Cells cultured on top of all the UPy-AA hydrogels are able to migrate or spread into the z-direction within a range of 55-70 µm. Despite the substantial difference in network formation for UPy-Lys, no differences in the cellular behavior were observed between the three UPy-AA hydrogels.

Furthermore, to explore the influence of the a positive, negative or neutral charged hydrogel on their ability to bind proteins a bicinchoninic acid (BCA) assay was performed with these three UPy-AA hydrogels (**Figure 12**). Two methods were used to study the binding of proteins; (1) at first the hydrogels were prepared with phosphate buffered saline (PBS) and after gelation the hydrogels were embedded in cell culture medium supplemented with fetal bovine serum (FBS), (2) secondly the hydrogels were prepared as usual with cell culture medium supplemented with FBS whereafter the hydrogels were embedded in PBS. After an incubation of 7 days, the results of the UPy-AA hydrogels embedded in culture medium with FBS (method 1) showed a decrease in measured protein concentration for the UPy-Lys hydrogel, suggesting that the proteins have a preference to bind to the hydrogel with a positive charge. This suggestion was strengthened by the results of the UPy-AA hydrogels embedded in PBS (method 2), which demonstrated a lower protein concentration for UPy-Lys compared with the concentrations measured for UPy-Glu and UPy-Gly. Again these results indicate that the proteins captured in the hydrogel during the preparation method, less easily dilute out of the positively charged UPy-Lys hydrogel compared with the UPy-Glu and UPy-Gly.
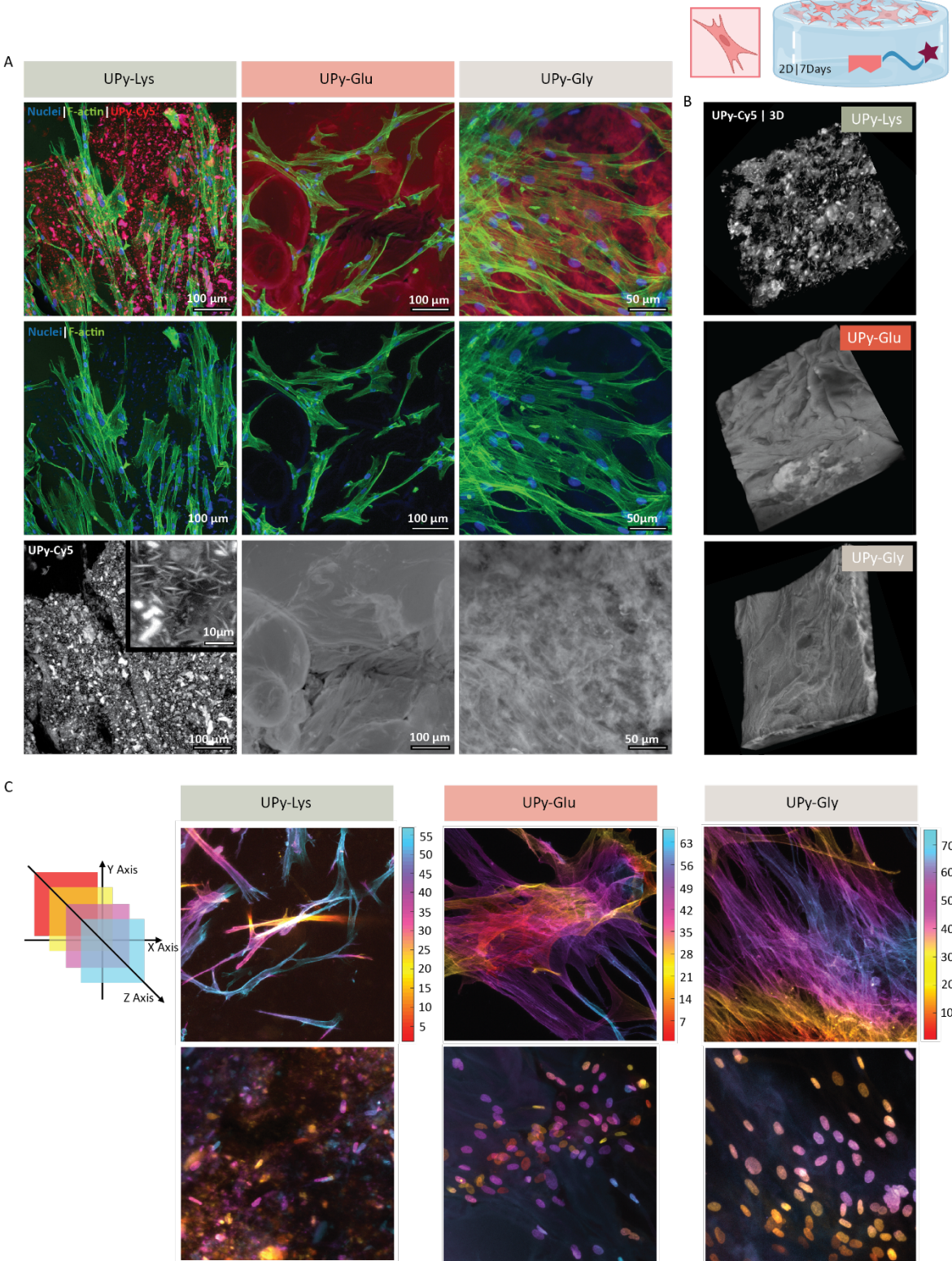
Figure 5. PKs cultured on top of Upy-Lys, UPy-Glu and UPy-Gly based hydrogels. The UPy-Cy5 additive is incorporated within all the hydrogels to visualize the network. **A)** From top to bottom: a merged immunofluorescent image representing the UPy-Cy5 in red, F-actin in green and nuclei in blue, a merged immunofluorescent image representing the F-actin and nuclei, a visualization of the UPy-Cy5. **B)** 3D visualization of the UPy-Cy5 within the hydrogel. **C)** Per UPy-AA, multicolored images visualize the original height in the obtained z-stack file. The top row represents the f-actin channel, the bottom row represents the nuclei channel. The color scale is in μm.

Encapsulation of primary keratocytes within a selection of supramolecular polyaminoacid hydrogels

Due to some interesting differences in cell behavior during the 2D cell culture on top of the various UPy-AA hydrogels, the effect of exposing cells to various UPy-AA within their microenvironment is further explored by encapsulating cells within UPy-AA hydrogels and start 3D cell culture. A selection of UPy-AA hydrogels was made by choosing at least one amino acid of each sub-group, *i.e.* UPy-Arg and UPy-Lys being positively charged amino acids, UPy-Glu being a negatively charged amino acid, UPy-Gln being a polar amino acid, UPy-Gly being a special amino acid, and UPy-Val being a hydrophobic amino acid. PKs were encapsulated within these UPy-AA hydrogels and cultured for 21 days, thereafter immunohistochemical analysis was performed to study the cellular morphology and ongoing mechanotransduction via yes-associated-protein (YAP) translocation (**Figure 6A**).

Elongated cells were observed for the positively charged UPy-Arg and UPy-Lys, rather comparable with the results of the 2D cell culture. Noteworthy is the large variation in cell compatibility of UPy-Arg, only a few spots within the hydrogel supported cell adhering and a spreaded morphology of the cells. The other UPy-AA hydrogels showed a homogenous distribution of cells throughout the whole hydrogel. In addition, some of the UPy-Arg hydrogels hosted no cells with a spreaded morphology, only small round-shaped cells that probably died during the culture. To this end, no analysis of YAP translocation or nuclei eccentricity could be performed for cells encapsulated within the UPy-Arg hydrogels. PKs with a spreaded morphology and the tendency to form cell clusters were observed within the negatively charged UPy-Glu hydrogel. An elongated cell morphology was also observed for the cells encapsulated within UPy-Gln hydrogels. These cells formed a less dense cellular network compared with the very dense sheets of cells, which were observed within the UPy-Gly and UPy-Val hydrogels. Especially the results of the cells encapsulated within the hydrophobic UPy-Val hydrogel were unexpected, since the results of the 2D cell culture previously demonstrated the lowest cell surface coverage for these hydrophobic hydrogels. Quantification of the number of cells per μL UPy-AA hydrogel showed the highest cell concentration for the UPy-Lys hydrogel, for all the other UPy-AA hydrogels the cell concentration turned out to be within the same range (**Figure 6B**).
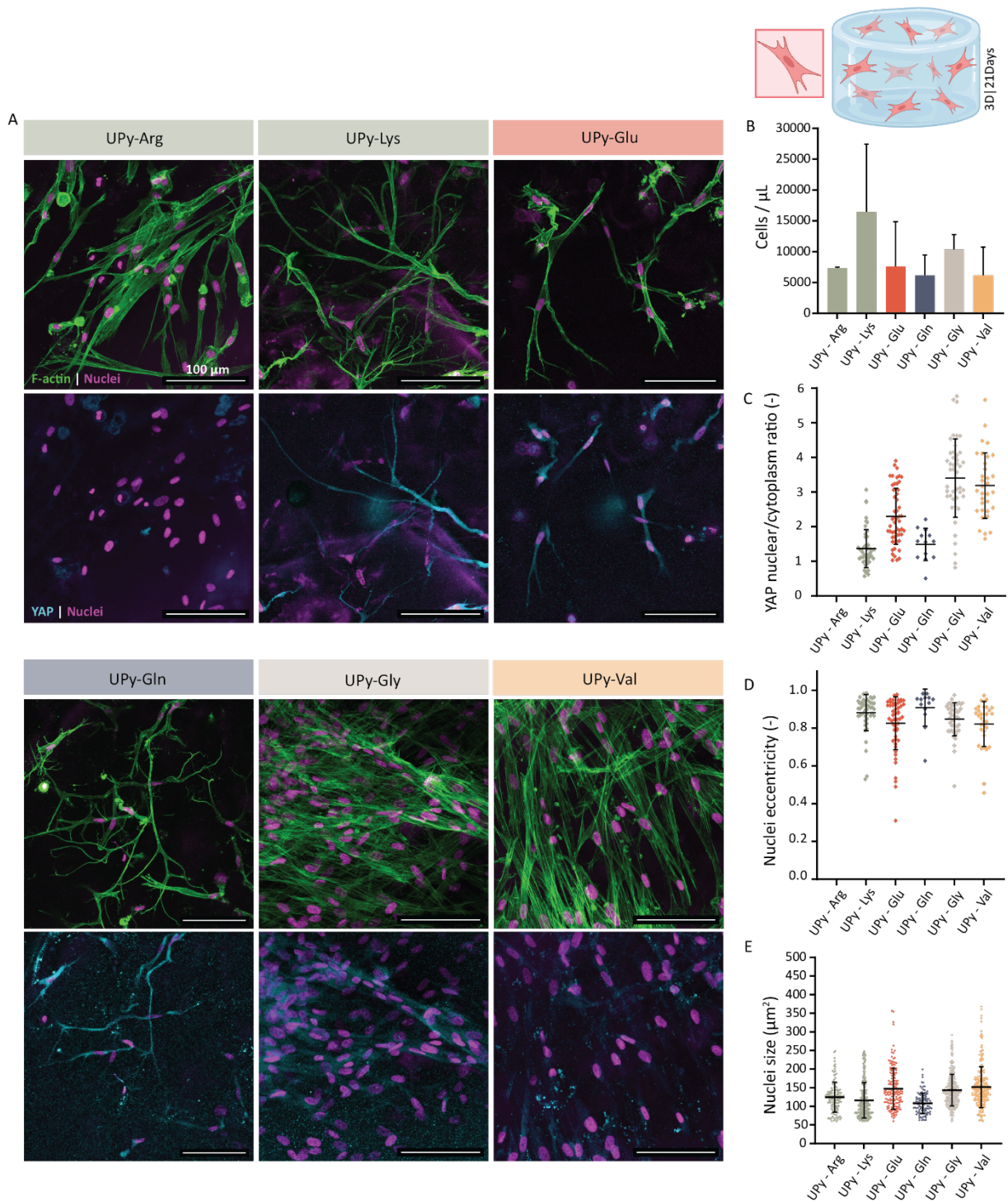
Figure 6. A selection of UPy-AAs: UPy-Arg, UPy-Lys, UPy-Glu acid, UPy-Gln, UPy-Gly and UPy-Val was used for 3D culture of PKs, which were treated towards stromal fibroblasts for 21 days. **A)** Immunofluorescent images of the PKs on day 21. The upper row of the images represents F-actin in green and nuclei in magenta. The bottom row of the images represents YAP in cyan and nuclei in magenta. Scale bar is 100 μm. **B)** Quantification of the number of cells per μL gel, calculated from 3 images per condition, n=3, mean ± standard deviation presented. **C)** Ratio of YAP expression intensity within the nuclei over the intensity within the cytoplasm, n=3, mean ± standard deviation presented. **D)** Nuclei eccentricity, where an eccentricity of 0 represents a perfect circle, n=3, mean ± standard deviation presented. **E)** Size of the nuclei measured in μm^2, n=3, mean ± standard deviation presented.

Mechanotransduction allows cells to sense and adapt to external forces by cytoskeleton remodeling or activating specific genetic programs.[51] To explore the interaction between the cells and their synthetic microenvironment in more detail, a YAP analysis was implemented in this study. YAP is a mechanosensitive transcriptional regulator, which is on a mechanical level regulated by mechanical cues such as ECM rigidity, strain or adhesive area.[52] Pathways involving YAP translocation to the nucleus, allow the cells to perceive ECM mechanics and to spread.[53] The expression of YAP within the cytoplasm is most substantially observed for the cells encapsulated within UPy-Lys and UPy-Gln hydrogels, slightly less expression of YAP within the cytoplasm is observed for the cells encapsulated within UPy-Glu hydrogels. Almost no expression of YAP within the cytoplasm is observed for the cells encapsulated within UPy-Gly and UPy-Val hydrogels. A custom-made cell profiler pipeline quantified the intensity of YAP expression inside the cytoplasm and inside the nuclei (**Figure 6C**). The ratio's between nuclear YAP intensity and YAP intensity within the cytoplasm of the cells encapsulated within UPy-Lys and UPy-Gln are similar to each other and slightly above 1, suggesting mechanotransduction within these hydrogels. The YAP nuclear/cytoplasm ratio of the cells encapsulated within UPy-Glu is significantly above the YAP nuclear/cytoplasm ratio of the cells encapsulated within UPy-Lys hydrogels. Overall, the YAP nuclear/cytoplasm ratios of the cells encapsulated within UPy-Gly and UPy-Val hydrogels are significantly above the YAP nuclear/cytoplasm ratios of the cells encapsulated within UPy-Lys, UPy-Glu and UPy-Gln hydrogels. These differences in mechanotransduction could be related to the observed differences in cellular morphology. The cells encapsulated within UPy-Lys as well as the cells encapsulated within UPy-Gln formed less dense cellular networks resulting in larger distances between the cells. On the contrary, cells encapsulated within UPy-Glu seemed to form cell clusters (SI Figure 6C) as a result, additional cellular interactions were introduced. The dense cellular networks observed for the cells encapsulated within the UPy-Gly and UPy-Val hydrogels exhibit probably even more cellular interactions and therewith an increased YAP nuclear/cytoplasm ratio. The nuclei eccentricity value of the cells encapsulated in all of the UPy-AA hydrogels is within a similar range of ~ 0.8-1.0, suggesting that the nuclei are oval-shaped instead of round-shaped (**Figure 6D**). The results showed similar nuclei sizes for the cells encapsulated in all of the UPy-AA hydrogels (**Figure 6E**). Overall, a YAP nuclear/cytoplasm ratio above 1 as well as oval-shaped nuclei, demonstrate mechanotransduction of the cells encapsulated with: UPy-Lys, UPy-Glu, UPy-Gln, UPy-Gly and UPy-Val hydrogel.

Differentiation of primary keratocytes encapsulated within a selection of UPy-AA hydrogels (3D)

Human primary keratocytes (PKs) are originally isolated from human donors corneal stroma and expanded *in vitro*. As described previously, the PKs are successfully encapsulated within a selection of UPy-AA hydrogels and cultured up to 21 days in a 3D environment. Here, the same selection of UPy-AA hydrogels is used to explore the ability of the hydrogels to support (re-)differentiation of the PKs during 3D culture. One day after encapsulation (day 1) the PKs are treated in two manners; (1) with serum towards stromal fibroblasts (SFs) or (2) with low serum and high glucose towards quiescent corneal stromal keratocytes (CSKs) (Figure 11).[54] A cell culture of 21 days is needed to allow successful (re-)differentiation of the PKs. During the 21-day cell culture of encapsulated cells, small amounts of cell culture medium were stored on day 7, 14 and 21 to perform an enzyme-linked-immunosorbent assay (ELISA) (**Figure 7A**). It is known that SFs secrete among others the cytokine Interleukin-8 (IL-8), which is a pro-inflammatory molecule important for neutrophil recruitment and T-cell activation. On the contrary, CSKs hardly secrete cytokines. Via an ELISA based on IL-8, this difference in cytokine secretion was analyzed, assuming a decrease in cellular IL-8 secretion for PKs differentiated into CSKs.[55] PKs were encapsulated within hydrogels based on UPy-Arg, UPy-Lys, UPy-Glu, UPy-Gln, UPy-Gly, and UPy-Val. The results of UPy-Arg differ substantially from the results of the other UPy-AA hydrogels, showing a lower concentration of the secreted IL-8 by the SFs treated cells. These results corelated with the large variability in cell compatibility, which was noticed for UPy-Arg hydrogels in previous experiments. All the other UP-AA hydrogels demonstrated a significant decrease in secreted IL-8 concentration between the PKs treated towards SFs and the PKs treated towards CSKs. Moreover, during culture a significant decrease in cellular secreted IL-8 was observed upon treating the PKs towards CSKs. Almost all hydrogels demonstrated a significant decrease in the secreted IL-8 between culture day 7 and day 21 as well as culture day 14 and day 21.
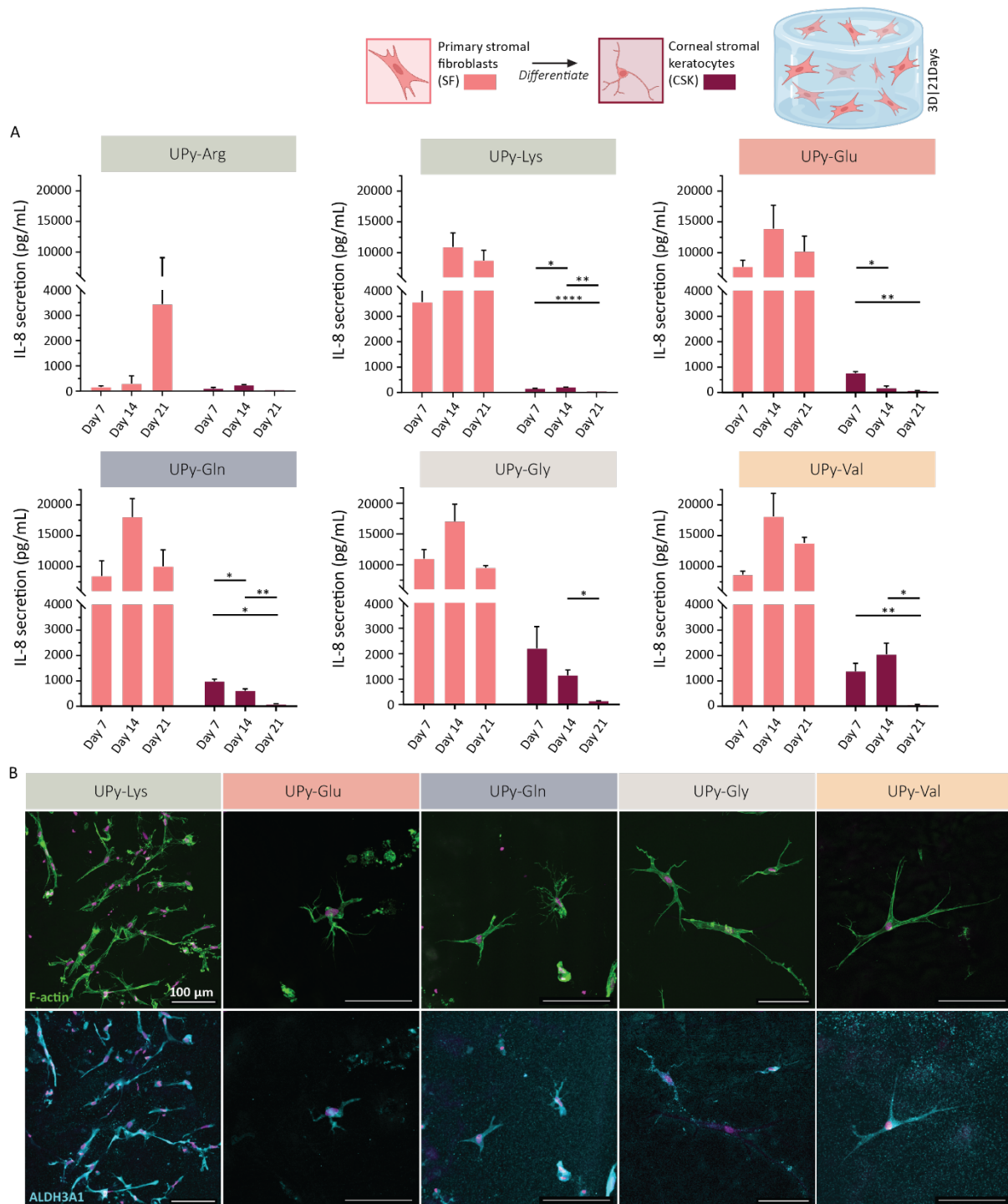
Figure 7. A selection of UPy-AAs: UPy-Arg, UPy-Lys, UPy-Glu, UPy-Gln, UPy-Gly and UPy-Val was used to 3D culture primary keratocytes, which were treated towards corneal stromal keratocytes (CSKs) for 21 days. **A)** Results of the enzyme linked immune sorbent assay (ELISA) to measure the cellular IL-8 secretion. The IL-8 concentration of cells treated towards stromal fibroblasts (left-side) and corneal stromal keratocytes (right-side) were measured at day 7, 14 and 21 with a sample size of n=3, mean ± standard deviation presented, * $p < 0.1$, ** $p < 0.01$, **** $p < 0.0001$. **B)** Immunofluorescent images of the PKs treated towards CSKs on day 21. The upper row of the images represents F-actin in green and nuclei in magenta. The bottom row of the images represents ALDH3A1 in cyan and nuclei in magenta. Scale bar is 100 μm.

Healthy human keratocytes do also express crystallin proteins that reduce light scattering and enhance the optical performance of the stromal tissue. One of these proteins is the enzyme aldehyde dehydrogenase 3 family member A1 (ALDH3A1), which is also the most common corneal crystallin in mammals.[56,57] ALDH3A1 is assumed to be a specific marker for keratocytes. Here, immunohistochemical staining showed the expression of ALDH3A1 in PKs treated towards CSKs (**Figure 7B**), suggesting that the encapsulated PKs successfully differentiated into CSKs.

The significant decrease in the secreted IL-8 concentration as well as the observed expression of ALDH3A1 for the encapsulated cells treated towards CSKs indicated that the UPy-Lys, UPy-Glu, UPy-Gln, UPy-Gly, UPy-Val hydrogels allowed PKs to (re-)differentiate into more quiescent CSKs.

Mixing supramolecular polyaminoacids to allow 3D cell culture and (re-)differentiation of PKs

During the previously described experiments PKs were exposed to one type of supramolecular polyaminoacid during 2D or 3D cell culture. Here, the curiosity arose to study combinations or mixtures of supramolecular polyaminoacids within one hydrogel by using the same bifunctional crosslinker combined with multiple supramolecular polyaminoacids. Herewith, hydrogels were created that contained supramolecular polyaminoacid fibers presenting various amino acids to the encapsulated cells. This approach allowed for the introduction of cellular-adhesive ligands in a supramolecular manner within the hydrogel, creating synthetic supramolecular proteins without the necessity of adding additional ligands to the hydrogel. To study these possibilities, three polyaminoacid mixtures were designed, *i.e.* (1) a mixture of UPy-Lys and UPy-Glu (K|E), (2) a mixture of UPy-Arg, UPy-Gly, UPy-Asp, UPy-Ser (R|G|D|S), (3) a mixture of UPy-Ile, UPy-Lys, UPy-Val and UPy-Ala (I|K|V|A). The first mixture is based on the combination of a positively and a negatively charged amino acid. The second mixture is based on the cell adhesive RGD ligand, which is commonly used in functional biomaterials to introduce bioactivity.[17,42] The third mixture is based on the heavenly examined and promising IKVAV peptide, which is a laminin derived peptide.[58–60]

The PKs were successfully encapsulated within the three polyaminoacid hydrogel mixtures and cultured up to 21 days in this 3D environment, whereafter differentiation possibilities of the PKs cultured within the polyaminoacid hydrogel mixtures were explored.

During the 21-day cell culture of encapsulated cells, again, small amounts of cell culture medium were stored on day 7, 14 and 21 to perform an enzyme-linked-immunosorbent assay (ELISA) (**Figure 8A**). The results of the R|G|D|S mixture differ substantially from the results of the other two polyaminoacid hydrogel mixtures, showing a lower concentration of the secreted IL-8 by the SFs treated cells. Immunohistochemical staining on day 21 of the cultures showed solely rounded, dead cells within this hydrogel mixture. To this end, no further cell analysis were performed with this condition. For the K|E mixture as well as the I|K|V|A mixture a significant decrease in secreted IL-8 concentration on day 21 is observed between the cells treated towards SFs and the cells treated towards CSKs. Moreover, during culture the results of the ELISA also showed a significant decrease in secreted IL-8 concentration by the cells treated towards CSKs. Both mixtures showed a significant decrease in the secreted IL-8 concentration between day 7 and day 21 as well as the decrease in secreted IL-8 concentration between day 14 and day 21, suggesting that both polyaminoacid mixtures allow the encapsulated cells to successfully differentiate into CSKs.   On culture day 21 immunohisto-chemical analysis were performed to study the cellular morphology and mechanotransduction via YAP translocation. After encapsulation the cells started to spread, proliferate and migrate within their new 3D environment. Analyzed confocal images only show the cellular morphology and network within the x- and y-direction. To study the ability of the cells to spread and migrate into the z-direction, multicolored images showing the height of the cells within the gel matrix were analyzed (**Figure 8B**). These results demonstrated a sparse network of elongated cells, capable to grow and migrate within the z-direction. The results of the immunohistochemical staining of YAP showed a clear expression of YAP within the cell nuclei for both the K|E (**Figure 8C**) and the I|K|V|A (**Figure 8D**) hydrogel mixture and almost no YAP expression within the cellular cytoplasm. Further quantification of the ratio's between nuclear YAP intensity and YAP intensity within the cytoplasm of the cells encapsulated within both mixtures are similar and slightly above 2, indicating mechanotransduction within both (**Figure 8E**). The nuclei eccentricity value of the cells encapsulated in both UPy-AA hydrogel mixtures is within a similar range of ~ 0.8-0.9, suggesting that the nuclei are oval-shaped instead of round-shaped (**Figure 8F**).

Overall, a YAP nuclear/cytoplasm ratio above 2 as well as oval-shaped nuclei, indicate mechanotransduction within both the K|E and I|K|V|A hydrogel mixture. Still, additional UPy-cRGD was used to allow cell adhering and survival within these UPy-AA hydrogel mixtures.
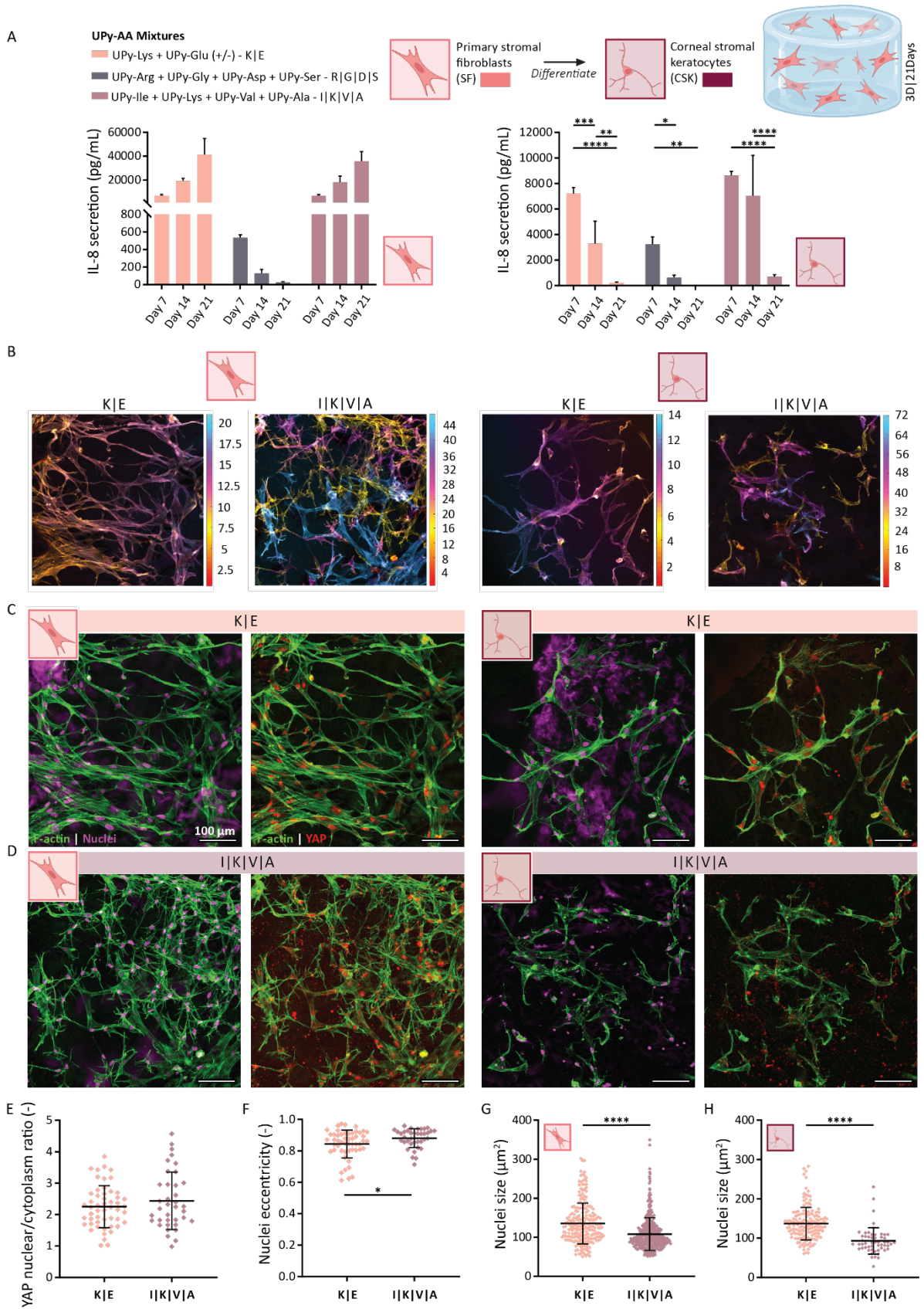
Figure 8. Three combinations of 2 or more UPy-AAs were used to 3D culture primary keratocytes for 21 days. During culture, the cells were either treated towards stromal fibroblasts (SFs) or corneal stromal keratocytes (CSKs). The following combinations were studied: (1) UPy-Lys + UPy-Glu / K|E, (2) UPy-Arg + UPy-Gly + UPy-Asp + UPy-Ser / R|G|D|S, (3) UPy-Ile + UPy-Lys + UPy-Val + UPy-Ala / I|K|V|A. **A)** Results of the enzyme linked immune sorbent assay to measure the cellular IL-8 secretion. The IL-8 concentration of cells treated towards stromal fibroblasts (left-side) and corneal stromal keratocytes (right-side) were measured at day 7, 14 and 21 with a sample size of n=3, mean ± standard deviation presented, * $p < 0.1$, ** $p < 0.01$, *** $p < 0.001$, **** $p < 0.0001$. **B)** Multicolored images showing the original height differences within the obtained z-stack. Color scale is in μm. **C)** Immunofluorescent images of the PKs, 3D culture within the K|E hydrogel on day 21, with F-actin in green, nuclei in magenta and YAP in red. SFs on the left and CSKs treated cells on the right. Scale bar is 100 μm. **D)** Immunofluorescent images of the PKs, 3D culture within the I|K|V|A hydrogel on day 21, with F-actin in green, nuclei in magenta and YAP in red. SFs on the left and CSKs treated cells on the right. Scale bar is 100 μm. **E)** Ratio of YAP expression intensity within the nuclei over the intensity within the cytoplasm, n=3, mean ± standard deviation presented. **F)** Nuclei eccentricity, where an eccentricity of 0.0 represents a perfect circle, n=3, mean ± standard deviation presented, * $p < 0.1$. **G)** Size of the nuclei of the SFs measured in $μm^2$, n=3, mean ± standard deviation presented, **** $p < 0.0001$. **H)** Size of the nuclei of the CSKs measured in $μm^2$, n=3, mean ± standard deviation presented, **** $p < 0.0001$.

It is very interesting to observe that combinations of UPy-moieties functionalized with single amino acids do not always improve the cell compatibility, while these single amino acid hydrogels on their own allow for good cell compatibility, cell adhering, encapsulation and even differentiation of cells.

CONCLUSION

Previously, small peptide additives are often used to design functional and bioactive biomaterials. Here, we focused on altering the core of the hydrogel by introducing a library of supramolecular amino acid monomers, which in solution assemble into supramolecular polyaminoacids. Via the introduction of a crosslinker various polyaminoacid based hydrogels were generated, suitable for encapsulation of PKs. Except for UPy-Arg, all the hydrogels supported the PKs to attain their spreaded morphology and to migrate through the hydrogels. Moreover, a significant decrease in secreted IL-8 during culture demonstrated the ability of these hydrogels to (re-)differentiate PKs into CSKs. Besides hydrogels with a core based on polyaminoacid fibers presenting only one amino acid to the cells, mixtures of supramolecular amino acid monomers were generated. These mixtures contained diverse supramolecular polyaminoacid fibers that provide different amino acids to the encapsulated cells. Both the hydrogels based on mixtures of UPy-Lys and UPy-Glu (K|E) as well as UPy-Ile, UPy-Lys, UPy-Ala, and UPy-Val (I|K|V|A) allowed the encapsulated PKs to spread, migrate and even (re-)differentiate. The hydrogels based on polyaminoacids presenting only UPy-Arg, UPy-Gly, UPy-Asp, or UPy-Ser to the cells supported a healthy cell behavior, this was surprisingly not observed for the R|G|D|S mixture. These results demonstrate a difficulty in the fabrication of mixtures based on estimated guesses, therewith indicating the need for a screening based approach to explore successful new supramolecular polyaminoacid mixtures. Yet, with the presented library of supramolecular amino acid monomers a novel minimalistic approach, allowing to create an even larger library of supramolecular polyaminoacids based biomaterials to synthetically mimic the natural protein presentation within the ECM, is introduced.

EXPERIMENTAL SECTION

Cryogenic transmission electron microscopy

Samples were prepared by dissolving 80 µM UPy-AA in basic PBS (80 mM NaOH) at 70 °C, after which the samples were neutralized by 1 M HCl. Lacey carbon film grids (Electron Microscopy Sciences, 200 mesh) were used for imaging. Prior to sample addition, grids were surface plasma treated (at 5 mA for 40s) using a Cressington 208 carbon coater. Using an automated vitrification robot (FEI VitrobotTM Mark III), 3 µL sample was applied to the grids and excess sample was removed by blotting using filter paper for 3 s at –3 mm. The thin film formed was vitrified by plunging the grid into liquid ethane just above its freezing point. On a FEI-Titan TEM equipped with a field emission gun operating at 300 kV the samples were examined. Post-GIF (Gatan imaging filter) 2x2 Gatan CCD camera was used for recording of the images. Micrographs were taken at low dose conditions, using a defocus setting of -10 µm at 25k magnification, or defocus setting of -40 µm at 6.5k magnification. The fiber thickness is determined in digital micrograph, where three images are taken at a magnification of 24kx, determining the fiber thickness of 6 fibers per image.

Maaike J.G. Schotman performed all the cryo-TEM experiments.

Zeta-potential measurements

The samples were annealed in basic PBS (80 mM NaOH) at a concentration of 4 mM for 30 minutes at 70 °C. After dissolving, the samples were neutralized to pH 7.0–7.1 with 1 M HCl. After neutralization, samples were 5x diluted with MiliQ, resulting in a PBS concentration of 0.1 x, 0.4 mM sample concentration. A DTS1070 cuvette was used for measuring the zeta potential, where the measurement duration was automated and automatic attenuation and voltage was selected. The samples were measured in triplo, at RT, with a 30 s equilibration time. Zetasizer software was used to analyze and process the zeta potential data.

Maaike J.G. Schotman performed all the Zeta-potential measurements.

Hydrogel preparation for rheology experiments and 2D cell culture experiments

UPy-AA hydrogels were prepared by dissolving the UPy-AA at 37.4 mM and the bifunctional molecules (UPy-PEG$_{10k}$-UPy) separately at 0.46 mM in basic PBS (80 mM NaOH) at 70 °C for 1 h. For the cellular adhesion analysis experiments, UPy-cRGD (1 mM) was included and dissolved together with the UPy-AA. Samples were neutralized by addition of HCl (1 M), and left to equilibrate for 15 min, whereafter the dissolved UPy-AA (50 µL of the neutralized solution) and bifunctional molecules (50 µL of the neutralized solution) were mixed in a cylindrical Teflon mold (diameter 8 mm, 2 mm

height) for rheology or 40 μL UPy-AA and 40 μL of bifunctional molecules in a 96-well plate (GREINER) for cellular experiments. The samples were left to gelate over night at 37 °C before rheological experiments were performed.

Rheology

UPy-AA hydrogels were prepared as stated above. Rheological measurements were performed on an Anton Paar Physica MCR501 rheometer. Hydrogels were measured at 37 °C using a 8 mm plate-plate with a distance of 1 mm. Low viscosity silicon oil (47 V 100m RHODORSIL®) was used to surround the hydrogels to prevent sample drying due to water evaporation. A time sweep was performed, with the storage and loss moduli were recorded for 10 minutes at 1% strain, 1 rad/s, whereafter the angular frequency (100 to 0.1 rad/s, 22 measurement points) at 1% strain and strain sweep (1 to 1000%, 22 measurement points) at 1 rad/s were recorded. The yield stress was determined by measuring the strain-sweep of each UPy-AA hydrogel, from which the cross-over point between the linear regime and a power fit plot for the final 10 points of the curve (strain 145-1000%) was determined, obtaining the yield stress.

Maaike J.G. Schotman performed all the rheological measurements.

Primary keratocyte (PK) cell culture

Primary human keratocytes were isolated from leftover human corneoscleral transplant material from Descemet Membrane Endothelial Keratoplasty surgery, which were obtained from the Cornea Department of the ETB-BISLIFE Multi-Tissue Center (Beverwijk, the Netherlands). The keratocytes were cultured in expansion medium (1:1 mixture of Dulbecco's modified Eagle's medium/F-12 supplemented with GlutaMAX (DMEM/F12 (Ham) + GlutaMAXTM, 10565-018; Gibco), 5% Fetal Bovine Serum (FBS, Biochrom AG), 1% penicillin/streptomycin (P/S, Biochrom AG), and 1 mM L-ascorbic acid 2-phosphate sesquimagnesium salt hydrate (Vitamin C, Sigma A8960)) at 37 °C, 21% O_2 and 5% CO_2 until ±80% confluency. Since the medium contained FBS, keratocytes were considered to be activated matrix-producing cells, referred to as stromal fibroblasts (SFs). To initiate cell (re-)differentiation towards corneal stromal keratocytes, another medium composition was used: differentiation medium (Dulbecco's modified Eagle's medium supplemented with GlutaMAX (GlutaMAXTM, 11880-028; Gibco), 1% penicillin/streptomycin (P/S, Biochrom AG), and 1 mM L-ascorbic acid 2-phosphate sesquimagnesium salt hydrate (Vitamin C, Sigma A8960), 1x ITS (Sigma, I3146), 2 mg/mL D-glucose (Invitrogen, 15023021), 2.5 mg/mL D-mannitol (Fluka, 63560)).[21] Cells were cultured with medium changes every 3 days, keratocytes from multiple donors were used up

to passage #3. TrypLE Express Enzyme (1x), no phenol red (12604013, Gibco) is used to detach the cells from the culture flask and to harvest them for experiments.

2D cell culture on top of UPy-AA hydrogels

UPy-AA hydrogels were prepared as stated above. Before cellular experiments were performed, the gels were sterilized by 20 minutes of UV exposure, whereafter the hydrogels were washed three times with culture medium. Cells were harvested from the culture flask and seeded at a density of 3500 cells/well (96-well plate) suspended in 200 µL medium.

Cell staining and Imaging – 2D culture

After three days, the culture medium was removed and the cells were gently washed with phosphate buffered saline (PBS) and fixated with 3.7% (v/v) formaldehyde solution (Merck) + 0.5% (v/v) Triton X-100 v/v (Merck) in PBS for 15 min at RT. The samples were subsequently washed with PBS and stained for the actin cytoskeleton with phalloidin-Atto 488 (Sigma-Aldrich, dilution 1:300) in PBS for 45 min at RT. Subsequently, the samples were washed and stained for the nucleus with 4'-6 diamidino-2-phenylindole (DAPI; 0.1 µg/mL; Sigma Aldrich). After an incubation of DAPI for 10 minutes, samples were washed again with PBS. For visualization, complete/intact hydrogels were place on a thin glass coverslip (24x69 mm, VWR 631-1575) immerged in mowiol 4-88 (Sigma Aldrich, 81381) and imaged using Leica TCS SP8 X inverted confocal microscope (Leica Microsystems) using HC PL APO CS2 objectives (20x/0.75, 40x/0.95). Each gel was measured in duplicate.

Metabolic activity – 2D culture

After three days, the culture medium was removed and the cells were gently washed with phosphate buffered saline (PBS). To each well 250 µL of 44 µM resazurin (Sigma-Aldrich) in medium was added and incubated at 37 °C for 3 hours. Subsequently, 2x 100 µL of the incubated resazurin/medium was collected and transferred to a black 96-well plate to measure fluorescence (excitation: 530/25 and emission: 590/35) with the plate reader (Synergy HTX, BioTek).

2D cell culture on top of UPy-Gly, UPy-Glu, and UPy-Lys hydrogel + UPy-Cy5

UPy-AA hydrogels were prepared by dissolving the UPy-AAs together with the 1mM UPy-cRGD in basic PBS (160 mM NaOH) at 70 °C for 20 minutes and the UPy-PEG$_{10K}$-UPy (bifunctional molecules) separately in PBS at 70 °C for 2 h. See **table 1** for the individual hydrogel compositions. Both solutions were cooled down to RT. UPy-Cy5 was dissolved in dimethyl-sulfoxide (DMSO, Sigma-Adrich, D8418) at a stock concentration of 1.23 mM and added to the monofunctional samples to reach a final UPy-Cy5 concentration of 0.06 mM, and thoroughly mixed for 10 minutes. The monofunctional samples were neutralized by addition of HCl (2 M), and left to equilibrate for 15 min, whereafter cell culture medium was added to both solutions 1:1. 40 µL UPy-AA and 40 µL bifunctional were mixed in a non-adhesive 96-well plate (Fisher Scientific, Nunclon Sphera-Treated, U-Shaped-Bottom plate 15227905), and left in the incubator to gelate overnight at 37 °C. The next day, the gels are washed 3x with medium and 5000 cells per well were seeded and cultured for 7 days. Staining and analysis were performed as described above, three dimensional images were generated by using the 3D viewer tool within Image J software.

Table 1. Overview of the three studied hydrogel compositions, namely; UPy-Lys, UPy-Glu, and UPy-Gly hydrogel. Calculations were made for one complete hydrogel with a volume of 80 µL.

Building block / additive	Ratio	µmol	mM	Wt/v %	
UPy-PEG$_{10K}$-UPy	1	0.018	0.23	0.26	
UPy-Cy5	0.27	0.0048	0.06	0.01	
UPy-Lysine	77.0	1.42	17.7	2.24	2.69 Total wt/v%
UPy-cRGD	4.6	0.08	1.06	0.18	
UPy-Glutamic acid	75.3	1.39	17.3	2.19	2.63 Total wt/v%
UPy-cRGD	4.3	0.08	0.98	0.17	
UPy-Glycine	76.9	1.41	17.7	2.11	2.56 Total wt/v%
UPy-cRGD	4.6	0.08	1.06	0.18	

3D Height indication cell images

A custom MatLab (The Mathworks, Natick, USA) script was written to pair a specific cell height within the obtained z-stack image to a specific color. Image stacks obtained from channels corresponding to the DAPI (nuclei) and phalloidin (F-actin) were used to create these 3D height indication cell images. LAS X Life Science Microscope Software was used to calculate the original µm distance in the z-direction from the original *lif* file. *The custom MatLab script was written by Mark C. van Turnhout.*

Cell Image Analysis

All image analysis were analyzed from maximum-intensity z-projections of confocal image stacks. Cell count was analyzed from images obtained after nuclei staining. To this end, ImageJ software was used to determine the number of nuclei per image. Fiji/ImageJ (NIH) software was used to determine the cell coverage as well. To determine the localization of YAP, z-projections of images were obtained from channels corresponding to the DAPI (nuclei), phalloidin (F-actin) and anti-YAP antibody staining (YAP). Afterwards CellProfiler™ (cell image analysis software) was used to design a pipeline, providing the nuclear areas and cytoplasmic areas. The mean intensity was determined in those respective areas and the ratio between the concentration present in nuclear and cytoplasmic regions of cell was then used as a measure of YAP nuclear translocation. The same pipeline was also used to determine the nuclei eccentricity and nuclei size.

Cell encapsulation in UPy-AA hydrogels – 3D culture

Bifunctional molecules (UPy-PEG$_{10K}$-UPy) were dissolved at 70 °C in an neutral PBS solution for 1.5 hours. UPy-AA (UPy-AA + UPy-cRGD) were dissolved at 70 °C in an alkaline PBS solution (containing 160 mM NaOH) for 20 minutes. After completely dissolving the powders of the bifunctional and monofunctional building blocks, the solutions were cooled down to room temperature. A specific volume of HCl solution (2 M) was added to the UPy-AA solution to reach neutral pH. Cell culture medium is added to both solutions 1:1, to provide the cells already with some nutrients during the gelation process later on in the procedure. Afterwards, both solutions were transferred from a glass vial to a sterile Eppendorf tube, from this step onwards a safety cabinet was used to guarantee a sterile work environment. The solutions were disinfected by exposing them to UV-light for 20 minutes. Subsequently, the cells were prepared and counted, the following cell concentrations were used during the experiments:

PKs treated towards SFs: 100 cells/µL | PKs treated towards CSKs: 200 cells/µL

Table 2. Overview of the six UPy-AA hydrogel compositions used for 3D encapsulation of the primary keratocytes, namely; UPy-Arg, UPy-Lys, UPy-Glu, UPy-Gln, UPy-Gly, and UPy-Val. Calculations were made for one complete hydrogel with a volume of 80 µL.

Building block / additive	Ratio	µmol	mM	Wt/v %	
UPy-PEG$_{10K}$-UPy	1	0.092	0.115	0.128	
UPy-Arginine	70.67	0.65	8.13	1.05	1.45
UPy-cRGD	13.41	0.12	1.54	0.27	
UPy-Lysine	70.45	0.65	8.10	1.03	1.43
UPy-cRGD	13.38	0.12	1.54	0.27	
UPy-Glutamic acid	70.12	0.65	8.06	1.02	1.41
UPy-cRGD	13.13	0.12	1.5	0.26	
UPy-Glutamine	69	0.63	7.94	1.0	1.39
UPy-cRGD	13.16	0.12	1.51	0.26	
UPy-Glycine	71.0	0.65	8.17	0.976	1.36
UPy-cRGD	13.4	0.12	1.54	0.26	
UPy-Valine	70.55	0.65	8.11	1.00	1.40
UPy-cRGD	13.4	0.12	1.54	0.27	

The cells needed for encapsulation were suspended in the correct amount of medium and this cell suspension was added to the bifunctional solution. Due to the addition of the cells suspension, the bifunctional molecules were diluted. To correct for this extra dilution step, the initial concentration of the bifunctional molecules was slightly higher (0.78 wt/v% instead of 0.52 wt/v%). For every experiment the bifunctional molecules were diluted with 1/3 of cell suspension, resulting in a final 0.52 wt/v% bifunctional molecules. All the gels were prepared in wells of a non-adhesive 96-well plate (Fisher Scientific, Nunclon Sphera-Treated, U-Shaped-Bottom plate 15227905).

At first 40 µL UPy-AA molecules solution were added to a well, than the cells were added to the bifunctional molecule solution and mixed thoroughly. Secondly 40 µL of bifunctional molecules / cell mixture were added to the 40 µL UPy-AA molecules solution inside the well. The molecules were mixed by carefully pipetting up and down (at least 3x per well), any air bubbles were removed by using a needle.

For the exact hydrogel compositions, see **table 2**. All the hydrogels were placed in the incubator at 37 °C, 21% O_2 and 5% CO_2 for 1 hour to allow for proper gelation. After 1 hour, medium to embed the gels was carefully added to the wells, and the hydrogels with encapsulated cells were

placed back in the incubator at 37 °C, 21% O_2 and 5% CO_2. After 1 day the cell culture medium, which surrounds the hydrogel, is refreshed and for the PKs treated towards CSKs the expansion medium is replaced by the differentiation medium. During the 21-day culture, the medium is refreshed every 2-3 days.

Cell staining and Imaging - 3D culture

Before immunohistochemical stainings were carried out, the hydrogels were washed 3x with PBS (5 min per wash). All cells encapsulated within the hydrogels were fixated for 20 minutes at room temperature using 3.7% paraformaldehyde (formalin 37%, Merck, 104033.1000). After washing with PBS, samples were permeabilized for 15 minutes with 0.5% Triton X-100 in PBS. Followed by adding a blocking solution of 10% goat serum in 0.05% Triton X-100 in PBS for 30 minutes. Next, the cells were incubated with the primary antibodies diluted in 2% donkey serum in 0.05% Triton X-100 in PBS overnight at 4 °C. Thereafter, the cells were washed thoroughly with 0.05% Triton X-100 in PBS, including wash waiting steps of 5-10 min. Next, the cells were incubated with the secondary antibodies and phalloidin at room temperature for 2 hours. Finally, the cells were stained with DAPI at a dilution of 1:250 for 10 min and washed thoroughly with PBS (including was waiting steps of 5-10 min). During imaging, complete/intact hydrogels were place on a thin coverslip (24x69 mm, VWR 631-1575) immerged in mowiol 4-88 (Sigma Aldrich, 81381) and imaged using Leica TCS SP8 X inverted confocal microscope (Leica Microsystems) using HC PL APO CS2 objectives (20x/0.75, 40x/0.95). Images were processed in ImageJ to create a max-projection image of the original z-stack. See **table 3** for an overview of al the used dyes and antibodies.

Table 3. Overview of the used dyes, primary and secondary antibodies.

Antibody / dye	Company / reference #	Dilution
4',6-diamidino-2-phenylindole dihydrochloride (DAPI)	Sigma-Aldrich, D9542	1:250
Phalloidin 488	Sigma-Aldrich	1:300
Phalloidin 555	Sigma-Aldrich	1:300
Anti-Vimentin	Ab20346, Abcam	1:300
Anti- tubulin β3	801202, BioLegend	1:100
Anti-YAP1	Ab52771, Abcam	1:100
Anti-ALDH3A1	Ab76976, Abcam	1:100
Secondary antibodies		
Anti-rabbit IgG (goat) 647	A21244, Molecular Probes	1:250
Anti-rabbit IgG (goat) 555	A211428, Molecular Probes	1:250
Anti-mouse IgG2a (goat) 555	A21137, Molecular Probes	1:250
Anti-mouse IgM (goat) 488	A21042, Molecular Probes	1:250
Anti-mouse IgM (goat) 555	A21426, Molecular Probes	1:250

Enzyme-linked immunosorbent assay (ELISA)

On culture day 7, 14, and 21 during the 3D cell culture, medium was refreshed and 150 μL medium surrounding the samples was collected in separate small Eppendorf tubes and stored in -80 °C upon use. All ELISA experiments were executed with n=3, and all the standards as well as the samples are ran in duplicate. The following IL-8 concentrations were used for the standard curve of IL-8:

1000 pg/mL, 500 pg/mL, 250 pg/mL, 125 pg/mL, 62.5 pg/mL, 31.3 pg/mL, 15.6 pg/mL.

Uncoated Nunc™MaxiSorp™ ELISA plates (BioLegend, 423501) were used, these plates were coated with capture antibody diluted in 1x coating buffer one day prior to running the ELISA (overnight incubation at 4 °C). See **table 4** for all the compositions of the used reagents. On the experiment day all the samples, the plates and the ELISA MAX™ Deluxe Set components (BioLegend®) were brought to room temperature. All the wash steps were executed in a similar manner, namely: 4 times with at least 300 μL wash buffer (0.05% Tween-20 in PBS) per well and residual buffer was blotted by firmly tapping the plate upside down on absorbent paper. After incubation with the capture antibody the plate was washed and blocked with 1x assay diluent A at room temperature

for 1 hour with shaking (500 rpm) to minimize non-specific binding and reduce background. During this incubation, the samples for the standard curve were prepared and every well plate comprised a standard. After blocking, the wells were washed and incubated with 100 µL of the samples and standards at room temperature for 2 hours with shaking (500 rpm), all samples were diluted 4x in 1x assay diluent (25 µL sample, 75 µL 1x assay diluent). Thereafter, the wells were washed and 100 µL of detection antibody solution was added to each well, and incubated at room temperature for 1 hour with shaking (500 rpm). The wells were washed again and incubated with 100 µL of diluted Avidin-HRP solution at room temperature for 30 min with shaking (500 rpm). Subsequently, the wells were washed 5x thoroughly with wash buffer, and soaked in buffer for 1 minute for each wash to minimize background. Then, 100 µL of substrate solution C was added and incubated in the dark for 15 minutes. During this step, positive wells turned blue in color. To stop the reaction, 100 µL Stop Solution for TMB Substrate (BioLegend, 4230021) was added to each well. All the positive wells turned from blue to yellow during this step. After adding the stop solution to the wells, the plate was softly tapped to the table a few times to proper mix the solutions and immediately the absorbance at 450 nm was measured with the plate reader (Synergy HTX, BioTek). In addition the absorbance at 570 nm was measured, this absorbance could be subtracted from the 450 nm absorbance. The standard curve for each ELISA was plotted in excel and polynomial curve-fitting software with order 3 or 4 was used to determine the best fit. Using this formula together with the measured absorbance value, resulted in the calculation of the amount of cytokine secretion.

Table 4. Reagents used to perform an ELISA with 2x a complete 96-well plate

4 mL Coating Buffer A (5x)	16 mL of Deionized Water
100 µL of Capture Antibody (200x)	20 mL of 1x Coating Buffer
12 mL of Assay Diluent A (5x)	48 mL of PBS
100 µL of Detection Antibody (200x)	20 mL of 1x Assay Diluent A
20 µL of Avidin-HRP (1000x)	20 mL of 1x Assay Diluent A
Substrate Solution C	-
Used ELSIA set: *ELISA MAX™ Deluxe Set Human IL-8 (BioLegend, 431504)*	

Cell encapsulation in UPy-AA mixture hydrogels – 3D culture

The same hydrogel preparation procedure for 3D cell culture is applied as described before. However to create the UPy-AA mixture, the start of the procedure is slightly different. Here, an individual stock solution is prepared for all the single UPy-AAs and UPy-cRGD. At first the UPy-AA and UPy-cRGD were dissolved, separately, at 70 °C in an alkaline PBS solution (containing 160 mM NaOH) for 20 minutes. After completely dissolving the polymers, the solutions were cooled down to room temperature. Afterwards the correct UPy-AA mixtures were prepared (including the right amount of UPy-cRGD), see **table 5** for the final hydrogel compositions. The UPy-AA mixture samples are again heated to 70 °C and stirred for 10 minutes. Subsequently the solutions were cooled down to room temperature again and the right volume of HCl solution (2 M) was added to the UPy-AA mixture solutions to reach neutral pH. Cell culture medium is added 1:1 to both the UPy-AA mixtures as well as the UPy-PEG$_{10K}$-UPy solution. From this step onwards the same procedure is followed as described above. During the 21-day culture, the medium is refreshed every 2-3 days.

Table 5. Overview of the compositions of the four UPy-AA hydrogel mixtures; K|E, R|G|D|S, and I|K|V|A. Calculations were made for one complete hydrogel with a volume of 80 μL.

	Building block / additive	Ratio	μmol	mM	Wt/v %	
	UPy-PEG$_{10K}$-UPy	1	0.0094	0.117	0.13	
KE	UPy-Lysine	37.8	0.35	4.43	0.56	
	UPy-Glutamic acid	37.8	0.35	4.43	0.56	1.34
	UPy-cRGD	4.4	0.041	0.52	0.09	
RGDS	UPy-Arginine	18.9	0.18	2.23	0.29	
	UPy-Glycine	18.9	0.18	2.23	0.26	
	UPy-Aspartic acid	18.9	0.18	2.23	0.28	1.32
	UPy-Serine	18.9	0.18	2.23	0.27	
	UPy-cRGD	4.4	0.041	0.52	0.09	
IKVA	UPy-Isoleucine	18.9	0.18	2.23	0.28	
	UPy-Lysine	18.9	0.18	2.23	0.28	
	UPy-Valine	18.9	0.18	2.23	0.27	1.32
	UPy-Alanine	18.9	0.18	2.23	0.27	
	UPy-cRGD	4.4	0.041	0.52	0.09	

Bicinchoninic acid (BCA) to determine protein binding to UPy-Gly, UPy-Glu, and UPy-Lys hydrogels.

The gels for this experiment were prepared similar to the procedures for hydrogels used in 3D culture, which are already described above. One set of gels (in the figure referred to as 'method 1' were prepared without addition of culture medium or specifically FBS, only PBS was used to dilute the hydrogels, while the other set of hydrogels is prepared with medium supplemented with FBS. All the gels were prepared in wells of a non-adhesive 96-well plate (Fisher Scientific, Nunclon Sphera-Treated, U-Shaped-Bottom plate 15227905). After a gelation time of 2 hours at 37 °C the gels were embedded in medium supplemented with FBS (method 1) or PBS without additives (method 2), whereafter the hydrogels were placed in an incubator at 37 °C, 21% O_2 and 5% CO_2. On day 2, 7, 14, and 21, 50 µL of the solvent surrounding the gels was used to perform a BCS assay and afterwards fresh medium with FBS or PBS without FBS were added to the gels. The Pierce™ BCA Protein Assay Kit (Thermo scientific, 23225) was used to perform the BCA assay and all the steps were executed according to the provided user guide of the kit. At first the diluted albumin standards were prepared, next the working dilution was prepared by mixing BCA reagent A 50:1 with BCA reagent B. In this experiment 3 replicates (n=3) were used per condition, and the protein content of each sample was measured twice. Of each sample (standard and unknown samples) 25 µL was pipetted into a transparent 96-well plate, and 200 µL of working dilution was added to each well, whereafter the plate was thoroughly mixed by using a plate shaker. The well plate was protected from light by using aluminum foil and incubated at 37 °C for 30 minutes. Finally the plate was cooled down to room temperature and the absorbance was measured at 562 nm on a plate reader (Synergy HTX, BioTek).

Statistical analysis

To test the significant differences of the results shown in figure 6, a Kruskal-Wallis test was performed with an additional Dunn's multiple comparisons test. No significant differences (ns) were observed between the cell concentration of the hydrogels. The following significant differences were observed for the YAP ratios: UPy-Lys vs. UPy-Glu **** $p < 0.0001$, UPy-Lys vs. UPy-Gly **** $p < 0.0001$, UPy-Lys vs. UPy-Val **** $p < 0.0001$, UPy-Glu vs. UPy-Gly *** p 0.0006, UPy-Glu vs. UPy-Val * $p < 0.0144$, UPy-Gln vs. UPy-Gly **** $p < 0.0001$, UPy-Gln vs. UPy-Val **** $p < 0.0001$. The following significant differences were observed for the nuclei eccentricity: UPy-Lys vs. UPy-Val * $p < 0.0426$, UPy-Glu vs. UPy-Gln * p 0.0373, UPy-Gln vs. UPy-Gly * $p < 0.0236$, UPy-Gln vs. UPy-Val ** $p < 0.0092$. The following significant differences were observed for the nuclei size: UPy-Arg vs. UPy-Glu ** p 0.0087, UPy-Arg vs. UPy-Gln * p 0.0294, UPy-Arg vs. UPy-Gly *** p 0.0002, UPy-Arg vs.

UPy-Val **** p < 0.0001, UPy-Lys vs. UPy-Glu , **** p < 0.0001, UPy-Lys vs. UPy-Val **** p < 0.0001, UPy-Glu vs. UPy-Gln **** p < 0.0001, UPy-Gln vs. UPy-Gly **** p < 0.0001, UPy-Gln vs. UPy-Val **** p < 0.0001.

To test the significant differences of the results shown in figure 7, a two-way Anova test was performed with an additional Tukey's multiple comparisons test. With significant differences in decrease or increase of secreted IL-8 concentration during culture (*i.e.* day 7 vs. day 14, day 14 vs. day 21, and day 7 vs. day 21), indicated as: * p < 0.1, ** p < 0.01, *** p < 0.001, **** p < 0.0001. A two-way Anova was performed with an additional Sidák's multiple comparisons test to observe significant differences between the secreted IL-8 secretion of SFs vs. CSKs per hydrogel. UPy-Lys: day 7 SF vs. CSK * p 0.0314, day 14 SF vs. CSK **** p < 0.0001, day 21 SF vs. CSK **** p < 0.0001 | UPy-Glu: day 7 SF vs. CSK ** p 0.0023, day 14 SF vs. CSK **** p < 0.0001, day 21 SF vs. CSK **** p < 0.0001 | UPy-Gln: day 7 SF vs. CSK ** p 0.0014, day 14 SF vs. CSK **** p < 0.0001, day 21 SF vs. CSK *** p 0.0001 | UPy-Gly: day 7 SF vs. CSK **** p < 0.0001, day 14 SF vs. CSK **** p < 0.0001, day 21 SF vs. CSK **** p < 0.0001 | UPy-Val: day 7 SF vs. CSK *** p 0.0004, day 14 SF vs. CSK **** p < 0.0001, day 21 SF vs. CSK **** p < 0.0001.

To test the significant differences of the results shown in figure 8, a two-way Anova test was performed with an additional Tukey's multiple comparisons test to demonstrate a significant decrease in IL-8 secretion by CSKs during culture. KE: day 7 vs. day 14 *** p 0.0005, day 7 vs. day 21 **** p < 0.0001, day 14 vs. day 21 ** p 0.0053 | RGDS: day 7 vs. day 14 * p 0.0189, day 7 vs. day 21 ** p < 0.0039, day 14 vs. day 21 ns | IKVA: day 7 vs. day 14 ns, day 7 vs. day 21 **** p < 0.0001, day 14 vs. day 21 **** p < 0.0001. A two-way Anova test was performed with an additional Sidák's multiple comparisons test to demonstrate a significant difference in the secreted IL-8 concentration between SFs and CSKs on day 21: KE **** p < 0.0001, IKVA **** p < 0.0001, RGDS ns. Mann-Whitney tests demonstrated the following differences between the cells encapsulated in the KE or the IKVA hydrogel: SF nuclei size **** p < 0.0001, CSK nuclei size **** p < 0.0001, YAP ratio ns p 0.5917, nuclei eccentricity * p 0.027.
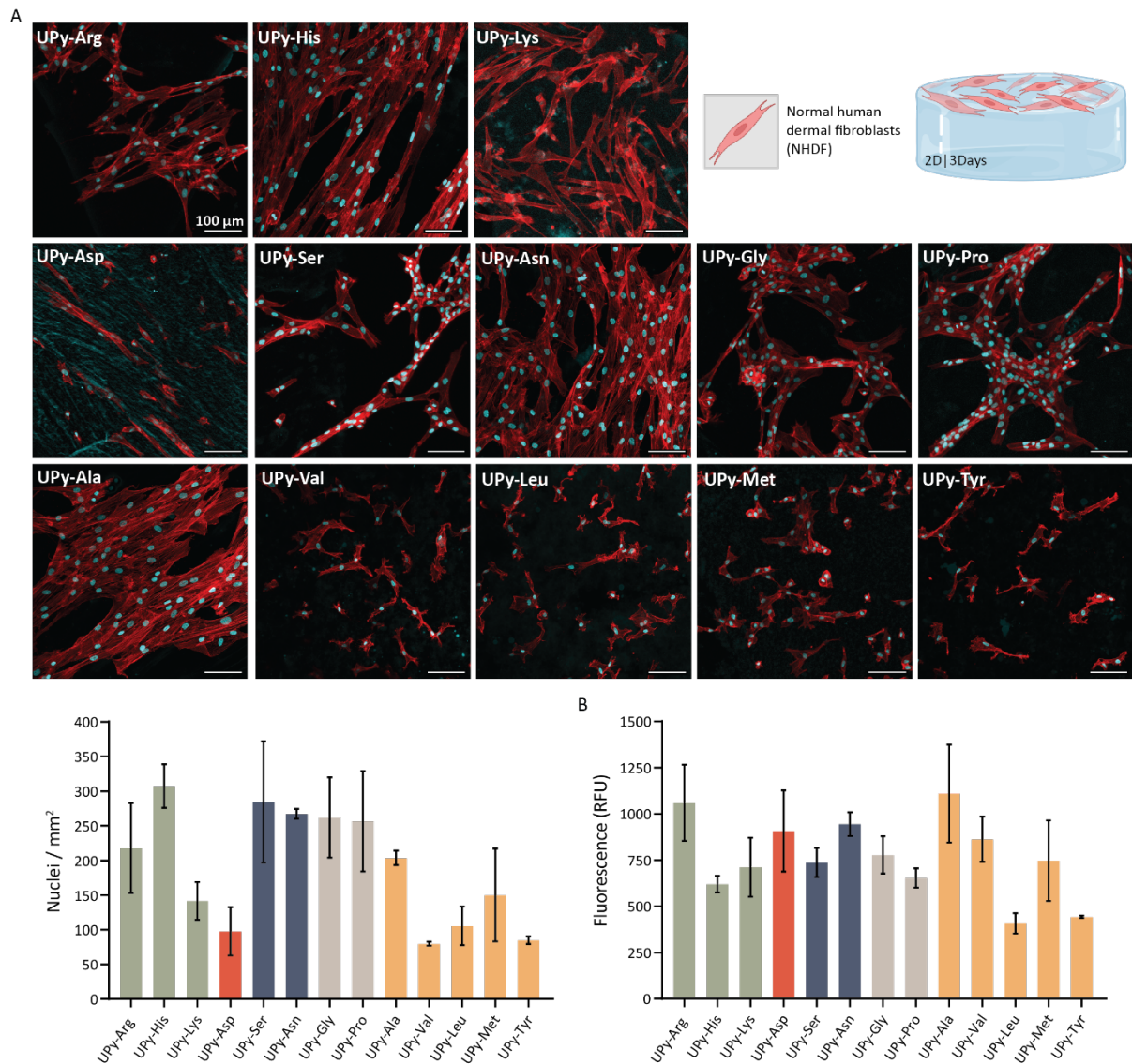
APPENDIX

Figure 9. 2D culture of normal human dermal fibroblasts (NHDFs) cultured on top of the AA hydrogels containing 1 mM UPy-cRGD. **A)** Immunofluorescent staining of f-actin (red) and nuclei (cyan). 3-day culture, scale bars are 100µm. Including, the average number of nuclei per mm^2 of fixated NHDFs quantification after 3 days of culture, data derived from two replicates, mean ± standard error of the mean presented. **B)** Metabolic activity of NHDFs after 7 days of culture, data derived from two replicates, mean ± standard error of the mean presented.
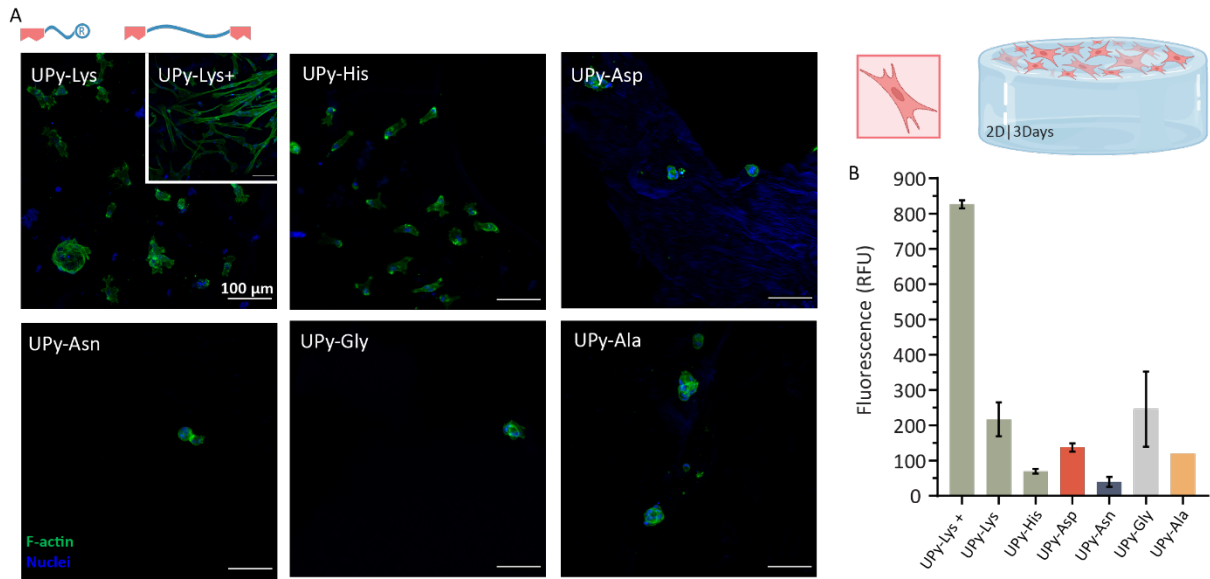
Figure 10. 2D culture of primary keratocytes (PKs) cultured on top of the AA hydrogels without UPy-cRGD. **A)** Immunofluorescent staining of f-actin (green) and nuclei (blue). 3-day culture, scale bars are 100µm. As a control UPy-Lys was used containing 1 mM UPy-cRGD (small insert). **B)** Metabolic activity of PKs after 7 days of culture, data derived from two replicates, mean ± standard error of the mean presented
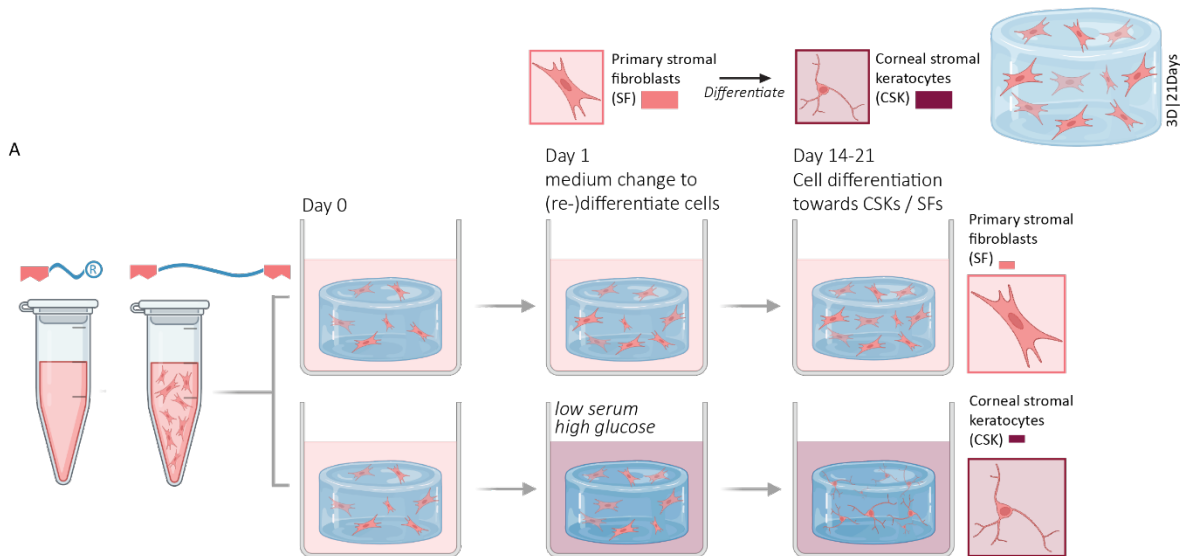

Figure 11. Experimental set-up and time-line of 3D culture primary keratocytes, which were treated towards corneal stromal keratocytes (CSKs) for 21 days
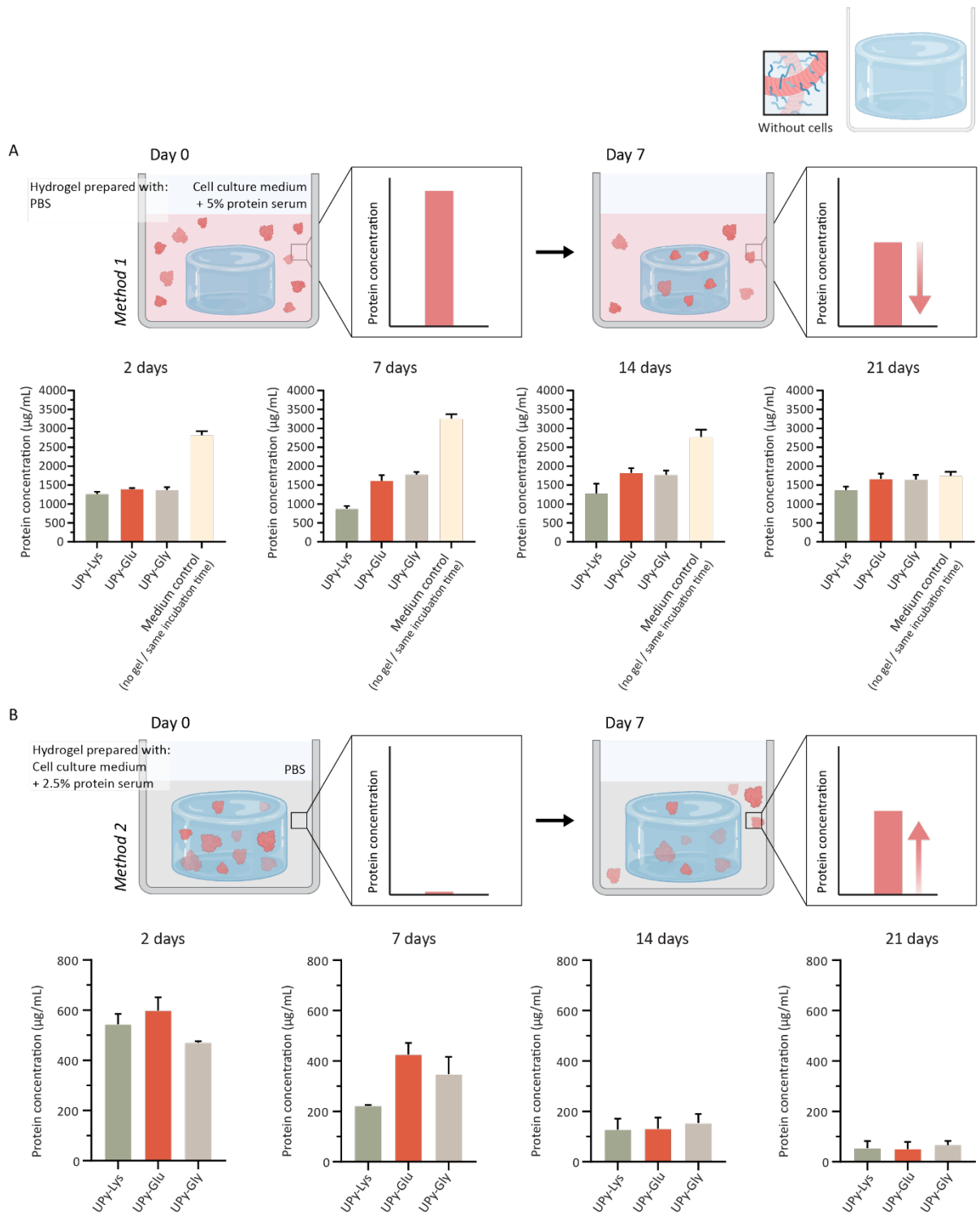
Figure 12. BCA assay to determine the ability of UPy-Lys, UPy-Glu, UPy-Gly hydrogel to bind proteins. Protein concentration were measured on day 2, 7, 14 and 21 with a sample size of n=3, mean ± standard deviation presented. **A)** Method 1: hydrogels were prepared with only PBS (without FBS) and embedded within cell culture medium (supplemented with 5% FBS). **B)** Method 2: hydrogels were prepared with medium supplemented with 2.5% FBS and embedded in PBS (without FBS).

REFERENCES

1. Berg, J. M., Tymoczko, J. L. & Stryer, L. Biochemistry - Chapter 2: Protein composition and Structure. in (eds. Berg, J. M., Tymoczko, J. L. & Stryer, L.) 25–65 (W. H. Freeman and Company , 2012).
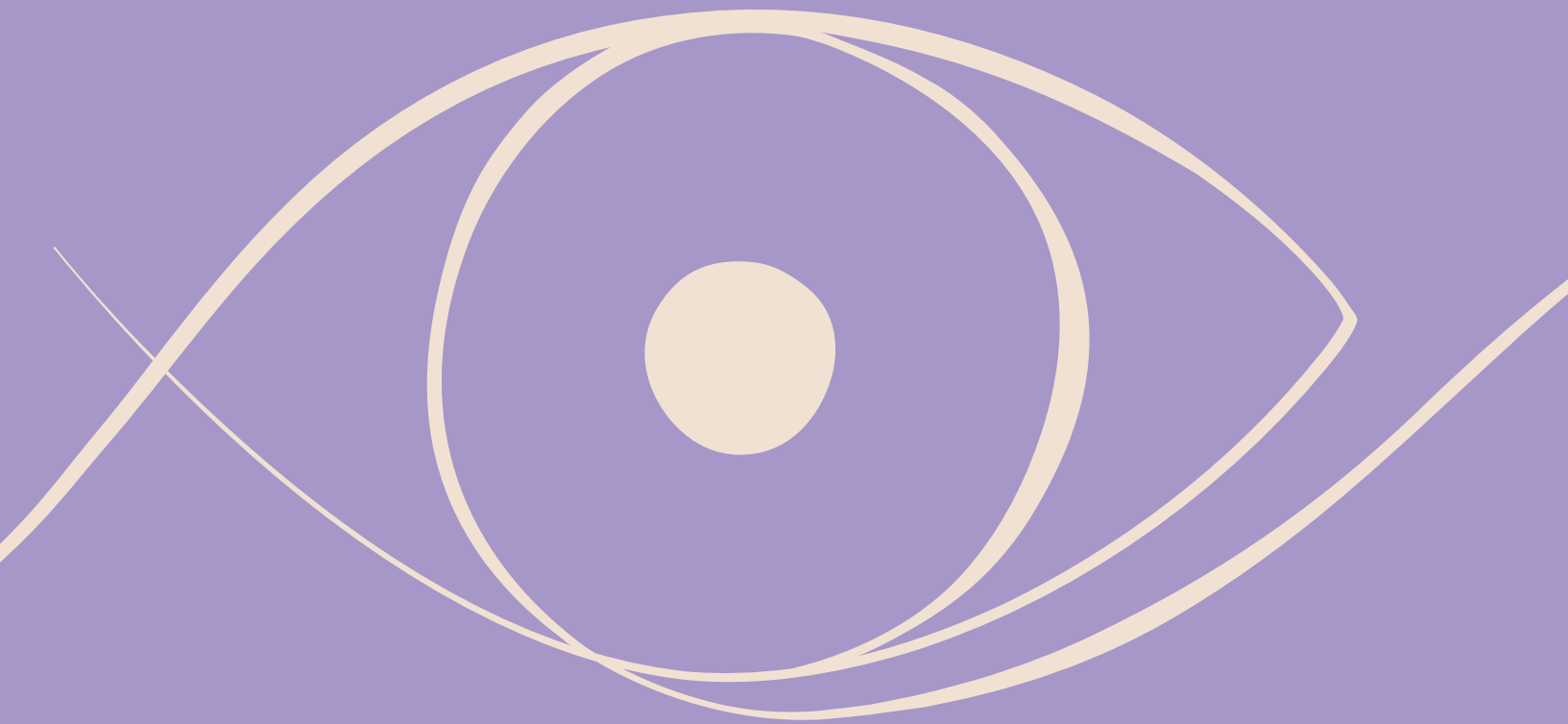
2. Groß, A., Hashimoto, C., Sticht, H. & Eichler, J. Synthetic Peptides as Protein Mimics. *Front Bioeng Biotechnol* 3, (2016).

3. Romano, N. H., Sengupta, D., Chung, C. & Heilshorn, S. C. Protein-engineered biomaterials: Nanoscale mimics of the extracellular matrix. *Biochimica et Biophysica Acta (BBA) - General Subjects* 1810, 339–349 (2011).

4. Numata, K. Poly(amino acid)s/polypeptides as potential functional and structural materials. *Polym J* 47, 537–545 (2015).

5. Rathore, O. & Sogah, D. Y. Self-Assembly of β-Sheets into Nanostructures by Poly(alanine) Segments Incorporated in Multiblock Copolymers Inspired by Spider Silk. *J Am Chem Soc* 123, 5231–5239 (2001).

6. Zarrintaj, P. *et al.* Polylysine for skin regeneration: A review of recent advances and future perspectives. *Bioeng Transl Med* 7, (2022).

7. Vandermeulen, G. W. M. & Klok, H.-A. Peptide/Protein Hybrid Materials: Enhanced Control of Structure and Improved Performance through Conjugation of Biological and Synthetic Polymers. *Macromol Biosci* 4, 383–398 (2004).

8. Song, Z. *et al.* Secondary structures in synthetic polypeptides from *N* -carboxyanhydrides: design, modulation, association, and material applications. *Chem Soc Rev* 47, 7401–7425 (2018).

9. Lu, H. *et al.* Ionic polypeptides with unusual helical stability. *Nat Commun* 2, 206 (2011).

10. Song, Z. *et al.* Synthesis of polypeptides via bioinspired polymerization of in situ purified *N* -carboxyanhydrides. *Proceedings of the National Academy of Sciences* 116, 10658–10663 (2019).

11. Jayawarna, V. *et al.* Nanostructured Hydrogels for Three-Dimensional Cell Culture Through Self-Assembly of Fluorenylmethoxycarbonyl–Dipeptides. *Advanced Materials* 18, 611–614 (2006).

12. Saiani, A. *et al.* Self-assembly and gelation properties of α-helix versus β-sheet forming peptides. *Soft Matter* 5, 193–202 (2009).

13. Jayawarna, V. *et al.* Introducing chemical functionality in Fmoc-peptide gels for cell culture. *Acta Biomater* 5, 934–943 (2009).

14. Zhou, M. *et al.* Self-assembled peptide-based hydrogels as scaffolds for anchorage-dependent cells. *Biomaterials* 30, 2523–2530 (2009).

15. Shah, R. N. *et al.* Supramolecular design of self-assembling nanofibers for cartilage regeneration. *Proceedings of the National Academy of Sciences* 107, 3293–3298 (2010).

16. Banwell, E. F. *et al.* Rational design and application of responsive α-helical peptide hydrogels. *Nat Mater* 8, 596–600 (2009).

17. Webber, M. J. *et al.* Development of bioactive peptide amphiphiles for therapeutic cell delivery. *Acta Biomater* 6, 3–11 (2010).

18. Chow, L. W. *et al.* A bioactive self-assembled membrane to promote angiogenesis. *Biomaterials* 32, 1574–1582 (2011).

19. Mishra, A. *et al.* Ultrasmall natural peptides self-assemble to strong temperature-resistant helical fibers in scaffolds suitable for tissue engineering. *Nano Today* 6, 232–239 (2011).

20. Hauser, C. A. E. *et al.* Natural tri- to hexapeptides self-assemble in water to amyloid β-type fiber aggregates by unexpected α-helical intermediate structures. *Proceedings of the National Academy of Sciences* 108, 1361–1366 (2011).

21. Hughes, M. *et al.* Differential supramolecular organisation of Fmoc-dipeptides with hydrophilic terminal amino acid residues by biocatalytic self-assembly. *Soft Matter* 8, 11565 (2012).

22. Mujeeb, A., Miller, A. F., Saiani, A. & Gough, J. E. Self-assembled octapeptide scaffolds for in vitro chondrocyte culture. *Acta Biomater* 9, 4609–4617 (2013).

23. Fleming, S., Debnath, S., Frederix, P. W. J. M., Tuttle, T. & Ulijn, R. V. Aromatic peptide amphiphiles: significance of the Fmoc moiety. *Chemical Communications* 49, 10587 (2013).

24. Castillo Diaz, L. A., Saiani, A., Gough, J. E. & Miller, A. F. Human osteoblasts within soft peptide hydrogels promote mineralisation in vitro. *J Tissue Eng* 5, 204173141453934 (2014).

25. Wan, S. *et al.* Self-assembling peptide hydrogel for intervertebral disc tissue engineering. *Acta Biomater* 46, 29–40 (2016).

26. Markey, A. *et al.* Peptide hydrogel *in vitro* non-inflammatory potential. *Journal of Peptide Science* 23, 148–154 (2017).

27. Scelsi, A. *et al.* Tuning of hydrogel stiffness using a two-component peptide system for mammalian cell culture. *J Biomed Mater Res A* 107, 535–544 (2019).

28. Mehrban, N. *et al.* Host macrophage response to injectable hydrogels derived from ECM and α-helical peptides. *Acta Biomater* 111, 141–152 (2020).

29. Chivers, P. R. A., Dookie, R. S., Gough, J. E. & Webb, S. J. Photo-dissociation of self-assembled (anthracene-2-carbonyl)amino acid hydrogels. *Chemical Communications* 56, 13792–13795 (2020).

30. Chiesa, I. *et al.* Modeling the Three-Dimensional Bioprinting Process of β-Sheet Self-Assembling Peptide Hydrogel Scaffolds. *Front Med Technol* 2, (2020).

31. Wychowaniec, J. K. *et al.* Role of Sheet-Edge Interactions in β-sheet Self-Assembling Peptide Hydrogels. *Biomacromolecules* 21, 2285–2297 (2020).

32. Rauf, S. *et al.* Self-assembling tetrameric peptides allow *in situ* 3D bioprinting under physiological conditions. *J Mater Chem B* 9, 1069–1081 (2021).

33. Alshehri, S., Susapto, H. H. & Hauser, C. A. E. Scaffolds from Self-Assembling Tetrapeptides Support 3D Spreading, Osteogenic Differentiation, and Angiogenesis of Mesenchymal Stem Cells. *Biomacromolecules* 22, 2094–2106 (2021).

34. Burgess, K. A. *et al.* Functionalised peptide hydrogel for the delivery of cardiac progenitor cells. *Materials Science and Engineering: C* 119, 111539 (2021).

35. Storrie, H. *et al.* Supramolecular crafting of cell adhesion. *Biomaterials* 28, 4608–4618 (2007).

36. Cui, H., Webber, M. J. & Stupp, S. I. Self-assembly of peptide amphiphiles: From molecules to nanostructures to biomaterials. *Biopolymers* 94, 1–18 (2010).

37. Silva, G. A. *et al.* Selective Differentiation of Neural Progenitor Cells by High-Epitope Density Nanofibers. *Science* 303, 1352–1355 (2004).

38.   Webber, M. J. *et al.* Supramolecular nanostructures that mimic VEGF as a strategy for ischemic tissue repair. *Proceedings of the National Academy of Sciences* 108, 13438–13443 (2011).

39.   Hendricks, M. P., Sato, K., Palmer, L. C. & Stupp, S. I. Supramolecular Assembly of Peptide Amphiphiles. *Acc Chem Res* 50, 2440–2448 (2017).

40.   Cui, H., Cheetham, A. G., Pashuck, E. T. & Stupp, S. I. Amino Acid Sequence in Constitutionally Isomeric Tetrapeptide Amphiphiles Dictates Architecture of One-Dimensional Nanostructures. *J Am Chem Soc* 136, 12461–12468 (2014).

41.   Ligorio, C., Hoyland, J. A. & Saiani, A. Self-Assembling Peptide Hydrogels as Functional Tools to Tackle Intervertebral Disc Degeneration. *Gels* 8, 211 (2022).

42.   Diba, M. *et al.* Engineering the Dynamics of Cell Adhesion Cues in Supramolecular Hydrogels for Facile Control over Cell Encapsulation and Behavior. *Advanced Materials* 33, 2008111 (2021).

43.   Bastings, M. M. C. *et al.* A Fast pH-Switchable and Self-Healing Supramolecular Hydrogel Carrier for Guided, Local Catheter Injection in the Infarcted Myocardium. *Adv Healthc Mater* 3, 70–78 (2014).

44.   Sargeant, T. D., Aparicio, C., Goldberger, J. E., Cui, H. & Stupp, S. I. Mineralization of peptide amphiphile nanofibers and its effect on the differentiation of human mesenchymal stem cells. *Acta Biomater* 8, 2456–2465 (2012).

45.   Tsimbouri, P. M., McNamara, L. E., Alakpa, E. V., Dalby, M. J. & Turner, L.-A. Cell–Material Interactions. in *Tissue Engineering* (eds. van Blitterswijk, C. A. & de Boer, J.) 217–251 (Elsevier, 2014).

46.   Mazia, D., Schatten, G. & Sale, W. Adhesion of cells to surfaces coated with polylysine. Applications to electron microscopy. *Journal of Cell Biology* 66, 198–200 (1975).

47.   Hejčl, A. *et al.* Macroporous hydrogels based on 2-hydroxyethyl methacrylate. Part 6: 3D hydrogels with positive and negative surface charges and polyelectrolyte complexes in spinal cord injury repair. *J Mater Sci Mater Med* 20, 1571–1577 (2009).

48.   Schneider, G. B. *et al.* The effect of hydrogel charge density on cell attachment. *Biomaterials* 25, 3023–3028 (2004).

49.   Camci-Unal, G. *et al.* Hydrogel surfaces to promote attachment and spreading of endothelial progenitor cells. *J Tissue Eng Regen Med* 7, 337–347 (2013).

50.   Bet, M. R., Goissis, G., Vargas, S. & Selistre-de-Araujo, H. S. Cell adhesion and cytotoxicity studies over polyanionic collagen surfaces with variable negative charge and wettability. *Biomaterials* 24, 131–137 (2003).

51.   Dupont, S. *et al.* Role of YAP/TAZ in mechanotransduction. *Nature* 474, 179–183 (2011).

52.   Elosegui-Artola, A. *et al.* Force Triggers YAP Nuclear Entry by Regulating Transport across Nuclear Pores. *Cell* 171, 1397-1410.e14 (2017).

53.   Nardone, G. *et al.* YAP regulates cell mechanics by controlling focal adhesion assembly. *Nat Commun* 8, 15321 (2017).

54.   Foster, J. W., Gouveia, R. M. & Connon, C. J. Low-glucose enhances keratocyte-characteristic phenotype from corneal stromal cells in serum-free conditions. *Sci Rep* 5, 10839 (2015).

55.   Yam, G. H.-F. *et al.* Nerve regeneration by human corneal stromal keratocytes and stromal fibroblasts. *Sci Rep* 7, 45396 (2017).

56. Jester, J. V. Corneal crystallins and the development of cellular transparency. *Semin Cell Dev Biol* 19, 82–93 (2008).

57. Jester, J. V. *et al.* The cellular basis of corneal transparency: evidence for 'corneal crystallins'. *J Cell Sci* 112, 613–622 (1999).

58. Tashiro, K. *et al.* A synthetic peptide containing the IKVAV sequence from the A chain of laminin mediates cell attachment, migration, and neurite outgrowth. *J Biol Chem* 264, 16174–82 (1989).

59. Silva, G. A. *et al.* Selective Differentiation of Neural Progenitor Cells by High-Epitope Density Nanofibers. *Science (1979)* 303, 1352–1355 (2004).

60. Álvarez, Z. *et al.* Artificial extracellular matrix scaffolds of mobile molecules enhance maturation of human stem cell-derived neurons. *Cell Stem Cell* 30, 219-238 (2023).

CHAPTER 6

Biohybrid corneal stromal tissue formation using keratocyte encapsulated supramolecular microgels

In comparison to bulk hydrogels, microgels possess some unique properties to make them favorable over bulk hydrogels for biomedical applications, i.e. an increased modularity and heterogeneity of biomaterials, their small size and reversible dynamic bonding being an advantage for minimally invasive delivery of cells, and increased tuning possibilities of the porosity scales resulting in the formation of porous microstructures. In this work, we aimed to fabricate single keratocyte encapsulated supramolecular microgels to generate a micro stromal tissue in-vitro. The fully synthetic microgels are fabricated via a combination of droplet-based microfluidics and the ureido-pyrimidinone (UPy) hydrogel functionalized with UPy-cRGD (chapter 2). A mix of microgels, equipped with a single encapsulated keratocyte or without a cell, were collected, embedded in medium and cultured for several days. Immunohistochemical analyses demonstrated the formation of stromal micro tissues, cellular extracellular matrix (ECM) deposition and substantial upregulation of nuclear yes-associated-protein (YAP) during culture, indicating cell-cell driven microgel assembly. The created interconnected pores within the microgel assembly facilitated migration and infiltration of the cells through the biohybrid stromal tissue construct. Herewith, this work demonstrates a novel supramolecular approach with promising outlooks for minimally invasive therapy to treat corneal defects in the clinic.

INTRODUCTION

At the outermost part of the eye the cornea is located, being a homogenously stratified tissue and covering the tear film. The cornea provokes two main functions, namely protection of the inner parts of the eye and refraction of light towards the retina.[1] The thickest layer within the corneal is the corneal stroma, which substantially affects the corneal functions. The corneal stroma exhibits a very specific and highly organized structure of packed collagen fibrils surrounded by specialized proteoglycans, resulting in a highly hydrated tissue.[2,3] Previously, to design a biomaterial mimicking the stromal extracellular matrix (ECM) we developed an injectable supramolecular synthetic hydrogel that proved to be a stable and biocompatible micro environment for the encapsulated primary stromal keratocytes. However, instead of creating bulk hydrogels, the formation of microgels as small building blocks to generate granular porous hydrogels raised our interests. The synthetic microgels are based on bifunctional and monofunctional molecules containing ureido-pyrimidinone (UPy) groups as supramolecular building blocks. UPy groups dimerize via fourfold hydrogen bonding into 1D stacks, whereafter the stacks start to bundle into fibers, generating a fibrous network. Interfiber cross-links are introduced upon addition of bifunctional UPy molecules, resulting in the formation of microgels.[4] The increased range of possibilities of using microgels as minimally invasive therapeutics allows them to become favorable over bulk hydrogels for clinical applications to treat corneal stromal defects.

Microgels are, by definition micrometer-scale gel beads with a particle size up to the micrometer range, *i.e.* ~ 100 nm – 100 μm. Particles smaller than 100 nm are usually considered nanogels, while gels with particle sizes bigger than 100 μm are usually called macrogels.[5] Compared with bulk hydrogels, microgels possess some unique properties that make them attractive for biomedical applications. First, multiple microgel populations with varying compositions, size, and contents can be mixed to design diverse materials. This provides the microgel system with a substantial modularity, and in addition contributes to an easily adaptable heterogeneity of the materials.[6] Second, their small sizes as well as their dynamic bonding within microgel assemblies make microgels highly favorable for injectability through small needles, which is a major advantage for minimally invasive delivery of cells and biologics.[6–8] Third, the assembly of microgels provides porous microstructures with interconnecting pores where the porosity scales can be easily tuned by adapting the packing density or size of the

microgels, to support cell migration.[7,9,10] Finally, the surface over volume ratio is one of the most substantial differences between microgels and bulk hydrogels. Compared with the low surface over volume ratio of bulk hydrogels, microgels have a large surface over volume ratio. Herewith, microgels rely in lower amount on hydrogel degradation and allow cells to easily infiltrate into the host tissue after injection.[8,11]

Taken together the above mentioned properties, microgels are found to be an attractive tool for biomedical applications, ranging from therapeutic delivery of cells and/or drugs to the production of scaffolds for tissue repair. Moreover, microgels allow the application of biomaterials in a minimally invasive manner.[7,8,12–15] Various researchers within the biomaterial and tissue engineering field are focusing on the design and development of microgels and are exploring their applications within the field. For instance, Allazetta *et al.* created a microfluidic platform to produce combinatorial microgels with varying elasticity, biochemical composition or both. Herewith, they generated an unpredicted, continuous landscape of microgel properties, enabling high-throughput applications of gels to explore novel compositions or applications of hydrogels.[16] Chen *et al.* combined an injectable bulk guest-host hydrogel with covalently-crosslinked microgels to create a composite hydrogel/microgel for therapeutic delivery of complex release profiles for broad applications, via decoupling of the release from the degradation of the bulk hydrogel.[11] Özkale *et al.* integrated magnetic nanoactuators into single-cell laden alginate microgels, herewith actuated microgels were generated that possess the ability of applying uniform and isotropic compressive stresses within a mechanically tunable 3D substrate. This microgel driven mechanically active single cell culture system enabled to explore biomechanical studies at a single cell level.[17] Another approach to create a microgel-based off-the-shelf material that can be easily tailored was designed by Wilson *et al.* They introduced bioactivity into microporous annealed particle scaffolds via tetrazine-norbornene chemistry to create a scaffold, which allowed for neural progenitor cell migration and differentiation.[18]

Our aim is to generate a biohybrid stromal tissue via keratocyte encapsulated supramolecular microgels, towards a minimally invasive *in vivo* treatment for corneal defects. To this end, single primary stromal keratocytes were trapped within supramolecular microgels. With the microgels a synthetic system is provided, allowing the cells to create their own microporous scaffold via cell-cell driven microgel assembly. Eventually, we want to design a system towards the application of these supramolecular microgels as injectable biomaterial to

treat corneal defects. For this purpose, the cells were encapsulated within the microgels to assure control and protection of the cells during future delivery processes. After cell encapsulation within the microgels, the cells were monitored during cell culture to study the microgel assembly driven by cell-cell interactions. Subsequently, the stromal tissue constructs were thoroughly analyzed with various immunohistochemical analyses.
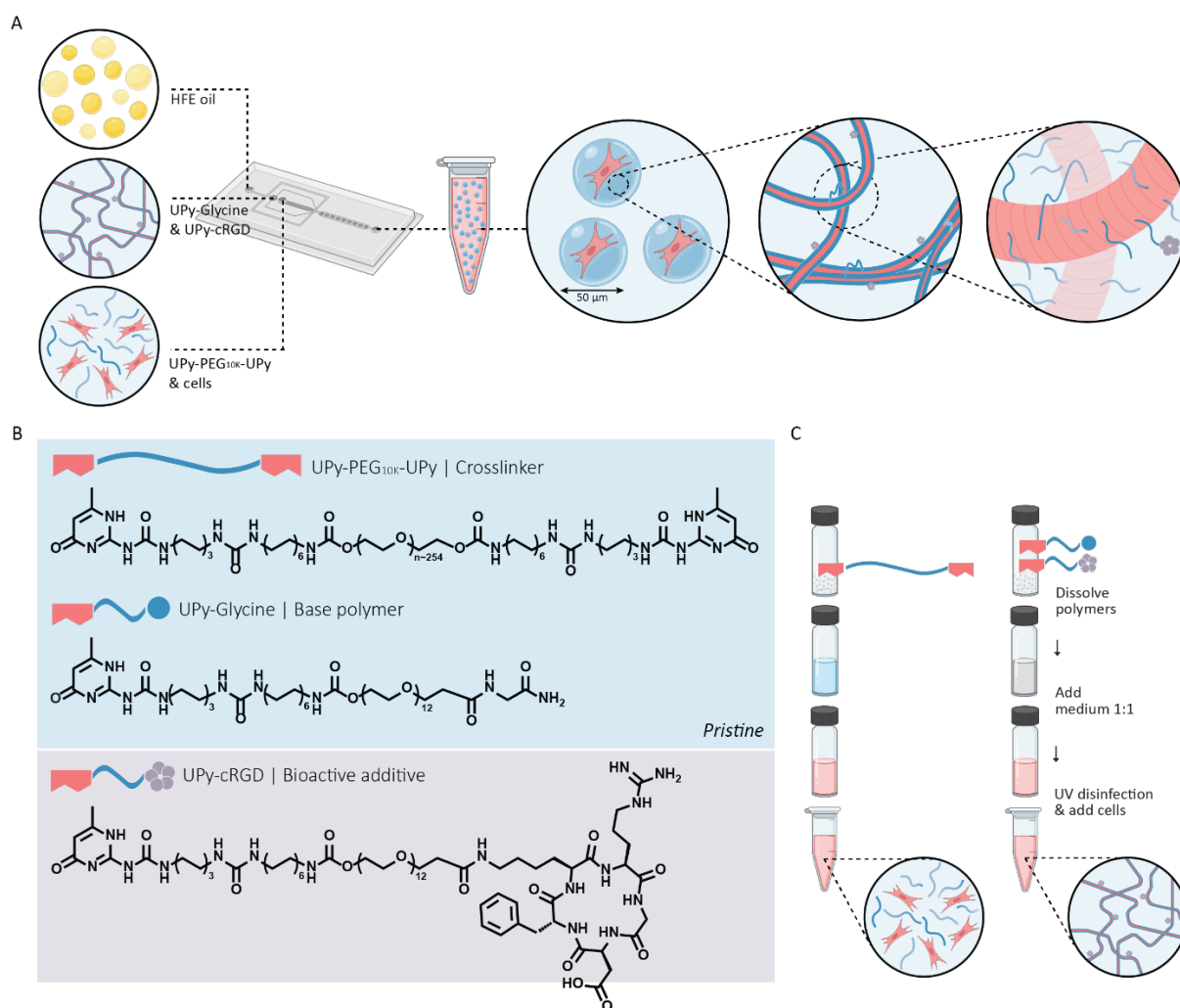

Figure 1. Schematic representation of microgel formulation by using a PDMS based droplet microfluidic device, chemical properties of the microgel and the formulation method of the microgels. **A)** Microgels with and without encapsulated cells are collected at the outlet of the microfluidic device due to a continuous flow of oil, dissolved monofunctional molecules and dissolved bifunctional molecules together with cells, respectively. **B)** The chemical structures of the monofunctional hydrogelator UPy-glycine, the bifunctional crosslinker UPy-PEG$_{10K}$-UPy, and the bioactive additive UPy-cRGD. **C)** Schematic microgel formation protocol.

RESULTS & DISCUSSION

Formation of supramolecular microgels

The core of the microgels comprised of a monofunctional UPy-Glycine hydrogelator and a bifunctional UPy-PEG$_{10K}$-UPy crosslinker, both containing functional hydrogen bonding UPy groups as supramolecular building blocks (**Figure 1B**). The molecular design of the monofunctional UPy moiety contained a 528 Da oligo(ethylene glycol) (OEG) chain, which was end-capped with a UPy moiety at one end and a Glycine group at the other end. It is assumed that the glycols' non-fouling properties are shielded, while the glycine groups are presented to the cells.[4] Integrin-binding cyclic arginine-glycine-aspartate (cRGD) ligands were introduced into the microgel network to allow for cell adhering, cellular infiltration and cell migration after microgel encapsulation. A monofunctional UPy moiety was functionalized with this cRGD end group, to act as a integrin binding supramolecular additive.

Human primary keratocytes (PKs) were isolated from human donor corneal stroma and expanded *in vitro*. The bifunctional and monofunctional molecules were received as a powder, and dissolved separately in aqueous solutions (**Figure 1C**). The dissolved bifunctional and monofunctional building blocks were both diluted with cell culture medium to provide the cells with some nutrients during gelation, subsequently the PKs were supplemented to the dissolved bifunctional molecules. A Polydimethylsiloxane (PDMS) based droplet microfluidic device with three inlets and one outlet is used to produce the microgels.[19] Syringes and tubing filled with mineral oil were used as hydraulic system to dispense the liquids computer-controlled from the syringes. The three inlets enable a continuous oil phase, dissolved monofunctional molecules, and dissolved bifunctional molecules together with cells, respectively (**Figure 1A**). The generated microgels, with and without encapsulated cells, were collected in an Eppendorf tube from the outlet and medium was poured on top of the emulsion to prevent evaporation of the oil. Whereafter, the microgels needed 2 hours at 37 °C to allow proper gelation before de-emulsification with 20 v/v% PFO in oil.

Encapsulation of primary keratocytes within supramolecular microgels

Single-cell encapsulation within supramolecular microgels is achieved with an initial cell-encapsulation rate of ~ 8% (**Figure 3A**). A mixture of round-shaped microgels with and without encapsulated single cells, with a uniform size of 50 µm in diameter, was added to each well and embedded in cell culture medium (day 0) (**Figure 3B**). Per well, both the number of encapsulated cells as well as the total number of microgels were counted to calculate obtain the cell-encapsulation rate. Subsequently, after three days of culture (day 3) the PKs were treated in two manners (**Figure 2**); (1) with serum to activate towards stromal fibroblasts (SFs) or (2) with low serum and high glucose to differentiate towards quiescent corneal stromal keratocytes (CSKs).[20] Various microgel assembling strategies exist, *i.e.* via physical reactions like hydrogen bonding, via external driving forces like fluid force or surface tension, or via cell-cell interactions.[7] However, upon the addition of culture medium no microgel assembly occurred, indicating that physical reactions or external fluid forces are not initiating the assembly of the microgels studied in this work.

An increase in the number of cells per well was observed on the third culture day, the PKs started to migrate from droplets and the cells initiated microgel assembly by pulling the droplets together via both cell-cell and cell-matrix interactions. From the third day onwards, the PKs were treated in two manners. For the PKs treated towards SFs the results showed cell proliferation and a substantial increase in the amount of cells (**Figure 3C**). Microgel assembly via cell-cell and cell-matrix interaction was clearly demonstrated by the increasing number of microgels per cluster from day 3 until day 7. Noteworthy is the substantial microgel assembly between day 7 and day 10, where it seems that the cells together with the microgels start to form a 3D tissue-like structure.

Although the proliferation rate of the PKs treated towards CSKs showed to be less pronounced than the proliferation rate of the PKs activated towards SFs, still an increase in the amount of cells was observed (**Figure 3D**). The results demonstrated an interesting difference in the degree of microgel assembly between the SF treated and the CSK treated condition. For the PKs differentiated towards CSKs the microgel assembly slowed down and resulted in a less dense cluster of microgels at culture day 10. Foster *et al.* already showed an increase in cell contractility when PKs are cultured with serum supplemented cell culture medium.[20] It is proposed that, this serum dependent cell contractility can be related to the differences in

microgel assembly between the condition of PKs activated towards SFs and the condition of PKs differentiated towards CSKs.

Overall, the results demonstrated the fabrication of single keratocyte encapsulated supramolecular microgels, succeeded by cell-cell and cell-matrix mediated microgel assembly. Eventually resulting in a cluster of microgels. Together, these results suggest that the cells dictate their scaffold of microgels, instead of a predesigned scaffold dictating the cells.

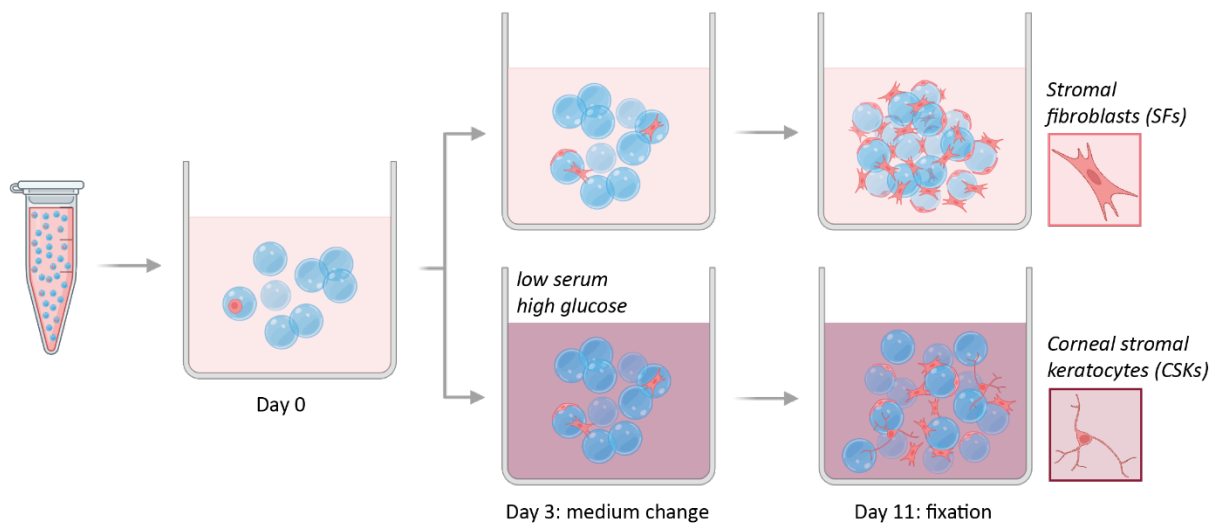**Figure 2**. Experimental set-up and timeline. A mixture of the collected microgels, with and without encapsulated single human primary keratocytes (PKs), are added to each culture well. From culture day 3 onwards the PKs are treated in two different manners. In the top-row the PKs are activated towards stromal fibroblasts (1), while in the bottom row the PKs are differentiated towards corneal stromal keratocytes (2).
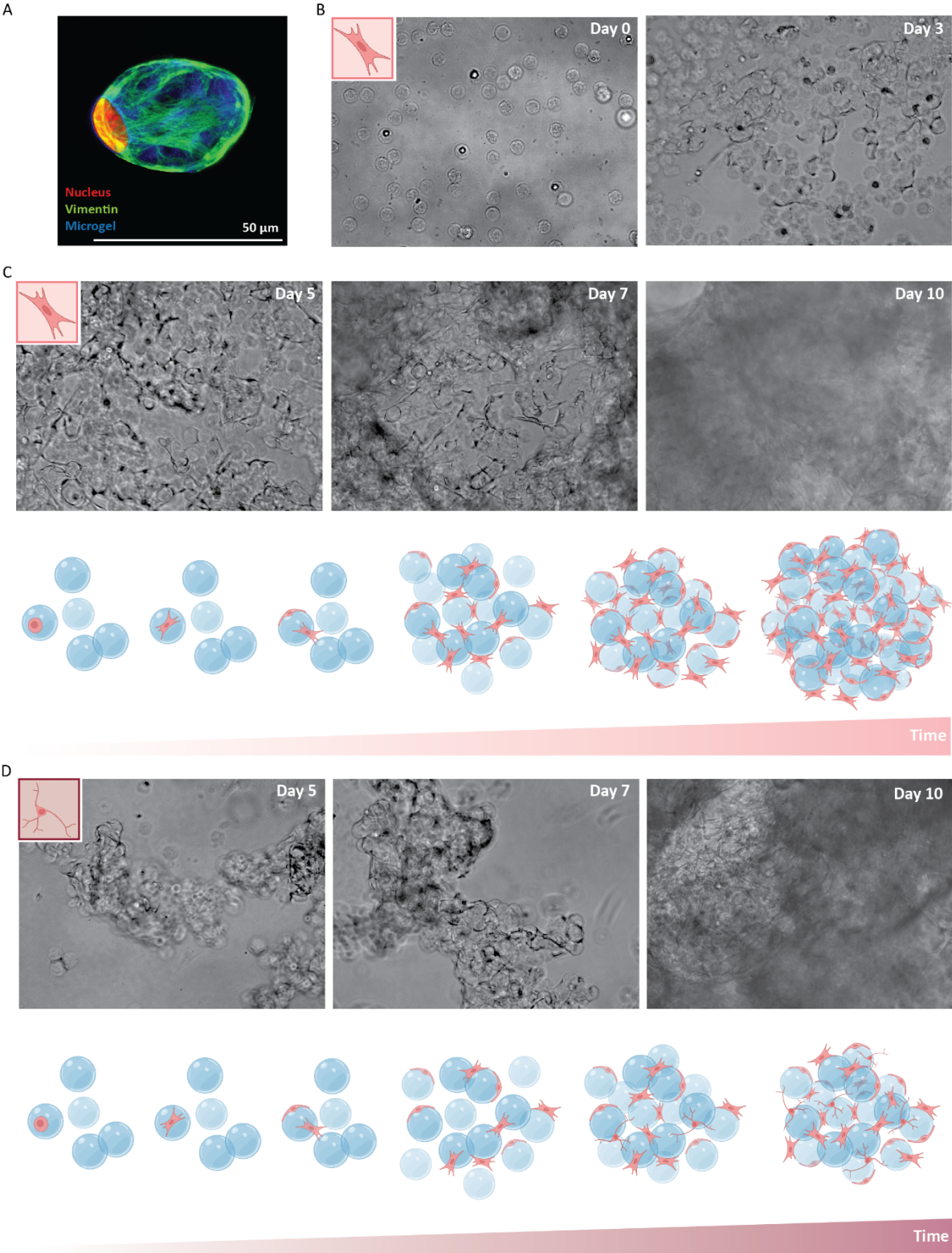
Figure 3. A mixture of collected microgel, with and without encapsulated single human primary keratocytes (PKs), from individual microgels with ~ 8% encapsulation rate on day 0 to a dense cluster of PKs and microgels on day 10. **A)** Visualization of a cell inside a single droplet, nucleus in red, vimentin in green, and microgel in blue. Scale bar represents 50 μm. **B)** Mixture of microgels with and without encapsulated PKs on day 0, followed by proliferated, spreaded and migrated PKs on day 3. **C)** A follow-up of PKs activated towards SFs from culture day 5 until day 10. With a very dense cluster of cells and microgels on day 10. **D)** A follow-up of PKs differentiated towards CSKs from culture day 5 until day 10. With a less dense cluster of cells and microgels on day 10.

From single cell encapsulation within microgels towards micro tissue formation

On day eleven of the cell culture, the cell/microgel clusters were fixated and various immunohistochemical analyses were performed. The PKs treated towards SFs formed dense cell/microgel clusters of approximately ~ 1 – 2 mm in diameter. The results demonstrated intracellular, granular deposition of the extracellular matrix (ECM) protein collagen type VI by the SFs within the cell/microgel cluster, as well as the intracellular expression of neural differentiation marker tubulin β3 (**Figure 4A**). The PKs differentiated towards CSKs formed loose cell/microgel clusters. Upon washing, these loose cell/microgel clusters fall apart into single microgels or preserved cell/microgel clusters of ~ 5 – 10 microgels. The CSKs deposited collagen type VI to a lower extend and solely around the nucleus, compared with the collagen type VI deposition of the SFs (**Figure 4B**). Corneal keratocytes possess the ability to heal the cornea throughout life. This property could be related to the origin of the keratocytes, being neural-crest derived mesenchymal cells.[21–23] Associated to this specific cell characteristic, some groups studied the differentiation behavior of corneal keratocytes and concluded that corneal keratocytes are not terminally differentiated but maintain a certain multipotency, which can contribute to the differentiation into neural crest derivatives.[23–25] The presence of tubulin β3 positive cells within the cell/microgel cluster could indicate that some of the PKs activated towards SFs still exhibit a multipotent differentiation potential. The multipotent differentiation capacity of the PKs differentiated towards CSKs is diminished, resulting in a less pronounced expression of tubulin β3.

Additional immunohistochemical staining showed that the PKs activated towards SFs expressed cytoplasmic alpha-smooth muscle actin (αSMA) with no specific architecture and no colocalization with the actin fibers (**Figure 5A**). The upregulated expression of αSMA was expected, and is supported by several studies where the keratocyte-fibroblast transition has been related to an upregulation of αSMA due to the presence of serum products within the culture media.[20,26–28]

Mechanotransduction allows cells to sense and adapt to external forces by cytoskeleton remodeling or activating specific gene pathways.[29] Mechanical signals are first sensed by cell surface receptors such as integrins or cadherins, which trigger and regulate multiple signaling pathways. One of these pathways is the Hippo signaling pathway, regulating tissue growth among other biological processes. The mechanosensitive transcriptional regulator yes-

associated protein (YAP) belongs to the Hippo pathway, and is involved in mechanotransduction pathways and regulated by mechanical cues such as cell-cell contact, ECM rigidity, flow, cell shape and cell tension.[30–32] Recent reports even point YAP as a master regulator of cell-ECM interaction, and analysis of YAP expression within the cell/microgel cluster is believed to aid in a better understanding of the ongoing mechanobiological interactions within the cell/microgel clusters.[33]
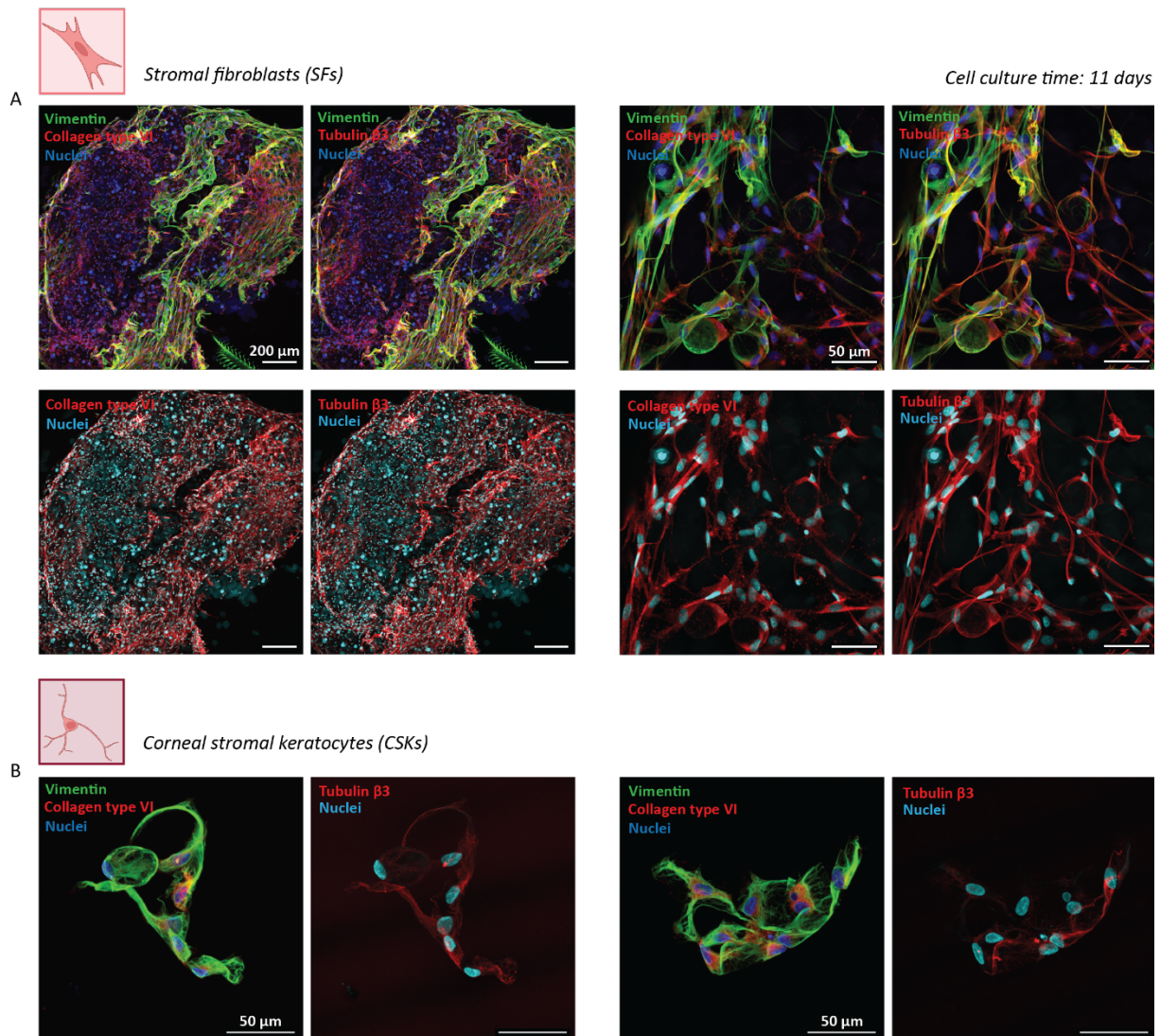
Figure 4. Human primary keratocytes (PKs) encapsulated within microgels and cultured for 11 days. **A)** Confocal images of immunohistochemical staining of PKs activated towards SFs. Vimentin in green, collagen type VI or tubulin β3 in red, and nuclei in blue or cyan. Scale bar for the four images on the left represents 200 μm and for the four images on the right it represents 50 μm. **B)** Confocal images of immunohistochemical staining of PKs differentiated towards CSKs. Vimentin in green, collagen type VI or tubulin β3 in red, and nuclei in blue or cyan. Scale bar represents 50 μm.
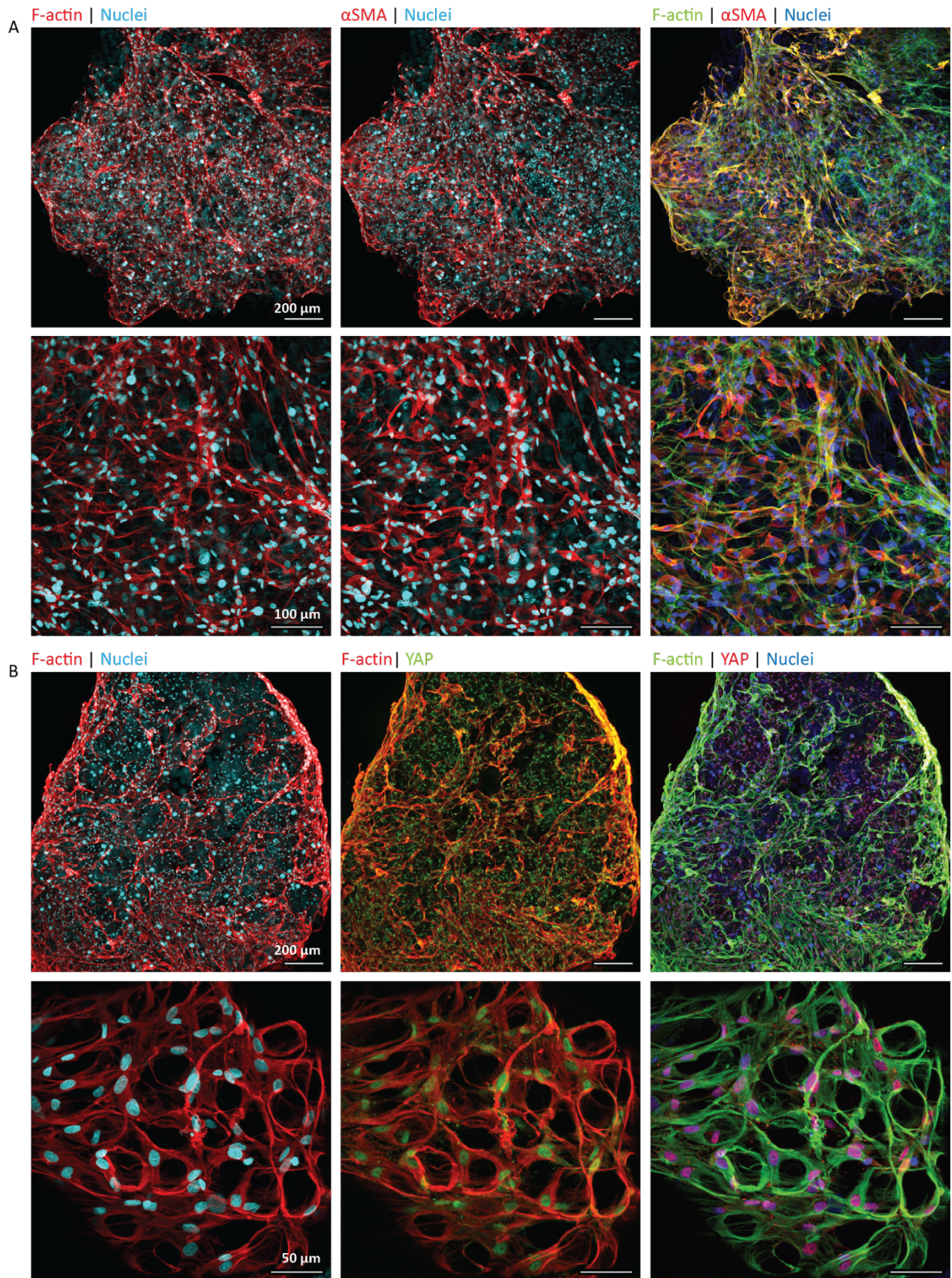
Figure 5. Immunohistochemical staining of cell/microgel clusters of human primary keratocytes (PKs) encapsulated within microgels and cultured for 11 days. **A)** From left to right; F-actin in red & nuclei in cyan, αSMA in red & nuclei in cyan, merged image of F-actin in green & αSMA in red & nuclei in blue. Scale bar of top row images represents 200 μm and bottom row represents 100 μm. **B)** From left to right; F-actin in red & nuclei in cyan, F-actin in red & YAP in green, merged image of F-actin in green & YAP in red & nuclei in blue. Scale bar of top row images represents 200 μm and bottom row represents 50 μm.

The results of all cell/microgel clusters showed expression of YAP solely within the nuclei of the cells, indicating a distinct nuclear translocation of YAP (**Figure 5B**). Nuclear translocation of YAP can be the result of various processes, for instance due to increased adhesive area caused by higher matrix stiffness or due to relieved mechanical strain in highly confluent cells by stretching the cells and increasing their spreading.[31]

The in-depth immunohistochemical analysis of microgel encapsulated PKs activated towards SFs aided in a better understanding of some of the ongoing biological processes within the cell/microgels clusters. Moreover, the results shown in figure 4 and 5 demonstrated that the microgels are still intact, allowing the cells to adhere to the microgel surface and to migrate or infiltrate between them. Dense cellular networks supported by the dynamic supramolecular microgels are formed within all the cell/microgel clusters.

Presence of proliferating cells within the core of the biohybrid stromal tissue construct

A major challenge in generating engineered tissues is gaining control over cell proliferation, more specifically, having cell division when more cells are needed or arresting them to avoid overgrowth.[32] Proliferation marker Ki-67 is a widely used and is highly expressed by cells during mitosis.[34] Small dots of Ki-67 are present in the nuclei as the cells exit the mitosis and enter the early G1 phase, followed by merged dots when the cells go through the mid G1 and late G1 phase.[35] Ki-67 is stable for ~ 36 hours, whereafter it will be degraded.[36] The obtained results showed the presence of Ki-67 positive nuclei on the edges and within the core of the cell/microgel clusters, suggesting the cells are still proliferating even within the core of the biohybrid tissue (**Figure 6**). Despite the already dense network of clustered cells and microgels, the presence of Ki-67 cells suggest that the cell number is still increasing within the core of the cluster.

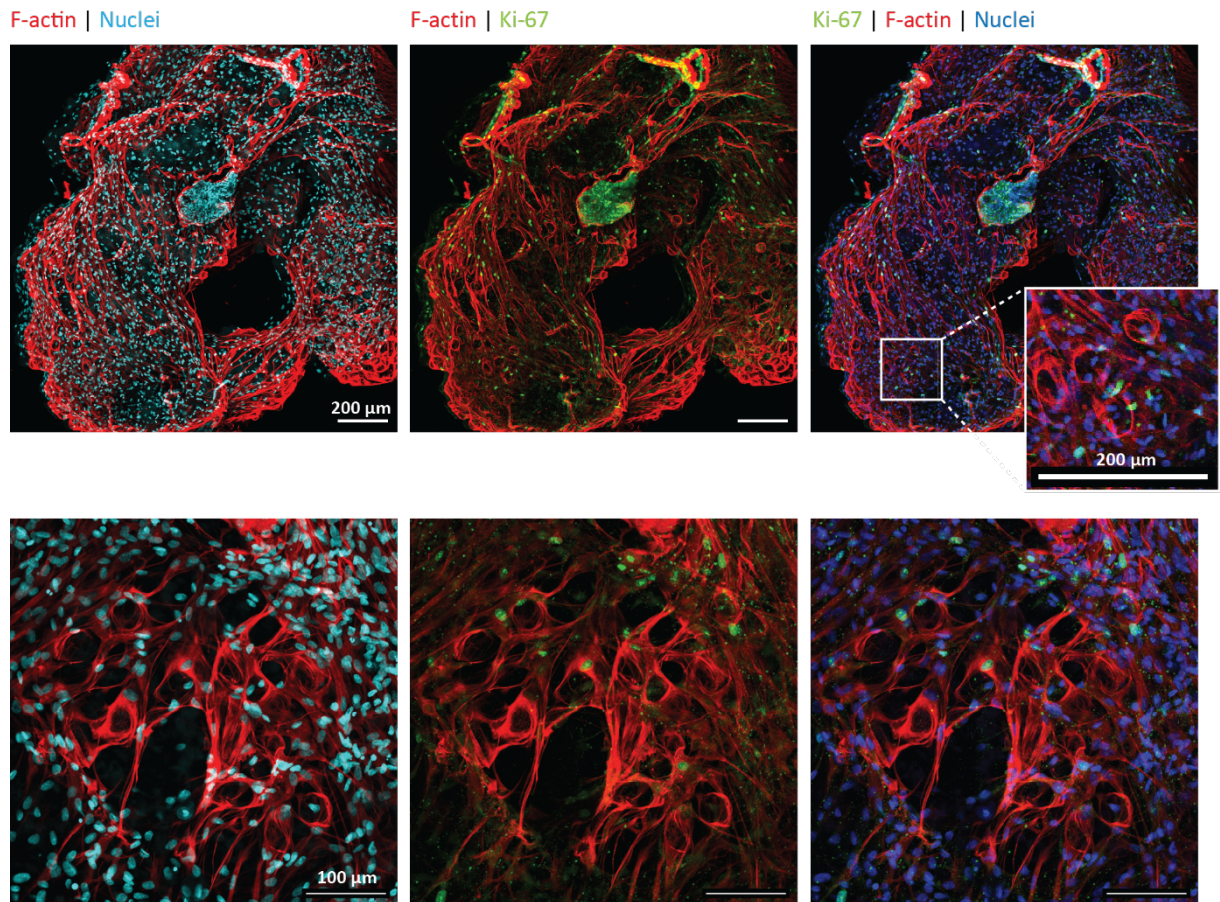**Figure 6.** Immunohistochemical staining of cell/microgel clusters of human primary keratocytes (PKs) encapsulated within microgels and cultured for 11 days. From left to right; F-actin in red & nuclei in cyan, F-actin in red & Ki-67 positive nuclei in green, merged image of F-actin in red & Ki-67 positive nuclei in green & nuclei in blue. Scale bar of top row images represents 200 μm and bottom row represents 100 μm.

Upregulation of YAP translocation in keratocytes encapsulated within microgels

The previous mentioned results demonstrated nuclear YAP expression within the cells of the studied cell/microgel cluster, cellular deposition of collagen type VI within the cell/microgel cluster, and proliferating cells within the core of the cluster. Here, the translocation of YAP was quantified and studied on day 5, day 7, day 14 and day 21 after cell culture. The nuclei eccentricity values were quantified and within the same range of ~ 0.7 − 0.8 for all the timepoints, suggesting that the nuclei are oval-shaped instead of round-shaped (**Figure 7A**). A custom-made cell profiler pipeline was used to quantify the intensity of YAP expression inside the cytoplasm and inside the nuclei. The ratios' between the nuclear YAP intensity and YAP intensity within the cytoplasm of the PKs are slightly above ~ 1 on day 5. Interestingly, during the culture YAP activation is upregulated and the nuclear YAP translocation increases significantly from just above ~ 1 for day 5 to just above ~ 6 for day 21 (**Figure 7B**). The confocal images of YAP expression showed a difference in cytoplasmic YAP and nuclear YAP as well (**Figure 7C,D**). As mentioned previously, the mechanosensitive transcription regulator YAP is involved in various biological processes, including cell proliferation and tissue homeostasis. Dupont *et al.* already speculated that the tissue architecture is regulated by a combination of growth factor signaling, localized control of YAP activation by cell-cell contacts, and mechanical cues.[29] Over-proliferation and excessive ECM deposition by cells can stiffen the matrix surrounding them and eventually trigger a fibrotic response, relating YAP activation to fibroblast activation and cell proliferation.[32] In contrast, if the cells reach a high cell confluency this will cause a reduction of adhesive areas and hence an altered cell shape. Similar to soft matrices, this geometrical change reduces stress fiber formation and thus inactivates YAP.[30,32]

Here, the results indicated that the interaction between the cells and the microgels acted as the key factor in activating nuclear YAP. The combination of a fibrotic response associated with ECM deposition and a less dynamic movement of the microgels due to an increase of cell-cell and cell-matrix interactions, resulted in an increased matrix stiffness sensed by the cells.
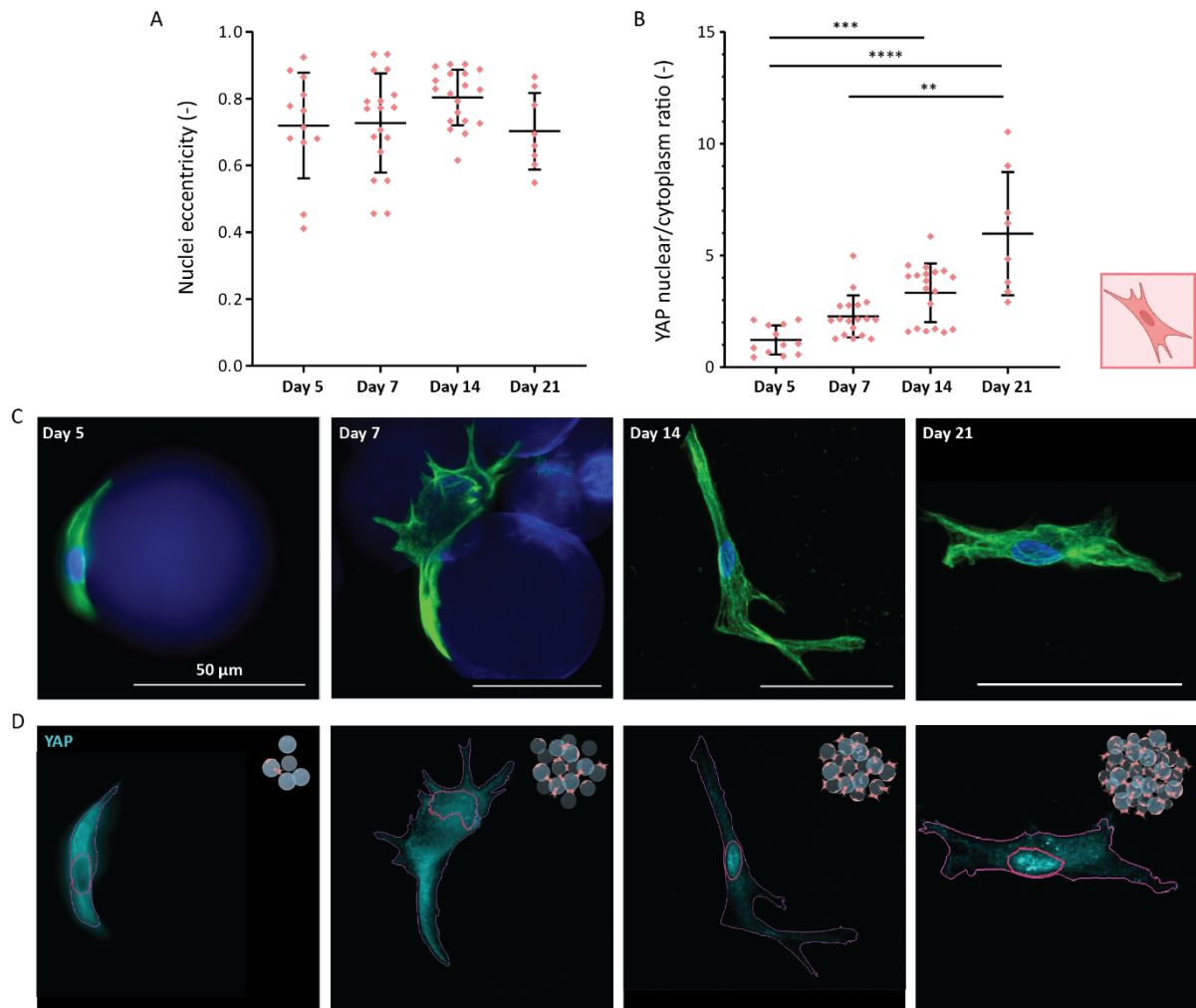
Figure 7. Upregulation of nuclear YAP translocation within PKs encapsulated within microgels, during pro-longed culture time of 21 days. **A)** Nuclei eccentricity, where 0.0 indicates a perfect circle and 1 a straight line, with a sample size of n=3, mean ± standard deviation presented. **B)** YAP nucleus/cytoplasm ratio, with significant differences between day 5 & 14, day 5 & 21 and day 7 & 21. With a sample size of n=3, mean ± standard deviation presented, ** $p < 0.01$, *** $p < 0.001$, **** $p < 0.0001$. **C)** Confocal images of the cells at the various time points, F-actin in green and nuclei in blue. Sale bar represents 50 µm. **D)** YAP expression within the cells of 7C, with the marked area in pink of the cytoplasm and the nucleus per cell.

CONCLUSION

Here, we combined droplet-based microfluidics with a supramolecular approach to fabricate single keratocyte encapsulated microgels. Compared with cells encapsulated and cultured within bulk hydrogels, the use of microgels demonstrated one important difference; the formation of a dense and connected cell network within a microporous construct consisting of cells and microgels. Via cell-cell mediated microgel assembly the cells generate their own scaffold (**Figure 8A**). The interconnected micropores inside the microgel assembly as well as the dynamic behavior of the microgels contributed to an enhanced cell migration and cell infiltration, both independent of hydrogel degradation. An initial single-cell encapsulation rate of ~ 8% resulted after several days in a dense cluster of cells and microgels with a diameter of ~ 1-2 mm (**Figure 8B**). Cellular expression of tubulin β3 suggests that the cells still exhibit a multipotent differentiation potential. While, cellular deposition of collagen type VI together with the intracellular αSMA expression indicates keratocyte-fibroblast transition of the cells. The summation of a fibrotic response, cellular ECM deposition, and diminished microgel dynamics due to cell-cell and cell-matrix mediated microgel assembly are assumed to result in an increased matrix stiffness sensed by the cells. This assumption was confirmed by the significant upregulation of nuclear YAP activation during culture.

Towards the future, the small size of the individual microgels combined with the dynamic bonding of microgel assemblies provides the microgel system with enhanced injection possibilities. To this end, the presented supramolecular microgel system has proven to be an attractive tool for biomedical applications in various minimally invasive therapies.
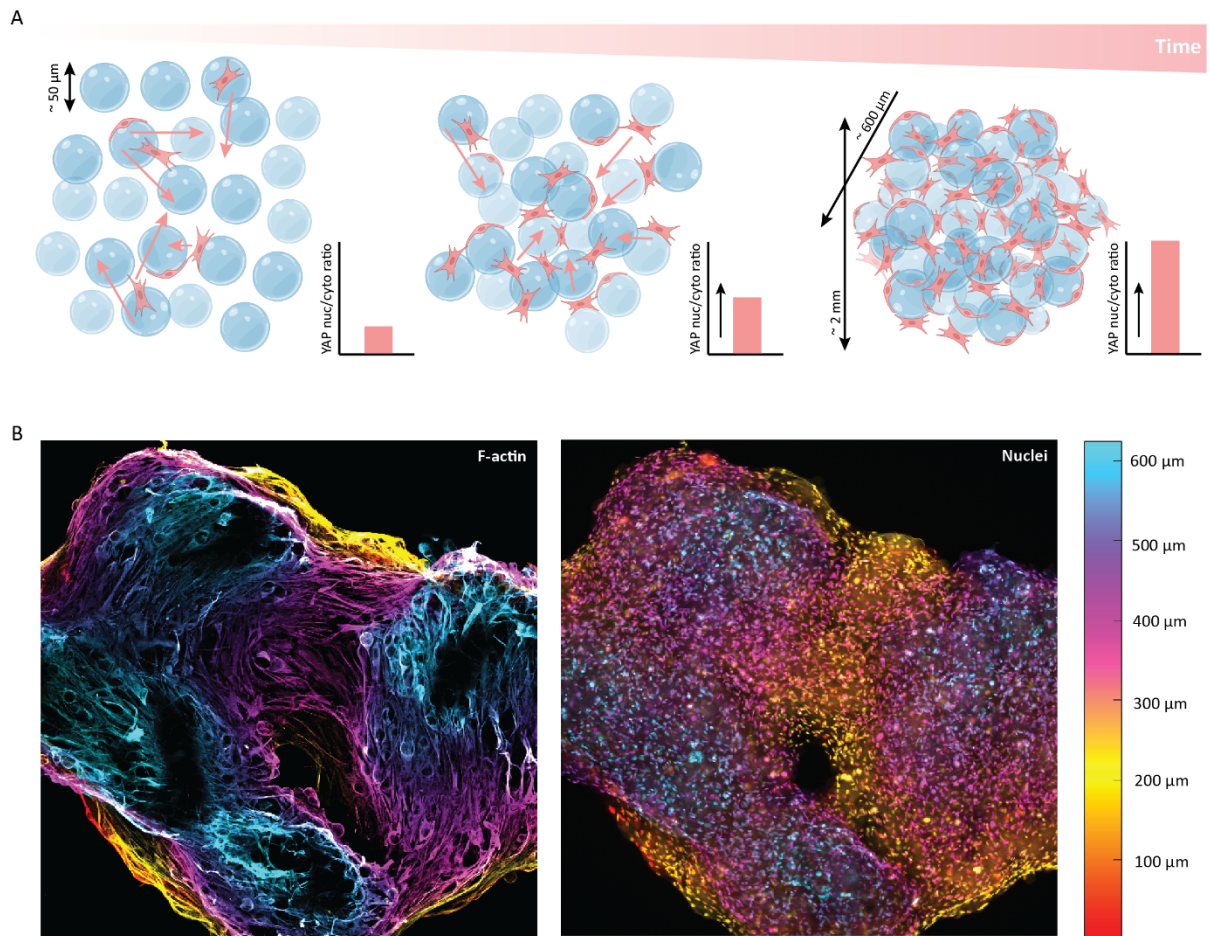
Figure 8. Conclusion figure of this study. **A)** Schematic representation of cell-cell interaction driven microgel assembly with related upregulation of nuclear YAP activation. **B)** Multicolored images show the original cell heights in the obtained z-stack files, indicating the formation of ~ 600 µm thick cell/microgel constructs.

EXPERIMENTAL SECTION

Microfluidic device production

Droplet-based microfluidics were used to generate single-cell laden supramolecular microgels, based on the published protocol of Sinha and coworkers who developed a pipette-tip based method for single cell encapsulation within droplets to enable cell isolation and perform single-cell analysis.[19] Maritza Rovers adapted this system and optimized it for the high throughput formation of single-cell laden supramolecular microgels. Microfluidic devices were produced from polydimethylsiloxane (PDMS) molds using soft lithography. Photomasks for soft photolithography were ordered from CAD/Art Services, Inc. (Bandon, Oregon). PDMS molds were produced by spin-coating wafers with SU-8 3000 photoresist (Microresist Technology's) according to manufacturer's protocol to obtain 70 µm of channel height. Microfluidic devices were fabricated by mixing PDMS base and curing agent (Sylgard) at a ratio of 10:1 w/w. After air bubble removing with vacuum, the mixture was poured onto a master silicon wafer containing the device layout and the mixture was cured at 65 °C for 3 hours. After curing, the PDMS was carefully removed from the wafer and 1 mm holes were punched for the inlets and outlet. The PDMS was bonded channels-down to glass slides to yield closed microchannels via OH-terminated by exposure to plasma (Emitech K1050X), whereafter the devices were incubated at 65 °C for 1 hour to increase binding. Finally, channels were treated with 5% silane in fluorinated HFE-7500 (Fluorchem UK, 3M Novec engineered fluid), incubated for one hour at 65 °C, flushed with HFE-7500, and incubated overnight at 65 °C for thermal bonding.

Primary keratocyte (PK) cell culture

Primary human keratocytes were isolated from leftover human corneoscleral transplant material from Descemet Membrane Endothelial Keratoplasty surgery, which were obtained from the Cornea Department of the ETB-BISLIFE Multi-Tissue Center (Beverwijk, the Netherlands). The keratocytes were cultured in expansion medium (1:1 mixture of Dulbecco's modified Eagle's medium/F-12 supplemented with GlutaMAX (DMEM/F12 (Ham) + GlutaMAXTM, 10565-018; Gibco), 5% Fetal Bovine Serum (FBS, Biochrom AG), 1% penicillin/streptomycin (P/S, Biochrom AG), and 1 mM L-ascorbic acid 2-phosphate sesquimagnesium salt hydrate (Vitamin C, Sigma A8960)) at 37 °C, 21% O_2 and 5% CO_2 until ±80% confluency. Since the medium contained FBS, keratocytes were considered to be activated matrix-producing cells, referred to as stromal fibroblasts (SFs). To initiate cell (re-)differentiation towards corneal stromal keratocytes, another medium composition was used: differentiation medium (Dulbecco's modified Eagle's medium supplemented with GlutaMAX

(GlutaMAXTM, 11880-028; Gibco), 1% penicillin/streptomycin (P/S, Biochrom AG), and 1 mM L-ascorbic acid 2-phosphate sesquimagnesium salt hydrate (Vitamin C, Sigma A8960), 1x ITS (Sigma, I3146), 2 mg/mL D-glucose (Invitrogen, 15023021), 2.5 mg/mL D-mannitol (Fluka, 63560)).[20] Cells were cultured with medium changes every 3 days, keratocytes from multiple donors were used up to passage #3. TrypLE Express Enzyme (1x), no phenol red (12604013, Gibco) is used to detach the cells from the culture flask and use them for experiments.

Preparation of hydrogelators

Bifunctional molecules (UPy-PEG$_{10K}$-UPy) were dissolved at 70 °C in an neutral PBS solution for 1.5 hours. Monofunctional molecules (UPy-Glycine or UPy-Glycine + UPy-cRGD) were dissolved at 70 °C in an alkaline PBS solution (containing 160 mM NaOH) for 20 minutes. After completely dissolving the monofunctional and bifunctional building blocks, the solutions were cooled down to room temperature. A specific volume of HCl solution (2 M) was added to the monofunctional solution to reach neutral pH. Cell culture medium is added to both solutions 1:1, to provide the cells already with some nutrients during the gelation process later on in the procedure. Afterwards, both solutions are transferred from a glass vial to a sterile Eppendorf tube, from this step onwards a safety cabinet is used to guarantee a sterile work environment. The solutions were disinfected by exposing them to UV-light for 20 minutes. The cells needed for encapsulation are suspended in the correct amount of medium and this cell suspension is added to the bifunctional solution with a cell concentration of 2000 cells/µL. This resulted in a dilution of the bifunctional molecules by the cell suspension. To correct for this extra dilution step, the initial concentration of the bifunctional molecules is slightly higher (0.78 wt/v% instead of 0.52 wt/v%). For every experiment the bifunctional molecules are diluted with 1/3 of cell suspension, resulting in a final 0.52 wt/v% bifunctional molecules.

Microgel formation

Single cell laden microgels based on supramolecular building blocks were generated using a tip-loading approach as previously described in Sinha et al.[19] All the components needed were disinfected by exposing them to UV-light for 20 minutes. Supramolecular hydrogels pre-solutions of bifunctional and monofunctional UPy-molecules with keratocytes were prepared separately as described previously. The pre-solutions were separately drawn into a 200 µL pipet tip and loaded according to **figure 9** to the inlets in the PDMS chip. Syringes and tubing filled with mineral oil were used as hydraulic system to dispense the liquids from the syringes driven by computer-controlled pumps (neMESYS microfluidic pump, Cetoni). HFE-7500 with 2.5 v/v% Pico-Surf (Sphere Fluidics)

was flushed into the oil inlet to form microgels. Microgel production was started with oil flow at a speed of 10 μL/min to prefill the channels of the microfluidic devices. The flow of the hydrogel pre-solution was started simultaneously at 5 μL/min. The flow of the oil was increased to 30 μL/min once the hydrogel pre-solutions started to mix at the droplet formation point. The microgels were collected in an Eppendorf tube from the outlet and medium was poured on top of the emulsion to prevent evaporation of the HFE oil. Single cell laden microgels were incubated for 2 hours in the dark at 37 °C to allow gelation of the microgel. Thereafter, the microgels were isolated by de-emulsification with 20 v/v% PFO (Sigma, 1H,1H,2H,2H-perfluorooctyl-triethoxysilane) in HFE-7500 oil (**Figure 10**). Microgels were collected and resuspended in fresh medium. The used cell concentration was 2 million cells per mL in BF solution. Mixtures of microgels with and without encapsulated cells were homogenously divided over the wells of a non-adhesive 96-well plate (Fisher Scientific, Nunclon Sphera-Treated, U-Shaped-Bottom plate 15227905) and additional cell culture medium to top of the well was added. The plates were placed in the incubator at 37 °C, 21% O_2 and 5% CO_2. After 3 days the cell culture medium, to embed the hydrogels, was refreshed and for the PKs treated towards CSKs the expansion medium was replaced by the differentiation medium. During culture, medium was partly refreshed every 2-3 days.
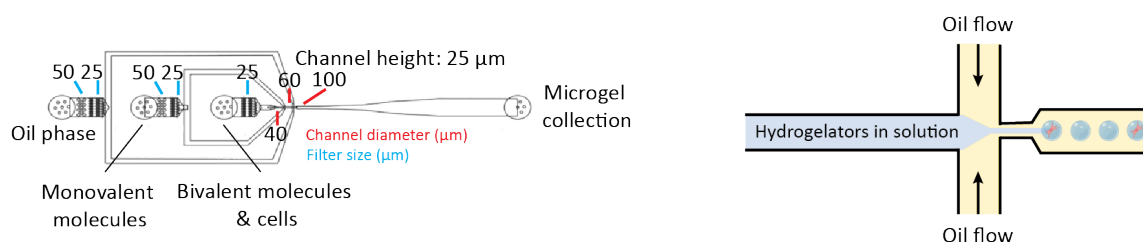

Figure 9. Schematic representation of the lay-out of the droplet based micro fluidic chip.
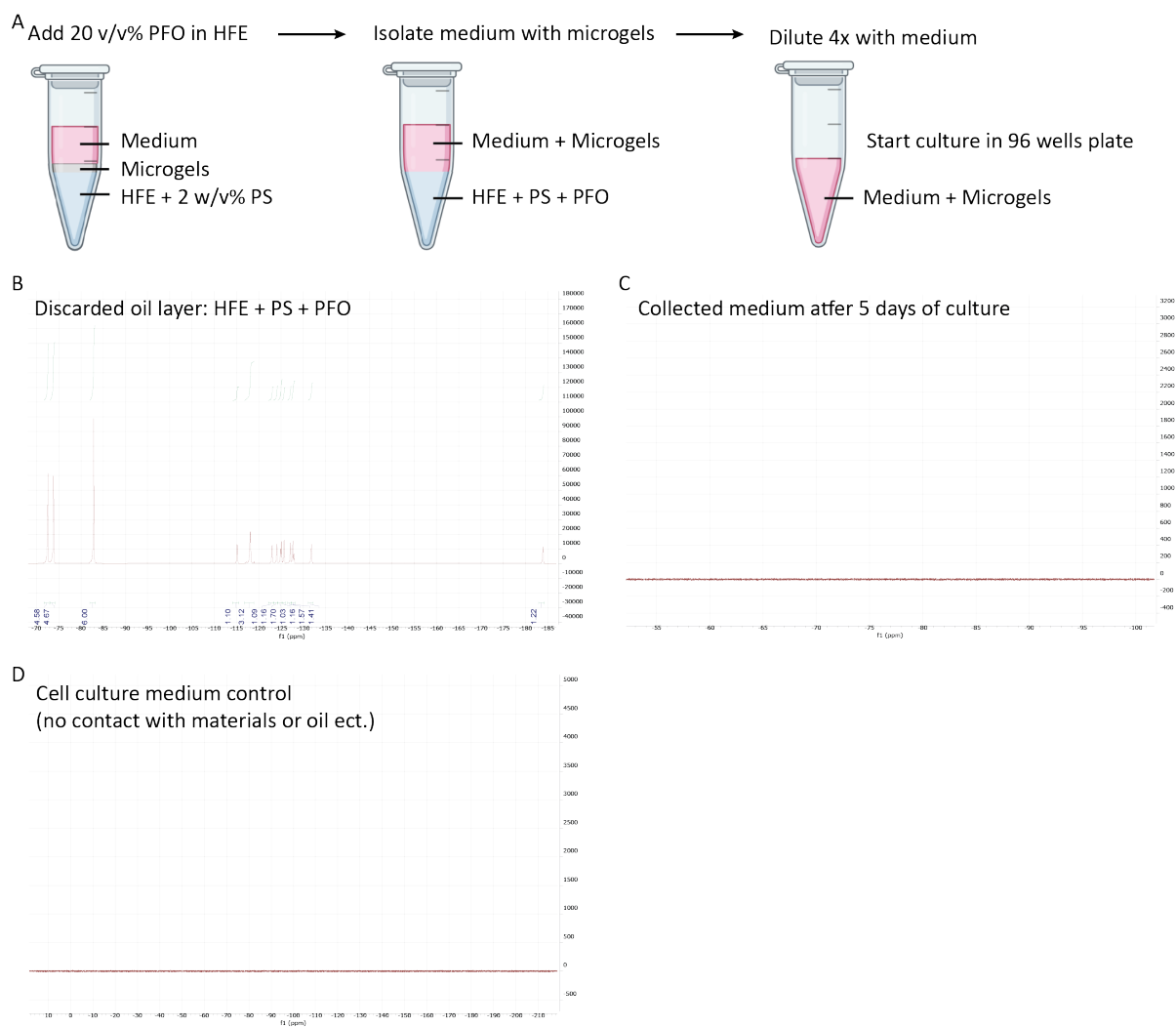
Figure 10. NMR results to check if the used PFO remains in the culture after removal of the oil from the microgels. **A)** Schematic representation of the protocol and steps needed to remove the oil. **B)** Discarded oil layer (positive control). **C)** Medium surrounding the microgels which was collected on day 5 of the cell culture; no oil or PFO present. **D)** Cell culture medium which was not in contact with the microgels or PFO (negative control).

Cell staining and Imaging

Before immunohistochemical stainings were carried out, the microgels were washed 3x with PBS (5 min per wash). All cells encapsulated within the microgels were fixated for 20 minutes at room temperature using 3.7% paraformaldehyde (formalin 37%, 104033.1000, Merck). After washing with PBS, samples were permeabilized for 15 minutes with 0.5% Triton X-100 in PBS. Followed by adding a blocking solution of 10% donkey or goat serum in 0.05% Triton X-100 in PBS for 30 minutes. Next, the cells were incubated with the primary antibodies diluted in 2% donkey serum in 0.05% Triton X-100 in PBS overnight at 4 °C. Thereafter, the cells were washed thoroughly with 0.05% Triton X-100 in PBS, including wash waiting steps of 5-10 min. Next, the cells were incubated with

the secondary antibodies and phalloidin at room temperature for 2 hours. Finally, the cells were stained with DAPI at a dilution of 1:250 for 10 min and washed thoroughly with PBS (including was waiting steps of 5-10 min). During imaging, microgels were place on a thin coverslip (24x69 mm, VWR 631-1575) immerged in mowiol 4-88 (Sigma Aldrich, 81381) and imaged using Leica TCS SP8 X inverted confocal microscope (Leica Microsystems) using HC PL APO CS2 objectives (20x/0.75, 40x/0.95).). Images were processed in ImageJ to create a max-projection image of the original z-stack. See **table 1** for the dyes, primary-, and secondary antibodies used within this study.

Cell Image Analysis

All image analysis were analyzed from maximum-intensity z-projections of confocal image stacks. To determine the localization of YAP, z-projections of images were obtained from channels corresponding to the DAPI (nuclei), phalloidin (F-actin) and anti-YAP antibody staining (YAP). Afterwards CellProfiler™ (cell image analysis software) was used to design a pipeline which determined the nuclear areas and cytoplasmic areas. The mean intensity was determined in those respective areas and the ratio between the concentration present in nuclear and cytoplasmic regions of cell was then used as a measure of YAP nuclear translocation. The same pipeline was also used to determine the nuclear eccentricity.

3D Height indication cell images

A custom MatLab script was written to pair a specific height of the cell within the obtained z-stack image to a specific color (**Figure 8B**). Image stacks obtained from channels corresponding to the DAPI (nuclei) and phalloidin (F-actin) were used to create these 3D height indication cell images. LAS X Life Science Microscope Software was used to calculate the original µm distance in the z-direction from the original lif file. *The custom MatLab script was written by Mark C. van Turnhout.*

Statistical analysis

To test the significant differences of the results shown in figure 7, a Kruskal-Wallis test was performed with an additional Dunn's multiple comparisons test. The following significant differences were observed for the YAP ratios: day 5 vs. day 14 *** p 0.0004, day 5 vs. day 21 **** $p < 0.0001$, day 7 vs. day 21 ** p 0.0062.

Table 1. Overview of the used dyes, primary-, and secondary antibodies.

Antibody / dye	Company / reference #	Dilution
4',6-diamidino-2-phenylindole dihydrochloride (DAPI)	Sigma-Aldrich, D9542	1:250
Phalloidin 488	Sigma-Aldrich	1:300
Phalloidin 555	Sigma-Aldrich	1:300
Anti-Collagen type VI	70R-CR009x, Fitzgerald	1:250
Anti-Vimentin	Ab20346, Abcam	1:300
Anti-Ki-67	Rb1510-P0, Thermo Scientific	1:200
Anti-tubulin β3	801202, BioLegend	1:100
Anti-YAP1	Ab52771, Abcam	1:100
Anti-α smooth muscle actin		1:100
Secondary antibodies		
Anti-goat IgG (donkey) 488	A11055, Molecular Probes	1:250
Anti-rabbit IgG (donkey) 555	A31572, Molecular Probes	1:250
Anti-rabbit IgG (donkey) 488	A21206, Molecular Probes	1:250
Anti-rabbit IgG (donkey) 647	711-605-152 Jackson	1:250
Anti-rabbit IgG (goat) 647	A21244, Molecular Probes	1:250
Anti-rabbit IgG (goat) 555	A211428, Molecular Probes	1:250
Anti-mouse IgG2a (goat) 555	A21137, Molecular Probes	1:250
Anti-mouse IgM (goat) 488	A21042, Molecular Probes	1:250
Anti-mouse IgM (goat) 555	A21426, Molecular Probes	1:250

All stainings were performed with a combination of solely donkey or goat secondary antibodies. Donkey serum was used for a combination of solely donkey based secondary antibodies, goat serum was used for a combination of solely goat based secondary antibodies.

REFERENCES

1. Kong, B. *et al.* Fiber reinforced GelMA hydrogel to induce the regeneration of corneal stroma. *Nat Commun* 11, 1435 (2020).

2. Mobaraki, M. *et al.* Corneal Repair and Regeneration: Current Concepts and Future Directions. *Front Bioeng Biotechnol* 7, (2019).

3. Formisano, N. *et al.* Mechanical Properties of Bioengineered Corneal Stroma. *Adv Healthc Mater* 10, 2100972 (2021).

4. Diba, M. *et al.* Engineering the Dynamics of Cell Adhesion Cues in Supramolecular Hydrogels for Facile Control over Cell Encapsulation and Behavior. *Advanced Materials* 33, 2008111 (2021).

5. Lima, C. S. A. de *et al.* An Updated Review of Macro, Micro, and Nanostructured Hydrogels for Biomedical and Pharmaceutical Applications. *Pharmaceutics* 12, 970 (2020).

6. Daly, A. C., Riley, L., Segura, T. & Burdick, J. A. Hydrogel microparticles for biomedical applications. *Nat Rev Mater* 5, 20–43 (2019).

7. Feng, Q., Li, D., Li, Q., Cao, X. & Dong, H. Microgel assembly: Fabrication, characteristics and application in tissue engineering and regenerative medicine. *Bioact Mater* 9, 105–119 (2022).

8. Choe, G., Park, J., Park, H. & Lee, J. Hydrogel Biomaterials for Stem Cell Microencapsulation. *Polymers (Basel)* 10, 997 (2018).

9. Sideris, E. *et al.* Particle Hydrogels Based on Hyaluronic Acid Building Blocks. *ACS Biomater Sci Eng* 2, 2034–2041 (2016).

10. Cunha, A. F. *et al.* Cell Response in Free-Packed Granular Systems. *ACS Appl Mater Interfaces* 14, 40469–40480 (2022).

11. Chen, M. H. *et al.* Injectable Supramolecular Hydrogel/Microgel Composites for Therapeutic Delivery. *Macromol Biosci* 19, 1800248 (2019).

12. Khademhosseini, A. & Langer, R. Microengineered hydrogels for tissue engineering. *Biomaterials* 28, 5087–5092 (2007).

13. Sivashanmugam, A., Arun Kumar, R., Vishnu Priya, M., Nair, S. V. & Jayakumar, R. An overview of injectable polymeric hydrogels for tissue engineering. *Eur Polym J* 72, 543–565 (2015).

14. Bidarra, S. J., Barrias, C. C. & Granja, P. L. Injectable alginate hydrogels for cell delivery in tissue engineering. *Acta Biomater* 10, 1646–1662 (2014).

15. Zhang, S. *et al.* Microsphere-containing Hydrogel Scaffolds for Tissue Engineering. *Chem Asian J* 17, (2022).

16. Allazetta, S., Negro, A. & Lutolf, M. P. Microfluidic Programming of Compositional Hydrogel Landscapes. *Macromol Rapid Commun* 38, 1700255 (2017).

17. Özkale, B. *et al.* Actuated 3D microgels for single cell mechanobiology. *Lab Chip* 22, 1962–1970 (2022).

18. Wilson, K. L., Pérez, S. C. L., Naffaa, M. M., Kelly, S. H. & Segura, T. Stoichiometric Post-Modification of Hydrogel Microparticles Dictates Neural Stem Cell Fate in Microporous Annealed Particle Scaffolds. *Advanced Materials* 34, 2201921 (2022).

19. Sinha, N., Subedi, N., Wimmers, F., Soennichsen, M. & Tel, J. A Pipette-Tip Based Method for Seeding Cells to Droplet Microfluidic Platforms. *Journal of Visualized Experiments* 2019, (2019).

20. Foster, J. W., Gouveia, R. M. & Connon, C. J. Low-glucose enhances keratocyte-characteristic phenotype from corneal stromal cells in serum-free conditions. *Sci Rep* 5, 10839 (2015).

21. West-Mays, J. A. & Dwivedi, D. J. The keratocyte: Corneal stromal cell with variable repair phenotypes. *Int J Biochem Cell Biol* 38, 1625–1631 (2006).

22. Zhu, Q. *et al.* Directed Differentiation of Human Embryonic Stem Cells to Neural Crest Stem Cells, Functional Peripheral Neurons, and Corneal Keratocytes. *Biotechnol J* 12, 1700067 (2017).

23. Lwigale, P. Y., Cressy, P. A. & Bronner-Fraser, M. Corneal keratocytes retain neural crest progenitor cell properties. *Dev Biol* 288, 284–293 (2005).

24. Kumar, A., Xu, Y., Yang, E. & Du, Y. Stemness and Regenerative Potential of Corneal Stromal Stem Cells and Their Secretome After Long-Term Storage: Implications for Ocular Regeneration. *Investigative Opthalmology & Visual Science* 59, 3728 (2018).

25. Du, Y., Funderburgh, M. L., Mann, M. M., SundarRaj, N. & Funderburgh, J. L. Multipotent Stem Cells in Human Corneal Stroma. *Stem Cells* 23, 1266–1275 (2005).

26. Berryhill, B. L. *et al.* Partial Restoration of the Keratocyte Phenotype to Bovine Keratocytes Made Fibroblastic by Serum. *Investigate Ophthalmology & Visual Science (IOVS)* 43, 3416–3421 (2002).

27. Jester, J. V. & Ho-Chang, J. Modulation of cultured corneal keratocyte phenotype by growth factors/cytokines control in vitro contractility and extracellular matrix contraction. *Exp Eye Res* 77, 581–592 (2003).

28. Jester, J. V, Barry-Lane, P. A., Cavanagh, H. D. & Petroll, W. M. Induction of alpha-smooth muscle actin expression and myofibroblast transformation in cultured corneal keratocytes. *Cornea* 15, 505–16 (1996).

29. Dupont, S. *et al.* Role of YAP/TAZ in mechanotransduction. *Nature* 474, 179–183 (2011).

30. Kwon, H., Kim, J. & Jho, E. Role of the Hippo pathway and mechanisms for controlling cellular localization of YAP/TAZ. *FEBS J* 289, 5798–5818 (2022).

31. Ma, S., Meng, Z., Chen, R. & Guan, K.-L. The Hippo Pathway: Biology and Pathophysiology. *Annu Rev Biochem* 88, 577–604 (2019).

32. Kim, S., Uroz, M., Bays, J. L. & Chen, C. S. Harnessing Mechanobiology for Tissue Engineering. *Dev Cell* 56, 180–191 (2021).

33. Nardone, G. *et al.* YAP regulates cell mechanics by controlling focal adhesion assembly. *Nat Commun* 8, 15321 (2017).

34. Scholzen, T. & Gerdes, J. The Ki-67 protein: From the known and the unknown. *J Cell Physiol* 182, 311–322 (2000).

35. Sun, X. & Kaufman, P. D. Ki-67: more than a proliferation marker. *Chromosoma* 127, 175–186 (2018).

36. Miller, I. *et al.* Ki67 is a Graded Rather than a Binary Marker of Proliferation versus Quiescence. *Cell Rep* 24, 1105-1112 (2018).

CHAPTER 7

Epilogue

Currently, corneal transplants from deceased human donors are the only curative form of treatment available for patients suffering from corneal disease or injury with the risk of blindness. Unfortunately, due to a global donor shortage only one corneal transplant for seventy patients in need is available, creating an urgent need for alternative solutions.[1] For patients with severe stromal injury for whom transplants are unavailable, pharmaceutical interventions allow to slow down the disease progression, yet do not restore vision.[2] An artificial cornea is often used as a replacement of the diseased or injured cornea and sutured into place, with the intention to preserve a minimal functionality of the cornea in patients without any perspective of other available treatments.[3–6] Such artificial corneas are neither restoring the damaged cornea nor supporting self-regeneration of the native tissue. Often, the implantation of an artificial cornea is even accompanied by unwanted harmful processes *i.e.* immune reactions and rejection, haze caused by scar tissue at the implant border, and alterations in oxygen permeability, which eventually can result in complete loss of the implant.[4,7–9] In recent decades, significant scientific progress is made by ophthalmologists and bioengineers, aiming to engineer biocompatible, implantable, and functional constructs that desirably induce self-regeneration of the compromised tissue. Despite their large investments and the presentation of diverse natural and synthetic materials as alternative implants, successful bioengineered constructs have not yet been integrated into clinical practice. [9–11] Especially the incorporation of biocompatibility is a burden in the development of fully synthetic artificial constructs, which is often solved by addition of a natural protein *i.e.* fibrinogen, laminin and collagen.[12–29] Here, a supramolecular approach is presented to design a fully synthetic hydrogel-based stromal construct.

A SUPRAMOLECULAR APPROACH TO DESIGN AN ARTIFICIAL STROMAL CONSTRUCT

The main focus of the research presented in this thesis is to design a hydrogel based corneal stromal construct. To achieve, we used a supramolecular approach to vary the bioactivity and mechanical properties of the designed supramolecular hydrogels. The characteristics of the native stromal microenvironment determined the design criteria for the various hydrogel designs studied. To this end we tried to mimic some of the characteristics of the stromal microenvironments as closely as possible, focusing on hydrogel designs that possess the
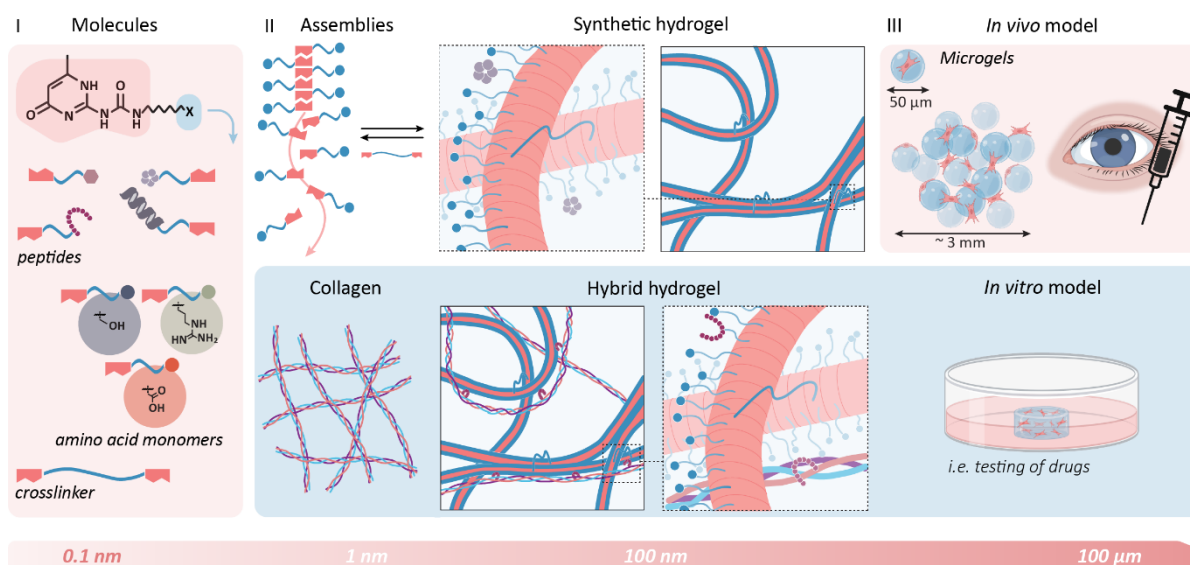
Figure 1. Length scales employed within this thesis. From left to right: I. Molecules as the supramolecular building blocks *i.e.* bioactive peptides, amino acid monomers, and the bivalent crosslinker. II. Assembly of the molecules into fibers and gel-like networks. III. Final application. The top row represents the length scales employed from the formation of synthetic microgels towards the *in vivo* application. Bottom row represents the length scales employed from the formation of hybrid hydrogels towards the *in vitro* application. Created with BioRender.com.

needed biochemical cues and mechanical properties to support stromal keratocytes. In addition, we focused on the clinical applicability of the hydrogel design, to eventually turn the supramolecular artificial stromal construct into an attractive tool for biomedical applications.

Within this thesis, a supramolecular approach was used to design various hydrogels and hydrogel systems. The non-covalent bonds within supramolecular assemblies are relatively low-energy bonds that allow an easy breakage or reformation of the bonds, and contribute to the great adaptability of supramolecular based hydrogels. This adaptability has a substantial impact on the success of cell encapsulation and cell culture within the hydrogels. Due to this characteristic, the supramolecular hydrogels allow for cellular matrix remodeling, and the ability to support important cellular activities, *i.e.* cell proliferation, cell migration, cell spreading, cell-cell interactions, and cell-gel interactions. In addition to adaptability, using a supramolecular approach allows for a great tunability of the materials. This tunability allowed for the incorporation of short peptide sequences conjugated to a supramolecular UPy-moiety. Within this thesis various molecular building blocks are introduced to provide the hydrogels with the needed biochemical cues and associated bioactivity. Both the incorporation of the UPy-cRGD and the UPy-GFOGER peptide additives demonstrated to introduce the desired bioactivity and to support essential cellular activities of the encapsulated primary keratocytes,

i.e. attaining a healthy cell morphology, cell migration, and cell differentiation. Both the UPy-cRGD and the UPy-GFOGER act as cell anchor points to allow for cell adherence within the generated hydrogels. In addition to these peptide additives, a collagen type I binding peptide additive was incorporated within the transient network to introduce an interaction between the synthetic and natural components within a hydrogel. The differences in bioactivity of these incorporated peptide additives, demonstrates the tunability of the supramolecular hydrogels. Besides the incorporation of diverse peptide additives, we demonstrated within this work the possibility to vary the molecular building blocks of the hydrogelators by introducing a library of supramolecular monomers. In solution, these supramolecular monomers formed supramolecular polyaminoacids. Due to the tunability of the used supramolecular approach hydrogels based on mixtures of diverse supramolecular polyaminoacid fibers were generated. With these hydrogels different amino acids are provided to the encapsulated cells, mimicking synthetically the natural protein presentation within the ECM. Taken together, we demonstrated that small adjustments in the molecular building blocks of the supramolecular hydrogels resulted in novel hydrogel designs. These designs are provided with an enhanced complexity and the associated ability to mimic more closely the complexity of the native cellular microenvironments (**Figure 1**). Besides synthetic building blocks to provide the hydrogel with bioactivity, the supramolecular approach allows for the formation of a hybrid hydrogel based on UPy-fibers and natural collagen type I fibers. With the hybrid hydrogel we demonstrated the ability of cells to rearrange their surrounding gel matrix. Herewith, we achieved to mimic the complex *in vivo* cell-matrix interplay within the hybrid hydrogel construct. This finding can contribute to the design of an *in vitro* model to, *i.e.* test new drugs. To turn the supramolecular hydrogel into an attractive tool for biomedical applications, we explored the possibilities to inject the hydrogel. Droplet-based microfluidics combined with the supramolecular approach resulted in the fabrication of single keratocyte encapsulated microgels. The small size of the individual microgels combined with the dynamic bonding of microgel assemblies provided the microgel system with enhanced injectability possibilities. To this end, the presented supramolecular microgel system has demonstrated to be an attractive tool for biomedical applications in various minimally invasive therapies.

WHAT IS NEXT ?

Towards a clinical applicable stromal construct

The corneal stromal tissue is very complex, and traditionally researchers tried to develop an artificial stromal construct, which incorporates all the essential design criteria, *i.e.* being biocompatible, being transparent, comprising the correct refractive index, possessing the correct biomechanics to function, and being elastic enough to be sutured in place or suitable to be injected. Within this thesis we focused on the bioactivity, mechanical properties, and clinical applicability of the hydrogel design, leaving the other design criteria uncovered. Our proposed strategy to cure corneal defects would be to design a synthetic stromal construct that upon a precise and minimally invasive injection allows for the recruitment of healthy native keratocytes. Ideally, due to the recruitment of healthy native keratocytes, the construct would stimulate and support *in vivo* self-regeneration of the comprised stromal tissue, resulting in the replacement of the damaged tissue by restored stromal tissue (**Figure 2**).

However to realize this proposed strategy, some essential design criteria still need to be explored. Despite the transparent appearance of the hydrogels, it is assumed to be a challenge to implement the correct breaking index and full transparency within the hydrogel construct. Besides the transparency, restoring the organized structure is another major challenge that remains. Perhaps the incorporation of novel biochemical cues is needed to stimulate the keratocytes to slowly regenerate the stromal tissue and restore the organized collagen structure. To translate the proposed strategy to the clinic, an important aspect to be considered is to provide the construct with or without cells. From a practical point of view, the presence of cells limits the storage possibilities and associated the off the shelf availability. In contrast, the absence of cells within the construct can result in a slower regeneration process. However, we assume that the development of stromal constructs without cells has multiple benefits to translate the proposed strategy to the clinic. For instance, easier and cheaper storage logistics of the materials, off the shelf availability, enhanced clinical applicability, more straightforward scalability, and lower risk of irreversible transition of the cells towards activate myofibroblasts. The developed supramolecular microgels are assumed to be an attractive tool to design an acellular stromal construct. Due to the ability to form a microporous scaffold with interconnected micropores, enhanced cell migration and cell infiltration, both independent of hydrogel degradation, is realized.
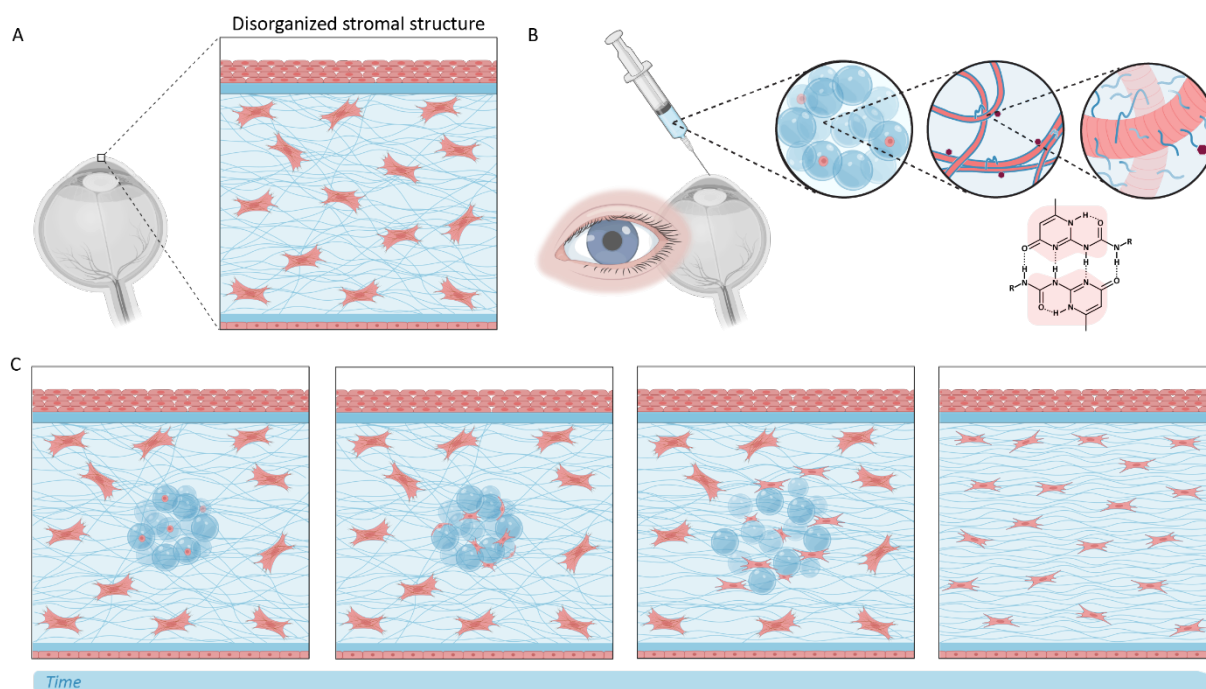
Figure 2. Schematic illustration of the proposed strategy to cure a stromal defects. **A)** Disorganized stromal structure with myofibroblasts. **B)** Injection of supramolecular single keratocyte encapsulated microgels functionalized with UPy-cRGD. **C)** Imagined mode of action of the induced healing process after injection: encapsulated keratocytes start to migrate and proliferate whereafter the keratocytes start to use the microgels as a scaffold providing the needed biochemical cues to trigger a self-regeneration response of the native tissue, resulting in a controlled regeneration process. Created with BioRender.com.

Screening of supramolecular hydrogels

Due to the modularity of the introduced supramolecular approach there are still numerous hydrogel compositions to be discovered. These compositions range from variations in molecular concentrations effecting the mechanical and dynamic properties of the hydrogels, to variations in molecular building blocks effecting the molecules presented to the cells. For instance, the introduced library of supramolecular polyaminoacids, resulted in the formulation and analyses of seventeen hydrogels. The associated introduction of the fabricated mixtures based on different supramolecular polyaminoacids in solution, allow the realization of transient networks presenting various amino acids to the cells. Within this work, this mixing approach is used to generate three combinations of different supramolecular polyaminoacids. These three studied combinations are based on theoretical knowledge of the successes of frequently used peptide additives.[30–34] However, supramolecular polyaminoacid combinations based on

educated guesses, proved to not guarantee an expected successful outcome. In order to discover the most successful combination of supramolecular polyaminoacids within a hydrogel, numerous combinations need to be formulated and analyzed. This exposes the major challenge of fabricating supramolecular polyaminoacids based hydrogels: the need of screening and automatization. In addition, the fabrication of supramolecular microgels allows for the formation of even more hydrogel designs. For instance by generating an heterogeneous collection of microgels with varying ratios, all comprising their specific amino acid building block, or functionalized with a different set of bioactive peptide additives.

As a first step, an automatization method needs to be implemented to decide, which combinations provide the most useful information and should be tested. Afterwards the process of hydrogel formulation needs to be automized, which will be a major challenge. Yet, atomization of hydrogel formation is not impossible, upon using very low molecular concentrations dissolved in strong alkaline based buffers. The biggest challenge will be to design a high throughput method for cell imaging of cells cultured in 3D within diverse hydrogels. A possible solution for this screening limitation is to use another analytical technique during the first screening round of the hydrogel library. An enzyme-linked immunosorbent assay (ELISA) can be useful to detect proteins secreted by the cells in an automized fashion, using this technique there is no need to lysate the cells or collect the cells from the gels. This approach even allows to first run the ELISA, store the samples and perform an immunohistochemical analysis of the interesting hits. Other techniques such as quantitative polymerase chain reaction (q-PCR) to quantify the gene expression in a cell or western blot to detect proteins present within the cells, could also be useful and designed in a less time consuming manner compared with immunohistochemical analysis. However, increase of knowledge is needed to determine if the presence of hydrogel parts influences the measurements, otherwise the cell lysates need to be separated from the gel, which could be challenging. Same limitation holds for fluorescent-activated cell sorting (FACS), which is a technique to detect and measure the expression of cell surface and intracellular proteins. To use this technique the cells need to be collected from the hydrogel, which is even more challenging because the cells preferably need to stay alive.

CONCLUDING REMARKS

This thesis describes the search for a hydrogel design, in which we strived to design a synthetic mimic of the native stromal microenvironment. Due to its modularity, supramolecular based hydrogels are a wonderful concept to design hydrogels with the ability to provide a specific mix of biochemical cues needed for a specific cell type or tissue. The designed fully synthetic hydrogel, based on supramolecular UPy-based microgels functionalized with UPy-cRGD to induce bioactivity, demonstrated to hold a great potential as an artificial corneal stromal construct. Due to its injectable properties, we proposed a strategy to inject supramolecular microgels to trigger and support self-regeneration of the damaged native tissue and eventually replace a part of the damaged stroma. The modularity of the introduced supramolecular approach allows for the development and the discovery of numerous hydrogel designs. Furthermore, it is assumed that screening and automation will contribute to the discovery of an even more favorable hydrogel-based stromal construct. Hopefully the findings of this thesis will, somewhere in the nearby future, contribute to the design of a successful therapy to restore the vision of patients suffering from stromal diseases or injuries.

REFERENCES

1. Gain, P. *et al.* Global Survey of Corneal Transplantation and Eye Banking. *JAMA Ophthalmol* 134, 167 (2016).

2. Whitcher, J. P., Srinivasan, M. & Upadhyay, M. P. Corneal blindness: a global perspective. *Bull World Health Organ* 79, 214–21 (2001).

3. Lee, R. *et al.* Long-term Visual Outcomes and Complications of Boston Keratoprosthesis Type II Implantation. *Ophthalmology* 124, 27–35 (2017).

4. Kanu, L. N. *et al.* Predictive factors of Boston Type I Keratoprosthesis outcomes: A long-term analysis. *Ocul Surf* 18, 613–619 (2020).

5. Cortina, M. & Cruz, J. *Keratoprostheses and Artificial Corneas*. (Springer Berlin Heidelberg, 2015).

6. Jirásková, N., Rozsival, P., Burova, M. & Kalfertova, M. AlphaCor artificial cornea: clinical outcome. *Eye* 25, 1138–1146 (2011).

7. Feiz, V. *et al.* Surface keratopathy after penetrating keratoplasty. *Trans Am Ophthalmol Soc* 99, 159–68; discussion 168-70 (2001).

8. Vannas, A., Holden, B. A. & Sweeney, D. F. Epithelial metabolism of the corneal graft is abnormal. *British Journal of Ophthalmology* 71, 593–597 (1987).

9. Matthyssen, S., Van den Bogerd, B., Dhubhghaill, S. N., Koppen, C. & Zakaria, N. Corneal regeneration: A review of stromal replacements. *Acta Biomater* 69, 31–41 (2018).

10. Formisano, N. *et al.* Mechanical Properties of Bioengineered Corneal Stroma. *Adv Healthc Mater* 10, 2100972 (2021).

11. Madl, A. C. & Myung, D. Supramolecular Host–Guest Hydrogels for Corneal Regeneration. *Gels* 7, 163 (2021).

12. Majumdar, S. *et al.* Cyclodextrin Modulated Type I Collagen Self-Assembly to Engineer Biomimetic Cornea Implants. *Adv Funct Mater* 28, 1804076 (2018).

13. Kong, B. *et al.* Fiber reinforced GelMA hydrogel to induce the regeneration of corneal stroma. *Nat Commun* 11, 1435 (2020).

14. Lee, H. J., Fernandes-Cunha, G. M., Na, K., Hull, S. M. & Myung, D. Bio-Orthogonally Crosslinked, In Situ Forming Corneal Stromal Tissue Substitute. *Adv Healthc Mater* 7, 1800560 (2018).

15. Chen, F., Le, P., Fernandes-Cunha, G. M., Heilshorn, S. C. & Myung, D. Bio-orthogonally crosslinked hyaluronate-collagen hydrogel for suture-free corneal defect repair. *Biomaterials* 255, 120176 (2020).

16. Chen, F., Le, P., Lai, K., Fernandes-Cunha, G. M. & Myung, D. Simultaneous Interpenetrating Polymer Network of Collagen and Hyaluronic Acid as an *In Situ* -Forming Corneal Defect Filler. *Chemistry of Materials* 32, 5208–5216 (2020).

17. Rafat, M. *et al.* PEG-stabilized carbodiimide crosslinked collagen–chitosan hydrogels for corneal tissue engineering. *Biomaterials* 29, 3960–3972 (2008).

18. Kong, B. *et al.* Tissue-engineered cornea constructed with compressed collagen and laser-perforated electrospun mat. *Sci Rep* 7, 970 (2017).

19.　Kim, J. I., Kim, J. Y. & Park, C. H. Fabrication of transparent hemispherical 3D nanofibrous scaffolds with radially aligned patterns via a novel electrospinning method. *Sci Rep* 8, 3424 (2018).

20.　Zhong, S. P. *et al.* Development of a novel collagen–GAG nanofibrous scaffold via electrospinning. *Materials Science and Engineering: C* 27, 262–266 (2007).

21.　Torbet, J. *et al.* Orthogonal scaffold of magnetically aligned collagen lamellae for corneal stroma reconstruction. *Biomaterials* 28, 4268–4276 (2007).

22.　Fernandes-Cunha, G. M. *et al.* In situ-forming collagen hydrogel crosslinked via multi-functional PEG as a matrix therapy for corneal defects. *Sci Rep* 10, 1–13 (2020).

23.　Fagerholm, P. *et al.* A Biosynthetic Alternative to Human Donor Tissue for Inducing Corneal Regeneration: 24-Month Follow-Up of a Phase 1 Clinical Study. *Sci Transl Med* 2, (2010).

24.　Fagerholm, P. *et al.* Stable corneal regeneration four years after implantation of a cell-free recombinant human collagen scaffold. *Biomaterials* 35, 2420–2427 (2014).

25.　Lagali, N. *et al.* Innervation of Tissue-Engineered Recombinant Human Collagen-Based Corneal Substitutes: A Comparative In Vivo Confocal Microscopy Study. *Investigative Opthalmology & Visual Science* 49, 3895 (2008).

26.　Merrett, K. *et al.* Tissue-Engineered Recombinant Human Collagen-Based Corneal Substitutes for Implantation: Performance of Type I versus Type III Collagen. *Investigative Opthalmology & Visual Science* 49, 3887 (2008).

27.　Fagerholm, P., Lagali, N. S., Carlsson, D. J., Merrett, K. & Griffith, M. Corneal Regeneration Following Implantation of a Biomimetic Tissue-Engineered Substitute. *Clin Transl Sci* 2, 162–164 (2009).

28.　Jangamreddy, J. R. *et al.* Short peptide analogs as alternatives to collagen in pro-regenerative corneal implants. *Acta Biomater* 69, 120–130 (2018).

29.　McTiernan, C. D. *et al.* LiQD Cornea: Pro-regeneration collagen mimetics as patches and alternatives to corneal transplantation. *Sci Adv* 6, (2020).

30.　Webber, M. J. *et al.* Development of bioactive peptide amphiphiles for therapeutic cell delivery. *Acta Biomater* 6, 3–11 (2010).

31.　Diba, M. *et al.* Engineering the Dynamics of Cell Adhesion Cues in Supramolecular Hydrogels for Facile Control over Cell Encapsulation and Behavior. *Advanced Materials* 33, 2008111 (2021).

32.　Tashiro, K. *et al.* A synthetic peptide containing the IKVAV sequence from the A chain of laminin mediates cell attachment, migration, and neurite outgrowth. *J Biol Chem* 264, 16174–82 (1989).

33.　Silva, G. A. *et al.* Selective Differentiation of Neural Progenitor Cells by High-Epitope Density Nanofibers. *Science (1979)* 303, 1352–1355 (2004).

34.　Álvarez, Z. *et al.* Artificial extracellular matrix scaffolds of mobile molecules enhance maturation of human stem cell-derived neurons. *Cell Stem Cell* 30, 219-238.e14 (2023).

One never notices what has been done;

one can only see what remains to be done

Marie Curie

Het ontwerpen van hoornvlies stroma micro-omgevingen gebaseerd op supramoleculaire hydrogelen

Aan de buitenkant van het oog bevindt zich, bedekt door de traanfilm, het hoornvlies. Het hoornvlies vervult twee belangrijke functies voor het oog; bescherming van de binnenste delen van het oog en breking van het licht wat op het oog valt naar het netvlies. De meest omvangrijke laag in het hoornvlies is het stroma. Hierdoor beïnvloeden de intrinsieke kenmerken van het stroma in grote mate de essentiële eigenschappen van het hoornvlies, zoals de transparantie van dit weefsel. Wanneer het stroma beschadigd raakt door ziekte of letsel, neemt het vermogen van het hoornvlies om het ingevallen licht zo exact mogelijk te focussen op het netvlies af. Uiteindelijk kan een hoornvliesaandoening of letsel aan het hoornvlies leiden tot slechtziendheid of in het ergste geval blindheid. Helaas zijn er voor patiënten met ernstig beschadigde hoornvliezen maar beperkte behandelingsmogelijkheden beschikbaar om het zicht te verbeteren. Daarom is het belangrijk dat we blijven zoeken naar nieuwe, succesvolle biomaterialen die als behandeling kunnen dienen voor deze patiënten.

De natuurlijke eigenschappen van het stroma bepalen de ontwerpcriteria voor nieuwe biomaterialen. Ons doel is om hydrogelen te ontwerpen die zo nauwkeurig mogelijk het stroma van het hoornvlies kunnen nabootsen. Om dit te bereiken maken we gebruik van supramoleculaire chemie, zodat we de bioactiviteit en de mechanische eigenschappen van de hydrogelen kunnen variëren en hydrogelen kunnen creëren die de cellen in het stroma op een gezonde manier kunnen ondersteunen. Hydrogelen zijn visco-elastisch en hebben een hoog watergehalte, waardoor ze de natuurlijke omgeving van cellen in het stroma, genaamd keratocyten, goed kunnen nabootsen. Synthetische biomaterialen op basis van supramoleculaire chemie zijn dusdanig ontworpen dat ze gemakkelijk aan te passen zijn en

dat verbroken connecties weer verbonden kunnen worden (self-healing). Deze dynamische eigenschappen maken het mogelijk om diverse biochemische signalen aan de hydrogelen toe te voegen, welke uiteindelijk ervoor kunnen zorgen dat regeneratie vanuit het weefsel zelf wordt gestimuleerd. In dit onderzoek hebben we gebruik gemaakt van polymeren gebaseerd op supramoleculaire ureido-pyrimidinone (UPy) motieven. Deze motieven fungeren als bouwstenen en kunnen onderling waterstofbruggen vormen die leiden tot de vorming van supramoleculaire polymeren, en uiteindelijk tot de totstandkoming van supramoleculaire hydrogelen.

Een ontwerp gebaseerd op deze UPy-motieven in combinatie met een UPy-cRGD als additief om bioactiviteit te introduceren, resulteerde in een volledig synthetische en injecteerbare supramoleculaire hydrogel. De biologische en mechanische eigenschappen van deze synthetische hydrogel werden vergeleken met een hybride hydrogel, gebaseerd op UPy-motieven gemengd met natuurlijk collageen type I. Beide hydrogelen toonden aan in staat te zijn om de benodigde biochemische signalen af te geven zodat de cellen zich succesvol in de hydrogelen konden verplaatsen (migreren), vermenigvuldigen (prolifereren) en ontwikkelen (differentiëren). Het ondersteunen van gezonde cellen in een 3D celkweek in combinatie met de mogelijkheid om de synthetische hydrogel te injecteren, tonen de potentie van deze synthetische hydrogel om ooit als synthetisch alternatief voor het stroma te dienen in de kliniek.

Naast UPy-cRGD zijn er drie andere bioactieve additieven gesynthetiseerd, geconjugeerd en gekarakteriseerd: een additief wat collageen type I kan binden, een wat langer additief wat collageen type I nabootst (inclusief de speciale structuur) en een kort maar relatief makkelijk te maken additief wat collageen nabootst (zonder speciale structuur). Alle drie deze additieven zijn individueel toegevoegd aan de synthetische supramoleculaire hydrogel. In tegenstelling tot het kortere collageen nabootsende additief, was het langere collageen nabootsende additief in staat om de benodigde biochemische signalen af te geven aan de cellen zodat deze zich konden hechten aan de hydrogel en een gezond fenotype van de cellen werd ondersteund. Verdere karakterisering van dit langere collageen nabootsende additief toonde aan dat dit additief de conformatie van een triple helix kan aannemen. Deze conformatie zien we ook terug bij het natuurlijke collageen type I eiwit. Hiermee tonen we

aan dat het nabootsen van deze conformatie van essentieel belang is voor het biologische succes van het additief.

Het toepassen van een supramoleculaire aanpak maakt het mogelijk om een groot aantal verschillende hydrogelen te maken. Naast het gebruik van verschillenden additieven in de hydrogelen, zijn ook verschillende variaties van de hoofd bouwstenen gebruikt om verschillende hydrogelen te formuleren. Deze verschillende variaties van hoofd bouwstenen zijn gecreëerd middels het introduceren van een supramoleculaire polyaminozuur bibliotheek, bestaande uit polymeren met dezelfde UPy bouwsteen maar met verschillende aminozuren als eindgroep. Hiermee hebben we een variatie van verschillende hydrogelen weten te maken die zowel 2D evenals 3D celkweken ondersteunen. Daarnaast hebben we aangetoond dat verschillende aminozuren in een hydrogel gecombineerd kunnen worden, waardoor de eiwitpresentatie in de natuurlijke extracellulaire matrix op een synthetische manier kan worden nagebootst. De introductie van deze supramoleculaire polyaminozuur bibliotheek draagt hierdoor bij aan het ontwerpen en maken van een groot aantal nieuwe functionele biomaterialen.

Naast de samenstelling van de hydrogelen hebben we ook onderzocht of het mogelijk is om de afmetingen van de hydrogelen te variëren. Door supramoleculaire hydrogelen te combineren met microfluïdica is het gelukt om hele kleine supramoleculaire gelen te maken, genaamd; microgelen. Het is ons gelukt om één cel te verpakken in één microgel. Door microgelen met en zonder verpakte cellen samen te voegen en te kweken hebben we aangetoond dat er poreuze microstructuren kunnen worden gevormd waarin cellen kunnen infiltreren en migreren. Omdat microgelen zo klein zijn en vanwege de reversibele bindingen tussen microgelen zelf en tussen microgelen en de cellen, zijn ze heel geschikt om bij te dragen aan de ontwikkeling van minimaal invasieve therapieën om hoornvlies letsel te herstellen.

De resultaten beschreven in dit proefschrift leveren belangrijke inzichten in verschillende ontwerpen van supramoleculaire hydrogelen, met de potentie om te kunnen functioneren als synthetisch hoornvlies. De vergaarde kennis bijeengebracht in dit proefschrift rijkt echter verder dan de toepassing in het hoornvlies veld. Het kan ook van toepassing zijn voor andere biomedische toepassingen die betrekking hebben op interacties tussen cellen en materialen.

Annika Vrehen was born on the 4th of September, 1994 in Nieuwstadt, the Netherlands. She grew up in Nieuwstadt and completed her secondary education (Atheneum) at Trevianum Scholengroep te Sittard in 2012. She than studied Medical Sciences and Technology at the Eindhoven University of Technology, where she obtained her Bachelor's degree in 2015. Her Bachelor end project focused on the evaluation of differences between various monocyte isolation techniques. She continued her Master Biomedical Engineering at the same university in the Biomaterials group of prof. dr. dr. Patricia Y.W. Dankers. During her master thesis, she focused on the development of a renal cellular read-out for biomaterial screening. For her internship abroad, she was granted a scholarship by het Prinses Beatrix Spierfonds, and went to King's College London, UK. Under supervision of prof. dr. Georgina Ellison-Hughes within the faculty of Life Sciences & Medicine, she investigated the therapeutic potential of PW1-positive interstitial cells in treating muscular dystrophy. She graduated in December 2018 after which she started as a PhD candidate in the same group under the supervision of prof. dr. dr. Patricia Y.W. Dankers. Within this project, she aimed to design corneal stromal microenvironments based on supramolecular hydrogels. The most important results of this research are presented in this thesis.

Annika Vrehen is geboren op 4 september 1994 in Nieuwstadt. Ze groeide op in Nieuwstadt en voltooide in 2012 haar middelbare schoolopleiding (Atheneum) aan Trevianum Scholengroep te Sittard. Daarna studeerde ze Medische Wetenschappen en Technologie aan de Technische Universiteit te Eindhoven, waar ze in 2015 haar bachelor diploma behaalde. Haar eindproject richtte zich op de evaluatie van verschillende isolatietechnieken voor monocyten. Ze vervolgde haar master Biomedical Engineering aan dezelfde universiteit in de Biomaterialen groep van prof. dr. dr. Patricia Y.W. Dankers. Tijdens haar masterscriptie richtte ze zich op de ontwikkeling van een read-out voor niercellen om biomaterialen te kunnen screenen. Voor haar buitenlandse stage kreeg ze een beurs van het Prinses Beatrix Spierfonds, en ging ze naar King's College London in Engeland. Binnen de faculteit Life Sciences & Medicine, onder supervisie van prof. dr. Georgina Ellison-Hughes onderzocht ze de therapeutische potentie van PW1-positieve interstitiële cellen voor de behandeling van spierdystrofie. In december 2018 studeerde ze af, waarna ze begon als promovendus in dezelfde groep onder begeleiding van prof. dr. dr. Patricia Y.W. Dankers. Binnen dit project richtte ze zich op het ontwerpen van micro-omgevingen voor het hoornvlies gebaseerd op supramoleculaire hydrogelen. De belangrijkste resultaten van dit onderzoek worden in dit proefschrift gepresenteerd.

Ronald C. van Gaal, **Annika F. Vrehen**, Johnick F. van Sprang, Peter-Paul K.H. Fransen, Mark C. van Turnhout, Patricia Y.W. Dankers. *Biomaterial screening of protein coatings and peptide additives: towards a simple synthetic mimic of a complex natural coating for a bio-artificial kidney*, *Biomaterials Science,* 2021, doi: 10.1039/D0BM01930E

Moniek G.J. Schmitz, Martijn Riool, Leonie de Boer, **Annika F. Vrehen**, Paul A.A. Bartels, Sebastian A.J. Zaat, Patricia Y.W. Dankers. *Development of an Antimicrobial Peptide SAAP-148-Functionalized Supramolecular Coating on Titanium to Prevent Biomaterial-Associated Infections*, *Advanced Materials Technologies,* 2023, doi: 10.1002/admt.202201846

Annika F. Vrehen, Martin G.T.A. Rutten, Patricia Y.W. Dankers. *Development of a Fully Synthetic Corneal Stromal Construct via Supramolecular Hydrogel Engineering*, *Advanced healthcare materials,* 2023, doi: 10.1002/adhm.202301392.

Laura Rijns, Martin G.T.A. Rutten, **Annika F. Vrehen**, Ana A. Aldana, Matthew B. Baker, Patricia Y.W. Dankers. *Using chemistry to recreate the complexity of the extracellular space: from natural to fully synthetic matrices utilizing supramolecular biomaterials*, in preparation.

Annika F. Vrehen, Maaike J.G. Schotman, Patricia Y.W. Dankers. *Creating a hydrogel library based on protein mimicking supramolecular polyaminoacids*, in preparation.

Annika F. Vrehen, Johnick F. van Sprang, Maaike J.G. Schotman, Jingyi Huang, Patricia Y.W. Dankers. *Collagen type I mimicking peptide additives to functionalize synthetic supramolecular hydrogels*, in preparation.

Annika F. Vrehen*, Maritza M. Rovers*, Patricia Y.W. Dankers. *Biohybrid corneal stromal tissue formation using keratocyte encapsulated supramolecular microgels*, in preparation.

DANKWOORD (ACKNOWLEDGEMENTS)

Na uren hydrogelen maken, cellen kweken, pipeteren, in het donker plaatjes maken met de microscoop, en al deze plaatjes en resultaten daarna weer uitwerken op kantoor is er uiteindelijk dit boekwerk uitgerold. De afgelopen jaren waarin deze thesis is gerealiseerd waren soms intens maar ook ontzettend mooi, en ik had ze absoluut niet willen missen. In deze tijd heb ik veel nieuwe mensen leren kennen, ben ik nog meer gefascineerd en geïnspireerd geraakt door de wetenschap en heb ik door mijn eigen grenzen te verleggen ook zelf ontzettend veel geleerd. Tijdens deze jaren heb ik veel hulp gehad van vele mensen om mij heen. Deels waren dit mensen die inhoudelijk hebben bijgedragen aan dit werk, en deels mensen die voor de nodige ontspanning zorgden naast het werk.

Patricia, allereerst wil ik jou bedanken voor de aangeboden kans om in jou mooie onderzoeksgroep te kunnen promoveren. Als ik het mij goed herinner, vond ons eerste gesprek plaats na het afronden van mijn bachelor en ging dit gesprek over het samenstellen van het vakkenpakket voor de master. Tijdens dit gesprek heb je mijn nieuwsgierigheid weten te wekken door te praten over de projecten die op dat moment gaande waren in de groep. Wat mijzelf toen (en ook nu nog steeds) heel erg aansprak was de duidelijke klinische toepassing van sommige lopende projecten. Zelf was ik ook opzoek naar een project met een duidelijk klinisch einddoel en zo is onze samenwerking in de master van start gegaan. Na de master volgde dit mooie promotie onderzoek, waarmee ook een nieuw orgaan werd geïntroduceerd in de groep: het oog. Ik weet nog dat ik mijn eerste consortium meeting best een beetje spannend vond en jou vroeg om tips. Jou tip was toen: kijk van te voren een paar filmpjes van oog operaties, want dat is vaak 'een beetje viezig'. Toen vond ik dat een beetje een rare tip, maar later bleek deze tip inderdaad een goeie. Samen hebben we de afgelopen jaren veel geleerd over het oog en wie weet komt er ooit wel weer een nieuw oogproject op gang in de groep. Patricia, bedankt voor je vertrouwen en de vrijheid die je me gegeven hebt om dit project echt van mij te maken. Jouw onuitputtelijke enthousiasme voor de wetenschap en het plezier waarmee je dit uitdraagt zijn de afgelopen jaren een inspiratie geweest voor mij, en waarschijnlijk ook voor vele anderen. Heel erg bedankt hiervoor!

Carlijn, als mijn tweede promotor hebben wij elkaar wat minder vaak gesproken tijdens de afgelopen jaren. Wel was er altijd jouw oprechte interesse in mijn werk. Bedankt voor jouw snelle en uitgebreide feedback op mijn eerste versie van dit proefschrift, deze hebben mij heel erg veel geholpen bij het afronden van dit proefschrift.

Naast mijn eerste en tweede promotor wil ook graag Maarten Merkx, Jan de Boer, Laura De Laporte, Rudy Nuijts, Matt Baker, en Willeke Daamen bedanken voor jullie deelname aan mijn promotie commissie. Ik kijk ernaar uit om met jullie van gedachten te kunnen wisselen tijdens mijn verdediging. **Rudy**, bedankt voor de inspirerende meetings die we vooral in het begin van mijn promotie onderzoek gehad hebben. Deze hebben me altijd ontzettend gemotiveerd om te blijven zoeken naar geschikte biomaterialen. **Matt**, thanks for all your help and input during the various EyeSciTe meetings. With a history at the TU/e you knew the UPy's very well, it was very nice to have someone in the room during these meetings who could help me out if others started to question the use of the UPy's.

Dan de twee meiden die straks aan mijn zijde staan tijdens deze bijzondere gebeurtenis. Ik ben super dankbaar, blij, en vereerd dat jullie dit voor mij willen doen. **Ellen**, als iemand er altijd voor mij is, en nooit iets te veel is, dan ben jij het wel. We gaan ondertussen al heel wat jaartjes terug maar ik ben onze vriendschap vooral gaan waarderen toen jij als een van de weinige mij bent komen bezoeken in het ziekenhuis. Ook kreeg ik om de dag hele lieve en motiverende appjes en trok jij me weer het huis uit toen ik dat zelf misschien nog wel wat spannend vond. Dit heeft mij toen ook echt super veel geholpen. Ondertussen hebben we heel wat mooie momenten gedeeld en soms ook minder mooie momenten. Ik geniet ontzettend van al onze bijklets momentjes, uitjes, klaagzangen en eigenlijk alles wat we samen ondernemen. Bedankt dat ik altijd met alles bij je terecht kan. **Maritza**, wij kennen elkaar nu ongeveer twee jaar en toch voelt het al veel langer. Iedere dag dat we samen op kantoor of in het lab aan het werk waren voelde voor mij als een feestje. Door veel samen te lachen over domme acties, of veel samen te klagen over de mannen thuis of over de hobbels tijdens de PhD vlogen de dagen voorbij. En niet te vergeten, onze grote klapper, beter bekend als de 'bolletjes' of 'druppeltjes'. Zonder verwachting met wat 'left-overs' op een vrijdagmiddag dit experiment afgetrapt, niet wetende wat voor schitterende resultaten hieruit zouden rollen. Dit project heeft zeker niet altijd de waardering gekregen wat het in mijn ogen verdiend, maar meid, ik ben er echt ontzettend trots op. Super knap dat je dat microgel system werkend hebt gekregen en ik weet wel bijna zeker dat er het komende jaar nog veel gave experimenten zullen volgen. Dat wordt een prachtig boekje!

Siri, bedankt voor het ontwerpen van de kaft. Zelf was ik al een beetje 'gewend' geraakt aan de microscopie plaatjes, maar door jou super enthousiaste reactie ben ik ze weer opnieuw gaan waarderen. Ik ben ontzettend blij en trots op het eindresultaat!

Door de jaren heen heb ik heel wat gezellige kantoormaten gehad die altijd klaarstonden om mij te helpen of om even gezellig koffie of water te halen en even te kletsen. Het begon heel rustig samen met Geert, maar al snel was met de komst van Martin en zijn snoep pot de rust voorbij. Met z'n drietjes introduceerde we de vrijdagmiddag disco en kregen we naast de postbode ook steeds vaker anderen op bezoek die even kwamen kletsen en snoepen. Geert vertrok, en Laura kwam erbij wat zorgde voor nog meer gezelligheid. **Geert**, bedankt voor al je adviezen en goede raad tijdens de eerste maanden van mijn PhD. Heel knap wat jij en Peter-Paul al bereikt hebben met UPy-ther en ik hoop dat er voor jullie nog veel meer moois volgt! De verhuizing naar het grote kantoor zorgde voor nog meer kantoormaten. **Martin**, **Laura**, **Jasper**, **Maritza**, **Victor**, **Paul**, en **Bram**, heel erg bedankt voor jullie behulpzaamheid, het bespreken van experimenten en natuurlijk de gezelligheid!

Al die jaren vond ik de Dankerslab groep een hele fijne omgeving om onderzoek in te doen. Mijn paranimfen heb ik een tegeltje gegeven met de tekst 'kennis wordt pas wijsheid wanneer je het deelt', en dit heb ik ook echt zo ervaren. Kritische vragen, discussies over de opzet van een experiment of over de resultaten, en de behulpzaamheid van iedereen binnen de groep hebben zeker een groot aandeel gehad in dit proefschrift. **Ronald** en **Bastiaan**, bedankt voor al jullie adviezen en kritische vragen tijdens het begin van mijn PhD. **Mani** en **Sergio**, jullie zijn de grondleggers van het hydrogel systeem waarvan ik veel gebruik heb gemaakt. Heel erg bedankt dat jullie dit systeem aan mij hebben willen overdragen! **Jingyi**, you are one of the kindest people that I met during my PhD. Both of us were in the same consortium, and you always had my back during the meetings. Thanks for all of your synthesis work, you are a real synthesis genius! I really hope we will meet again someday, hopefully you are enjoying your time back in China with your family. **Alex**, after Jingyi left you became my consortium buddy. It's amazing what you achieved with the material films, the transparency, the ease of making them, the rolling part, you are a genius too! I hope you and your family will stay save in these uncertain times. Thanks for all your humor and help! **Maaike**, wij werden samen op het UPy-amino zuren project gezet. Een immens project zonder duidelijk doel, maar uiteindelijk hebben we er toch een mooi project van weten te maken. Mede door jouw enthousiasme begon ik het project ook steeds leuker en interessanter te vinden. Samenwerken met jou was altijd gezellig, of we nu samen aan het kweken waren, onze duo presentatie aan het voorbereiden waren of urenlang de polymeren aan het afwegen waren, samen met jou was het nooit saai. Ik heb ervan genoten om dit project samen met jou aan te pakken. Heel erg bedankt! Heel veel geluk samen met Lenne in jullie nieuwe huis en heel veel succes met je verdere carrière! **Johnick**, ik denk dat ik samen met jou de meeste uurtjes in het lab heb doorgebracht. En zeker de helft van die uren vond in de vroege ochtend plaats, waardoor de dag al meteen goed en gezellig

van start ging. Samen bespraken we de set-up van experimenten, de resultaten, wat er mis gegaan kon zijn, of hoe gaaf de resultaten eruit zagen, en deze discussies/gesprekken hebben een hele belangrijke bijdrage geleverd aan dit proefschrift. Daarnaast natuurlijk ook nog onze samenwerking aan het UPy-GFOGER project, wat zonder jou enthousiasme nooit zo mooi was geworden. **Dan Jing**, ik denk dat ik in mijn leven zelden iemand ben tegengekomen die zo ambitieus is als dat jij bent. Het is fascinerend en inspirerend om te zien hoe jij alles aanpakt en wat jij allemaal weet te bereiken. Het lijkt wel alsof jij iedere kleine tegenslag weet om te buigen in een nieuw nog groter succes, een echte carrière tijger! Ik vind het een ware eer dat je mij gevraagd hebt om te komen werken bij VivArt-x, hopelijk lukt het ons om hier samen met Muhabbat en Patricia wat moois van te maken! **Muhabbat**, bedankt voor alle laatste tips omtrent het afronden van dit boekje. Ik kijk uit naar onze verdere samenwerking binnen VivArt-X. **Jolanda**, ik wil niet weten wat voor papierwinkel jij af en toe voor je kiezen krijgt. Bedankt voor alles wat je de afgelopen jaren voor mij geregeld hebt! **Marcel**, bedankt voor alle feedback met betrekking tot het presenteren van data tijdens de groupmeetings en natuurlijk voor de laatste check van alle structuur formules in dit proefschrift. **Moniek**, **Boris**, **Joyce**, **Paul**, **Simone**, **Riccardo**, **Jasper**, **Vincent**, **Saptarshi**, **Victor**, **Fenna**, **Roos**, and **Bram**, thanks for all the nice and helpful discussions we had over the years. Goodluck with your own PhD projects and/or future careers, I'm certain that you all will do well!

Het cel lab zou niet zo'n fijne werkplek zijn zonder alle mensen van het **Tech-team**. Dames en heren van het Tech-team ontzettend bedankt voor jullie inzet iedere dag. **Mark**, bedankt voor het 'up and running' houding van de SP8, zonder deze microscoop waren de plaatjes vast een stuk minder mooi geworden. Ook bedankt voor je hulp met het matlab scriptje! **Dylan**, als mede limbo eindigde we de werkdag best vaak toevallig in dezelfde trein en dit waren altijd gezellige en interessante ritjes. Heel veel succes met het afronden van je eigen promotie onderzoek en je verdere carrière! **Cas**, jij bent vanaf mijn eerste werkdag mijn oog en consortium maatje binnen de TU/e. Wat was het fijn dat jij de keratocyten al naar het lab had gehaald en dat we altijd samen konden sparren over experimenten en resultaten. Ook onze gesprekken bij het koffieapparaat over ons promotie onderzoek, het consortium, en allerlei andere zaken heb ik altijd heel erg gewaardeerd. Ik ben trots op al het werk wat we beiden hebben neergezet met betrekking tot het oog, heel veel succes met je verdere carrière!

Laura, Martin en Maritza, ofwel de LAMM, waar moet ik beginnen. Terugkeren uit het lab met jullie 3 aanwezig op kantoor maakte de dag meteen weer helemaal goed. Wat hebben we veel gelachen samen op kantoor en ook zeker daarbuiten. **Martin**, ook al ben je 3 maanden na mij begonnen, jij

bent mijn PhD maatje van het eerste uur. Jou eerste werkdag was volgens mij carnavalsvrijdag en ik weet nog dat Patricia heel enthousiast op ons kantoor met Geert en mij over carnaval begon te praten en liedjes te zingen. Jou gezicht, als toen nog niet carnaval vierder, sprak boekdelen. En nu 4 jaar later, ben je met de carnaval ontembaar. Ik ben zo trots. Ik ken ook niemand die zo behulpzaam is als jij, jij stond/staat altijd klaar om me te helpen met experimenten, met metingen of om gewoon mijn klaagzang aan te horen en lekker mee te klagen. ICT'er, BHV'er, rheologie master, thuis bakker, kantoor versierder, jij bent het allemaal. Samen hebben we het hydrogel systeem verder geoptimaliseerd met ontelbare rheologie metingen, en hebben we vele legendarische rheologie marathon dagen meegemaakt. We hebben zoveel gelachen samen op kantoor, ik had me echt geen beter PhD maatje kunnen wensen. Heel veel succes met het afronden van je eigen PhD en met je verdere carrière! **Laura**, welke ruimte jij ook binnenloopt, jouw aanwezigheid brengt meteen gezelligheid met zich mee. Legendarische uitspraken als 'pffffff ik kan niet meer' om 9:30 in de ochtend of 'vroeg pieken is lang genieten' zal ik niet snel meer vergeten. En dan nog die legendarische acties zoals die telefoon in een pak rijst of was het toch misschien zout? Jouw enthousiasme en drive voor de wetenschap is enorm en ik hoop echt dat het Rijnslab er ooit van komt! Heel veel succes met de verdediging van je eigen PhD en met je aankomende postdoc in Amerika, je bent een topper! Lieve LAMM, ik hoop dat we elkaar blijven zien ondanks dat onze wegen binnenkort uit elkaar gaan! Wie stemt er 'voor' om van de oktoberfeesten een vaste traditie te maken?

Evelien, Eef, we zien elkaar eigenlijk veel te weinig. Maar als we elkaar spreken is het weer net zo gezellig als vroeger en is er altijd die oprechte interesse, hopelijk doen we snel weer een drankje!

Rim, **Melle**, **Natalie** en **Koen**, bedankt voor jullie altijd oprechte interesse in mijn werk en alle gezellige en lekkere wijnavondjes, deze zorgde voor de nodige ontspanning buiten het werk. Jullie zijn ook alle vier ambitieuze en harde werkers, ik ben heel benieuwd hoe onze carrières er over een aantal jaar uitzien!

De Kennedymars deise neit op die janboerefluitjes, mer un proefschrift sjrieve zonger alle leuke en vaak spontane feeskes mit uch auch neit. **Ken**, jij staat altijd klaar om ons te helpen en geen klusje is jou te gek. Bedankt voor het afbeulen van Martijn in de sportschool, en voor het entertainen van Charlie tijdens de formule 1 races. **Joyce**, met jou is elke wandeling en elk feestje nog net een beetje leuker. Hopelijk volgen er nog veel meer legendarische momenten samen. Durven we volgend jaar weer de mars van 80 km aan?

Ellen, **Lars**, **Tim** en **Claudia**, ofwel de Johnny's en Anita's bedankt voor alle gezellige spelletjes avonden, BBQ's, uitjes, en de klapper het weekendje weg in 2022. Ik waardeer onze vriendschap enorm en zonder al deze fijne afleiding waren de afgelopen jaren een stuk saaier geweest. **Larseman**, bedankt voor je oprechte interesse in mijn werk en je o zo nuchtere tips en onnozele oplossingen die ik zelf dan even totaal niet zie. Heel veel succes met opzetten van je eigen bedrijf! **Tim**, als mede onderzoeker begrijp jij als geen ander de up's en down's in de onderzoekswereld. **Claudia**, de eetclub etentjes samen met Houbie zorgde altijd voor een fijne afleiding, bedankt!

Des, **Lex**, **Féline** en **Fenna**, jullie zijn nu nog veel te jong om een woord van dit boekje te begrijpen. Maar wat is het fijn om naast al dit serieuze werk af en toe even af te kunnen dwalen in jullie fantasie en weer opnieuw van alle kleine dingen te genieten.

Lieve familie, ook jullie wil ik allemaal bedanken voor alle steun de afgelopen jaren. We zien elkaar niet meer zo vaak als vroeger maar toch staan we altijd voor elkaar klaar en dat waardeer ik enorm.

Marlies† en **Jos**, bedankt voor jullie steun en oprechte interesse de afgelopen jaren. **Bjorn**, je bent altijd oprecht geïnteresseerd in mijn werk en je enthousiaste reactie op wat ik in het lab probeer te bereiken werkt toch altijd motiverend, bedankt daarvoor!

Truus en **Hans**, jullie staan altijd klaar om ons te helpen. Puinruimen tijdens de verbouwing, het onderhouden van onze tuin, en de ontzettend liefdevolle opvang van Charlie, niets is jullie te gek. Vooral het oppassen op Charlie heeft mij heel erg geholpen om mijn experimenten af te ronden en me thuis te kunnen concentreren op het schrijven van deze thesis. Ontzettend bedankt!

Mia† en **Fien**, mijn oma's, zelf hebben jullie door oorlog of de geest van de tijd niet de kans gekregen om de lagere school af te maken of een studie te beginnen. Jullie hebben me altijd gesteund en verteld hoe trots jullie op me waren. Dit motiveerde me keer op keer om mijn best te blijven doen. Jullie waren/zijn beide in mijn ogen powervrouwen, zo jong en al zo hard moeten werken. Door de verhalen wat jullie mij altijd verteld hebben, besef ik me nog meer hoe dankbaar ik mag zijn dat er door de jaren heen toch al heel veel is veranderd. **Oma Vrehen**, u heeft me nadat ik ziek ben geweest ontzettend veel geholpen. Samen hebben we vele dagen doorgebracht, samen naar de fysio, samen bakken en iedere dag weer net een stapje meer gezet. Hier ben ik u nog steeds heel dankbaar voor!

Sander, **Sandra**, **Celine** en **Yard**, bedankt voor jullie onvoorwaardelijke steun. Ik kan altijd op jullie rekenen en ik hoop dat jullie weten dat dat omgekeerd ook zo is. Ik geniet er altijd enorm van als we samen zijn. Het afgelopen jaar heb ik helaas wat weinig tijd gehad om samen leuke dingen te

ondernemen, maar dit halen we dubbel en dik weer in. Met de komst van Féline en Fleur blijft ons gezin groeien en dit brengt alleen maar meer gezelligheid met zich mee.

Pap en **mam**, ik kan me geen fijnere ouders voorstellen dan jullie. Waar jullie kunnen, staan jullie voor mij klaar en willen jullie mij altijd helpen. De afgelopen jaren waren soms intens, en vooral de periode in het ziekenhuis hebben we heel veel tijd samen doorgebracht en was voor jullie bijna net zo zwaar als voor mijzelf. Mam, door jou ben ik al die jaren geleden met Sander naar de open dag geweest van de TU/e. Zonder die tip was dit proefschrift waarschijnlijk nooit gemaakt. Jij bent zo'n lieve en hardwerkende vrouw, ik kan alleen maar hopen dat ik ooit net zo wordt als jij. Als verpleegkundige heb jij gezorgd voor mijn interesse in het menselijk lichaam en het willen helpen van mensen. Pap, beide hebben we gestudeerd aan de universiteit en beide zijn voor stage naar de UK geweest. De verhalen over alle experimenten die jij als landbouw scheikundige en bioloog hebt uitgevoerd hebben mij altijd gefascineerd. Onze gesprekken over de wetenschap, en het proberen verbeteren van de natuur motiveren mij altijd enorm. Je doorzettingsvermogen en in mijn ogen soms onmogelijke vertrouwen in een goede afloop zijn de laatste jaren een voorbeeld voor mij geweest. Pap en mam, bedankt voor alles, ik ben trots om jullie dochter te zijn.

Tenslotte is er nog een speciaal persoon die er achter de schermen misschien nog wel het meest voor heeft gezorgd dat dit proefschrift nu voor ons ligt. Lieve **Martijn**, bedankt voor al je steun en motivatie op momenten waarop ik even niet meer goed voor me zag hoe dit ooit nog wat moest gaan worden. Samen hebben we al ontzettend veel meegemaakt, vooral de laatste jaren waren soms intens en niet altijd even gemakkelijk. Ik ben er ontzettend trots op hoe we naast alle zorgen ons toch zijn blijven focussen op ons werk, en zelfs ons eerste huis hebben gekocht en dit ook nog, op de buitenmuren na, volledig hebben verbouwd. Iedere dag samen met jou is een feestje en met de komst van Charlie, ons hondenkind, is het nog veel leuker geworden. Naast alle grote momenten, feestjes en vakanties samen met jou geniet ik ook ontzettend van alle kleine en simpele dingen die we samen ondernemen. Lieve Martijn, ik hou van je, ik hou van ons, en ik kijk ontzettend uit naar alle avonturen die nog voor ons liggen.

Veel liefs,

Annika

" Ik heb vurleupig wir genog geproat

Ik heb 't allemoal gezeen, allemoal gehad

Ik wil danse, danse met ow "